



Mackenzie, Ruth M. (2010) *Oxidative stress in endothelial cells of patients with coronary artery disease*. PhD thesis.

<http://theses.gla.ac.uk/1531/>

Copyright and moral rights for this thesis are retained by the author

A copy can be downloaded for personal non-commercial research or study, without prior permission or charge

This thesis cannot be reproduced or quoted extensively from without first obtaining permission in writing from the Author

The content must not be changed in any way or sold commercially in any format or medium without the formal permission of the Author

When referring to this work, full bibliographic details including the author, title, awarding institution and date of the thesis must be given

# **Oxidative Stress in Endothelial Cells of Patients with Coronary Artery Disease**

This being a thesis submitted for the degree of Doctor of Philosophy (Ph.D.)  
in the Faculty of Medicine, University of Glasgow  
September 2009

Ruth M. Mackenzie, M. Sci.

BHF Glasgow Cardiovascular Research Centre  
Division of Cardiovascular and Medical Sciences  
Faculty of Medicine  
University of Glasgow

# Declaration

I declare that this thesis has been written entirely by myself and is a record of research performed by myself with the exception of recruitment and clinical assessment of study participants (Dr Jane Dymott), measurements of endothelial function and vascular superoxide production (Dr Carlene A. Hamilton) and some of the methods involved in analysis of microarray data (Dr Martin W. McBride and Dr John D. McClure). This work has not been submitted previously for a higher degree and was carried out under the supervision of Dr William H. Miller and Professor Anna F. Dominiczak.

---

(Ruth M. Mackenzie)

# Acknowledgements

Firstly, I wish to acknowledge my supervisors, Dr William Miller and Professor Anna Dominiczak, for their support and advice. In particular, I would like to thank Professor Dominiczak for the wonderful opportunities afforded to me over the last four years.

I extend my extreme gratitude to Dr Ian Salt without whose help and guidance, this project would not have been possible.

I also wish to thank Dr Carlene Hamilton for her constant encouragement and her assistance with vascular studies.

Special thanks go to Professor Salvador Moncada for allowing me to spend time in his laboratory and introducing me to AMPK.

I am grateful to Dr Jane Dymott and Dr Christian Delles for their help in obtaining human tissue samples. In addition, I would like to thank Dr Wai Kwong Lee and Dr Angelika Kritz-Wilson for their training in molecular techniques, and Dr Martin McBride and Dr John McClure for their help in analysing microarray data.

Thanks also to Dr Sergio Colombo, Dr Marisol Quintero, Jim McCulloch, Dr Maria Moreno, Dr James Reihill, Pamela Jane Logan, Dr Mike Murphy, Dr James Polke and Dr Caline Koh Tan for their technical expertise.

Finally, and most importantly, I would like to thank my wonderful friends and family, in particular my parents, for their unwavering support. I could not have achieved this without them.

# Contents

Declaration .....	2
Acknowledgements .....	3
Contents .....	4
List of Figures .....	8
List of Tables.....	10
Publications, Awards & Presentations .....	11
List of Abbreviations, Acronyms & Symbols.....	15
Summary .....	21
<b>1. Introduction</b> .....	24
1.1 Cardiovascular Disease .....	25
1.1.1 Type 2 Diabetes Mellitus .....	25
1.1.1.1 Hormonal Regulation of Metabolic and Hemodynamic Homeostasis.....	28
1.1.1.2 Insulin Secretion.....	28
1.1.1.3 Insulin Signalling .....	30
1.1.1.4 Insulin Resistance.....	32
1.1.1.5 Type 2 Diabetes Mellitus & Cardiovascular Disease .....	35
1.1.1.6 Genetics & Environment.....	36
1.1.1.7 Treatment of Type 2 Diabetes Mellitus .....	38
1.2 The Vascular Endothelium.....	40
1.2.1 Endothelial Dysfunction.....	41
1.3 Oxidative Stress in Cardiovascular Disease.....	41
1.3.1 Reactive Oxygen Species .....	41
1.3.2. Nitric Oxide.....	42
1.3.3 Oxidative Stress .....	45
1.3.4 Reactive Oxygen Species: Sources in The Vasculature.....	46
1.3.4.1 Endothelial Nitric Oxide Synthase.....	46
1.3.4.2 NAD(P)H Oxidase .....	46
1.3.4.2.1 NAD(P)H Oxidase In Type 2 Diabetes Mellitus .....	49
1.3.4.3 Mitochondria .....	49
1.3.4.3.1 Mitochondria in Type 2 Diabetes Mellitus .....	51
1.4 Mechanisms in Defence Against Oxidative Stress .....	53
1.4.1 Superoxide Dismutases .....	53
1.4.2 Catalase .....	54
1.4.3 Glutathione Peroxidases.....	54
1.5 AMP-activated Protein Kinase.....	55
1.5.1 AMP-activated Protein Kinase in Type 2 Diabetes Mellitus .....	57
1.5.2 AMP-activated Protein Kinase in The Vascular Endothelium .....	59
1.6 Aims .....	61
<b>2. Materials &amp; Methods</b> .....	62
2.1 General Laboratory Practice .....	63
2.2 Recruitment & Clinical Assessment of Study Participants.....	64
2.3 Human Vascular Tissue .....	66
2.4 Isolation & Culture of Primary Cells .....	66
2.4.1 Isolation of Primary Endothelial Cells from Human Saphenous Vein .....	66
2.4.2 Isolation of Primary Vascular Smooth Muscle Cells from Human Saphenous Vein.....	67
2.4.3 Primary Cell Culture & Passage .....	68
2.4.4 Immunocytochemical Characterisation of HSVECs & HSVSMCs.....	68
2.4.5 Cryo-preservation of HSVECs.....	69

2.5 Extraction, Purification & Quantification of RNA from HSVECs.....	69
2.5.1 RNA Extraction.....	69
2.5.2 DNase Treatment of Extracted Total RNA.....	70
2.5.3 RNA Quantification .....	70
2.6 Extraction & Quantification of Protein from HSVECs .....	71
2.6.1 Protein Extraction.....	71
2.6.2 Determination of Protein Concentration .....	71
2.6.3 Cell Lysate Preparation .....	71
2.7 HSVEC mRNA Expression .....	72
2.7.1 Reverse Transcription Polymerase Chain Reaction (RT-PCR) .....	72
2.7.2 TaqMan <sup>®</sup> Real-Time RT-PCR .....	73
2.8 HSVEC Protein Expression .....	74
2.8.1 Western Blot Assessment of Protein Expression.....	74
2.8.2 Densitometric Quantification of Protein Bands .....	75
2.9 Statistical Analysis .....	75
<b>3. Mechanisms of Oxidative Stress in Coronary Artery Disease .....</b>	<b>77</b>
3.1 Introduction .....	78
3.2 Materials & Methods.....	82
3.2.1 Study Participants .....	82
3.2.2 Human Vascular Tissue & Primary Cell Culture.....	82
3.2.3 Assessment of Endothelial Function.....	82
3.2.4 Assessment of Vascular Superoxide Production.....	83
3.2.5 Assessment of HSVEC Superoxide Production.....	83
3.2.5.1 Lucigenin-Enhanced Chemiluminescence .....	83
3.2.5.2 Electron Paramagnetic Resonance Spectroscopy.....	84
3.2.6 HSVEC mRNA Expression .....	86
3.2.7 Western Blot Analysis .....	86
3.2.7.1 Primary Antibodies .....	87
3.2.7.2 Secondary Antibodies .....	87
3.2.7.3 Densitometric Quantification of Protein Bands .....	87
3.2.8 Relative Quantitation of HSVEC Mitochondria by qRT-PCR .....	87
3.2.8.1 DNA Extraction .....	87
3.2.8.2 DNA Quantification .....	90
3.2.8.3 Quantitation of Single-copy Mitochondrial & Nuclear DNA.....	90
3.2.9 Statistical Analysis .....	90
3.3 Results .....	91
3.3.1 Endothelial Function .....	91
3.3.2 Vascular Superoxide Production.....	91
3.3.3 Isolation & Characterisation of HSVECs & HSVSMCs .....	91
3.3.4 HSVEC Superoxide Production.....	95
3.3.4.1 Lucigenin-Enhanced Chemiluminescence .....	95
3.3.4.2 Electron Paramagnetic Resonance Spectroscopy.....	95
3.3.5 HSVEC Superoxide Dismutase Expression.....	95
3.3.6 Relative Quantitation of HSVEC Mitochondria by qRT-PCR .....	101
3.3.7 Characterisation of Enzymatic Sources of Superoxide Generation .....	101
3.3.7.1 Mitochondria .....	101
3.3.7.2 Endothelial Nitric Oxide Synthase.....	105
3.3.7.3 NAD(P)H Oxidase .....	107
3.4 Discussion .....	109
<b>4. Endothelial AMP-activated Protein Kinase Activity in Coronary Artery Disease .....</b>	<b>117</b>
4.1 Introduction .....	118
4.2 Materials & Methods.....	119

4.2.1 Study Participants .....	119
4.2.2 Human Vascular Tissue & Primary Cell Culture.....	119
4.2.3 Determination of ATP Production in HSVECs .....	120
4.2.4 Western Blot Analysis .....	120
4.2.4.1 Primary Antibodies .....	121
4.2.4.2 Secondary Antibodies .....	121
4.2.4.3 AMPK Thr172 Phosphorylation at Different Oxygen Concentrations.....	121
4.2.4.4 Densitometric Quantification of Protein Bands .....	125
4.2.5 <i>PRKAA1</i> & <i>PRKAA2</i> mRNA Expression .....	125
4.2.6 AMPK Activity Assay .....	125
4.2.6.1 Preparation of HSVEC Lysates.....	125
4.2.6.2 Immunoprecipitation of AMPK .....	126
4.2.6.3 Assaying AMPK Activity .....	127
4.2.7 Statistical Analysis .....	127
4.3 Results .....	127
4.3.1 HSVEC ATP Production .....	127
4.3.2 Effect of Oxygen Concentration on HSVEC AMPK Thr172 Phosphorylation	128
4.3.3 HSVEC AMPK Activity .....	128
4.3.4 HSVEC <i>PRKAA1</i> & <i>PRKAA2</i> mRNA Expression .....	132
4.3.5 HSVEC AMPK Substrate Phosphorylation .....	132
4.3.6 HSVEC AMPK Upstream Kinase Phosphorylation .....	135
4.3.7 Mitochondrial ROS-Mediated AMPK Activation in HSVECs .....	139
4.4 Discussion .....	142
<b>5. Gene Expression Profiling of Endothelial Cells in Coronary Artery Disease .....</b>	<b>148</b>
5.1 Introduction .....	149
5.2 Materials & Methods.....	150
5.2.1 Study Participants .....	150
5.2.2 Human Vascular Tissue & Primary Cell Culture.....	150
5.2.3 RNA Extraction, Quantification & Validation.....	150
5.2.4 Biotinylated cRNA Synthesis .....	151
5.2.4.1 First & Second Strand cDNA Synthesis .....	151
5.2.4.2 Double Stranded cDNA Purification .....	151
5.2.4.3 <i>In Vitro</i> Transcription to Synthesise cRNA .....	152
5.2.4.4 cRNA Purification & Validation.....	152
5.2.5 Microarray Hybridisation & Data Collection .....	153
5.2.6 Microarray Data Analysis .....	154
5.2.6.1 Quality Control .....	154
5.2.6.2 Gene Expression Data Analysis .....	154
5.2.6.2.1 Illumina <sup>®</sup> BeadStudio Analysis .....	154
5.2.6.2.2 Ingenuity Pathway Analysis.....	155
5.2.6.2.3 Rosetta Resolver <sup>®</sup> Analysis .....	155
5.2.6.2.4 Integration of Analyses Results .....	156
5.2.7 TaqMan <sup>®</sup> Real-Time RT-PCR .....	156
5.3 Results .....	156
5.3.1 Total RNA & cRNA Validation.....	156
5.3.2 Microarray HSVEC mRNA Expression Profiling .....	158
5.3.2.1 Microarray Data Quality Control .....	158
5.3.2.2 Beadstudio Analysis.....	158
5.3.2.2.1 Ingenuity Pathway Analysis.....	158
5.3.2.2.2 Confirmation of Differential Expression of Candidate Genes by TaqMan <sup>®</sup> Real-Time RT-PCR.....	164
5.3.2.3 Rosetta Resolver <sup>®</sup> Analysis .....	168

5.3.2.3.1 Ingenuity Pathway Analysis.....	168
5.3.2.3.2 Confirmation of Differential Expression of Candidate Genes by TaqMan <sup>®</sup> Real-Time RT-PCR.....	173
5.3.2.4 Identification of Differentially Expressed Genes Common to BeadStudio & Rosetta Resolver <sup>®</sup> Microarray Data.....	173
5.4 Discussion .....	177
<b>6. General Discussion</b> .....	184
Appendix .....	190
Reference List .....	202



# List of Figures

		Page
Figure 1.1	Cardiovascular Disease Risk Factors	26
Figure 1.2	Regulation of Glucose Metabolism	29
Figure 1.3	Insulin Secretion	31
Figure 1.4	Overview of Insulin Signalling	33
Figure 1.5	Oxidative Stress in Cardiovascular Disease	43
Figure 1.6	Nitric Oxide Signalling in the Vessel Wall	44
Figure 1.7	Structure of the Active NAD(P)H Oxidase Complex	48
Figure 1.8	Mitochondrial Oxidative Phosphorylation and Superoxide Production	50
Figure 1.9	Insulin Resistance and Hyperglycaemia-induced Mitochondrial Superoxide Production in Activation of Atherogenic Signalling Pathways	52
Figure 1.10	AMPK-regulated Pathways in Endothelial Cells	56
Figure 3.1	Accumulation of MitoQ <sub>10</sub> in Cells and Mitochondria	81
Figure 3.2	Vasorelaxation in Rings of Saphenous Vein	92
Figure 3.3	Vascular Superoxide Production	93
Figure 3.4	Representative Photomicrographs Showing Vascular Cells in Primary Culture	94
Figure 3.5	HSVEC Basal Superoxide Production Measured by Lucigenin Chemiluminescence	96
Figure 3.6	HSVEC Basal Superoxide Production Measured by Electron Paramagnetic Resonance Spectroscopy	97
Figure 3.7	HSVEC <i>SOD1</i> mRNA Expression Relative to $\beta$ -actin ( <i>ACTB</i> ) as Assessed by TaqMan <sup>®</sup> qRT-PCR	99
Figure 3.8	HSVEC <i>SOD2</i> mRNA and Protein Expression	100
Figure 3.9	Comparison of HSVEC Mitochondrial Numbers by Polymerase Chain Reaction	102
Figure 3.10	Effects of Mitochondrial Respiratory Chain Inhibition on HSVEC Superoxide Production as Assessed by Electron Paramagnetic Resonance Spectroscopy	103
Figure 3.11	Effects of a Mitochondria-Targeted Antioxidant on HSVEC Superoxide Production as Assessed by Electron Paramagnetic Resonance Spectroscopy	104
Figure 3.12	eNOS mRNA Expression & Contribution to Superoxide Production in HSVECs	106
Figure 3.13	p22 <sup>phox</sup> mRNA Expression and NAD(P)H Oxidase Contribution to Superoxide Production in HSVECs	108
Figure 4.1	ATP Production in HSVECs	129
Figure 4.2	Effect of Oxygen Concentration on AMPK $\alpha$ 1 Thr172 Phosphorylation in HSVECs from CAD Patients	130

Figure 4.3	Comparison of Total AMPK Activity in Immunoprecipitates from HSVEC Lysates Cultured at 21% Oxygen	131
Figure 4.4	Comparison of AMPK $\alpha$ 1 Thr172 Phosphorylation in HSVEC Lysates Cultured at 21% Oxygen	133
Figure 4.5	HSVEC <i>PRKAA1</i> mRNA Expression Relative to <i>GAPDH</i> as Assessed by TaqMan <sup>®</sup> qRT-PCR	134
Figure 4.6	Comparison of ACC Ser80 Phosphorylation in HSVEC Lysates Cultured at 21% Oxygen	136
Figure 4.7	Comparison of eNOS Ser1177 Phosphorylation in HSVEC Lysates Cultured at 21% Oxygen	137
Figure 4.8	Comparison of LKB1 Protein Expression in HSVEC Lysates Cultured at 21% Oxygen	138
Figure 4.9	Comparison of CaMKK $\alpha$ Protein Expression in HSVEC Lysates Cultured at 21% Oxygen	140
Figure 4.10	Effect of Mitochondrial-ROS on AMPK Activation in HSVEC Lysates Cultured at 21% Oxygen	141
Figure 4.11	Proposed Mechanism of Mitochondrial Reactive Oxygen Species-Mediated AMPK Activation in Endothelial Cells	147
Figure 5.1	Agilent Bioanalyzer 2100 Assessment of Total RNA Quality	157
Figure 5.2	Agilent Bioanalyzer 2100 Assessment of cRNA Quality	159
Figure 5.3	Microarray Data Quality Control	160
Figure 5.4	IPA Canonical Pathway Analysis of BeadStudio Microarray Data	161
Figure 5.5	Citrate Cycle Canonical Pathway	163
Figure 5.6	Retinoic Acid Receptor (RAR) Activation Canonical Pathway	166
Figure 5.7	BeadStudio Candidate Gene mRNA Expression Relative to $\beta$ -actin ( <i>ACTB</i> ) as Assessed by TaqMan <sup>®</sup> qRT-PCR	167
Figure 5.8	Differentially Expressed Probes Identified by Rosetta Resolver <sup>®</sup> Analysis	169
Figure 5.9	IPA Canonical Pathway Analysis of Rosetta <sup>®</sup> Resolver Microarray Data	170
Figure 5.10	G-protein Coupled Receptor Signalling Canonical Pathway	172
Figure 5.11	Rosetta Resolver <sup>®</sup> Candidate Gene mRNA Expression Relative to $\beta$ -actin ( <i>ACTB</i> ) as Assessed by TaqMan <sup>®</sup> qRT-PCR	174
Figure 5.12	Differentially Expressed Genes Common to BeadStudio & Rosetta Resolver <sup>®</sup> Analyses of Microarray Data	175
Figure 5.13	Renin-Angiotensin System Enzymatic Cascades	180

# List of Tables

		<b>Page</b>
Table 1.1	Common Variants in MODY Genes	37
Table 1.2	Type 2 Diabetes Susceptibility Genes	39
Table 2.1	Characteristics of the Study Cohort	65
Table 3.1	Test Substances for Electron Paramagnetic Resonance Spectroscopy Experiments	85
Table 3.2	Primary Antibodies	88
Table 3.3	Secondary Antibodies	89
Table 4.1	Primary Antibodies	122
Table 4.2	Secondary Antibodies	124
Table 5.1	Differentially Expressed Citrate Cycle Genes	162
Table 5.2	Differentially Expressed Genes Involved in Retinoic Acid Receptor (RAR) Activation	165
Table 5.3	Differentially Expressed G-protein Coupled Receptor Signalling Genes	171
Table 5.4	Differentially Expressed Genes Common to BeadStudio & Rosetta Resolver® Analyses of Microarray Data	176

# **Publications, Awards & Presentations**

## **Publications**

**Mackenzie RM**, Salt IP, Miller WH, Hamilton CA, Degasperi A, Calder M, Murphy MP, Delles C, Dominiczak AF. MitoQ<sub>10</sub> decreases AMPK activation in endothelial cells from patients with coronary artery disease and diabetes. 2009

Submitted for publication August 2009

## **Awards**

University of Glasgow Biomedical Faculties' Poster Competition 2008: first prize

Scottish Society for Experimental Medicine 2009: Clinical Science Young Investigator Award

## **Presentations**

XI Workshop of the ESH Young Investigator Initiative Group

Milan, June 16<sup>th</sup> and 18<sup>th</sup>, 2007

Molecular Determinants of Oxidative Stress In Human Endothelial Cells

**R.M. Mackenzie**, W.H. Miller, C.A. Hamilton, I.P. Salt, A.F. Dominiczak  
(oral communication)

Scottish Society For Experimental Medicine

Glasgow, November 23<sup>rd</sup>, 2007

Oxidative Stress & AMP-Dependent Kinase In Human Endothelial Cells

**R.M. Mackenzie**, W.H. Miller, C.A. Hamilton, I.P. Salt, A.F. Dominiczak  
(poster communication)

Scottish Cardiovascular Forum

Edinburgh, February 2<sup>nd</sup>, 2008

Oxidative Stress & AMP-Activated Protein Kinase In Human Endothelial Cells

**R.M. Mackenzie**, W.H. Miller, C.A. Hamilton, I.P. Salt, A.F. Dominiczak

(poster communication)

2<sup>nd</sup> International Cardiovascular Symposium

Glasgow, June 9<sup>th</sup> and 10<sup>th</sup>, 2008

AMP-Activated Protein Kinase (AMPK) & Oxidative Stress In Human Endothelial Cells

**R.M. Mackenzie**, W.H. Miller, C.A. Hamilton, I.P. Salt, C. Delles, A.F. Dominiczak

(poster communication)

ISH (Hypertension 2008)

Berlin, June 16<sup>th</sup>-19<sup>th</sup>, 2008

AMP-Activated Protein Kinase (AMPK) & Oxidative Stress In Human Endothelial Cells

**R.M. Mackenzie**, W.H. Miller, C.A. Hamilton, I.P. Salt, C. Delles, A.F. Dominiczak

(poster communication)

Abstract published in the Journal of Hypertension

ISH (Hypertension 2008)

Berlin, June 16<sup>th</sup>-19<sup>th</sup>, 2008

Characterisation Of Metabolic Phenotypes In The SHRSP Using Chromosome 2 Congenic Strains

W.H. Miller, D. Graham, K. Douglas, **R.M. Mackenzie**, N.N. Huyn, A.F. Dominiczak

(poster communication)

Abstract published in the Journal of Hypertension

XII Workshop of the ESH Young Investigator Initiative Group

Berlin, June 18<sup>th</sup> and 19<sup>th</sup>, 2008

Oxidative Stress & Mitochondrial Dysfunction In Vessels From Patients With Coronary Artery Disease (CAD)

**R.M. Mackenzie**, C.A. Hamilton, W.H. Miller, C. Delles, I.P. Salt, A.F. Dominiczak

(oral communication)

British Hypertension Society Annual Meeting

Cambridge, September 15<sup>th</sup>-17<sup>th</sup>, 2008

Oxidative Stress & Mitochondrial Dysfunction In Vessels From Patients With Coronary Artery Disease (CAD)

**R.M. Mackenzie**, C.A. Hamilton, W.H. Miller, C. Delles, I.P. Salt, A.F. Dominiczak  
(oral communication)

British Hypertension Society Annual Meeting

Cambridge, September 15<sup>th</sup>-17<sup>th</sup>, 2008

Metabolic Phenotypes in SHRSP & Chromosome 2 Congenic Strains

W.H. Miller, D. Graham, K. Douglas, **R.M. Mackenzie**, N.N. Huyn, A.F. Dominiczak  
(poster communication)

University of Glasgow Biomedical Faculties' Open Day

Glasgow, November 21<sup>st</sup>, 2008

Cellular Mechanisms of Oxidative Stress

**R.M. Mackenzie**, C.A. Hamilton, I.P. Salt, M.W. McBride, J.D. McClure, C. Delles, W.H. Miller, A.F. Dominiczak  
(poster communication)

British Hypertension Society Annual Meeting

Cambridge, September 14<sup>th</sup>-16<sup>th</sup>, 2009

MitoQ<sub>10</sub> Reduces Mitochondrial Reactive Oxygen Species (ROS) Production and AMP-activated Protein Kinase (AMPK) Activity in Vessels from Patients with Type 2 Diabetes and Coronary Artery Disease (CAD)

**R.M. Mackenzie**, C.A. Hamilton, W.H. Miller, I.P. Salt, M.P. Murphy, C. Delles, A.F. Dominiczak  
(oral communication)

AHA 63rd High Blood Pressure Research Conference

Chicago, September 23<sup>rd</sup>-26<sup>th</sup>, 2009

MitoQ<sub>10</sub> Reduces Mitochondrial Reactive Oxygen Species (ROS) Production and AMP-activated Protein Kinase (AMPK) Activity in Vessels from Patients with Type 2 Diabetes and Coronary Artery Disease (CAD)

**R.M. Mackenzie**, C.A. Hamilton, W.H. Miller, I.P. Salt, M.P. Murphy, C. Delles, A.F. Dominiczak

(oral communication)

Abstract published in the Journal of Hypertension

Scottish Society for Experimental Medicine

Glasgow, November 27<sup>th</sup>, 2009

MitoQ<sub>10</sub> Decreases AMP-Activated Protein Kinase (AMPK) Activation in Endothelial Cells from Patients with Coronary Artery Disease and Diabetes

**R.M. Mackenzie**, C.A. Hamilton, W.H. Miller, I.P. Salt, M.P. Murphy, C. Delles, A.F. Dominiczak

(poster communication)

## List of Abbreviations, Acronyms & Symbols

2DG	2-deoxy-D-glucose
µg	microgram
µM	micromolar (micromoles per litre)
µM	microlitre
ACAD	acyl-Coenzyme A dehydrogenase
ACC	acetyl CoA carboxylase
ACE	angiotensin converting enzyme
ACTB	β-actin
ADP	adenosine diphosphate
AGE	advanced glycation end-product
AGTR2	angiotensin II type 2 receptor
AICAR	5-aminoimidazole-4-carboxamide ribonucleoside
AMP	adenosine monophosphate
AMPK	AMP- activated protein kinase
AMPKK	AMPK kinase
Ang I	angiotensin I
Ang II	angiotensin II
ANOVA	analysis of variance
ANT	adenine nucleotide translocase
aPKC	atypical PKC
APS	ammonium persulphate
ARB	angiotensin-II receptor blocker
AS160	Akt substrate of 160kDa
AT <sub>1</sub>	angiotensin II type 1
AT <sub>2</sub>	angiotensin II type 2
ATP	adenosine triphosphate
ATP5G3	ATP synthase, H <sup>+</sup> transporting, mitochondrial F0 complex, subunit C3 (subunit 9)
BAEC	bovine aortic endothelial cell
BCA	bicinchoninic acid
BH <sub>4</sub>	tetrahydrobiopterin
BMI	body mass index
bp	base pair
BSA	bovine serum albumin
Ca <sup>2+</sup>	calcium
CABG	coronary artery bypass graft
CAD	coronary artery disease
CaMKK	Ca <sup>2+</sup> /calmodulin-dependent kinase kinase
cAMP	cyclic AMP
cDNA	complementary DNA
cGMP	cyclic GMP
CM	3-methoxy-carbonyl



CMH	1-hydroxy-3-methoxycarbonyl-2,2,5,5-tetramethylpyrrolidine
CP	3-carboxy-proxyl
CPH	1-hydroxy-3-carboxy-2,2,5-tetramethyl-pyrrolidine hydrochloride
cpm	counts per minute
cRNA	complementary RNA
CRP	C-reactive protein
Ct	cycle threshold
Cu	copper
CVD	cardiovascular disease
CYBA	cytochrome b, $\alpha$ polypeptide
cyt c	cytochrome c
DBP	diastolic blood pressure
dH <sub>2</sub> O	distilled water
DHE	dihydroethidium
DMEM	Dulbecco's Modified Eagle's Medium
DMSO	dimethyl sulphoxide
DNA	deoxyribonucleic acid
dNTP	deoxyribonucleotide triphosphate
DPI	diphenylene iodonium
DTT	dithiothreitol
DTTP	decyl triphenylphosphonium bromide
e <sup>-</sup>	electron
EC	endothelial cell
ECL	enhanced chemiluminescence
ECM	extracellular matrix
ecSOD	extracellular SOD
EDHF	endothelium-derived hyper-polarisation factor
EDRF	endothelium-derived relaxing factor
EDTA	ethylenediamine tetra-acetic acid
EGTA	ethylene glycol tetra-acetic acid
eIF4E	eukaryotic translation initiation factor 4E
eNOS	endothelial nitric oxide synthase
EPR	electron paramagnetic resonance
ET-1	endothelin-1
ETC	electron transport chain
FAD	flavin adenine dinucleotide
FADH <sub>2</sub>	reduced flavin adenine dinucleotide
FCS	foetal calf serum
FDR	false discovery rate
FFA	free fatty acid
FITC	fluorescein isothiocyanate
FMN	flavin mononucleotide
G6Pase	glucose-6-phosphatase
GAPDH	glyceraldehyde 3-phosphate dehydrogenase
GCK	glucokinase

GLUT	glucose transporter
GMP	guanosine monophosphate
GPx	glutathione peroxidase
GSH	reduced glutathione/glutathione
GSK	glycogen synthase kinase
GSSG	oxidised glutathione
GST	glutathione-s-transferase
GTP	guanosine triphosphate
GWAS	genome wide association study
H <sup>+</sup>	proton
H <sub>2</sub> O	water
H <sub>2</sub> O <sub>2</sub>	hydrogen peroxide
HbA <sub>1c</sub>	glycosylated haemoglobin A <sub>1c</sub>
HBB	β-haemoglobin
HDL	high density lipoprotein
HEPES	4-(2-hydroxyethyl)-1-piperazineethanesulfonic acid
HNF	hepatic nuclear factor
HOCl	hypochlorous acid
HPLC	high performance liquid chromatography
HSVEC	human saphenous vein endothelial cell
HSVSMC	human saphenous vein smooth muscle cell
HUVEC	human umbilical vein endothelial cell
IDH3G	isocitrate dehydrogenase 3 (NAD <sup>+</sup> ) γ
IL	interleukin
IP	immunoprecipitate
IPA	Ingenuity Pathway Analysis
IPF1	insulin promoter factor 1
IPKB	Ingenuity Pathways Knowledge Base
IRS	insulin receptor substrate
IU	international unit
IVT	<i>in vitro</i> transcription
K <sup>+</sup>	potassium
kb	kilobase
kDa	kilodalton
kg	kilogram
KRH	Krebs-Ringer HEPES
L	litre
LDL	low density lipoprotein
L-NAME	N <sup>G</sup> -nitro-L-arginine methyl ester
LOO <sup>•</sup>	lipid radical
mA	milliAmp
MAPK	mitogen-activated protein kinase
MCP	monocyte chemoattractant protein
mg	milligrams

MHRA	Medicines and Healthcare products Regulatory Agency
miRNA	microRNA
MitoQ <sub>10</sub>	mitochondrial coenzyme Q/mitoquinone
ml	millilitre
mM	millimolar (millimoles per litre)
mm	millimetre
mmHg	millimetres of mercury
Mn	manganese
MODY	maturity onset diabetes of the young
mRNA	messenger RNA
MT-CYB	mitochondrially encoded cytochrome b
mtDNA	mitochondrial DNA
mTOR	mammalian target of rapamycin
mtROS	mitochondrial reactive oxygen species
NAD(P)H	nicotinamide adenine (phosphate) dinucleotide
NADH	nicotinamide adenine dinucleotide
ND	non (type 2) diabetic
NF-κB	nuclear factor κB
ng	nanogram
NHS	National Health Service
nM	nanomolar (nanomoles per litre)
NO	nitric oxide
NOS	nitric oxide synthase
NOX	nicotinamide adenine dinucleotide phosphate oxidase
O <sub>2</sub>	oxygen
O <sub>2</sub> <sup>-</sup>	superoxide
ODU	optical density unit
OH <sup>-</sup>	hydroxyl radical
ONOO <sup>-</sup>	peroxynitrite
OXPHOS	oxidative phosphorylation
p70S6K	p70 ribosomal S6 kinase
PAGE	polyacrylamide gel electrophoresis
PAI	plasminogen activator inhibitor
pAMPK	phosphorylated AMPK
PBS	phosphate buffered saline
PCA	principal component analysis
PCR	polymerase chain reaction
PDE	phosphodiesterase
PDGF	platelet-derived growth factor
PDK1	phosphoinositide-dependent protein kinase 1
PEPCK	phosphoenolpyruvate carboxylkinase
PGC-1α	PPAR-γ co-activator-1α
PGI <sub>2</sub>	prostacyclin
phox	phagocyte oxidase
Pi	inorganic phosphate

PI3K	phosphatidylinositol 3-kinase
PIK3R2	phosphoinositide-3-kinase, regulatory subunit 2 ( $\beta$ )
PKB	protein kinase B
PKC	protein kinase C
PMSF	phenylmethylsulfonylfluoride
PPAR- $\gamma$	peroxisome proliferator-activated receptor- $\gamma$
PRKAA	AMPK catalytic $\alpha$ -subunit
PRKAG	AMPK regulatory $\gamma$ -subunit
PSS	physiological salt solution
PtdIns	phosphatidylinositol
PTEN	phosphatase and tensin homologue
qRT-PCR	quantitative reverse transcription polymerase chain reaction
RAR	retinoic acid receptor
RAS	renin-angiotensin system
rcf	relative centrifugal force
RIN	RNA Integrity Number
RNA	ribonucleic acid
ROS	reactive oxygen species
rpm	revolutions per minute
rRNA	ribosomal RNA
RT	reverse transcription
SBP	systolic blood pressure
SDHAL1	succinate dehydrogenase complex, subunit A, flavoprotein pseudogene 1
SDHC	succinate dehydrogenase complex, subunit C, integral membrane protein, 15kDa
SDS	sodium dodecyl sulphate
SEM	standard error of the mean
Ser	serine
SHIP2	SH2 domain-containing inositol-5-phosphatase
SHRSP	stroke prone spontaneously hypertensive rat
SOD	superoxide dismutase
SOS	son-of-sevenless
STRAD	STE-20 related adaptor protein
T2D	type 2 diabetes
TCA	tricarboxylic acid
TCF	transcription factor
TGF	transforming growth factor
Thr	threonine
TNF- $\alpha$	tumour necrosis factor- $\alpha$
tPA	tissue plasminogen activator
TPP	triphenylphosphonium
TSC	tuberous sclerosis complex
ubiq	ubiquinol
UCP	uncoupling protein
v/v	volume/volume
VCAM-1	vascular cell adhesion molecule-1

VEGF	vascular endothelial growth factor
VSMC	vascular smooth muscle cell
vWF	von Willebrand factor
w/v	weight/volume
WHO	World Health Organisation
ZMP	5'-aminoimidazole-4-carboxamide ribonucleotide
Zn	zinc

## Summary

There is increasing evidence to support a role for vascular oxidative stress in the development of endothelial dysfunction and coronary artery disease (CAD). The prevalence of CAD in patients with type 2 diabetes (T2D) is more than ten times greater than in the general population and CAD patients with T2D display poorer clinical outcomes than those without. Previous investigations carried out within this laboratory have demonstrated endothelial dysfunction and elevated superoxide ( $O_2^-$ ) production throughout the vessel wall in saphenous veins from patients with advanced CAD. However, the molecular basis for these findings was not investigated, nor was the effect of T2D. Consequently, the aim of this study was to investigate a number of molecular determinants of oxidative stress in primary human saphenous vein endothelial cells (HSVECs) from CAD patients both with and without T2D, the hypothesis being that oxidative stress leads to endothelial dysfunction in CAD and is exacerbated in those patients with T2D.

Initial experiments confirmed the findings of previous studies, revealing significantly elevated  $O_2^-$  levels and impaired endothelium-dependent relaxation in portions of saphenous vein from patients with CAD related to those from healthy control subjects. In addition, results demonstrated more severe endothelial dysfunction in vessels from CAD patients with T2D relative to those CAD patients without this additional cardiovascular risk factor.

Attempts to characterise cellular sources of elevated  $O_2^-$  production in the endothelium of patients with CAD revealed that while HSVEC endothelial nitric oxide synthase (eNOS) is not a major source of  $O_2^-$  generation in CAD, nicotinamide adenine (phosphate) dinucleotide (NAD(P)H) oxidase contributes to excess  $O_2^-$  production in the endothelium of patients with this cardiovascular disease.

Further cellular investigation revealed a significant increase in expression of mitochondrial superoxide dismutase (SOD2) in HSVECs from CAD patients, in particular those with T2D. Mitochondrially-derived reactive oxygen species (mtROS) are reported to contribute to oxidative stress and endothelial dysfunction in CAD and T2D and, as such, this increase in SOD2 expression is likely to represent an adaptive response to elevated mitochondrial  $O_2^-$  production. In addition, analysis of gene expression microarray data revealed

differential expression of a number of genes potentially linked to mitochondrial function, serving to support a key role for mitochondrial dysfunction in the pathogenesis of CAD and T2D.

Additional molecular studies focused on AMP-activated protein kinase (AMPK). Proposed as a candidate target for therapeutic intervention in endothelial dysfunction, AMPK stimulates eNOS, leading to nitric oxide (NO) production in cultured endothelial cells. Furthermore, it has recently been reported that endothelial AMPK is activated in a mtROS-mediated manner. With SOD2 expression data indicating an increase in mtROS production in the endothelium of patients with CAD, AMPK activity was investigated and compared in HSVECs isolated from these patients and control subjects. AMPK activity was significantly greater in cells from patients with CAD, despite no change in activity of upstream kinases, LKB1 and  $\text{Ca}^{2+}$ /calmodulin-dependent kinase kinase (CaMKK). On stratifying CAD patients according to the presence of T2D, AMPK activity was found to be significantly increased in the endothelium of those patients with CAD and T2D as compared to those with CAD alone. Given the potentially elevated levels of mtROS production in the endothelium of patients with CAD, it seemed likely that endothelial AMPK activation in CAD patients was occurring in an mtROS-mediated manner and that this activation was enhanced in those CAD patients with T2D who display more severe endothelial dysfunction and increased SOD2 expression, consistent with increased mtROS production. In order to test this hypothesis, HSVECs isolated from vessels of CAD patients were treated with the mitochondria-targeted antioxidant, MitoQ<sub>10</sub>. Results demonstrated a significant decrease in AMPK activation in cells from those CAD patients with T2D on treatment with MitoQ<sub>10</sub>. The same effect was not seen in cells from CAD patients without T2D. These findings indicate that AMPK is activated in a mtROS-mediated manner in endothelial cells isolated from CAD patients with T2D and suggest a role for the kinase in defence against oxidative stress and endothelial dysfunction in these individuals.

In summary, a wide range of molecular techniques have been employed to investigate cellular mechanisms underlying the oxidative stress and endothelial dysfunction associated with CAD. Results suggest mitochondria contribute to the increased  $\text{O}_2^-$  production and endothelial dysfunction observed in vessels from CAD patients. In addition, findings indicate a novel, mtROS-mediated activation of AMPK in the endothelium of patients with CAD and T2D. Therefore, mitochondria-targeted antioxidants, used in combination with

pharmacological activators of AMPK, may have enhanced potential in prevention and treatment of coronary artery disease in patients with type 2 diabetes.



# **1. Introduction**

## **1.1 Cardiovascular Disease**

Cardiovascular disease (CVD) refers to disorders of the heart and circulatory system and represents a major cause of morbidity and mortality in the world today. Indeed, according to the World Health Organisation (WHO), an estimated 17.5 million, or approximately 30% of total global deaths resulted from CVD in 2005 and of these deaths, 7.6 million were due to coronary artery disease (CAD) (1). Furthermore, in the United Kingdom in 2006, the calculated annual direct cost of the care of patients with CAD was around £3.2 billion, with the indirect cost of loss of productivity even greater at over £3.9 billion (2). Consequently, the identification and characterisation of molecular mechanisms contributing to the pathogenesis of CAD is highly desirable.

In addition to CAD, stroke, peripheral vascular disease and renal failure / end stage renal disease are among cardiovascular disease phenotypes. CVD aetiology is observed to be multifactorial in nature with lifestyle, environmental and genetic factors implicated (3-6). Hypertension, type 2 diabetes mellitus and atherosclerosis are often observed in early development of CVD and are considered major modifiable risk factors for disease (3;4). Further modifiable risk factors include hypercholesterolaemia, obesity and those associated with low socioeconomic status, such as cigarette smoking, sedentary lifestyle, unhealthy diet and alcohol consumption (2). Conversely, aging, family history of CVD, gender and ethnicity represent non-modifiable disease risk factors (3) (Figure 1.1). Recent WHO statistics suggest that the major modifiable CVD risk factors account for around 80% of new CAD and stroke cases (1), highlighting the overwhelming need for research into conditions such as type 2 diabetes.

### **1.1.1 Type 2 Diabetes Mellitus**

It is universally recognised that diabetes mellitus increases CVD risk (7;8). One of the most common chronic diseases, diabetes mellitus results from a combination of defects in insulin secretion and action (9) and affects more than 180 million people worldwide, a number predicted to more than double by 2030 (10). While microvascular complications of the condition, such as nephropathy and retinopathy, are well documented, macrovascular complications, including diseases of coronary arteries, peripheral arteries and carotid

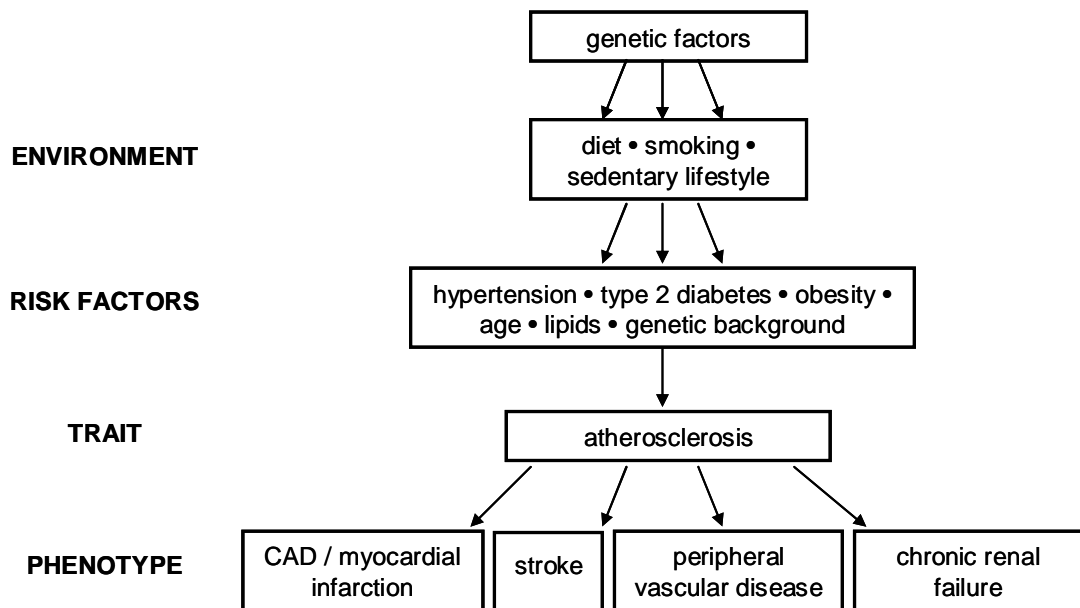


**Figure 1.1. Cardiovascular Disease Risk Factors.** Multiple interactions between genetic and environmental factors result in the target organ damage characteristic of cardiovascular disease. Adapted from (3).

vessels are reaching epidemic proportions (7). Diabetic macrovascular disease is observed to have a more severe course with greater prevalence of multiple vessel coronary artery disease and more diffuse, elongated atheromas in affected blood vessels (11-14). With the NHS reportedly spending £1 million an hour, 10% of its yearly budget, treating the condition and its complications (15), diabetes mellitus represents a major public health concern.

There are two major diabetes mellitus categories; type 1 and type 2. Type 1 diabetes is characterised by a lack of insulin production, rendering patients absolutely dependent on exogenous insulin. This form of the disease accounts for only 5%-10% of all diabetes cases and its diagnosis is made most commonly in childhood. Type 1 diabetes is thought to result from the autoimmune destruction of the insulin-producing pancreatic  $\beta$ -cells of the islets of Langerhans. Type 2 or non-insulin dependent diabetes mellitus represents the far more common form of the disease, usually with onset in adult life and associated with insulin resistance and relative insulin deficiency, as opposed to the absolute deficiency observed in type 1 (9). Type 2 diabetes (T2D) is a heterogenous disorder with clinical expression requiring interaction between genetic and environmental factors (16).

There are currently over 2.5 million people with diabetes in the United Kingdom and it is believed a further half a million cases remain undiagnosed (17). Recent findings suggest that the prevalence and incidence of diabetes in the U.K. has increased over the past decade and is mainly attributable to an increase in T2D (18). Patients with type 2 diabetes have almost twice the risk of CVD of non diabetic individuals after adjustment for other cardiovascular risk factors (19). Consequently, while the relative burden of CVD attributable to traditional risk factors, such as smoking, hypertension and hypercholesterolaemia, has declined in recent years, findings, such as those from The Framingham Heart Study, suggest an increasing prevalence of T2D has led to an increase in the proportion of CVD due to diabetes mellitus (20;21). Furthermore, after their first CV event, patients suffering from T2D and CAD consistently display poorer clinical outcomes than their non diabetic counterparts (22-27), potentially the result of impaired insulin-related metabolism (28), increased oxidative stress and/or an altered inflammatory response (29). Indeed, the mortality rate for patients with T2D has been observed to be almost twice as high as those without (30) with around 65% of deaths in these individuals related to CAD or stroke (8).

#### 1.1.1.1 Hormonal Regulation of Metabolic and Hemodynamic Homeostasis

A continuous supply of glucose is necessary to ensure appropriate function and survival of all organs. Glucose homeostasis is regulated primarily by the opposing actions of insulin and glucagon, hormones secreted by pancreatic  $\beta$ -cells and  $\alpha$ -cells respectively (31;32). Under physiological conditions, insulin secretion is increased in response to elevated blood glucose (i.e. after consumption of a meal). Insulin acts to maintain normoglycaemia by stimulating glucose uptake, utilisation and storage in classical insulin responsive tissues, namely skeletal muscle, adipose tissue and liver, and by reducing glucose production via inhibition of hepatic gluconeogenesis (33;34). Conversely, stimulation of glucagon secretion occurs during periods of hypoglycaemia when the hormone promotes hepatic glucose production and ultimately raises blood glucose levels (31;32) (Figure 1.2). Type 2 diabetes develops as a consequence of failure to regulate glucose metabolism efficiently.

In addition to its role in regulation of glucose metabolism, insulin has an important role in cardiovascular physiology, regulating vascular tone by stimulating production of the vasodilator, nitric oxide (NO) (35), and the vasoconstrictor, endothelin-1 (ET-1) (35-38), from the vascular endothelium. As such, the insulin resistance of T2D contributes to endothelial dysfunction, a common feature of cardiovascular diseases, and thus is a potential contributor to the pathogenesis of vascular disease in type 2 diabetes (39).

#### 1.1.1.2 Insulin Secretion

At a cellular level, elevated blood glucose triggers exocytosis of insulin secretory vesicles and release of insulin into the bloodstream. During normal insulin secretion, glucose transporter 2 (GLUT2) facilitates the entry of glucose into the pancreatic  $\beta$ -cells. Once inside the cell, glucose is converted by a specific glucokinase to glucose 6-phosphate before being metabolised to form adenosine triphosphate (ATP). The resultant alteration in the ATP:ADP (adenosine diphosphate) ratio causes inhibition of ATP-sensitive potassium channels in the cellular membrane. The ensuing inhibition of potassium efflux results in depolarisation of the  $\beta$ -cell and activation of voltage-sensitive calcium channels, enabling an influx of calcium. It is this increase in the intracellular calcium concentration which

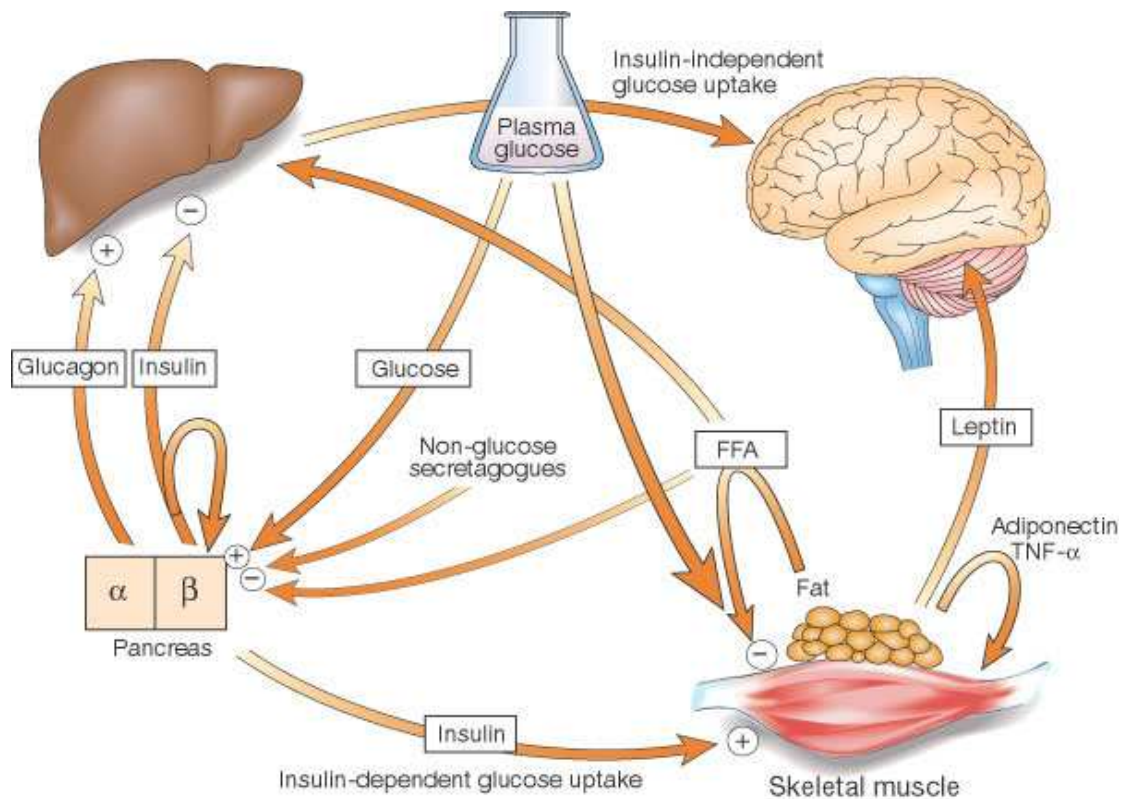


**Figure 1.2. Regulation of Glucose Metabolism.** Insulin is secreted from the  $\beta$ -cells of the pancreas in response to elevations in plasma glucose. The hormone decreases glucose production from the liver (gluconeogenesis), and increases glucose uptake, utilisation and storage in fat (adipose tissue) and skeletal muscle, thus reducing plasma glucose levels. Glucose is stored as glycogen in liver and muscle and as lipid in adipocytes. When plasma glucose levels fall (during fasting or exercise), glucagon promotes the release of stored and newly synthesised glucose into the bloodstream. In this way glucose homeostasis is maintained (34). The fat cell is important in metabolic regulation, releasing free fatty acids (FFAs) which reduce glucose uptake in muscle, insulin secretion from the  $\beta$ -cell, and increase glucose production from the liver. The fat cell can also secrete adipokines, such as leptin, adiponectin and tumour necrosis factor- $\alpha$  (TNF- $\alpha$ ), which regulate food intake, energy expenditure and insulin sensitivity (34;40). Figure from (34). Reprinted with permission from Macmillan Publishers Ltd: Nature; 414(6865):799-806, copyright 2001.

stimulates fusion of the insulin-containing secretory vesicles with the plasma membrane, resulting in the pulsatile release of insulin into the bloodstream (9;34) (Figure 1.3).

### 1.1.1.3 Insulin Signalling

In addition to serving as a primary regulator of glucose and cardiovascular homeostasis, insulin regulates gene transcription, protein synthesis and cell proliferation and differentiation (34;41). On its release, the hormone binds to a high affinity transmembrane receptor, promoting phosphorylation of intrinsic tyrosine kinases (42), resulting in activation of insulin receptor substrates (IRS) (43). Subsequent downstream signalling events ultimately determine which physiological response occurs (34;41;44;45) (Figure 1.4).

In conventional insulin-sensitive tissues, the hormone acts through Akt / protein kinase B (PKB) to promote translocation of glucose transporter 4 (GLUT4) which facilitates glucose uptake (46;47) (Figure 1.4). A second, PKB-independent pathway, involving the Cbl protooncogene, has also been reported to facilitate insulin-stimulated glucose transport (48-50) (Figure 1.4).

Acting through PKB, insulin is able to stimulate glycogen synthesis through inhibition of glycogen synthase kinase-3 (GSK3) (51) (Figure 1.4). Gluconeogenesis in the liver is inhibited by insulin via phosphatidylinositol (PtdIns) 3-kinase (PI3K)-mediated suppression of the genes for the key gluconeogenic enzymes, phosphoenolpyruvate carboxylkinase (PEPCK) (52) and glucose-6-phosphatase (G6Pase) (53). In addition, insulin inhibits lipolysis by reducing cyclic adenosine monophosphate (cAMP) levels through PKB-mediated activation of phosphodiesterase 3B (PDE3B) (54).

Insulin activates cellular protein synthesis via the mTOR (mammalian target of rapamycin) complex 1 (mTORC1) (55-57) and exerts mitogenic effects by means of the mitogen-activated protein kinase (MAPK) cascade (58) (Figure 1.4).

In cardiovascular tissue, the MAPK signalling pathway also stimulates the secretion of ET-1 (36-38) (Figure 1.4), in addition to the cellular adhesion molecules, vascular cell

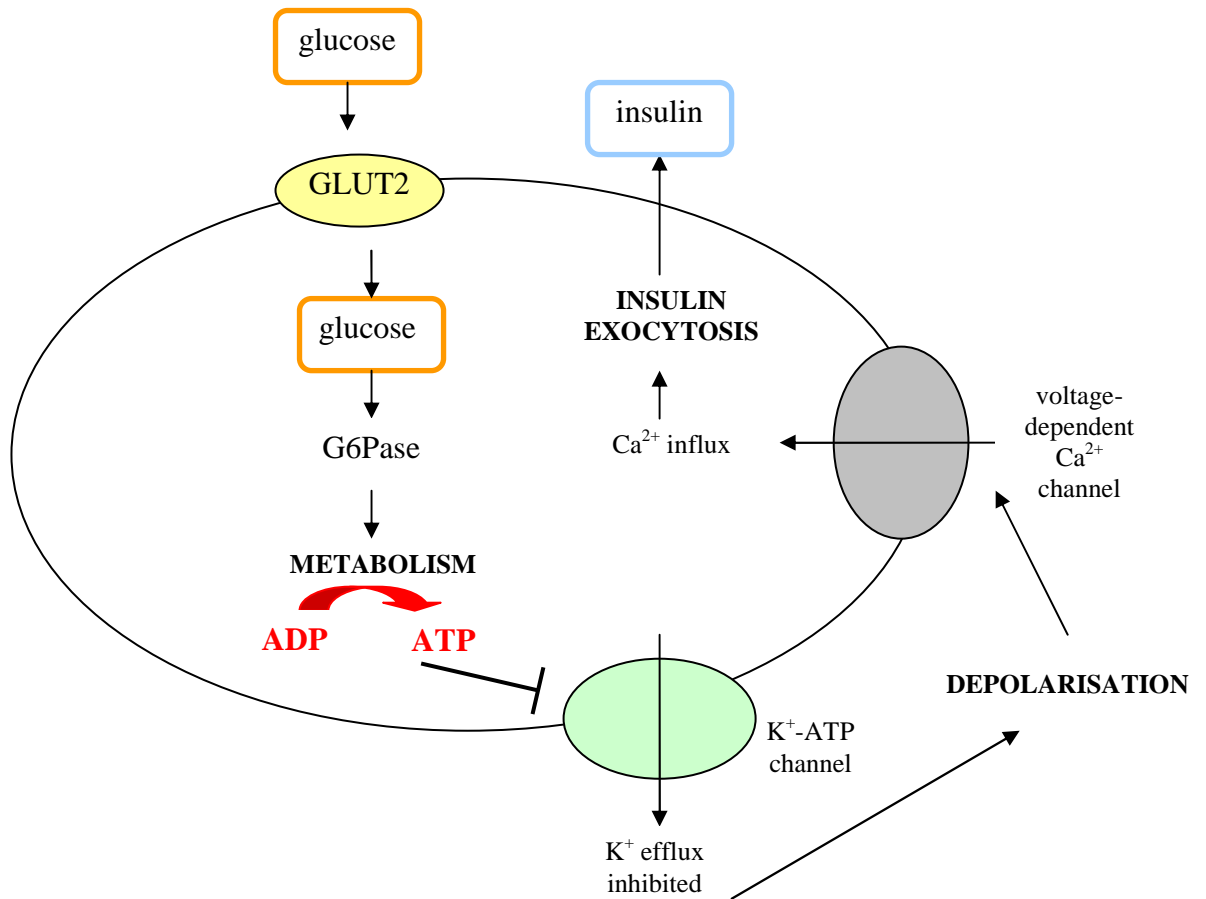


**Figure 1.3. Insulin Secretion.** Insulin secretion in  $\beta$ -cells is triggered by rising blood glucose levels. Starting with the uptake of glucose by the glucose transporter 2 (GLUT2), the glycolytic phosphorylation of glucose causes a rise in the ATP:ADP ratio. This rise subsequently activates the potassium ( $K^+$ ) channel which depolarises the membrane, causing the calcium ( $Ca^{2+}$ ) channel to open, allowing  $Ca^{2+}$  ions to flow in to the cell. Elevated  $Ca^{2+}$  levels result in insulin exocytosis (9;34). G6Pase, glucose-6-phosphatase



adhesion molecule-1 (VCAM-1) and E-selectin (59), while PKB directly phosphorylates and activates endothelial nitric oxide synthase (eNOS), leading to production of NO (35;60;61) (Figure 1.4).

#### 1.1.1.4 Insulin Resistance

Insulin resistance describes a decreased sensitivity and / or responsiveness to metabolic actions of insulin (34;40). Insulin resistance is present and precedes the development of T2D in the majority of patients (62) and is characterised by a variety of defects in insulin signalling, including decreases in receptor concentration and kinase activity, the concentration and phosphorylation of IRS, PI3K and PKB activity, glucose transporter translocation, and the activity of intracellular enzymes (40;63;64). In many cases, insulin resistance can be attributed to an increase in visceral adiposity (62;65-67) (Figure 1.2).

The underlying pathogenic mechanisms by which visceral adiposity contributes to the etiology of insulin resistance and T2D are complex and still partially undetermined but studies have shown that on comparison with peripheral fat, visceral fat is more resistant to the metabolic effects of insulin and more sensitive to lipolytic hormones (68;69). Consequently, visceral adipocytes contribute to elevated free fatty acid (FFA) levels in the circulation. FFAs adversely affect the insulin signalling cascade, inhibiting glucose uptake, glycogen synthesis and glucose oxidation, while stimulating hepatic gluconeogenesis (70) (Figure 1.2). These effects have been attributed to the ability of FFAs to promote accumulation of triglycerides and fatty acid-derived metabolites (diacylglycerol, fatty acyl-CoA and ceramides) in non-adipose cells, such as hepatocytes and myocytes, a phenomenon termed 'lipotoxicity' (67;71). Recent evidence suggests elevated concentrations of FFAs may also induce endoplasmic reticulum stress (increased unfolded protein response due to the disruption of the smooth operation of endoplasmic reticulum) which in turn has been implicated in the development of peripheral insulin resistance (72).

Increased visceral adiposity is often accompanied by a disproportionate increase in pro-inflammatory adipokines (73;74), including tumour necrosis factor- $\alpha$  (TNF- $\alpha$ ) (75;76) (Figure 1.2), monocyte chemoattractant protein (MCP-1) (77), interleukin-6 (IL-6) (78)

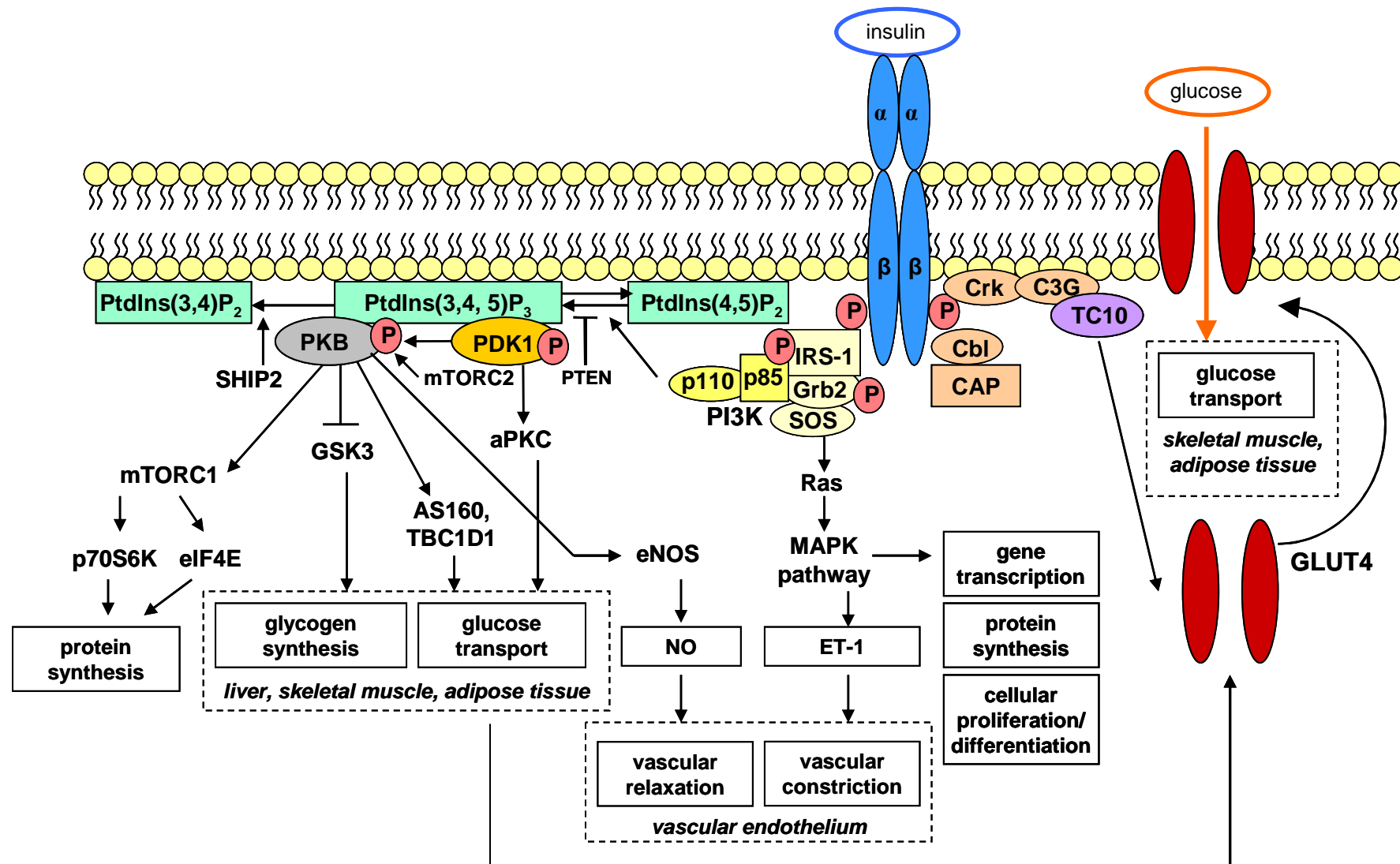


Figure 1.4. Overview of Insulin Signalling – continued overleaf

**Figure 1.4. Overview of Insulin Signalling.** The interaction of insulin with its receptor on the outer surface of the plasma membrane activates the protein-tyrosine kinase activity associated with the  $\beta$  subunit of the receptor. The receptor then phosphorylates itself and insulin receptor substrate-1 (IRS-1) which binds the regulatory p85 subunit of phosphatidylinositol (PtdIns) 3-kinase (PI3K). The catalytic p110 subunit of PI3K then phosphorylates PtdIns-4-5-biphosphate (PtdIns (4,5)  $P_2$ ) at the plasma membrane, thus converting it to PtdIns-3,4,5-triphosphate (PtdIns (3,4,5)  $P_3$ ). The increased amount of PtdIns (3,4,5)  $P_3$  results in recruitment of AKT / protein kinase B (PKB) and phosphoinositide-dependent protein kinase 1 (PDK1) to the membrane. This positions PDK1 and PKB such that PDK1 can phosphorylate (activate) PKB on Thr 308. Activated PtdIns (3,4,5)  $P_3$  also triggers activation of the mammalian target of rapamycin complex-2 (mTORC2) which further phosphorylates PKB at Ser 473 for maximum activation. PDK1 additionally acts to activate the atypical protein kinase C (aPKC) isoforms, PKC- $\zeta$  and  $-\lambda$ , which appear to be required for insulin-stimulated glucose transport in classically insulin-responsive tissues. Activity of the PI3K pathway is partly determined by phosphatidylinositol-3-phosphatases such as phosphatase and tensin homologue (PTEN) and the SH2 domain-containing inositol-5-phosphatase (SHIP2). Protein tyrosine phosphatases, including PTP1B, that dephosphorylate the insulin receptor and IRS-1, also play an important role in negative regulation of insulin-signalling pathways. Effects of PKB activation include phosphorylation of glycogen synthase kinase-3 (GSK3) which reduces GSK3 activity, thus enhancing the conversion of blood glucose to glycogen. Another downstream effect of activated PKB is activation of the mTOR complex 1 (mTORC1) which acts to control cellular translation machinery by phosphorylation of p70 ribosomal S6 kinase (p70S6K) and the inhibitor of the initiation factor 4E for eukaryotic translation (eIF4E), resulting in its activation. Insulin binding also results in activation of the adaptor protein, Grb-2 which recruits the Son-of-sevenless (SOS) exchange protein to the plasma membrane for activation of Ras, thus stimulating gene transcription and cellular proliferation or differentiation through the mitogen-activated protein kinase (MAPK) cascade. In addition, binding of insulin to its receptor causes tyrosine phosphorylation of the Cbl protein which, in most insulin responsive cells, is associated with the adaptor protein, CAP. This results in the Cbl-CAP complex being recruited to a region of the plasma membrane termed a lipid raft. Here, Cbl interacts with the adaptor protein, Crk, which is constitutively associated with the Rho-family guanine nucleotide exchange factor, C3G. C3G in turn activates the G-protein, TC10 which acts to promote glucose transporter 4 (GLUT4) translocation to the membrane. This occurs in parallel with activated PKB which phosphorylates the Rab GTPase-activating protein, Akt substrate of 160kDa (AS160) and its paralogue, TBC1D1, also promoting translocation of GLUT4 and uptake of glucose from blood. In cardiovascular tissue, the MAPK pathway controls secretion of ET-1 in the vascular endothelium while PKB directly phosphorylates endothelial nitric oxide synthase (eNOS), thus stimulating NO production (34;45).

and interleukin-8 (IL-8), all of which have been implicated in the development of insulin resistance (79). Unlike these adipokines, adiponectin, which signals via AMP-activated protein kinase (AMPK) (80), is found at decreased concentrations in visceral obesity, resulting in a reduction in its insulin-sensitising effects in liver and muscle (81;82) (Figure 1.2).

Under conditions of insulin resistance, the  $\beta$ -cells of the pancreas initially compensate, facilitating an increase in insulin secretion to prevent the hyperglycaemia of T2D. However, as insulin resistance worsens,  $\beta$ -cell compensation becomes less effective and hyperglycaemia of progressively greater magnitude occurs as the patient progresses towards frank type 2 diabetes (83).

#### 1.1.1.5 Type 2 Diabetes Mellitus & Cardiovascular Disease

Recent medical literature has highlighted the importance of insulin resistance in increasing CVD risk (62;84-86), a risk which gradually increases as an individual progresses from insulin resistance to T2D (62). Insulin resistance is associated with a dramatic downregulation of the insulin signalling pathway leading from PI3K, PDK1 and PKB to phosphorylation and activation of eNOS. However, the MAPK pathway remains unaffected, perhaps allowing for some of the detrimental effects of chronic hyperinsulinemia on cellular growth in the vasculature (39). In the endothelium, a decrease in PI3K signalling and an increase in MAPK signalling may lead to decreased production of NO and increased secretion of ET-1, characteristic of the endothelial dysfunction of many cardiovascular diseases (39;87).

The elevated circulating FFA levels of visceral obesity and insulin resistance are also known to contribute to diabetic vascular complications by reducing eNOS activity and increasing reactive oxygen species (ROS) production in the vasculature (39;88). FFA-associated ROS production is known to enhance protein kinase C (PKC) activity and increase formation of advanced glycation end-products (AGEs) which interact with AGE-binding receptors to promote atherosclerosis directly through changes in the function of endothelial, macrophage and smooth muscle cells (39;88;89). Furthermore, circulating adipokines recruit and activate inflammatory cells, thus perpetuating a systemic

inflammatory milieu which can strongly affect vascular function and development of atherosclerosis (90).

It has been reported that visceral adiposity and insulin resistance impair thrombolysis via a mechanism involving increased levels of plasminogen activator inhibitor-1 (PAI-1) (65;91-94). Levels of this atherogenic factor have been observed to be particularly high in patients with T2D (91;92), serving as a predictor for CVD (95;96).

In addition, hyperglycaemia itself is implicated in the pathogenesis of diabetic macrovascular disease (97;98), facilitating PKC activation and AGE formation (88;89;99) in a similar manner to FFAs. AGEs induce ROS production and promote vascular inflammation through activation of nuclear factor  $\kappa$ B (NF- $\kappa$ B) which enhances expression of VCAM-1 and MCP-1 (87;88). Acute hyperglycaemia can also reduce eNOS activation and NO production, thus contributing to endothelial dysfunction and the vascular complications of type 2 diabetes (100).

#### 1.1.1.6 Genetics & Environment

There is a wealth of evidence to support a profound influence of genetic factors on the development of T2D, including twin studies which reveal an approximate 70% concordance in monozygotic twins, as compared to 20-30% in dizygotic twins (101;102). Furthermore, the life-time risk of developing the disease is around 40% in offspring of one parent with T2D but is seen to approach 70% if both parents have the disease (103). Large ethnic differences in the prevalence of T2D have also been explained by way of a genetic component (104;105). Additionally, there are a number of relatively uncommon monogenic forms of T2D, known as maturity onset diabetes of the young (MODY), which have roughly the same phenotypic expression as the adult onset form and follow a clear Mendelian mode of inheritance (106) (Table 1.1). While the incidence of MODY is not precisely known, it is believed to account for < 5% of all T2D cases, the remainder being attributed to polygenic defects (9).

Type	Gene	Chromosome	Defect
MODY 1	hepatic nuclear factor-4 $\alpha$ ( <i>HNF4A</i> )	20q	progressive $\beta$ -cell failure
MODY 2	glucokinase ( <i>GCK</i> )	7p	impaired glucose-regulated insulin secretion
MODY 3	hepatic nuclear factor-1 $\alpha$ ( <i>HNF1A</i> )	12q	progressive $\beta$ -cell failure
MODY 4	insulin promoter factor 1 ( <i>IPF1</i> )	13q	impaired pancreatic development, impaired glucose-mediated stimulation of insulin gene transcription
MODY 5	hepatic nuclear factor-1 $\beta$ ( <i>HNF1B</i> ) / hepatic transcription factor 2 ( <i>TCF2</i> )	17 cen-q	progressive $\beta$ -cell failure, renal disease
MODY 6	NEUROD1	2q	abnormal $\beta$ -cell development and function

**Table 1.1. Common Variants in MODY Genes.** There are a minimum six forms of MODY, each caused by mutations in a distinct gene. Common to all forms is that they result in impaired insulin secretion. MODY patients are identified clinically as having a form of non-insulin dependent diabetes mellitus, characterised by a mild to moderate insulin secretory deficiency, an autosomal dominant mode of inheritance and onset at less than 25 years of age in some family members (106;107).

Attempts to define the more common, polygenic form of T2D, including linkage analysis, candidate gene studies and, more recently, genome wide association studies (GWAS), have identified a number of genes as being associated with the disease (16;108) (Table 1.2). Of particular interest are the results from several recent GWAS on both T2D and its risk factor, obesity, which have revealed at least eighteen genes consistently associated with T2D (109-118). Many of these genes implicate pancreatic  $\beta$ -cell function in disease pathogenesis whereas only one appears clearly associated with insulin resistance (16) (Table 1.2). It is likely these discoveries represent but a small proportion of the genetic variation underlying the susceptibility to the disorder and further investigation will be required to provide a more complete picture of the genetic complexity of T2D.

While type 2 diabetes has a strong genetic component, its development is triggered by environmental factors in genetically susceptible individuals. The epidemic increase in T2D prevalence across the globe in the past 50 years can be ascribed to a change in environment as the world advances towards a more affluent, westernised lifestyle and the calorie rich diet and physical inactivity with which it is associated (9). One explanation for the interaction between genes and environment in polygenic T2D etiology is outlined in the *thrifty genotype hypothesis* (119) and concerns evolution of a genotype which conferred survival benefits in the past but is detrimental in the current environment. An opposing theory, the so called *thrifty phenotype hypothesis* (120), proposes that the condition represents an adult metabolic response to foetal malnutrition.

#### 1.1.1.7 Treatment of Type 2 Diabetes Mellitus

Lifestyle modifications targeting weight reduction, and in particular reduction in visceral adiposity, have been shown to be beneficial as a first-line approach in treating glycaemic abnormalities and reducing the risk for diabetes and CVD (121-123). However, pharmacological therapies are used adjunctively in patients at higher risk and in those noncompliant with lifestyle modification (62).

Given the key role of insulin resistance in the development of T2D, development of pharmaceuticals has been primarily focused on insulin sensitising agents. At present, two classes of insulin sensitising agents are in use: biguanides, including metformin, and the

Year of Major Publication	Reference	Suggested Gene	Disease Mechanism
2000	(113;114;117;124)	<i>PPARG</i> *	insulin sensitivity
2000	(125)	<i>CAPN10</i> **	glucose transport
2003	(113;114;117;126)	<i>KCNJ11</i> *	β-cell dysfunction
2006	(113;114;117;127;128)	<i>TCF7L2</i>	β-cell dysfunction
2007	(113;114;117;129;130)	<i>CDKAL1</i>	β-cell dysfunction
2007	(113;114;117;131)	<i>CDKN2A/2B</i>	β-cell dysfunction
2007	(113;114;117;128-132)	<i>HHEX/IDE</i>	β-cell dysfunction
2007	(113;114;117;128;130)	<i>SLC30A8</i>	β-cell dysfunction
2007	(113;114;117;131)	<i>IGF2BP2</i>	β-cell dysfunction
2007	(113;114;117)	<i>WFS1</i> *	unknown
2007	(133)	<i>TCF2</i> *	unknown
2007	(109;110)	<i>FTO</i>	obesity
2008	(112)	<i>MC4R</i>	obesity
2008	(111;118)	<i>NOTCH2</i>	unknown
2008	(111;118)	<i>ADAMTS9</i>	unknown
2008	(111;118)	<i>THADA</i>	unknown
2008	(111;118)	<i>TSPAN8/LGR5</i>	unknown
2008	(111;118)	<i>CDC123/CAMK1D</i>	unknown
2008	(111;118)	<i>JAZF1</i>	unknown
2008	(115;116)	<i>KCNQ1</i>	β-cell dysfunction

**Table 1.2. Type 2 Diabetes Susceptibility Genes.** *PPARG*, peroxisome proliferator-activated receptor gamma; *CAPN10*, calpain 10; *KCNJ11*, potassium inwardly rectifying channel, subfamily J, member 11; *TCF7L2*, transcription factor 7-like 2; *CDKAL1*, CDK5 regulatory subunit associated protein 1-like 1; *CDKN2A/B*, cyclin-dependent kinase inhibitor 2A/B; *HHEX*, haematopoietically expressed homeobox; *IDE*, insulin-degrading enzyme; *SLC30A8*, solute carrier family 30 member 8; *IGF2BP2*, insulin-like growth factor 2mRNA binding protein 2; *FTO*, fat mass and obesity associated; *MC4R*, melanocortin 4 receptor; *NOTCH2*, Notch homolog 2 Drosophila; *ADAMTS9*, ADAM metalloproteinase with thrombospondin type 1 motif, 9; *THADA*, thyroid adenoma associated; *TSPAN8*, tetraspanin 8; *LGR5*, leucine-rich repeat-containing G protein-coupled receptor 5; *CDC123*, cell division cycle 123 homolog; *CAMK1D*, calcium/calmodulin-dependent protein kinase ID; *JAZF1*, juxtaposed with another zinc finger gene 1; *KCNQ1*, potassium voltage-gated channel, KQT-like subfamily, member 1. \*, indicates a biological candidate gene confirmed by GWAS. \*\*, indicates gene implicated in type 2 diabetes by considerable functional and genetic evidence but not by GWAS. All other genes have been identified by GWAS. Adapted from (16).



thiazolidinediones (134). Metformin is relatively more active in the suppression of hepatic glucose production, exerting a portion of its effect through AMPK (135-137). Metformin has been shown to have a beneficial effect on cardiovascular outcomes (138-140). Thiazolidinediones act on the peroxisome proliferator-activated receptor- $\gamma$  (PPAR- $\gamma$ ) and are more active in stimulation of muscle glucose uptake (141;142). They are also known to activate AMPK (143) and enhance vascular function, ameliorating the dyslipidemia and inflammatory milieu of T2D (144). In addition, certain antihypertensive therapies, known to act on the renin-angiotensin system (RAS), such as angiotensin converting enzyme (ACE) inhibitors and angiotensin-II receptor blockers (ARBs), have been shown to have beneficial effects in T2D. Treatment of type 2 diabetics with lipid-lowering statins has also been shown to be of therapeutic benefit (39;40).

## **1.2 The Vascular Endothelium**

More than a trillion endothelial cells line the luminal surface of the human vasculature, representing a critical interface between circulating blood and tissue (145-148). An important endocrine organ, the endothelium plays a pivotal role in maintaining cardiovascular homeostasis under physiological conditions by releasing a number of vasoactive substances which act to regulate vascular tone, antiproliferation and antiaggregation, in addition to limiting increases in blood pressure, controlling tissue blood flow and inflammatory responses and maintaining blood fluidity (146-148). The endothelium releases these vasoactive substances in response to mechanical stimuli, such as pressure and shear stress, and various hormonal stimuli, such as insulin (39;87;146). Endothelium-derived substances with vasodilatory and antiproliferative effects include, endothelium-derived hyper-polarisation factor (EDHF) (149;150), NO (151;152) and prostacyclin (PGI<sub>2</sub>) (153), while ET-1 (154), angiotensin II (Ang II) and ROS are among those mediators which exert vasoconstrictor effects (87). All forms of cardiovascular disease have been shown to be associated with some degree of endothelial dysfunction (87;146).

### **1.2.1 Endothelial Dysfunction**

Endothelial dysfunction describes the situation when a shift in the equilibrium between vasodilators and vasoconstrictors occurs, allowing vasoconstrictor and proliferative effects to predominate, leading to the development of hypertension, atherosclerosis, platelet aggregation and ischemia (87;145-148;155). With respect to functional investigation, the term endothelial dysfunction generally relates to an impaired maximal dilative response and/or an impaired sensitivity to endothelium dependent vasodilators such as acetylcholine, bradykinin and calcium ionophore, under conditions of preserved response to endothelium-independent dilators including sodium nitroprusside (87;146).

Endothelial dysfunction is an early and independent predictor of poor prognosis in most forms of CVD (87;156-158), with alterations in endothelial function consistently found in hypertension, atherosclerosis, CAD, T2D and obesity (39;87;157-162). An increasing body of evidence suggests oxidative stress underlies the endothelial dysfunction of CVD.

## **1.3 Oxidative Stress in Cardiovascular Disease**

### **1.3.1 Reactive Oxygen Species**

All layers of the vascular wall have enzymatic systems capable of producing ROS and, under physiological conditions, these ROS act as important signalling molecules (146), stimulating vascular smooth muscle cell (VSMC) and endothelial cell mitogenic and apoptotic signalling (163-166). ROS is a collective term encompassing both oxygen radicals and certain nonradicals which act as oxidising agents and/or are easily converted into radicals. ROS include the superoxide anion ( $O_2^-$ ), the hydroxyl radical ( $OH^\cdot$ ), NO, lipid radicals ( $LOO^\cdot$ ), hydrogen peroxide ( $H_2O_2$ ), hypochlorous acid (HOCl) and peroxynitrite ( $ONOO^-$ ) (167). Principal among these ROS is the superoxide anion, formed from the univalent reduction of oxygen, its unpaired electron renders it highly reactive and unstable with a short half-life. Superoxide acts as both an oxidising agent, being reduced to

H<sub>2</sub>O<sub>2</sub> (168), and a reducing agent, donating its extra electron to form ONOO<sup>-</sup> with NO (169) (Figure 1.5).

### 1.3.2. Nitric Oxide

Nitric oxide, first identified as endothelium-derived relaxing factor (EDRF) (151;152), is a potent signalling molecule and vasodilator, responsible for mediating many functions of the endothelium, including control of vascular tone, inhibition of platelet aggregation and leukocyte adhesion, and suppression of VSMC proliferation (145;147;148). Each of these events has been implicated in the initiation and progression of atherosclerosis and NO is therefore considered an anti-atherosclerotic agent (147;155;170).

A freely diffusible molecule with a short half-life of 6-10 seconds *in vivo*, vascular NO is formed from L-arginine by the constitutively expressed endothelial isoform of NOS which requires Ca<sup>2+</sup>/calmodulin, flavin adenine dinucleotide (FAD), flavin mononucleotide (FMN), nicotinamide adenine dinucleotide phosphate (NADPH) and tetrahydrobiopterin (BH<sub>4</sub>) as cofactors (147;148;161;171-173). Endothelial NOS is activated in response to elevated cytosolic Ca<sup>2+</sup> which occurs on exposure to various stimuli, including shear stress. In addition, eNOS is known to be activated by hormones (including insulin) and platelet-derived substances and agonists, such as bradykinin and acetylcholine (161;174). It has recently been demonstrated that eNOS is regulated by reversible phosphorylation and both PKB and AMPK have been shown to phosphorylate and activate the enzyme at serine 1177 (Ser1177) in cultured endothelial cells (175;176).

On its release from endothelial cells, NO diffuses to the lumen of the vessel where it exerts its effects on platelet and blood element functions, and to adjacent VSMCs where it induces vasodilation and inhibits vascular remodelling and smooth muscle cell proliferation via activation of soluble guanylyl cyclase, present in the cytosol. Activation of guanylyl cyclase causes an increase in intracellular cGMP, which in turn activates protein kinase G (PKG), leading to reduced intracellular calcium and vasodilation (177) (Figure 1.6). While this represents the predominant sensing pathway for NO in the vasculature, it has been reported that under certain conditions, NO may cause vasodilation by activation of K<sup>+</sup> channels (178).

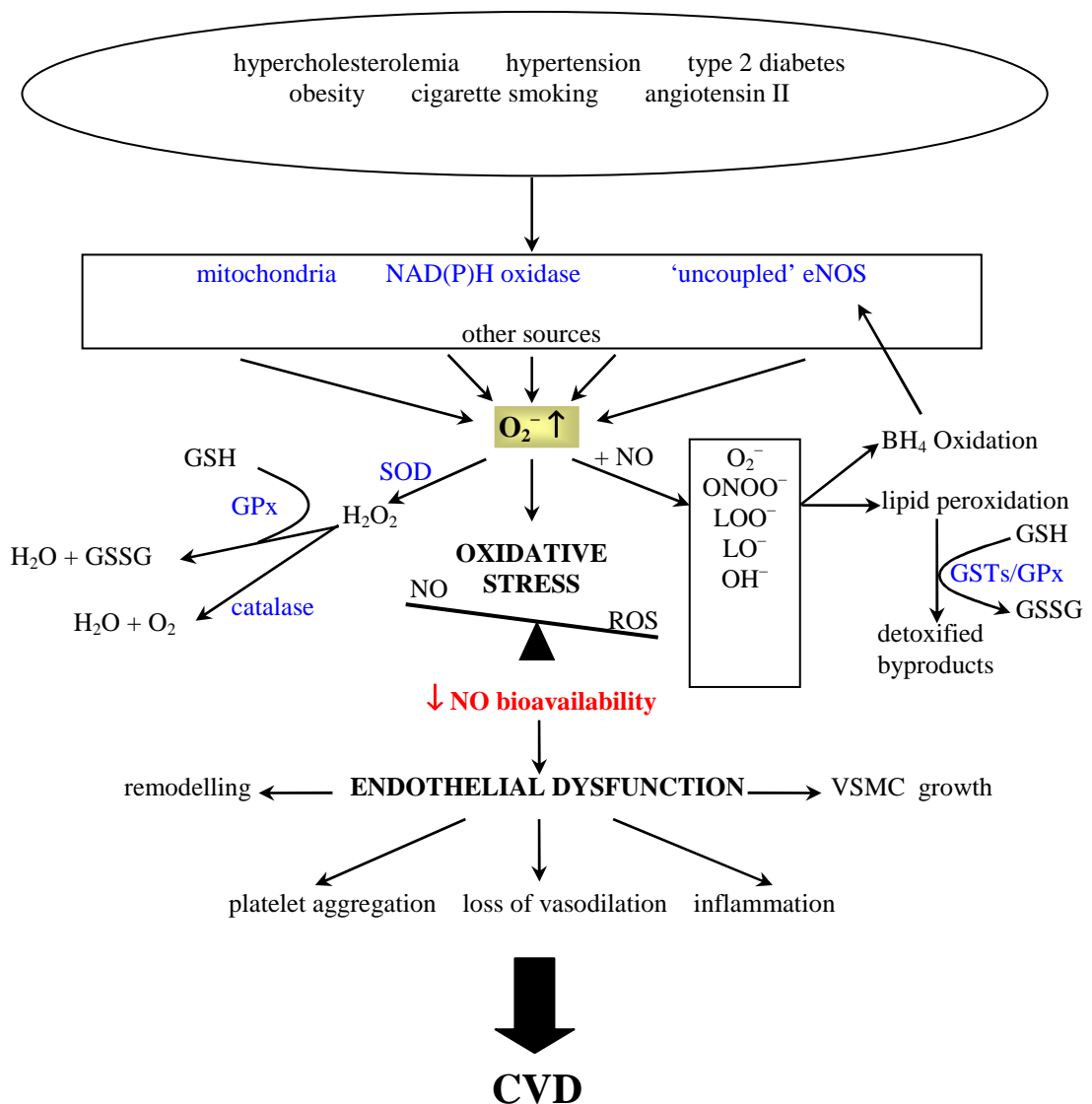


**Figure 1.5. Oxidative Stress in Cardiovascular Disease.** Environmental and physiological factors lead to the generation of superoxide ( $O_2^-$ ) in the vasculature.  $O_2^-$  is enzymatically converted to hydrogen peroxide ( $H_2O_2$ ) by superoxide dismutases (SODs) and further processed by catalase and glutathione peroxidase (GPx). However, excess  $O_2^-$  can generate a number of other reactive oxygen species (ROS), disrupting the balance of nitric oxide (NO) and ROS. Increased oxidative stress leads to reduced NO bioavailability, associated with endothelial dysfunction and cardiovascular disease (CVD). Adapted from (167).

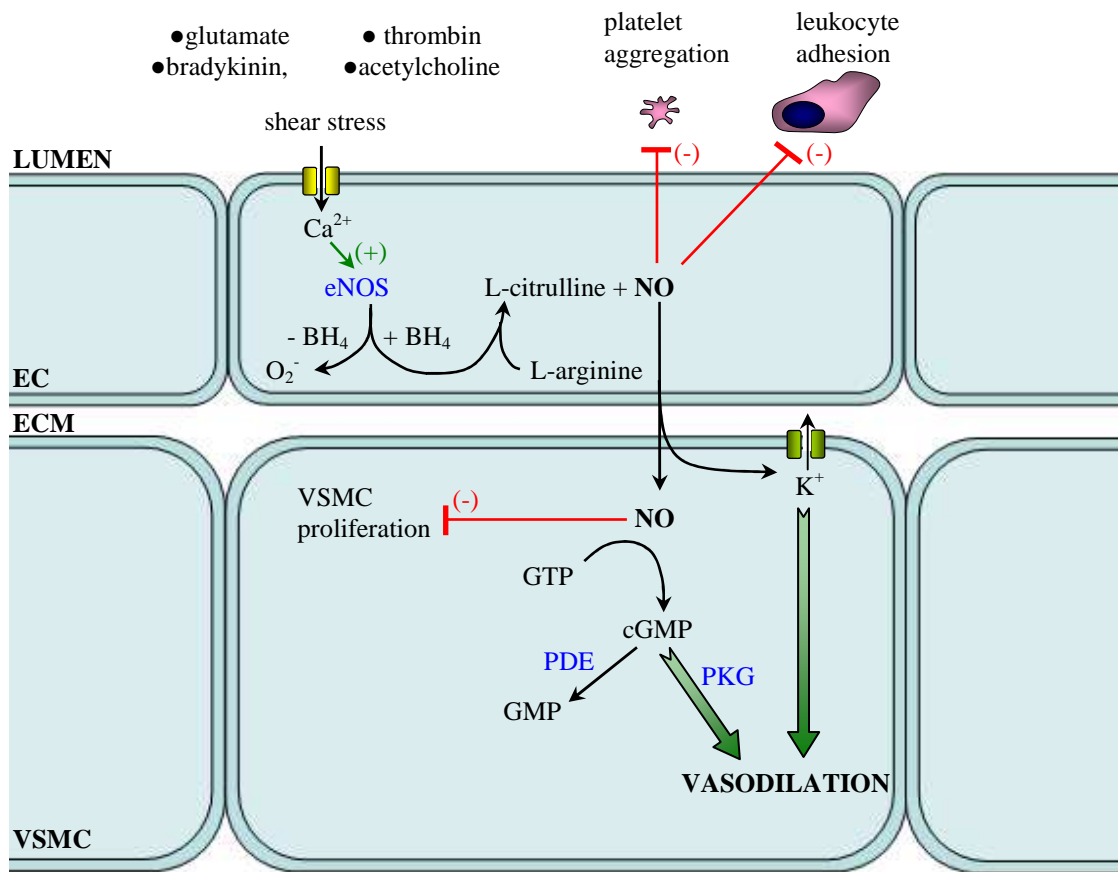


**Figure 1.6. Nitric Oxide Signalling in the Vessel Wall.** Nitric oxide (NO), produced in the endothelial cell (EC), acts to regulate vascular tone and inhibit platelet aggregation and leukocyte adhesion (177;178). BH<sub>4</sub>, tetrahydrobiopterin; Ca<sup>2+</sup>, calcium; cGMP, cyclic guanosine monophosphate; ECM, extracellular matrix; eNOS, endothelial nitric oxide synthase; GMP, guanosine monophosphate; GTP, guanosine triphosphate; K<sup>+</sup>, potassium; O<sub>2</sub><sup>-</sup>, superoxide anion; PDE, phosphodiesterases; PKG, protein kinase G; VSMC, vascular smooth muscle cell.

Given its cardioprotective function and fundamental role in maintaining vascular homeostasis, loss of endothelial NO bioavailability is a maladaptive event and, unsurprisingly, represents a common manifestation of endothelial dysfunction (87;148;161). Indeed, decreased NO bioavailability has been observed in T2D (179), hypertension (180), hypercholesterolaemia (181) and cigarette smoking (182). Reduction of NO bioavailability in the endothelium may be the result of impaired NO production due to reduced expression of eNOS (183), lack of substrate or cofactor (171-173), or alterations in cellular signalling leading to reduced eNOS activation (184). However, the reduced endothelial NO bioavailability associated with CVD has been reported to occur as a consequence of elevated ROS production under conditions of oxidative stress (161;167).

### **1.3.3 Oxidative Stress**

Oxidative stress describes the condition wherein an excessive production of ROS overwhelms endogenous anti-oxidant defence mechanisms (Figure 1.5). The resultant elevation in ROS levels has a detrimental effect on cellular function, a consequence of ROS-induced damage to lipid membranes, enzymes and nucleic acids (167). CAD and its risk factors, including T2D, are characterised by excess vascular production of ROS (167;185). One of the earliest measurable consequences of oxidative stress in human subjects is impaired endothelium-dependent vasodilation which occurs as a result of accelerated NO degradation by ROS (167).

The most likely candidate for accelerating NO degradation is  $O_2^-$ . When present in excess, the superoxide anion rapidly inactivates NO (186), yielding the highly reactive radical,  $ONOO^-$  as a by-product. Peroxynitrite is more stable than either NO or  $O_2^-$  and is a potent oxidant, capable of inducing oxidation of deoxyribonucleic acid (DNA), proteins and lipids (187;188) (Figure 1.5).

### 1.3.4 Reactive Oxygen Species: Sources in The Vasculature

Principal sources of ROS in the vasculature include NAD(P)H oxidase (189-191), xanthine oxidase (167;192) and the mitochondrial electron transport chain (193-196). In addition, 'uncoupled' eNOS produces  $O_2^-$  rather than NO under conditions of substrate (L-arginine) or co-factor ( $BH_4$ ) deficiency (170;173) (Figure 1.5). Other potential sources of ROS include arachidonic acid pathway enzymes, such as lipoxygenase and cyclooxygenase, cytochrome p450s, peroxidases and other haemoproteins (167).

#### 1.3.4.1 Endothelial Nitric Oxide Synthase

Under conditions of oxidative stress, eNOS may generate  $O_2^-$  rather than NO, a phenomenon termed eNOS uncoupling (Figures 1.5 and 1.6). Nitric oxide generation is dependent on eNOS homodimerisation in the presence of  $BH_4$ . However,  $BH_4$  is highly susceptible to oxidative degradation by  $ONOO^-$  and in the absence of its cofactor, eNOS fails to dimerise fully, resulting in uncoupling of the enzyme and amplification of oxidative stress (197) (Figure 1.5 and 1.6). Uncoupled eNOS has been shown to contribute to increased superoxide production and endothelial dysfunction in a number of CVDs, including CAD (161) and T2D (179).

#### 1.3.4.2 NAD(P)H Oxidase

NAD(P)H oxidase is the predominant source of  $O_2^-$  in the human vasculature, catalysing the one electron reduction of oxygen using NADH or NAD(P)H as the electron donor (189;191). The enzyme was originally characterised in neutrophils but is present in VSMCs (198;199) and endothelial cells (200-202). A multisubunit enzyme, vascular NADPH oxidase consists of membrane integrated cytochrome  $b_{558}$  and a number of cytosolic regulatory components;  $p47^{phox}$ ,  $p67^{phox}$ ,  $p40^{phox}$  (where *phox* represents *phagocyte oxidase*) and the GTP-binding protein, Rac1. The cytochrome  $b_{558}$  is itself comprised of two subunits,  $p22^{phox}$  and nicotinamide adenine dinucleotide phosphate

oxidase (NOX) protein, NOX2 (gp91<sup>phox</sup>) or a functional isoform of this differentially expressed catalytic subunit (189;190) (Figure 1.7). Vascular NADPH oxidase is a constitutive enzyme but can also be regulated in VSMCs by humoral factors such as Ang II and a number of growth factors, including TNF $\alpha$  and platelet-derived growth factor (PDGF) (190;203-205). In the endothelium, activity of the enzyme is upregulated by shear stress caused by increased blood flow (201).

Vascular NAD(P)H oxidase-stimulated O<sub>2</sub><sup>-</sup> production has been shown to be positively correlated with endothelial dysfunction and clinical risk factors for CVD in humans (206) and inhibition of the enzyme is seen to improve endothelial function in both rat and human blood vessels (207).

Antisense inhibition of the constitutively expressed p22<sup>phox</sup> subunit of NAD(P)H oxidase identified it as being critical for enzymatic function (199) and significantly increased p22<sup>phox</sup> protein levels and upregulation of p22<sup>phox</sup> messenger ribonucleic acid (mRNA) have been shown to be associated with enhanced NAD(P)H oxidase activity in vessels from patients with CAD (208). Consequently, common genetic polymorphisms within both promoter and coding regions of the p22<sup>phox</sup> gene (*CYBA*) have been the object of considerable research, the hypothesis being that they confer important functional effects, contributing to interindividual variation in enzyme activity. Studies have shown that a number of these allelic variants are associated with cardiovascular disease (209-211).

NAD(P)H oxidase NOX subunit expression varies among vascular cells. Endothelial cells predominantly express the NOX4 isoform with expression of NOX2 occurring to a lesser extent (212). Subunit expression has been shown to be associated with CAD, correlating with severity of atherosclerosis (212) and with features of plaque stability in human coronary arteries (213). Recent studies have demonstrated that NOX2 and NOX4-based NAD(P)H oxidases are the predominant contributors to oxidative stress in coronary arteries from patients with advanced CAD (208), while NOX5 has been identified as a novel, calcium-dependent source of ROS in these vessels (214).



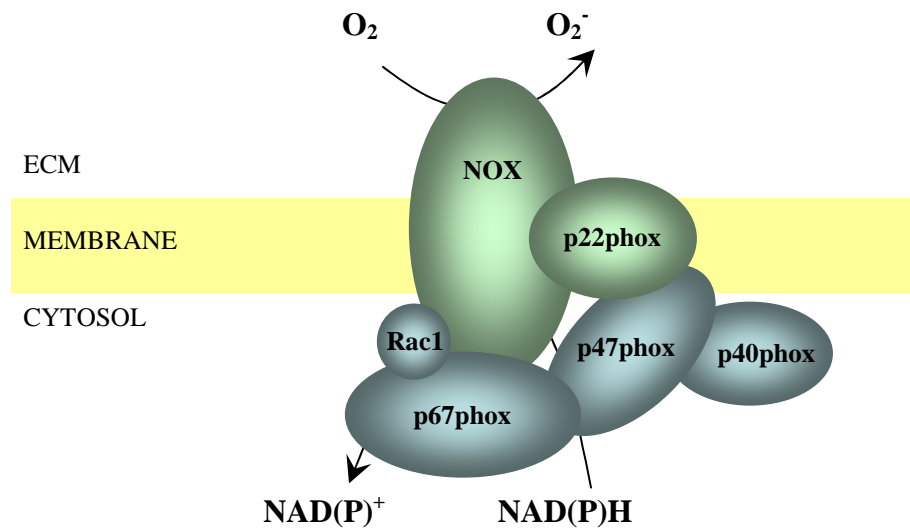


**Figure 1.7. Structure of the Active NAD(P)H Oxidase Complex.** Vascular NAD(P)H oxidase is a heterodimer, consisting of membrane-bound p22<sup>phox</sup> and NOX subunits and cytoplasmic subunits, p67<sup>phox</sup>, p47<sup>phox</sup> and p40<sup>phox</sup>. Rac1 is required for assembly of the subunits. The NAD(P)H-binding domain is predicted to be on one side of the membrane, while superoxide (O<sub>2</sub><sup>-</sup>) generation is predicted to occur on the other. The oxidase may be located either on the plasma membrane or on intracellular membranes (190;191). ECM, extracellular matrix. Adapted from (190).

#### 1.3.4.2.1 NAD(P)H Oxidase In Type 2 Diabetes Mellitus

It has been shown that elevated  $O_2^-$  production in human blood vessels from patients with T2D is mediated by upregulated NAD(P)H oxidase activity (179). Increased activity of the enzyme has also been implicated in the impaired endothelium-dependent vasodilation observed in the OLETF rat, a model of T2D (215). In addition, a number of *in vitro* studies have demonstrated that the hyperglycaemia and AGE formation characteristic of T2D increases NAD(P)H oxidase-induced  $O_2^-$  production in endothelial cells (216-218). Furthermore, increased protein levels of p22<sup>phox</sup>, p47<sup>phox</sup> and p67<sup>phox</sup> have been observed in human vessels from patients with T2D (179) while p22<sup>phox</sup> mRNA was shown to be upregulated in vessels from streptozotocin-induced diabetic and OLETF rats (215;219). The specific mechanisms underlying enhanced NAD(P)H oxidase activity in T2D are yet to be fully elucidated but recent studies have indicated a crucial role for protein kinase C. A recognised stimulant of NAD(P)H oxidase activation, activity of PKC is increased as a result of hyperglycaemia (220;221).

#### 1.3.4.3 Mitochondria

The oxidative phosphorylation (OXPHOS) pathway is essential for energy production in mitochondria of eukaryotic cells. Enzymes of the inner mitochondrial membrane transfer electrons along the electron transport chain (ETC) which generates a proton gradient, enabling ATP synthase to generate ATP. Under physiological conditions, this process produces ROS as byproducts, a result of the one electron reduction of molecular oxygen ( $O_2$ ) to superoxide (196;222;223) (Figure 1.8). As such, a network of mitochondrial antioxidant systems is in place to protect against ROS-induced damage to mitochondrial proteins, lipids and nucleic acids (Figure 1.8). However, under conditions of oxidative stress, these antioxidant systems are overwhelmed, allowing ROS to exert their damaging effects and ultimately alter mitochondrial function (196;222). Increased production of mitochondrial ROS (mtROS), leading to accumulation of mitochondrial DNA (mtDNA) damage and progressive mitochondrial dysfunction, has been shown to be associated with vascular diseases, including CAD and T2D (88;222;224;225).

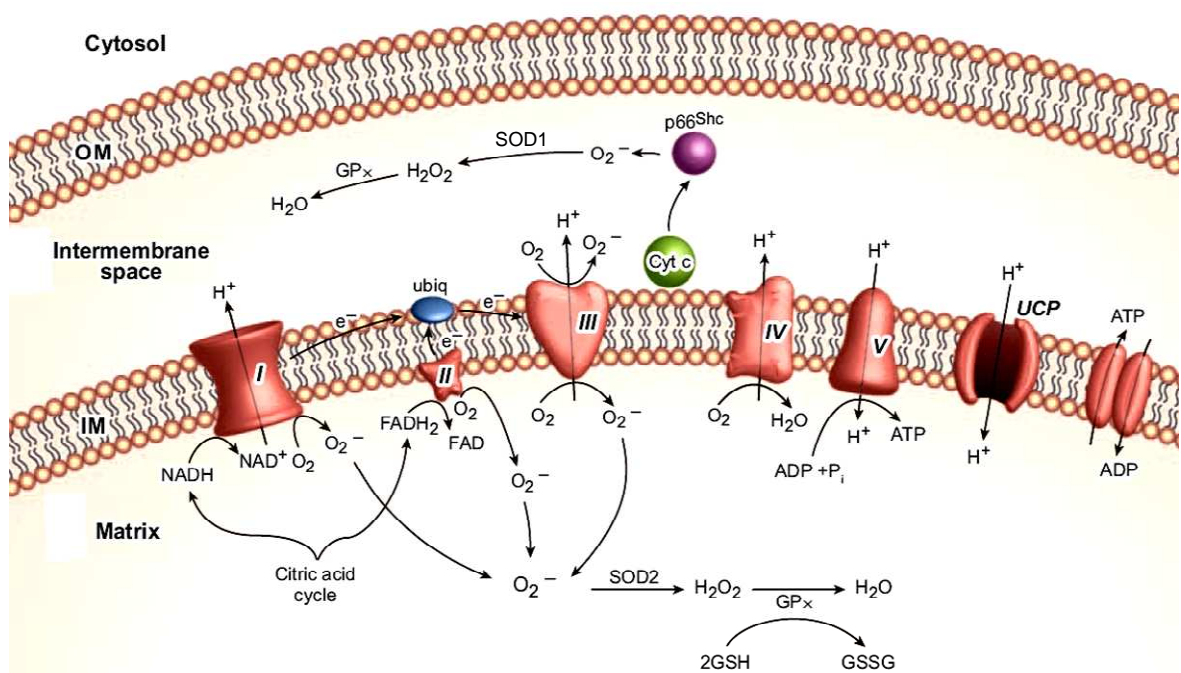


**Figure 1.8. Mitochondrial Oxidative Phosphorylation and Superoxide Production.** Oxidative phosphorylation (OXPHOS) is composed of 5 multiple subunit complexes embedded in the inner mitochondrial membrane. Electrons ( $e^-$ ) from reduced nicotinamide adenine dinucleotide (NADH) and flavin adenine dinucleotide ( $FADH_2$ ) pass through complex I (NADH dehydrogenase) and complex II (succinate ubiquinone oxidoreductase) respectively and are then shuttled to complex III (ubiquinol cytochrome oxidoreductase) via ubiquinol (ubiq). Cytochrome *c* (cyt *c*) transfers electrons from complex III to complex IV, with the reduction of molecular oxygen ( $O_2$ ) to water ( $H_2O$ ), a reaction inhibited by nitric oxide. Flow of electrons is accompanied by proton ( $H^+$ ) transfer across the inner mitochondrial membrane at complexes I, III and IV, creating an electrochemical gradient ( $\Delta\psi$ ). Protons re-enter the mitochondrial matrix through complex V (ATP synthase) which utilises the proton-motive force to generate ATP. This force also drives ATP-ADP exchange by the adenine nucleotide translocase (ANT). Uncoupling proteins (UCPs) allow protons to return to the matrix, reducing ROS formation. Of the electrons entering the transport chain, it is estimated 2-4% are involved in superoxide ( $O_2^-$ ) formation. Complex I leaks electrons to generate  $O_2^-$  in the matrix, whereas complex III generates  $O_2^-$  in both the matrix and intermembrane space. The  $P66^{Shc}$  intermembrane protein has been identified as being involved in mitochondrial ROS production, subtracting electrons from cytochrome *c* to produce  $O_2^-$ . Superoxide is dismutated to hydrogen peroxide ( $H_2O_2$ ) by superoxide dismutase 2 (SOD2) in the matrix and by SOD1 or SOD3 in the intermembrane space.  $H_2O_2$  is then reduced by enzymes such as glutathione peroxidase (GPx) which uses reduced glutathione (GSH) as an electron donor, resulting in oxidised glutathione (GSSG) formation (88;196;222;223). Pi, inorganic phosphate. Adapted from (88).

One important regulator of mtROS production is NO which, at physiological concentrations, modulates O<sub>2</sub> consumption by inhibiting cytochrome *c* oxidase in a reversible manner (88;226). In this way, NO is able to regulate the mitochondrial redox state, facilitating release of the O<sub>2</sub><sup>-</sup> anion and other free radicals which act as NO-regulated signalling molecules (88;227). Nitric oxide-mediated inhibition of cytochrome *c* oxidase is also thought to underlie the increased mtROS production observed in hypoxic conditions (228). However, during periods of oxidative stress, mitochondrial NO reacts with O<sub>2</sub><sup>-</sup> to form ONOO<sup>-</sup> which, in turn, enhances O<sub>2</sub><sup>-</sup> production by the ETC and disrupts mitochondrial integrity, thus contributing to the pathogenesis of vascular disease (88;222;223).

Recent studies have also revealed a potential link between NAD(P)H oxidase-derived ROS and mitochondrial dysfunction in endothelial cells. Superoxide produced by NAD(P)H oxidase is believed to directly activate mitochondrial ATP-sensitive K<sup>+</sup> channels or react with NO to form ONOO<sup>-</sup>, leading to respiratory complex damage and impaired mitochondrial function (229).

#### *1.3.4.3.1 Mitochondria in Type 2 Diabetes Mellitus*

Mitochondrial ROS have a fundamental role in the development and progression of endothelial dysfunction and macrovascular disease in T2D, with hyperglycaemia shown to increase generation of O<sub>2</sub><sup>-</sup> from the mitochondrial ETC in endothelial cells (230). Intracellular hyperglycaemia causes an increase in the mitochondrial proton gradient, a consequence of electron donor (NADH and reduced flavin adenine dinucleotide, FADH<sub>2</sub>) overproduction by the citric acid cycle (also known as the tricarboxylic acid (TCA) cycle or citrate cycle). This, in turn, leads to increased mitochondrial production of ROS. Increased levels of mtROS are implicated in processes known to contribute to the pathogenesis of diabetic macrovascular disease, including PKC activation and AGE formation (88;222;230;231) (Figure 1.9). In addition, the elevated FFA flux and oxidation characteristic of visceral obesity and insulin resistance is known to induce mitochondrial ETC ROS production in endothelial cells (232) (Figure 1.9).

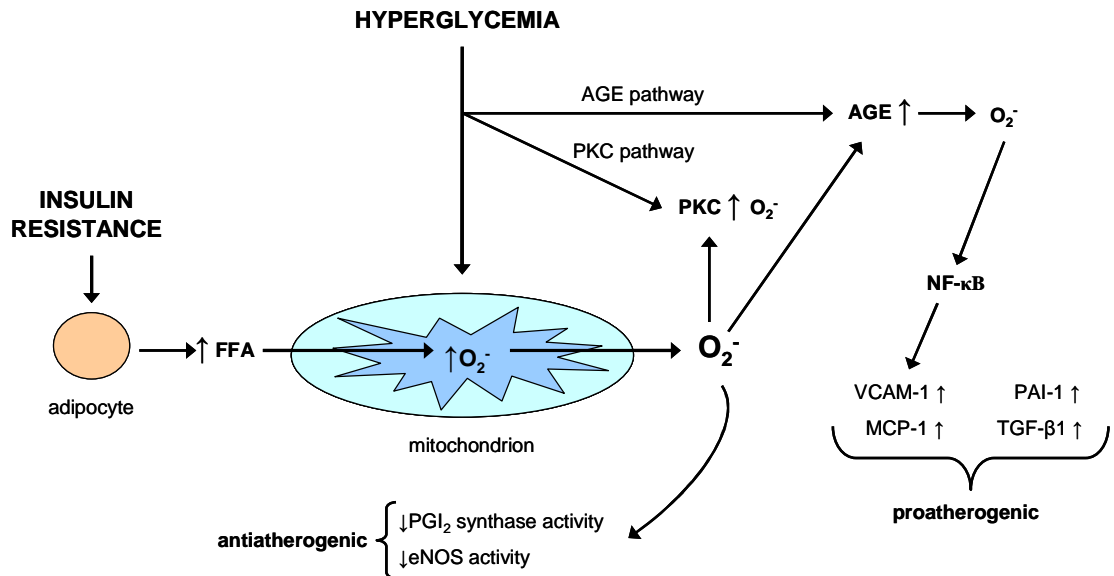


**Figure 1.9. Insulin Resistance and Hyperglycaemia-induced Mitochondrial Superoxide Production in Activation of Atherogenic Signalling Pathways.** Elevated mitochondrial superoxide ( $O_2^-$ ) production caused by high glucose flux through endothelial cells, leads to increased protein kinase C (PKC) activation and advanced glycation end-product (AGE) formation. This results in downstream activation of nuclear factor  $\kappa$ B (NF- $\kappa$ B) which induces transactivation of vascular cell adhesion molecule-1 (VCAM-1) and monocyte chemoattractant protein-1 (MCP-1). Transactivation of additional proatherogenic genes, such as plasminogen activator inhibitor-1 (PAI-1) and transforming growth factor  $\beta_1$  (TGF- $\beta_1$ ), occurs via a similar pathway. Increased flux of free fatty acids (FFAs), released from insulin-resistant adipocytes through vascular endothelial cells, also activates atherogenic signalling pathways, including PKC and AGE pathways. Furthermore, FFA-induced excess mitochondrial  $O_2^-$  production inactivates antiatherogenic enzymes such as prostacyclin (PGI<sub>2</sub>) synthase and endothelial nitric oxide synthase (eNOS) (88;222;230;231). Adapted from (88).

## **1.4 Mechanisms in Defence Against Oxidative Stress**

A number of endogenous anti-oxidant defence mechanisms, both enzymatic and non-enzymatic, operate to limit ROS levels in the vasculature. Non-enzymatic anti-oxidant molecules include ascorbic acid (vitamin C),  $\alpha$ -tocopherol (vitamin E) and glutathione, while superoxide dismutases (SODs), catalase and glutathione peroxidases (GPxs) represent important anti-oxidant enzymes which act to directly scavenge ROS, converting them to less reactive species (188;233) .

### **1.4.1 Superoxide Dismutases**

The SODs represent the first and most important line of enzymatic anti-oxidant defence against ROS. A ubiquitous family of enzymes, SODs catalyse the conversion of  $O_2^-$  to  $H_2O_2$  and  $O_2$  (188;233;234) (Figures 1.5 and 1.8). Three distinct isoforms of SOD have been identified in vascular tissue. The first isoform, cytosolic copper/zinc (Cu/Zn) SOD, is an unusually stable homodimer encoded by the *SOD1* gene. SOD1 is believed to be the predominant SOD isoform in the endothelium and is thought to lower  $O_2^-$  concentrations from the nanomolar to picomolar range (188;233;234). A second isoform, encoded by *SOD2*, is localised in mitochondria (Figure 1.8). This mitochondrial SOD functions as a homotetramer and utilises manganese (Mn) as a cofactor (234). *SOD3* encodes the extracellular SOD (ecSOD), a copper/zinc-containing tetramer which has a C terminal heparin-binding region and is principally located in arterial smooth muscle cells in the vascular wall (234).

The importance of SODs as an anti-oxidant defence mechanism has been highlighted by gene transfer studies wherein SOD overexpression improved endothelial function (235;236) and provided protection against myocardial infarction (237). Overexpression of SOD2 has also been shown to prevent hyperglycaemia-associated production of  $O_2^-$ , activation of PKC and AGE formation (230), supporting a role for mtROS production in diabetic macrovascular disease.

Expression of *SOD* genes may be upregulated by mechanical, chemical or biological stimuli and downregulated in certain pathological conditions (234). In addition, *SOD2* expression is regulated post-transcriptionally by a specific RNA-binding protein (238).

### 1.4.2 Catalase

Catalase is the homotetrameric, haem-containing enzyme principally responsible for  $\text{H}_2\text{O}_2$  metabolism following dismutation of  $\text{O}_2^-$  by SOD (188;233). An intracellular anti-oxidase, catalase is primarily located in peroxisomes but also functions in the cytosol and catalyses the conversion of  $\text{H}_2\text{O}_2$  to water and  $\text{O}_2$  (188;233;239) (Figure 1.5). Inherited catalase deficiency has been linked to elevated cardiovascular risk and increased incidence of diabetes mellitus in affected families (233). However, experimental investigation has provided evidence that catalase affords only moderate protection against oxidative stress (240) and while gene transfer studies showed reduced ROS production on co-expression of SOD and catalase, the relative contribution of each gene was not ascertained (241).

### 1.4.3 Glutathione Peroxidases

Glutathione, a tripeptide comprised of glutamate, cysteine and glycine, is the principal low molecular weight, non-protein thiol in the cell (188). Mainly found in the reduced state (GSH), glutathione has numerous functions in metabolism, signal transduction and gene expression (242). GSH acts as an electron donor and can directly scavenge ROS but also acts as a cofactor in the conversion of  $\text{H}_2\text{O}_2$  to  $\text{H}_2\text{O}$  by GPxs (188;233).

The GPxs are a family of tetrameric enzymes with a role in both first and second line anti-oxidant defence. Like catalase, GPxs act to reduce the  $\text{H}_2\text{O}_2$  produced as a result of the dismutation of  $\text{O}_2^-$  by SOD, transferring electrons from GSH to  $\text{H}_2\text{O}_2$  with the subsequent formation of  $\text{H}_2\text{O}$  and  $\text{O}_2$  and conversion of GSH to oxidised glutathione disulphide (GSSG) (188;233;242;243) (Figures 1.5 and 1.8).

Despite the actions of first line anti-oxidant defence mechanisms, interactions between ROS and cellular macromolecules do occur, giving rise to reactive species capable of causing damage to lipids, proteins and nucleic acids. Detoxification of secondary oxidation products is therefore crucial and GPxs play their part, reducing lipid peroxides to their corresponding alcohols via the conjugation and oxidation of GSH (188;233;243) (Figure 1.5).

There are four known GPx isoforms, each containing selenocysteine at the active site (233). GPx1 knockout mice displayed increased susceptibility to ROS-induced oxidative stress (244), while induction of this isoform has been shown to offer protection against oxidative damage in endothelial cells (245). Furthermore, transgenic GPx1 expression was observed to impair endothelial dysfunction (246). Similarly, deficiency of GPx3 has been associated with decreased NO bioavailability and increased platelet-dependent thrombosis (233).

Additional selenoproteins with similar anti-oxidant activities to GPxs include the thioredoxins (233), while the glutathione-s-transferases (GSTs) are examples of non-selenocysteine containing enzymes of significant importance in secondary oxidative stress defence, acting to detoxify reactive electrophiles (233;243).

### **1.5 AMP-activated Protein Kinase**

AMPK is a key molecule in the regulation of cellular energy homeostasis. A heterotrimeric serine-threonine kinase, human AMPK consists of a catalytic  $\alpha$ -subunit and regulatory  $\beta$ - and  $\gamma$ -subunits, each of which has two or more isoforms which are encoded by distinct genes and are differentially expressed in various tissues (Figure 1.10) (247;248). AMPK is activated in response to metabolic stresses, such as glucose deprivation, hypoxia and exercise, which cause a decrease in the cellular energy charge (247-250). When ATP levels fall, there is a corresponding increase in intracellular AMP levels. When present at increased concentration, AMP binds to the  $\gamma$ -subunit of AMPK, allosterically activating the enzyme. AMP binding also promotes phosphorylation at a critical threonine residue (Thr172) of the  $\alpha$ -subunit by an upstream kinase, generating full activation of AMPK (251) (Figure 1.10). This upstream AMPK kinase (AMPKK) has been identified as a complex



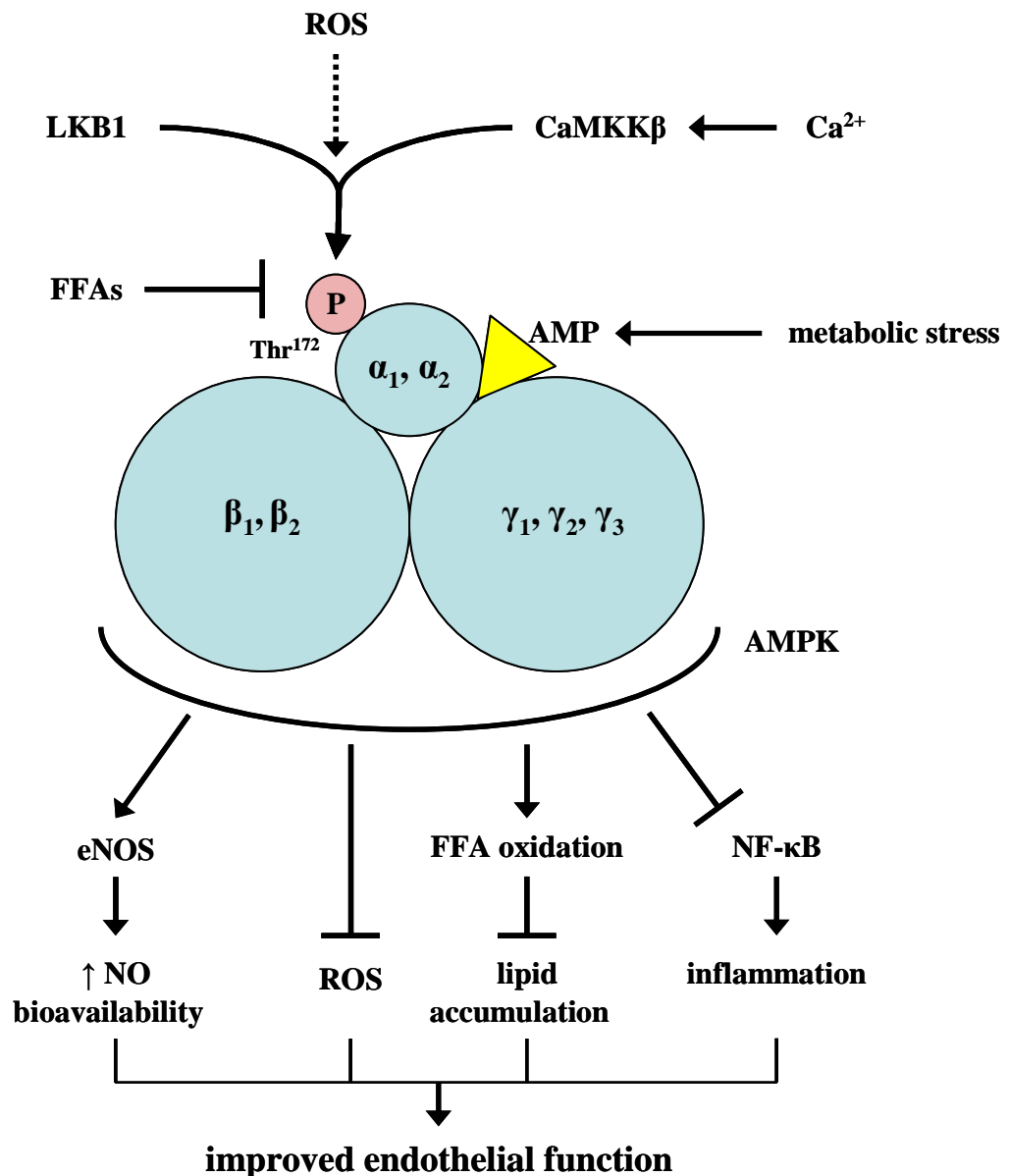


**Figure 1.10. AMPK-regulated Pathways in Endothelial Cells.** The AMPK heterotrimer consists of  $\alpha$ -,  $\beta$ - and  $\gamma$ - subunits. The  $\alpha$ -subunit is responsible for the catalytic activity of the enzyme, involved in transferring a phosphate (P) molecule from ATP to a target protein to activate or inactivate it. The  $\alpha$ -subunit also contains a phosphorylation site for regulation of AMPK activity. The  $\beta$ - and  $\gamma$ - regulatory subunits are important for regulation and cellular localisation of the protein. Assembly of the heterotrimeric complex is essential for enzyme activity. When the  $\gamma$ -subunit binds AMP, AMPK is allosterically activated and becomes a better substrate for LKB1. AMPK is also regulated by upstream kinase Ca<sup>2+</sup> calmodulin-dependent kinase kinase  $\beta$  (CaMKK $\beta$ ) and elevated free fatty acid (FFA) and reactive oxygen species (ROS) levels. Studies suggest AMPK activation improves hyperglycaemia-mediated endothelial dysfunction via a number of pathways, including endothelial nitric oxide synthase (eNOS) activation, protection against the adverse effects of ROS formation, FFA oxidation, and prevention of inflammation via the inhibition of nuclear factor  $\kappa$ B (NF- $\kappa$ B). Adapted from (252).

between the tumour suppressor, LKB1, and two accessory subunits, STRAD (STE-20 related adaptor protein) and MO25 (251;253;254).

Activated AMPK (pAMPK) acts to restore cellular ATP levels via mechanisms including the insulin-independent translocation of GLUT4 to the plasma membrane in skeletal muscle and the subsequent activation of glycolysis (247;248;255). AMPK activation also promotes fatty acid oxidation, inhibition of acetyl CoA carboxylase (ACC) and fatty acid synthesis (256) and, as recently suggested, modulation of gene expression (257;258). In addition, pAMPK mediates the effects of hormones, such as ghrelin (259), and adipokines, including resistin (248), leptin (260) and adiponectin (80;261), and is therefore involved in maintenance of energy balance at both the cellular and whole body level. Already a target for anti-diabetic drugs, metformin (137) and the thiazolidinediones (143), the finding that artificial activation of AMPK with 5-aminoimidazole-4-carboxamide ribonucleoside (AICAR) (262) can mimic the effects of repeated exercise / endurance training in mice (263) has led to heightened interest in the enzyme as a potential therapeutic target for intervention in obesity, T2D and cardiovascular diseases.

More recently, mechanisms independent of bioenergetic changes have been shown to be involved in AMPK activation. A second AMPKK has been identified as  $\text{Ca}^{2+}$ /calmodulin-dependent protein kinase kinase (CaMKK), in particular the  $\beta$  isoform (CaMKK $\beta$ ) (264;265), revealing increased intracellular  $\text{Ca}^{2+}$  as an alternative stimulus for AMPK activation. Additionally, signalling by ROS has been implicated in activation of the enzyme (228;266). Such findings imply AMPK may have a role outwith the regulation of energy homeostasis.

### **1.5.1 AMP-activated Protein Kinase in Type 2 Diabetes Mellitus**

A key effect in the up-regulation of ATP-generating catabolic pathways by AMPK is the stimulation of glucose uptake which occurs as a result of increased translocation of GLUT4 to the plasma membrane, activation of GLUT1 at the plasma membrane and enhanced transcription of the GLUT4 gene. The latter effect may be responsible for increased expression of GLUT4 in response to endurance training which can subsequently lead to increased insulin-stimulated glucose uptake (247). With reduced insulin-stimulated

glucose uptake via GLUT4 a central feature of insulin resistance, the mechanism by which exercise and AMPK activation stimulate this process in an insulin-independent manner is currently of great interest in diabetes research. The exact manner in which AMPK mediates GLUT4 translocation remains to be fully elucidated but studies suggest a potential role for Akt substrate of 160kDa (AS160) (267;268) (Figure 1.4).

As previously described, the hyperglycaemia of T2D results from a reduced ability of insulin to both repress glucose production by the liver and increase glucose uptake in peripheral tissues. Hepatic AMPK activation has been shown to down-regulate expression of the gluconeogenic enzymes PEPCK and G6Pase (269) and activation of the kinase is thought to underlie the ability of adiponectin to reduce hepatic glucose production (80). The transcriptional co-activator, TORC2, a target of AMPK, has recently been proposed as being involved in mediating this effect (270).

By inhibiting fatty acid synthesis and stimulating fatty acid oxidation, AMPK activation reduces excessive storage of triglycerides, which in non-adipose cells results in the lipotoxicity associated with insulin resistance. AMPK inhibits fatty acid synthesis both acutely, by phosphorylating and inactivating the ACC1 isoform of acetyl-CoA carboxylase (262), and in the longer term by switching off expression of lipogenic genes, including ACC1 and fatty acid synthase (271). The kinase stimulates oxidation of fatty acids by phosphorylating and inactivating the ACC2 isoform of acetyl-CoA carboxylase. This lowers malonyl-CoA, thus relieving inhibition of fatty acid uptake into mitochondria (272).

A further catabolic action of AMPK is the promotion of mitochondrial biogenesis via up-regulation of PPAR- $\gamma$  co-activator-1 $\alpha$  (PGC-1 $\alpha$ ) (273). Again, this is likely to prove beneficial in insulin resistant states where a deficit in mitochondrial function is thought to predispose to development of T2D (225).

In addition, AMPK activation is known to inhibit activation of the mTORC1 pathway by the insulin signalling pathway (Figure 1.4), via phosphorylation of the tuberous sclerosis complex (TSC), an upstream regulator of mTORC1 (55). The insulin-mTORC1 pathway is believed to exert a negative feedback effect on insulin signalling via activation of p70 ribosomal S6 kinase (p70S6K) (see Figure 1.4) and subsequent phosphorylation and down-regulation of IRS-1. Consequently, AMPK activation may increase insulin sensitivity by

inhibiting mTORC1 (55;247;274). This effect could explain the ability of AMPK activator, AICAR to mimic the effects of exercise in increasing muscle insulin sensitivity.

AICAR was the first relatively specific compound shown to activate AMPK in intact cells (262). The nucleoside is taken up and accumulates inside the cell as the monophosphorylated nucleotide 5'-aminoimidazole-4-carboxamide ribonucleotide (ZMP), which activates AMPK without disturbing cellular adenine nucleotide ratios (262;275). As such, effects observed on administration of AICAR are not merely due to depletion of ATP. AICAR has been shown to reverse insulin resistance and lower blood pressure in animal models such as the ob/ob mouse (276), the fa/fa rat (277) and the high fat-fed rat (278).

As previously mentioned, anti-diabetic drugs, metformin and the thiazolidinediones also activate AMPK. Neither activate the kinase directly, potentially achieving activation by inhibiting complex I of the ETC, thus increasing the cellular AMP:ATP ratio (279). However, as stated, the major target of the thiazolidinediones is the transcription factor, PPAR- $\gamma$ . In adipocytes, the thiazolidinediones act on PPAR- $\gamma$  to stimulate release of adiponectin and the effects of the drugs in reversing insulin resistance and improving glucose tolerance are greatly reduced in adiponectin knockout mice (280;281). Recent evidence suggests adiponectin acts primarily by activating AMPK, indicating the thiazolidinediones exert a portion of their therapeutic benefit via two independent mechanisms serving to activate AMPK (247).

### **1.5.2 AMP-activated Protein Kinase in The Vascular Endothelium**

Activated AMPK is known to phosphorylate eNOS at Ser1177 in cultured endothelial cells (176;282) and has been shown to increase endothelium-dependent vasodilation in response to shear stress (283). Infection of endothelial cells with adenoviruses expressing dominant-negative mutant AMPK has demonstrated a key role for AMPK in NO production in response to AICAR, hypoxia, ONOO<sup>-</sup>, metformin, adiponectin, shear stress, vascular endothelial growth factor (VEGF) and rosiglitazone (176;283-289). It has also been proposed that AMPK mediates adiponectin- and hypoxia-stimulated angiogenesis (290;291). Incubation with AICAR has recently been reported to reduce TNF $\alpha$ -stimulated

monocyte adhesion, NF- $\kappa$ B activation and mRNA expression of ICAM-1, VCAM-1 and E-selectin in mouse brain endothelial cells (292;293), while metformin has been reported to have similar effects in human umbilical vein endothelial cells (HUVECs) (294), revealing the potential anti-atherogenic benefits of AMPK activation. With increasing evidence to suggest AMPK is activated in a ROS-mediated manner (228;266;289;295-297), it has been proposed that the enzyme exerts its beneficial effect on endothelial function by increasing NO bioavailability and facilitating an anti-oxidative response in the endothelium (252) (Figure 1.10).

As stated, the endothelial dysfunction characteristic of T2D is associated with elevated levels of circulating FFAs (39;88;232). Activated AMPK phosphorylates and inhibits ACC, thus accelerating mitochondrial fatty acid oxidation (256). However, high levels of FFAs may trigger inhibition of AMPK (252) (Figure 1.10) and reduced AMPK activation has been linked to FFA-induced development of endothelial dysfunction in obese rats (298). Furthermore, AMPK activation inhibits fatty acid-induced increases in NF- $\kappa$ B transactivation in vascular endothelial cells (252;294), further supporting a protective role for the enzyme in atherogenic and inflammatory vascular disease.

These downstream consequences of endothelial AMPK activation may explain the beneficial effects of metformin and the thiazolidinediones on vascular outcomes in patients with T2D and highlight why AMPK is increasingly recognised as a potential therapeutic target in defence against oxidative stress and prevention of endothelial dysfunction in cardiovascular diseases such as CAD and T2D.

## **1.6 Aims**

Previously, studies within this laboratory have demonstrated endothelial dysfunction and elevated  $O_2^-$  production in vessels from patients with advanced CAD (159). However, the molecular basis for this increase was not investigated, nor was the effect of type 2 diabetes. The aim of this study therefore, is to investigate a number of molecular determinants of oxidative stress and T2D in primary human vascular cells from patients with CAD, the hypothesis being that oxidative stress leads to endothelial dysfunction in CAD and is exacerbated in those patients with T2D.

The specific aims of this study are:

- (1) to establish sources of  $O_2^-$  production in primary vascular cells isolated from patients with advanced CAD and determine how the presence of T2D affects their contribution to cellular ROS generation;
- (2) to examine the activity and activation of AMPK in primary cultures of endothelial cells isolated from patients with CAD and T2D;
- (3) to investigate how T2D alters gene expression in the endothelium of CAD patients.

## **2. Materials & Methods**

This chapter outlines general laboratory practices and methods that are common to more than one chapter. Each individual results chapter has a specific Materials & Methods section.

## **2.1 General Laboratory Practice**

Laboratory equipment and reagents were of the highest available grades. A laboratory coat and latex powder-free gloves were worn during all procedures. Handling of hazardous reagents was in accordance with Control of Substances Hazardous to Health regulations, utilising laboratory spectacles, facemasks and fume hoods where necessary.

Laboratory glassware was cleaned in Decon 75 detergent (Decon Laboratories Ltd.), rinsed with distilled water and dried in a 37°C cabinet. Sterile, disposable plastic-ware utilised included 0.5 ml, 1.5 ml and 2 ml microcentrifuge tubes (Greiner Bio-One), 15 ml and 50 ml Corning centrifuge tubes and 5 ml and 20 ml Universal containers (Sterilin). Laboratory-ware requiring sterilisation was autoclaved in a Priorclave Tactrol 2.

Reagents were weighed using an Ohaus Portable Advanced balance (sensitive to 0.01 g), or a Mettler HK160 balance (sensitive to 0.0001 g). The pH of solutions was determined using a Mettler Toledo digital pH meter, calibrated on a regular basis with solutions of pH 4.0, 7.0 and 10.0 prepared from buffer tablets [Sigma-Aldrich Company Ltd (Sigma), St Louis, MO, U.S.A.]. Volumes from 0.1 µl to 1,000 µl were dispensed using appropriate Gilson pipettes (Gilson Medical Instruments). Volumes from 1 ml to 25 ml were measured with sterile disposable pipettes (Corning) and a Gilson battery-powered pipetting aid. Distilled water (dH<sub>2</sub>O) was used to prepare aqueous solutions unless otherwise indicated and a Jenway 1000 hotplate/stirrer used to aid dissolving and mixing. Vortexing was carried out using an FSA Laboratory Supplies WhirliMixer. Centrifugation of samples up to 2 ml was performed at 4 - 20°C in an Eppendorf 4515 microcentrifuge while samples of larger volumes were centrifuged in a Sigma 4K15, compatible with 15 ml and 50ml centrifuge tubes, 20 ml Universal tubes and including carriers for standard reaction plates. A Julabo TW8 water bath was utilised for experiments requiring incubations from 37°C to 90°C and a Grant SBB14 boiling water bath used where temperatures up to 100°C were required.



For experiments involving ribonucleic acid (RNA), certified nuclease-free reagents and plastic-ware were used, including nuclease-free H<sub>2</sub>O (Ambion, Austin, TX, U.S.A.), Ambion RNase-free microcentrifuge tubes and RAININ nuclease-free pipette tips. Pipettes and benches were wiped with Ambion RNaseZap reagent prior to all RNA experiments.

## **2.2 Recruitment & Clinical Assessment of Study Participants**

Recruitment and clinical assessment of patients was carried out by Dr Jane Dymott.

Seventy nine patients with severe CAD from cardiothoracic pre-operative clinics were recruited. Twenty three patients had a history of T2D for at least 4 weeks prior to admission for surgery. Type 2 diabetes was defined as having fasting venous blood glucose  $\geq 6.1$  mM or  $\geq 10$  mM two hours post oral glucose load (75 g). Nineteen control subjects free of evidence of CAD who were undergoing surgery for the removal of varicose veins were also recruited. The study was approved by the Glasgow West Ethics Committee and participants gave their written informed consent prior to participation.

Demographic and clinical characteristics of patients and control subjects are given in Table 2.1. As expected, patients with CAD were older and more likely to be on cardiovascular medication than control subjects. Total and low density lipoprotein (LDL) cholesterol levels were lower in patients with CAD compared to control subjects, consistent with lipid lowering therapy in the CAD patient group. High density lipoprotein (HDL) cholesterol levels were significantly greater in control subjects compared to patients. Patients with T2D had greater body mass index and greater percentage of glycosylated haemoglobin A<sub>1c</sub> but no other significant differences to patients without diabetes were observed. Forty three percent of patients with T2D were treated with metformin.

	<b>CAD</b>		<i>P</i> value T2D vs ND	<b>Controls</b>	
	T2D  n=23	ND  n=56		 n=19	<i>P</i> value CAD vs controls
Age (years)	65±11	65±9	0.961	44±19	<0.001
Sex (m:f)	20/3	45/11	0.747	8/11	0.001
BMI (kg/m <sup>2</sup> )	31.7±5.2	28.6±4.7	0.026	26.5±1.9	0.004
SBP (mmHg)	138±22	138±26	0.897	132±23	0.471
DBP (mmHg)	73±13	80±11	0.065	84±12	0.162
Total cholesterol (mmol/L)	3.95±1.10	4.11±0.99	0.542	4.96±0.99	0.029
LDL cholesterol (mmol/L)	1.80±0.83	2.00±0.78	0.314	2.69±1.11	0.024
HDL cholesterol (mmol/L)	1.11±0.22	1.17±0.27	0.366	1.72±0.30	<0.001
Triglycerides (mmol/L)	2.54±1.97	2.04±0.97	0.262	1.17±0.47	0.052
CRP (mg/L)	2.5±2.9	5.0±10.5	0.280	3.5±4.2	0.843
HbA <sub>1c</sub> (%)	7.2±1.3	5.6±0.4	<0.001	5.4±0.2	0.111
Active smoking (y/n)	2/22	2/54	0.579	2/17	0.324
ACEI/ARB (y/n)	18/5	32/24	0.122	1/18	<0.001
Statin (y/n)	21/2	53/3	0.625	2/17	<0.001
Metformin (y/n)	10/13	0/56	<0.001	0/19	<0.001

**Table 2.1. Characteristics of the Study Cohort.** Continuous data are given as mean ± standard deviation irrespective of distribution or skewness. *P* values, however, derive from Student's t-test or Mann-Whitney U-test as appropriate. Comparison between categorical data was performed using Fisher's exact test. CAD, coronary artery disease; BMI, body mass index; SBP, systolic blood pressure; DBP, diastolic blood pressure; LDL, low density lipoprotein; HDL, high density lipoprotein; CRP, C-reactive protein; HbA<sub>1c</sub>, glycosylated haemoglobin A<sub>1c</sub>; ACEI, angiotensin-converting enzyme inhibitor; ARB, angiotensin receptor blocker

## **2.3 Human Vascular Tissue**

Freshly obtained saphenous veins from patients undergoing coronary artery bypass graft (CABG) surgery were stored in sterile saline solution by the surgical team at Glasgow Western Infirmary until collection. Control vessels from patients undergoing elective varicose vein removal were stored in the same way by the surgical team at Glasgow's Gartnavel General. Maximum storage time was 2 hours. Only non-varicosed portions of veins from control patients, as identified by the surgical team, were utilised. Samples were taken to the laboratory and cleaned of excess connective tissue. Endothelial cells were isolated from portions of vessels on the day of surgery and the remainder of samples stored at 4°C in a Krebs 4-(2-hydroxyethyl)-1-piperazineethanesulfonic acid (HEPES) buffer [118 mM NaCl, 10 mM Hepes, pH 7.4, 25 mM NaHCO<sub>3</sub>, 4.7 mM KCl, 1.2 mM MgSO<sub>4</sub>, 1.2 mM KH<sub>2</sub>PO<sub>4</sub>, 11 mM glucose, 10 µM indomethacin, 50 µM ethylenediamine tetra-acetic acid (EDTA)] for study of endothelial function and O<sub>2</sub><sup>-</sup> production the following day.

## **2.4 Isolation & Culture of Primary Cells**

Primary cells were handled under sterile conditions using class II biological safety cabinets (Holten Safe 2010). Cabinets were cleaned before and after use with dH<sub>2</sub>O and 70% ethanol. Waste plastics and fluid were decontaminated by steeping for 24 hours in (10%) bleach before plastics were incinerated and fluids emptied into domestic waste drains. Cells were cultured in 100 mm x 20 mm cell culture dishes and 25 cm<sup>2</sup>, 75 cm<sup>2</sup> and 150 cm<sup>2</sup> culture flasks with vented caps (Corning).

### **2.4.1 Isolation of Primary Endothelial Cells from Human Saphenous Vein**

Human saphenous vein endothelial cells (HSVECs) were isolated on the day of surgery by standard collagenase digestion based on a modified version of the protocol described by

Jaffe and colleagues (299). In summary, saphenous veins were gently flushed of remaining blood with wash medium [Dulbecco's Modified Eagle's Medium (DMEM), 1000 mg/l glucose, without phenol red (Invitrogen<sup>TM</sup>, Paisley, U.K.) and supplemented with 100 IU/ml penicillin, 100 µg/ml streptomycin and 2 mM L-glutamine]. Veins were then filled with a solution of filter-sterilised collagenase [(Sigma), 2 mg/ml in wash medium] and the vessel incubated at 37°C in a sterile petri dish in 5% CO<sub>2</sub> for 15 minutes. Endothelial cell suspensions were obtained by flushing the vein with wash medium and collecting flow-through. Veins were then refilled with collagenase and incubated at 37°C for a further 10 minutes. Collagenase was flushed through and cells collected and pelleted by centrifugation (2,000 x g, 5 minutes, room temperature). Cells were resuspended in complete Large Vessel Endothelial Cell Basal Medium (TCS Cellworks Ltd, Botolph Claydon, Bucks, U.K.), supplemented with 20% (v/v) foetal calf serum (FCS), 100 IU/ml penicillin, 100 µg/ml streptomycin and 2 mM L-glutamine (endothelial cell growth medium), and then incubated for 24 hours before a complete medium change. Cells were cultured in complete growth medium and used between passages 1 and 5.

#### **2.4.2 Isolation of Primary Vascular Smooth Muscle Cells from Human Saphenous Vein**

Following HSVEC isolation, vessel portions were stored overnight at 4°C in a HEPES-containing buffer [DMEM, 1000 mg/l glucose, + L-glutamine, + 25 mM HEPES, + pyruvate (Invitrogen<sup>TM</sup>), supplemented with 10% (v/v) FCS, 100 IU/ml penicillin, 100 µg/ml streptomycin]. The following day human saphenous vein smooth muscle cells (HSVSMCs) were obtained from medial explants of these portions of saphenous veins according to the method described by Southgate and Newby (300). Briefly, segments of vein were cut longitudinally and pinned out with the endothelial surface uppermost. The medial layer was scored with a sterile scalpel, peeled away from the adventitial layer and then cut into 1mm<sup>2</sup> size pieces using a McIlwain Tissue Chopper. Explants were then incubated at 37°C in 5% CO<sub>2</sub> in minimal medium until they adhered to the flask (approximately 24 hours). Subsequently, explants were cultured in 7.5 ml of DMEM (4500 mg/L glucose, + Glutamax-1), supplemented with 100 IU/ml penicillin, 100 µg/ml streptomycin and 20% (v/v) FCS (smooth muscle cell growth medium), at 37°C in 5%

CO<sub>2</sub>. Medium was changed once a week until HSVSMCs had migrated from the explants and then every 3 days for subsequent passages.

### **2.4.3 Primary Cell Culture & Passage**

As stated, cells were maintained in complete growth medium. Confluent cultures of primary cells were passaged by trypsin-EDTA. Cells were washed twice in sterile Dulbecco's calcium and magnesium free phosphate buffered saline (PBS, Lonza, Verviers, Belgium) and incubated at 37°C in trypsin-EDTA (0.05% trypsin, 0.02% EDTA) for 5 minutes or until the majority of cells had detached from the flask. The action of trypsin-EDTA was then blocked by the addition of an equal volume of growth medium containing 20% (v/v) FCS. Cells were harvested by centrifugation at 1,500 x g and resuspended in fresh growth media before plating.

### **2.4.4 Immunocytochemical Characterisation of HSVECs & HSVSMCs**

HSVECs were identified by immunofluorescent staining for von Willebrand factor (vWF) and HSVSMCs by immunofluorescence for SMC- $\alpha$ -actin. Primary antibodies were mouse-anti-human vWF (clone F8/86, MO616) and mouse-anti-human smooth muscle  $\alpha$  actin (clone 1A4, M0851), both from Dako-Cytomation (Dako, Glostrup, Denmark).

At passage 1 HSVECs and HSVSMCs were harvested and plated onto sterile coverslips in 6 well plates. Sixteen hours later media were removed, cells washed twice in PBS and fixed in 4% paraformaldehyde for 5 minutes at room temperature. Cells were washed twice more in PBS and then incubated with the appropriate primary antibody (1:50 for anti-vWF and 1:2000 for anti-SMC- $\alpha$ -actin, both in 20% goat serum/PBS) at room temperature for 30 minutes. This was followed by 3 washes in PBS. Cells were then incubated with goat-anti-mouse IgG-fluorescein isothiocyanate (FITC) conjugate (Dako) secondary antibody (1:200 in 20% goat serum/PBS) for 30 minutes at room temperature and washed a further 3 times in PBS. Cell-free sides of coverslips were subsequently washed with dH<sub>2</sub>O, coverslips mounted in Vectashield (Vector Laboratories Inc., Burlingame, CA, U.S.A.),

containing propidium iodide for nucleic counter-staining, and cells visualised under a fluorescence microscope at x 40 and x 100 magnifications.

### **2.4.5 Cryo-preservation of HSVECs**

At passage 3, cell cultures were harvested as described in section 2.4.3 and resuspended at a density of approximately  $1 - 2 \times 10^7$  cells/ml in cryo-preservation media [complete culture media supplemented with 10% (v/v) dimethyl sulphoxide (DMSO, Fisher Scientific, Pittsburgh, PA, U.S.A.). Cell suspensions were aliquoted into sterile 2 ml cryo-vials and cooled at a constant  $-1^\circ\text{C}/\text{minute}$  to  $-80^\circ\text{C}$  using isopropanol. Vials were then transferred to liquid nitrogen and stored until required for analysis.

For resuscitation, vials were removed from the liquid nitrogen store and pre-warmed culture medium slowly added until contents thawed. Cells were then plated and DMSO-containing medium replaced with fresh medium the following day.

## **2.5 Extraction, Purification & Quantification of RNA from HSVECs**

### **2.5.1 RNA Extraction**

RNA was routinely extracted from HSVECs at passage 3.

RNA was isolated using the RNeasy<sup>®</sup> Mini Kit (QIAGEN) and according to the manufacturer's guidelines. Cells were pelleted, supernatants removed and pellets loosened by flicking the tube. Cells were then resuspended in one volume (600  $\mu\text{l}$ ) Buffer RLT containing 0.01% (v/v)  $\beta$ -mercaptoethanol. Samples were homogenised by repeated pipetting. One volume of 70% ethanol was added to the homogenised lysate and samples mixed well by pipetting. Up to 700  $\mu\text{l}$  of sample was then applied to an RNeasy mini column placed in a collection tube and centrifuged for 15 seconds at  $8,000 \times g$  and room temperature. Flow-through was discarded and 700  $\mu\text{l}$  Buffer RW1 added to columns.

Samples were then centrifuged as before and flow-through discarded. Columns were transferred to fresh collection tubes and 500 µl Buffer RPE added. Centrifugation was carried out as before to wash columns and flow-through discarded before another 500 µl Buffer RPE was added and samples centrifuged (2 minutes, 8,000 x g, room temperature) to dry the RNeasy silica-gel membrane. To eliminate the possibility of Buffer RPE carryover, collection tubes containing flow through were discarded and columns placed in fresh tubes for centrifugation at 14,000 x g (room temperature) for 1 minute. RNeasy columns were transferred to new collecting tubes and 40 µl RNase-free water pipetted directly onto the silica-gel membrane. Samples were then centrifuged for 1 minute at 8,000 x g and room temperature to elute. To increase RNA yield, the elution step was repeated, re-using the original volume of RNase-free water. RNA samples were stored at -70°C until time of analysis.

### **2.5.2 DNase Treatment of Extracted Total RNA**

In order to remove any contaminating DNA, extracted total RNA was treated with DNase using the TURBO DNA-free™ kit from Ambion and according to the manufacturer's instructions. In summary, 0.1 volume (4 µl) 10 X TURBO DNase Buffer and 1 µl TURBO DNase (2 U/µl) were added to RNase-free tubes containing 40 µl RNA samples. Samples were then incubated at 37°C for 25 minutes. Following incubation, 0.1 volume (4.4 µl) DNase Inactivation Reagent was added to tubes. Samples then underwent a further 2 minute incubation at room temperature with occasional mixing, before a 1.5 minute centrifugation at 10,000 x g and 4°C. Supernatants containing DNase treated total RNAs were transferred to fresh, RNase-free tubes and stored at -70°C for downstream applications.

### **2.5.3 RNA Quantification**

Total RNA concentrations were quantified using the NanoDrop® ND-100 Spectrophotometer and ND-1000 v3.1.0 programme (Labtech International Ltd, Lewes, East Sussex, U.K.). For each sample, 2 µl total RNA was quantified.

## **2.6 Extraction & Quantification of Protein from HSVECs**

### **2.6.1 Protein Extraction**

Protein was routinely extracted from HSVECs at passage 3.

For protein extraction, cells were permeabilised in 0.2% Triton X 100 (Sigma) and samples homogenised by at least 20 passes through a 21-gauge needle (0.8 mm diameter) fitted to a syringe. Protein samples were stored at -20°C until required.

### **2.6.2 Determination of Protein Concentration**

Protein concentrations were determined using a Pierce BCA (bicinchoninic acid) Protein Assay kit (Thermo Scientific, Waltham, MA, U.S.A.) according to the manufacturer's instructions. Assays were performed in 96-well plates. Dilutions of an albumin protein standard (provided) ranging from 25 ng/μl – 2 μg/μl were made in PBS and used to generate a standard curve for each assay. Reagents A and B included in the kit were mixed at a ratio of 50:1 respectively before being added to protein samples and standards at a ratio of 8:1 (25 μl sample/standard, 200 μl BCA reagents mixture). Plates were subsequently protected from light in aluminium foil and placed at 37°C for 30 minutes. Absorbance at 560 nm was determined for all wells using a Wallac Victor<sup>2</sup> plate reader (Wallac, Turku, Finland). Both samples and standards were measured in duplicate and an average value calculated. Concentration of protein in each sample was then interpolated from the standard curve by Work-Out software (Wallac).

### **2.6.3 Cell Lysate Preparation**

Passage 3 HSVECs were grown in 100 mm diameter cell culture dishes until confluent and then serum-starved overnight. Medium was removed and cell lysates prepared. Briefly, 0.4 ml of ice-cold lysis buffer [50 mM Tris-HCl, pH 7.4 at 4°C, 50 mM NaF, 5 mM Na<sub>4</sub>P<sub>2</sub>O<sub>7</sub>, 1



mM NaVO<sub>3</sub>, 1mM EDTA, 1mM ethylene glycol tetra-acetic acid (EGTA), 0.1 mM benzamidine, 0.1 mM phenylmethylsulfonylfluoride (PMSF), 5 µg/ml soybean trypsin inhibitor, 1% (w/v) glycerol, 1% (w/v) Triton X 100] was added and cell extract scraped off and transferred to a microcentrifuge tube. Extracts were then vortexed-mixed and centrifuged (14,000 x g, 1 min, 4°C). Total protein concentration of each sample was determined as outlined in section 2.6.2. Cell lysates were stored at -20°C when not required immediately.

## **2.7 HSVEC mRNA Expression**

RNA was routinely isolated from passage 3 HSVECs as described in section 2.5.

### **2.7.1 Reverse Transcription Polymerase Chain Reaction (RT-PCR)**

First strand complementary DNA (cDNA) was synthesised from 1 µg of DNase-treated total RNA using the TaqMan<sup>®</sup> Reverse Transcription Reagents kit from Applied Biosystems and following the manufacturer's guidelines. RNA samples were reverse transcribed to cDNA in a 20 µl reaction containing a final concentration of 5.5 mM MgCl<sub>2</sub>, 500 µM of each deoxyribonucleotide triphosphate (dNTP), 2.5 µM Random Hexamers, 0.4 U/µL RNase Inhibitor, 1.25 U/µL MultiScribe Reverse Transcriptase and 1 X TaqMan<sup>®</sup> RT Buffer. Selected samples were used for negative control reactions which did not contain MultiScribe Reverse Transcriptase. Samples were then incubated at 25°C for 10 minutes to maximize primer-RNA template binding before being held at 48°C for 30 minutes to facilitate reverse transcription. Reverse Transcriptase was inactivated by incubating samples at 95°C for 5 minutes before samples were placed on ice and diluted, in nuclease-free water, to a final volume of 50 µl. When not being used immediately, samples were stored at -20°C.

### 2.7.2 TaqMan<sup>®</sup> Real-Time RT-PCR

Real-time RT-PCR quantitation of samples was carried out via a two-step RT-PCR assay utilising TaqMan<sup>®</sup> Gene Expression Assays (Applied Biosystems).

Prior to real-time RT-PCR reactions, an efficiency assay was performed for each gene of interest. Serial dilutions of pooled, neat cDNAs were set up in singleplex and multiplex reactions to determine whether the gene of interest amplified with equal efficiency to that of a reference/housekeeping gene [ $\beta$ -actin or glyceraldehyde 3-phosphate dehydrogenase (GAPDH)]. Efficiencies, as calculated according to the manufacturer's instructions (ABI PRISM 7700 Sequence Detection System User Bulletin #2), were considered to be equal if the absolute value of the slope was  $< 0.1$ .

Following efficiency tests, multiplex reactions were carried out for genes of interest reacting with similar efficiency to a reference gene. Each multiplex reaction was of 5  $\mu$ l volume, consisting of 2.5  $\mu$ l TaqMan<sup>®</sup> Universal PCR Master Mix, 1 X VIC-labelled reference probe, 1 X FAM-labelled probe for gene of interest and 2  $\mu$ l cDNA. Reactions were carried out in barcoded 384-well plates. For genes of interest with relative efficiencies dissimilar to those of reference genes, reactions were carried out in singleplex (with equal volumes of nuclease-free water in place of the relevant probe) but within the same plate. The  $2^{-\Delta\Delta C_t}$  comparative method (301) was used for the relative quantitation of gene expression according to the manufacturer's instructions (ABI PRISM 7700 Sequence Detection System User Bulletin #2).

## **2.8 HSVEC Protein Expression**

Cell lysates were prepared and protein routinely isolated from passage 3 HSVECs as described in section 2.6.

### **2.8.1 Western Blot Assessment of Protein Expression**

Protein samples were mixed with an equal amount of reducing loading dye (125 mM Tris pH 6.8, 4% (v/v) SDS, 10% (v/v) glycerol, 0.006% (v/v) bromophenol blue, 2% (v/v)  $\beta$ -mercaptoethanol) and subsequently denatured by incubating them for 10 minutes at 99°C. Equal amounts (in the range of 20  $\mu$ g to 50  $\mu$ g) of total protein were then resolved using sodium dodecyl sulphate polyacrylamide gel electrophoresis (SDS/PAGE). 12% polyacrylamide gels (containing 40% (v/v) polyacrylamide (30%), 11.25 mM Tris pH 8.8, 0.1% (v/v) SDS, 300  $\mu$ l ammonium persulphate (APS) and 30  $\mu$ l TEMED) were used. A 4% stacking gel (13.3% (v/v) polyacrylamide (30%), 3.75 mM Tris pH 6.8, 0.1% SDS, 300  $\mu$ l APS and 30  $\mu$ l TEMED) was used with each gel. 15  $\mu$ l of Amersham Rainbow Markers (GE Healthcare U.K. Ltd, Bucks, U.K.) were included in each blot. These protein molecular weight markers were either low range [2.5 kilodaltons (kDa) – 45 kDa] or full range (10 kDa – 250 kDa).

Proteins were transferred onto Hybond-P nitrocellulose membranes (Amersham Bioscience U.K. Ltd) overnight at 90 milliAmps (mA) in transfer buffer containing 0.025 M Tris, 0.2 M glycine, 20% (v/v) methanol, 0.01% (v/v) SDS. Membranes were then blocked (with shaking) in TBS-T [150 mM NaCl, 50 mM Tris, 0.1% (v/v) Tween-20] + 10% (w/v) fat-free milk powder (blocking buffer) for approximately 6 hours before overnight incubation at 4°C (with shaking) in a primary antibody solution. Primary antibodies were diluted to appropriate concentrations in blocking buffer. Membranes were then washed 6 times in TBS-T at room temperature with each wash lasting approximately 5 minutes. Secondary antibodies were also diluted in blocking buffer and incubated with membranes at room temperature for 2 hours with shaking. A further six 5 minute washes in TBS-T were then performed.

Proteins were visualised using Amersham™ ECL™ (enhanced chemiluminescence) Western Blotting Detection Reagents (GE Healthcare) as per the manufacturer's instructions. Films were exposed for varying lengths of time, ranging from 30 seconds to overnight.

### **2.8.2 Densitometric Quantification of Protein Bands**

Immuno-detected bands on photographic film were scanned on a Mercury 1200c scanner, using Adobe Photoshop software, to generate a digital image. Individual bands were labeled and demarcated by boxes using a drawing tool and the intensity of bands measured using Scion Image or ImageJ software and expressed in units of optical density per mm<sup>2</sup> (ODU/mm<sup>2</sup>).

Two methods of background subtraction were used for densitometrical analyses. For blots with clean and constant background intensities, a 'global' background subtraction method was used. This involved drawing a box in an area of the image representative of the background, thus allowing the software to calculate the average intensity of pixellation in this box and subtracting this value from pixel intensity in all boxes containing bands. Alternatively, a 'local' background subtraction method was used for blots where the background intensity level was variable across the blot. Here, the software calculated an average background intensity for each box by measuring the average intensity of all pixels in a one pixel border around each box and subtracted this from each pixel in the box to determine band intensity.

## **2.9 Statistical Analysis**

For clinical data and measurements in whole vessels, continuous data are given as mean ± standard deviation or median (interquartile range), unless otherwise indicated. Values stated are means ± standard error of the mean (SEM) for cellular data, unless otherwise indicated. For comparisons of a continuous variable between 2 experimental groups, paired and unpaired Student's t-tests and Mann-Whitney U-tests were applied as appropriate. For comparisons of a continuous variable in data sets with more than 2 groups, analysis of

variance (ANOVA) was applied, followed by the Tukey's post-hoc test for all possible pairwise comparisons. Categorical data were analysed by Fisher's exact test. A *P*-value of less than 0.05 (two tailed) was considered significant.

### **3. Mechanisms of Oxidative Stress in Coronary Artery Disease**

### **3.1 Introduction**

Levels of  $O_2^-$  have been shown to be elevated in vessels from patients with advanced CAD relative to those from control subjects with no documented CAD (159;208;302) and studies carried out within our laboratory have shown endothelial dysfunction to be associated with this elevated  $O_2^-$  production in saphenous veins from CAD patients (159). However, while these studies demonstrated elevated  $O_2^-$  generation throughout the vessel wall in patients with CAD (159), the molecular basis for this increase was not investigated nor was the effect of the additional CVD risk factor, T2D.

Traditional methods for the detection of  $O_2^-$  in vascular tissue include lucigenin-enhanced chemiluminescence and fluorescence techniques involving the use of probes such as dihydroethidium (DHE). Employing these methods, vascular  $O_2^-$  production has been shown to be increased in a number of conditions recognised as risk factors for CVD and in which endothelial function is impaired, including T2D (303;304) and various forms of hypertension such as Ang II-induced hypertension (180;305) and that found in the stroke prone spontaneously hypertensive rat (SHRSP) (306;307). In addition, more recent applications of these techniques have succeeded in demonstrating increased levels of  $O_2^-$  in vascular tissue from patients with advanced CAD as compared to individuals with no documented vascular disease (159;208), as previously described. However, the validity of lucigenin-enhanced chemiluminescence assays has been questioned, with evidence to suggest that at high concentrations, lucigenin itself may act as a source for  $O_2^-$  via redox cycling (308;309). Similarly, DHE has been associated with potential artefacts (310). Consequently, the use of two independent methods for superoxide detection is considered necessary by most investigators in order to obtain reliable results.

Cytochrome c reduction is another well established approach for measurement of  $O_2^-$  production. While this method is useful for quantifying  $O_2^-$  released in large amounts during the respiratory burst of neutrophils or by isolated enzymes, for other tissues, such as vessels and endothelial cells, where the level of  $O_2^-$  production is much lower, its application is more difficult as investigators find themselves operating at the lower limit of the assay's sensitivity (311).

In recent years, intracellular  $O_2^-$  production has increasingly been detected using DHE and high performance liquid chromatography (HPLC) (311;312) and/or electron paramagnetic

resonance (EPR) spectroscopy (311;313). Currently one of the most accurate methods for the detection of radical species, EPR detects the transitions of unpaired electrons in an applied magnetic field (311) and has been used in conjunction with cyclic hydroxylamine spin probes to investigate  $O_2^-$  levels in vascular tissue (314) and cultured endothelial cells (315-317). Cyclic hydroxylamines include 1-hydroxy-3-carboxy-2,2,5-tetramethylpyrrolidine hydrochloride (CPH) and 1-hydroxy-3-methoxycarbonyl-2,2,5,5-tetramethylpyrrolidine (CMH) and are effective scavengers of  $O_2^-$ , oxidised to form stable nitroxide radicals which can readily be detected by EPR (311).

As stated previously (section 1.3), principal sources of  $O_2^-$  in the vasculature include uncoupled eNOS and NAD(P)H oxidase and inhibitors of these enzymes have been shown to reduce  $O_2^-$  production in saphenous veins from CAD patients (159;302;318). Preincubation of sections of saphenous vein with  $N^G$ -nitro-L-arginine methyl ester (L-NAME), an eNOS inhibitor, and diphenylene iodonium (DPI), an inhibitor of flavin-containing oxidases such as NAD(P)H oxidases, caused significant reductions in vascular  $O_2^-$  generation in patients with CAD (302), suggesting they represent enzymatic sources of  $O_2^-$  generation in saphenous veins. Furthermore, incubation of saphenous veins with the NAD(P)H oxidase inhibitor, apocynin has been shown to improve endothelium-dependent relaxations in CAD patients, suggesting NAD(P)H oxidase contributes to  $O_2^-$  production and endothelial dysfunction in these patients (159).

As previously outlined, mitochondria are major sites of ROS generation within cells of the vasculature. However, the precise contribution of mitochondria to total ROS production in the vessel wall and other cardiovascular tissues remains unclear, a consequence of limited efficacy of conventional antioxidants due to the difficulty associated with delivering them to mitochondria *in situ* (319). Furthermore, although specific antagonists of the respiratory chain, such as the complex I inhibitor, rotenone, or the complex III inhibitor, antimycin, can modify mitochondria-derived ROS production, they have confounding effects on mitochondrial ATP production and membrane potential, rendering interpretation of their effects on cellular ROS levels difficult (320).

A recently developed mitochondria targeted ubiquinone, MitoQ<sub>10</sub>, has been shown to overcome the problem of direct delivery to the mitochondria. MitoQ<sub>10</sub> is composed of a lipophilic triphenylphosphonium (TTP) cation covalently attached to an ubiquinol antioxidant (321;322). Lipophilic cations can easily move through phospholipid bilayers



without requiring a specific uptake mechanism and, as such, the TTP cation concentrates MitoQ<sub>10</sub> several hundred fold within the mitochondria, driven by the large mitochondrial membrane potential (321-324) (Figure 3.1). Within mitochondria, MitoQ<sub>10</sub> is reduced by the respiratory chain to its active ubiquinol form, a highly effective antioxidant which prevents lipid peroxidation and mitochondrial damage (321;323-325). MitoQ<sub>10</sub> has been shown to prevent oxidative damage in endothelial cells *in vitro* (326) and to be effective against such damage *in vivo*, in rodent models of sepsis and reperfusion injury (327;328).

The aims of the experimental work outlined in this chapter were as follows:

- 1) to compare endothelial function and levels of O<sub>2</sub><sup>-</sup> production in vessels from control subjects and CAD patients with and without T2D;
- 2) to isolate and culture HSVECs and HSVSMCs from control subjects and patients with CAD;
- 3) to compare levels of O<sub>2</sub><sup>-</sup> production in HSVECs isolated from control subjects and CAD patients with and without T2D;
- 4) to investigate SOD expression and characterise enzymatic sources of O<sub>2</sub><sup>-</sup> production in HSVECs from CAD patients with and without T2D

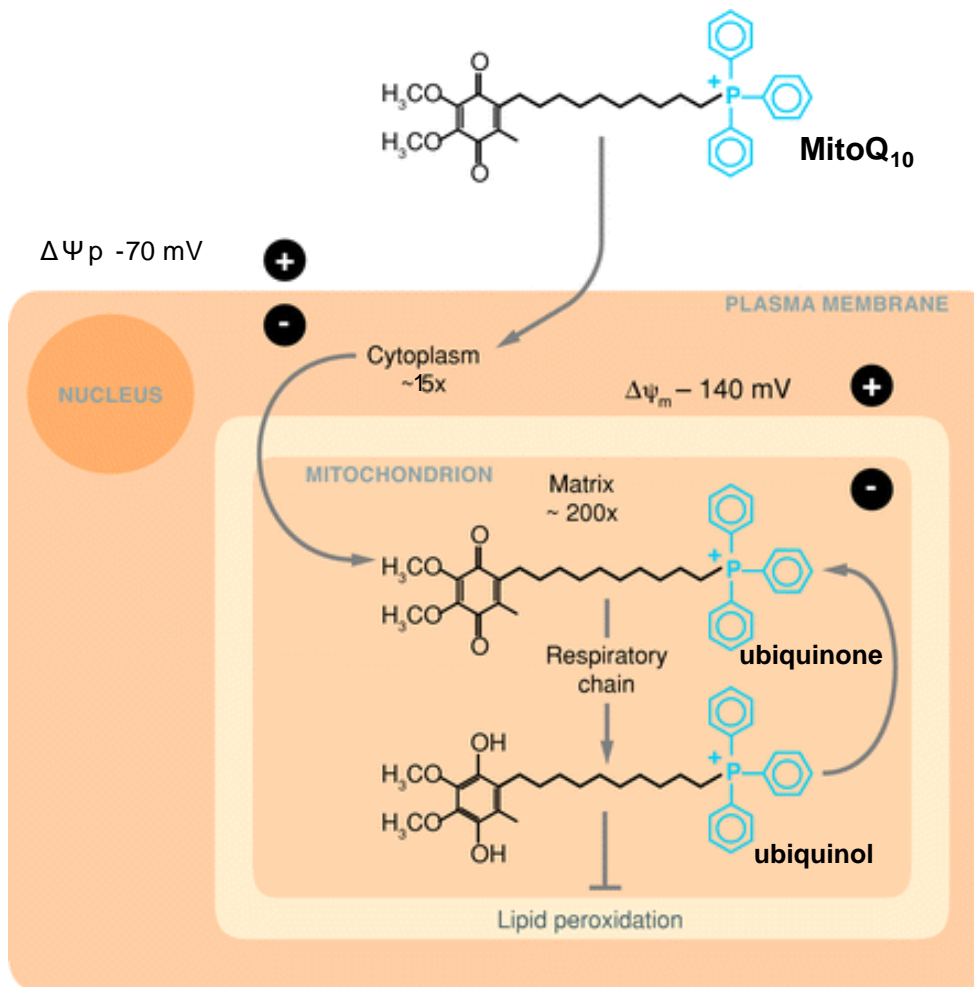


**Figure 3.1. Accumulation of MitoQ<sub>10</sub> in Cells and Mitochondria.** MitoQ<sub>10</sub> accumulates (~10- to 20-fold) within the cell driven by the plasma membrane potential ( $\Delta\Psi_p$ ). Further accumulation (~150- to 200-fold) in mitochondria is driven by the mitochondrial membrane potential ( $\Delta\Psi_m$ ). Within the mitochondrial matrix, MitoQ<sub>10</sub> is reduced to the active antioxidant form, ubiquinol by the respiratory chain. Ubiquinol in turn acts to prevent lipid peroxidation. Antioxidant activity produces the ubiquinone form which is recycled back to ubiquinol by the respiratory chain (continual recycling). Adapted from (329).

## **3.2 Materials & Methods**

### **3.2.1 Study Participants**

Patients with CAD and control subjects were as described in section 2.2.

### **3.2.2 Human Vascular Tissue & Primary Cell Culture**

Vascular tissue was obtained and prepared as described in section 2.3 and HSVECs and HSVSMCs isolated, characterised and cultured as outlined in section 2.4.

### **3.2.3 Assessment of Endothelial Function**

Portions of saphenous vein were studied in organ bath chambers as outlined by Hamilton and colleagues (330). Vessels were cleaned of connective tissue and cut into 2–3 mm rings. Rings were then suspended on wires in 10 ml organ chambers filled with physiological salt solution [(PSS), 130 mM NaCl, 4.7 mM KCl, 14.9 mM NaHCO<sub>3</sub>, 1.18 mM KH<sub>2</sub>PO<sub>4</sub>, 5.5 mM glucose, 1.17 mM MgSO<sub>4</sub>·7H<sub>2</sub>O, 1.6 mM CaCl<sub>2</sub>·2H<sub>2</sub>O, and 0.03 mM CaNa<sub>2</sub>EDTA, 0.02 mM indomethacin dissolved in DMSO (pH 7.49 ± 0.1)], maintained at 37°C, and aerated with a mixture of 95% O<sub>2</sub>-5% CO<sub>2</sub>. The rings were connected to force transducers, and changes in isometric tension were recorded. Vessels were constricted with phenylephrine and relaxation in response to the endothelium dependent vasodilator, calcium ionophore A23187 (0.01-10 µM) was studied. Maximum relaxation was calculated and expressed as a percentage of constriction to phenylephrine.

### 3.2.4 Assessment of Vascular Superoxide Production

Superoxide production was measured in 3-4 mm rings by chemiluminescence using lucigenin as described by Berry *et al.* (318). Samples were analysed in a liquid scintillation counter (Hewlett Packard Tricarb 2100TR). Readings were taken every 10 seconds for 3 minutes and absolute counts quantified with a xanthine / xanthine oxidase calibration curve for  $O_2^-$  generation and standardised to wet weight of the tissue. Calibration curves were in the range of 28 nM to 280 nM xanthine and prepared by adding 20  $\mu$ l xanthine oxidase (0.1 U/ml), 5  $\mu$ M lucigenin and increasing volumes of 20  $\mu$ M xanthine to a scintillation vial containing 2 ml Krebs-Ringer HEPES (KRH) buffer (119 mM NaCl, 20 mM Na-HEPES, pH 7.4, 5 mM  $NaHCO_3$ , 4.7 mM KCl, 1.3 mM  $CaCl_2$ , 1.2 mM  $MgSO_4$  ( $7H_2O$ ), 10 mM glucose,  $NaH_2PO_4$ ). Counts were reported as nmol/mg tissue/min. It has previously been shown that the lucigenin assay responds in the same way to  $O_2^-$  as the conversion of dihydroethidine to ethidium, with ethidium production being measured by its fluorescence (159).

### 3.2.5 Assessment of HSVEC Superoxide Production

#### 3.2.5.1 Lucigenin-Enhanced Chemiluminescence

For measurement of HSVEC  $O_2^-$  levels by lucigenin chemiluminescence, cells were grown in 100 mm diameter cell culture dishes until confluent and then serum-starved overnight. Medium was removed and cell lysates prepared as per section 2.6.3. Serum-free medium was removed following overnight incubation and replaced with 5 ml KRH buffer +/- MitoQ<sub>10</sub> as indicated. Cells were then incubated for 1 hour at 37°C in a CO<sub>2</sub>-free incubator and lysates prepared as previously described. Total protein concentration of each sample was determined by Pierce BCA Protein Assay kit according to the manufacturer's protocol and using the Wallac Victor<sup>2</sup> plate reader.

Lucigenin (5  $\mu$ M) was added to 350  $\mu$ g lysate and samples analysed immediately in a Hewlett Packard Tricarb 2100TR liquid scintillation counter. Readings were taken every 10 seconds for 3 minutes and absolute counts quantified with a xanthine/xanthine oxidase

calibration curve for  $O_2^-$  generation. Calibration curves were prepared as per section 3.2.3 and were in the range of 28 nM to 280 nM xanthine. Counts were reported as nmol/mg lysate/min.

### 3.2.5.2 Electron Paramagnetic Resonance Spectroscopy

Passage 3 HSVECs were grown in 100 mm diameter cell culture dishes until confluent and then serum-starved overnight (unless otherwise indicated) before being incubated in the presence or absence of test substances (Table 3.1). Concentrations and incubation times for test substances were as previously optimised within the laboratory or from relevant literature where indicated. Cells were then detached using trypsin-EDTA as described in section 2.4.3. Numbers of cells from each dish were determined in triplicate using a Beckman Coulter AcT Diff II Haematology Analyser and an average value calculated. HSVECs were then diluted in PBS to a concentration of  $5 \times 10^6$  cells/ml and test substances re-added at appropriate concentrations before addition of the spin probe, CMH (331;332) (Noxygen, Elzach, Germany) to a final concentration of 500  $\mu$ M, determined optimal during previous studies within the laboratory. Cell suspensions were subsequently assessed in triplicate for  $O_2^-$  release in an EPR spectrometer (e-scan R Bruker BioSpin GmbH, Rheinstetten Germany). Between assessments, suspensions were stored at 37°C in an Eppendorf® Thermomixer Compact, shaking at 800 rpm to ensure cells did not re-pellet.

10 mM stock solutions of CMH dissolved in Krebs-HEPES buffer (99 mM NaCl, 4.69 mM KCl, 2.5 mM  $CaCl_2 \cdot 2H_2O$ , 1.2 mM  $MgSO_4 \cdot 7H_2O$ , 25 mM  $NaHCO_3$ , 1.03 mM  $KH_2PO_4$ , 5.6 mM D(+) glucose, 20 mM HEPES, pH 7.4) containing chelating agents, deferoxamine (25  $\mu$ M, Sigma) and Na diethyldithiocarbamate trihydrate (5  $\mu$ M, Sigma) were prepared daily and kept on ice. Krebs-HEPES buffer was prepared using double distilled water and ultra pure chemicals from Sigma with concentrations of Fe and Cu <0.0005 %. Prior to addition of chelators, buffer was sterile-filtered using a 0.22  $\mu$ m filter system.

EPR spectra and kinetics were recorded from cell suspensions in 50  $\mu$ l glass capillary tubes (Hirschmann Laborgeräte, Eberstadt, Germany) at 37°C. Instrument settings were: centre field, 3375 G; modulation amplitude, 2.27 G; sweep time, 5.24 seconds; sweep width, 60 G; and 10 scans. Oxidation of CMH by  $O_2^-$  results in formation of the stable nitroxide

Test Substance	Final Concentration	Incubation Time	Diluent	Source
apocynin	2.5 $\mu$ M	1 hour	DMSO	Sigma-Aldrich, St Louis, MO, U.S.A.
DTPP (328)	1 $\mu$ M	1 hour	ethanol	A generous gift from Dr M. P. Murphy, MRC Mitochondrial Biology Unit, Cambridge, U.K.
DPI	5 $\mu$ M	1 hour	DMSO	Sigma-Aldrich, St Louis, MO, U.S.A.
L-NAME	1 mM	30 minutes	dH <sub>2</sub> O	Sigma-Aldrich, St Louis, MO, U.S.A.
MitoQ <sub>10</sub> (328)	1 $\mu$ M	1 hour	ethanol	A generous gift from Dr M. P. Murphy, MRC Mitochondrial Biology Unit, Cambridge, U.K.
rotenone (228)	0.5 $\mu$ M	2 hours	DMSO	Sigma-Aldrich, St Louis, MO, U.S.A.

**Table 3.1. Test Substances for Electron Paramagnetic Resonance Spectroscopy Experiments.**

DTPP, decyl triphenylphosphonium (TPP) bromide; dH<sub>2</sub>O, distilled water; DMSO, dimethyl sulphoxide; DPI, diphenyleneiodonium chloride; L-NAME, *N*<sup>G</sup>-nitro-L-arginine methyl ester

radical, 3-methoxy-carbonyl (CM) (331). Therefore, the amount of CM formed equals the concentration of the reacting oxidant species. The concentration of CM was determined from the amplitude of the low field component of EPR spectra according to a calibration curve, generated using standard solutions of the 3-carboxy-proxyl (CP) radical (Noxygen). CP standard solutions of 1  $\mu$ M, 5  $\mu$ M and 10  $\mu$ M were prepared from a 1 mM stock solution of CP dissolved in Krebs-HEPES buffer. Counts were recorded once a minute for 10 minutes and  $O_2^-$  formation recorded as  $\mu$ mol/minute.

Measurements of the background activity of PBS +/- test substances to final concentrations, Krebs-HEPES buffer +/- chelators, and CMH dissolved in buffer with chelators to 500  $\mu$ M were routinely carried out prior to assessment of HSVEC  $O_2^-$  release. Signals were not usually observed for PBS +/- diluents and buffer +/- chelators but due to normal auto-oxidation of the probe, CMH dissolved in buffer with chelators produced a low-level background signal which was noted and subtracted from all sample readings obtained that day.

### 3.2.6 HSVEC mRNA Expression

RNA was extracted from HSVECs as per section 2.5 and mRNA expression levels assessed as outlined in section 2.7. Applied Biosystems Custom TaqMan<sup>®</sup> Gene Expression Assays for eNOS (*NOS3*, Hs00167166\_m1), p22<sup>phox</sup> (*CYBA*, Hs00164370\_m1), *SOD1* (Hs00166575\_m1), *SOD2* (Hs00167309\_m1) and *SOD3* (Hs00162090\_m1) were used with TaqMan<sup>®</sup> Endogenous Controls,  $\beta$ -actin (*ACTB*, 4326315E) and *GAPDH* (4326317E) as indicated. Reactions were carried out in singleplex or multiplex as indicated.

### 3.2.7 Western Blot Analysis

Protein was isolated from HSVECs as outlined in section 2.6.1 and protein expression assessed by western blotting as described in section 2.8.1.

### 3.2.7.1 Primary Antibodies

Primary antibodies utilised during this study are listed in Table 3.2.

### 3.2.7.2 Secondary Antibodies

Secondary antibodies utilised during this study are listed in Table 3.3.

### 3.2.7.3 Densitometric Quantification of Protein Bands

Densitometric quantification of protein bands was carried out as outlined in section 2.8.2.

## 3.2.8 Relative Quantitation of HSVEC Mitochondria by qRT-PCR

### 3.2.8.1 DNA Extraction

Total DNA was isolated from HSVECs using the QIAamp<sup>®</sup> DNA Mini Kit (QIAGEN) according to the manufacturer's protocol. Passage 3 HSVECs were pelleted and resuspended in PBS to a final volume of 200 µl before addition of 20 µl QIAGEN Protease (or proteinase K). 200 µl Buffer AL was then added to samples which were subsequently mixed by pulse-vortexing for 15 seconds. Samples were then incubated at 56°C for 10 minutes before 200 µl of 100% ethanol was added and samples mixed again by pulse-vortexing for 15 seconds. Samples were then applied to a QIAamp Mini spin column placed in a collection tube and centrifuged for 1 minute at 6,000 x g. Flow-through was discarded and columns transferred to fresh collection tubes. 500 µl Buffer AW1 was then added to columns and centrifugation carried out as before. Columns were again transferred to clean collection tubes and flow-through discarded before 500 µl Buffer AW2 was added and samples centrifuged at 20,000 x g for 3 minutes. To eliminate the possibility of Buffer



<b>Epitope</b>	<b>Clonality</b>	<b>Host Species</b>	<b>Dilution</b>	<b>Diluent (w/v in TBS-T)</b>	<b>Source</b>
$\alpha$ -p22 <sup>phox</sup> (MW1866)	monoclonal	mouse	1:250	5% fat-free milk powder	Mast, Liverpool, U.K.
$\alpha$ -p22 <sup>phox</sup> (FL-195)	polyclonal	rabbit	1:200	5% fat-free milk powder	Santa Cruz Biotechnology, CA, U.S.A.  (sc-20781)
$\alpha$ -p22 <sup>phox</sup>	monoclonal	mouse	1:1000	5% fat-free milk powder	A generous gift from Prof. M. T. Quinn, Montana State University, Montana, U.S.A.
$\alpha$ -p22 <sup>phox</sup>	polyclonal	rabbit	1:1000	5% fat-free milk powder	A generous gift from Dr. F. Wientjes, University College London, London, U.K.
$\alpha$ -p22 <sup>phox</sup>	monoclonal	mouse	1:1000	5% fat-free milk powder	A generous gift from Prof. D.G. Harrison, Emory University, Atlanta, Georgia, U.S.A.
$\alpha$ -SOD2	monoclonal (clone: 2A1)	mouse	1:3000	5% fat-free milk powder	AbCam, Cambridge, U.K.  (ab16956)

**Table 3.2. Primary Antibodies**

<b>Linked Molecule</b>	<b>Epitope</b>	<b>Host Species</b>	<b>Dilution</b>	<b>Diluent (w/v in TBST)</b>	<b>Source</b>
HRP	$\alpha$ -mouse IgG	rabbit	1:2000	5% fat-free milk powder	Dako-Cytomation, Glostrup, Denmark (#P0260)
HRP	$\alpha$ -rabbit IgG	goat	1:5000	5% fat-free milk powder	Vector Laboratories Inc., Burlingame, CA, U.S.A (#PI-1000)

**Table 3.3 Secondary Antibodies.** IgG, immunoglobulin G

AW2 carryover, collection tubes containing flow-through were discarded and columns placed in fresh tubes for centrifugation at 20,000 x *g* for 1 minute. QIAamp Mini spin columns were transferred to new collection tubes and 200 µl Buffer AE added. Samples were then incubated at room temperature for 1 minute before being centrifuged at 6,000 x *g* for 1 minute to elute. To increase DNA yield, the elution step was repeated using the original volume of Buffer AE. DNA samples were stored at -20°C until time of analysis.

### 3.2.8.2 DNA Quantification

DNA concentrations were quantified using the NanoDrop<sup>®</sup> ND-100 Spectrophotometer and ND-1000 v3.1.0 programme. For each sample, 2 µl DNA was quantified.

### 3.2.8.3 Quantitation of Single-copy Mitochondrial & Nuclear DNA

Using TaqMan<sup>®</sup> probes for single copy nuclear β-haemoglobin (*HBB*, Hs00758889\_s1) and mitochondrially encoded cytochrome b (*MT-CYB*, Hs02596867\_s1) genes, abundance of mtDNA relative to nuclear DNA was determined by calculating Ct (cycle threshold value) ratios for each patient, a variation on the method of Miller and colleagues (333). Singleplex TaqMan<sup>®</sup> real-time RT-PCR reactions were carried out as per section 2.7.2, using 2 µl DNA (12.5 ng/µl) in place of cDNA.

### 3.2.9 Statistical Analysis

Statistical analyses were performed as outlined in section 2.9.

### **3.3 Results**

#### **3.3.1 Endothelial Function**

Endothelium-dependent relaxation was impaired in vessels of patients with CAD compared to those obtained from control subjects (maximum relaxation to A23187,  $43 \pm 16$  vs  $62 \pm 16\%$ ;  $P=0.001$ ; Figure 3.2A). Patients with CAD and T2D had significantly reduced endothelium dependent relaxation compared to those with CAD alone (maximum relaxation to A23187,  $34 \pm 11\%$  vs  $47 \pm 16\%$ ;  $P=0.008$ ; Figure 3.2B).

#### **3.3.2 Vascular Superoxide Production**

Vascular  $O_2^-$  production was greater in patients with CAD compared to control subjects ( $0.752 \pm 0.482$  vs  $0.431 \pm 0.284$  nmol/mg/min;  $P=0.001$ ; Figure 3.3A), as assessed by lucigenin chemiluminescence. Within the group of patients with CAD there was no difference in vascular  $O_2^-$  generation in patients with and without T2D ( $0.640 \pm 0.433$  vs  $0.791 \pm 0.502$  nmol/mg/min;  $P=0.226$ ; Figure 3.3B).

#### **3.3.3 Isolation & Characterisation of HSVECs & HSVSMCs**

HSVECS and HSVSMCs were successfully isolated from both control subjects and patients with CAD. HSVECs showed typical cobblestone morphology and demonstrated positive immunofluorescent staining for the endothelial cell marker, von Willebrand factor (Figure 3.4A). Similarly, HSVSMCs displayed characteristic ‘hill and valley’ morphology and phenotype was further confirmed by positive immunofluorescence for SMC- $\alpha$ -actin (Figure 3.4B). Unfortunately, HSVSMCs demonstrated prohibitively slow growth in culture and, consequently, all subsequent investigation was performed in HSVECs.

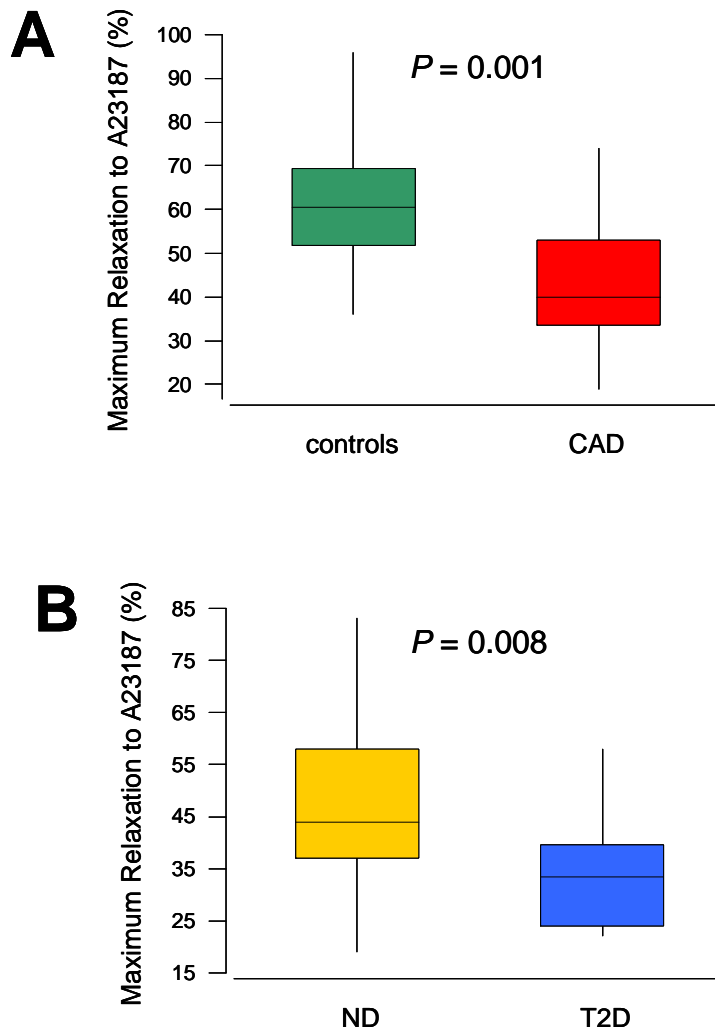


**Figure 3.2. Vasorelaxation in Rings of Saphenous Vein.** Vessel rings were constricted with phenylephrine and maximum relaxation to calcium ionophore A23187 examined and expressed as a percentage of constriction. (A) Endothelium-dependent relaxation was significantly impaired in vessels from patients with CAD (n=49) compared to vessels from controls (n=10). (B) Patients with CAD and type 2 diabetes (T2D, n=14) had significantly reduced endothelium dependent relaxation compared to those with CAD alone (ND, n=35).

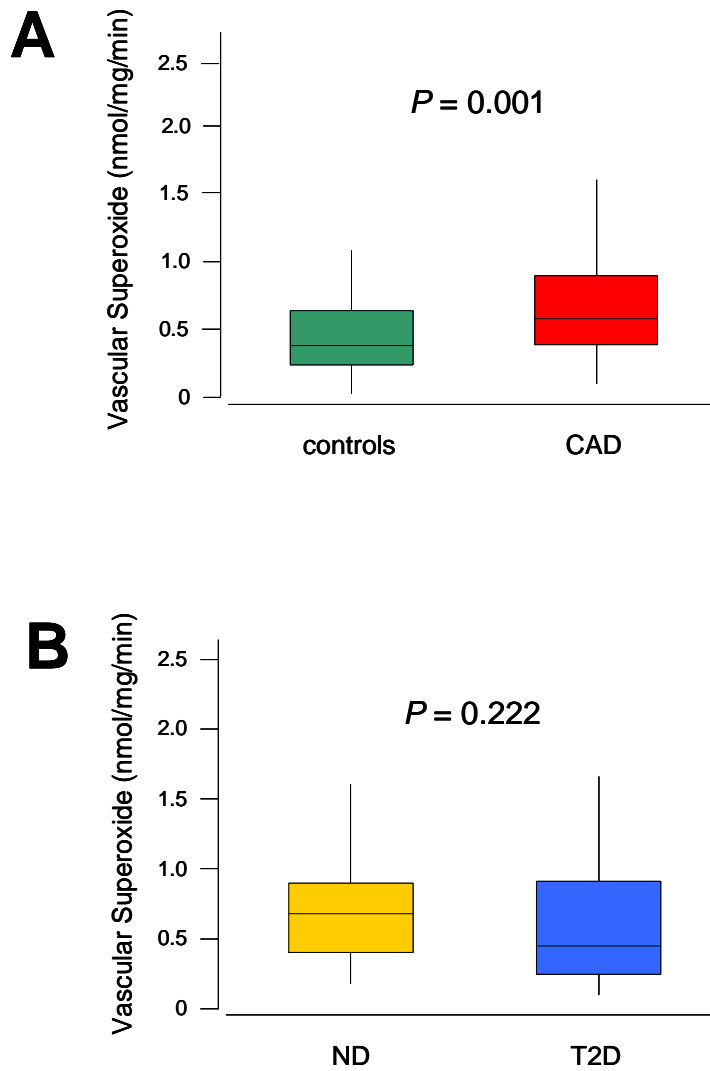


**Figure 3.3. Vascular Superoxide Production.** Superoxide levels in rings of saphenous vein were measured by lucigenin chemiluminescence. (A) Vascular lucigenin chemiluminescence was significantly greater in patients with CAD (n=76) compared to controls (n=19), consistent with elevated superoxide production in these samples. (B) Within the group of patients with CAD, there was no statistically significant difference in vascular lucigenin chemiluminescence between patients with (T2D, n=22) and without (ND, n=54) type 2 diabetes.

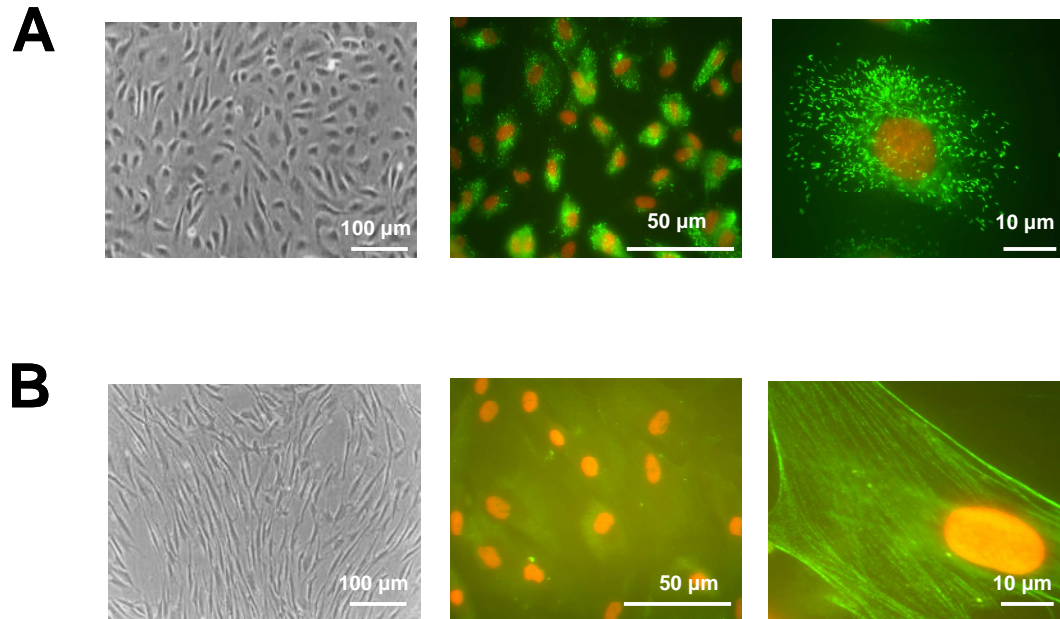


**Figure 3.4 Representative Photomicrographs Showing Vascular Cells in Primary Culture.** (A) Endothelial cells were successfully isolated from portions of human saphenous vein, as determined by characteristic cobblestone morphology (left-hand panel). Endothelial cell phenotype was further confirmed by positive staining (green) for von Willebrand Factor (middle and right-hand panels). (B) Successful isolation of smooth muscle cells from human saphenous vein was determined by observation of characteristic ‘hill and valley’ morphology in culture (left-hand panel) and positive staining (green) for smooth muscle cell- $\alpha$ -actin (middle and right-hand panels). For both cell types, nuclei are stained red (propidium iodide).

### 3.3.4 HSVEC Superoxide Production

#### 3.3.4.1 Lucigenin-Enhanced Chemiluminescence

To determine whether endothelial cells isolated from vascular tissue retained the elevated  $O_2^-$  phenotype, levels of basal  $O_2^-$  production in cultured HSVECs were investigated. Lucigenin chemiluminescence was greater in HSVECs isolated from patients with CAD compared to control subjects ( $16.246 \pm 1.262$  vs  $11.294 \pm 1.024$  nmol/mg/min;  $P=0.0382$ ; Figure 3.5), consistent with elevated  $O_2^-$  production in these samples.

#### 3.3.4.2 Electron Paramagnetic Resonance Spectroscopy

In order to confirm lucigenin chemiluminescence findings showing increased  $O_2^-$  production in HSVECs isolated from CAD patients, EPR spectroscopy was employed. Results demonstrated a trend towards elevated  $O_2^-$  levels in patients with CAD as compared to control subjects but just failed to reach statistical significance ( $0.371 \pm 0.012$  vs  $0.308 \pm 0.019$   $\mu$ mol/min;  $P=0.061$ ; Figure 3.6). On stratifying CAD patients according to the presence or absence of T2D,  $O_2^-$  levels were observed to be elevated in patients with T2D on comparison with control subjects ( $0.391 \pm 0.034$  vs  $0.308 \pm 0.019$   $\mu$ mol/min;  $P=0.058$ ; Figure 3.6) and CAD patients without T2D ( $0.391 \pm 0.034$  vs  $0.360 \pm 0.011$   $\mu$ mol/min;  $P=0.537$ ; Figure 3.6). However, results did not reach statistical significance.

### 3.3.5 HSVEC Superoxide Dismutase Expression

Given results indicating a trend towards increased  $O_2^-$  production in HSVECs isolated from patients with CAD as compared to control subjects and in those CAD patients with T2D as compared to those without, it was of interest to investigate expression of the superoxide dismutases, SOD1, SOD2 and SOD3, in cells from all patient groups.

Expression of *SOD3* mRNA was undetectable in HSVECs from all patient groups.



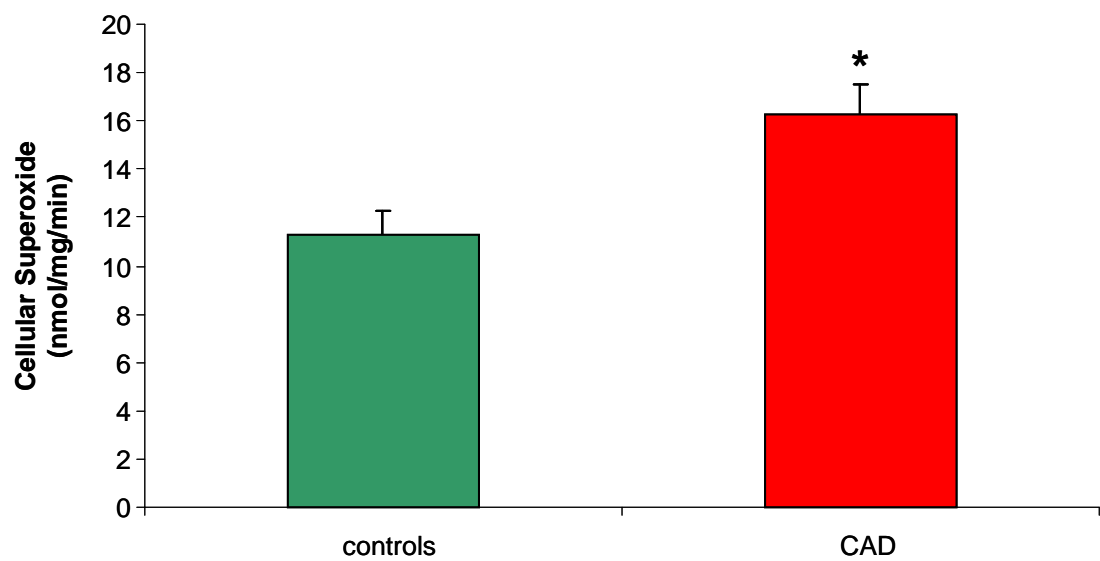


**Figure 3.5 HSVEC Basal Superoxide Production Measured by Lucigenin Chemiluminescence.** Basal superoxide levels were assessed in HSVECs isolated from controls (n=3) and patients with CAD (n=3). Superoxide production was observed to be significantly elevated in HSVECs from patients with CAD as compared to controls. \*,  $P < 0.05$

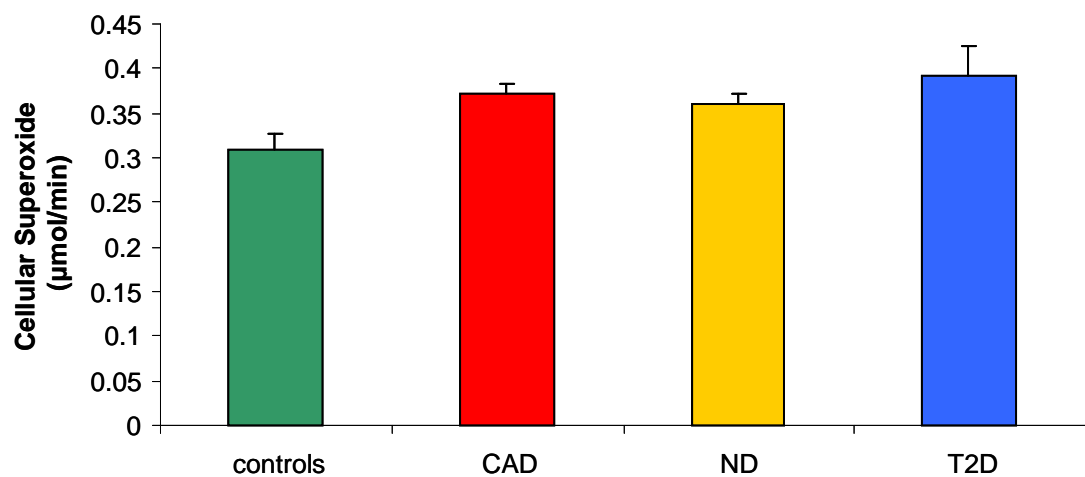


**Figure 3.6. HSVEC Basal Superoxide Production Measured by Electron Paramagnetic Resonance Spectroscopy.** Basal superoxide levels were assessed in HSVECs isolated from controls (n=4) and patients with CAD (n=8). A trend towards elevated superoxide production was observed in HSVECs from patients with CAD as compared to controls but results failed to reach statistical significance. Within the group of patients with CAD, there was a trend towards increased basal superoxide levels in HSVECs from patients with type 2 diabetes (T2D, n=4) as compared to those from patients with CAD alone (ND, n=4) and control subjects but again numbers were not statistically significantly different.

As shown in Figure 3.7, no significant difference in HSVEC *SOD1* mRNA expression was observed between patient groups, although a trend towards increased expression in CAD patients relative to control subjects ( $\Delta\text{Ct}$ ,  $-0.818 \pm 0.335$  vs  $-0.078 \pm 0.313$ ;  $P=0.250$ ) was noted, consistent with elevated  $\text{O}_2^-$  levels in cells from CAD patients. Levels of *SOD1* mRNA appeared slightly lower in HSVECs from CAD patients with T2D than in those with CAD alone ( $-0.669 \pm 0.379$  vs  $-0.846 \pm 0.395$ ;  $P=0.853$ ; Figure 3.7) but, as stated, results failed to reach statistical significance.

Expression of *SOD2* mRNA in HSVECs was found to be increased by approximately three-fold in cells from CAD patients relative to those from control subjects ( $\Delta\text{Ct}$ ,  $-5.522 \pm 0.821$  vs  $-3.904 \pm 1.224$ ;  $P=0.34$ ; Figure 3.8A). When stratified according to T2D status, there was a greater than two-fold increase in *SOD2* expression in cells from CAD patients with T2D as compared to those without ( $\Delta\text{Ct}$ ,  $-6.514 \pm 0.815$  vs  $-5.191 \pm 1.061$ ;  $P=0.338$ ; Figure 3.8B) but results did not reach statistical significance. No significant increase was observed in CAD patients without T2D as compared to controls ( $\Delta\text{Ct}$ ,  $-5.191 \pm 1.061$  vs  $-3.905 \pm 1.203$ ;  $P=0.501$ ; Figure 3.8A) but there was a significant, almost six-fold increase in those CAD patients with T2D ( $\Delta\text{Ct}$ ,  $-6.514 \pm 0.815$  vs  $-3.922 \pm 1.225$ ;  $P=0.044$ ; Figure 3.8A).

This finding was confirmed at protein level (Figure 3.8B) using mouse anti-SOD2 primary antibody and rabbit anti-mouse IgG-HRP secondary antibody. Densitometry revealed significantly increased SOD2 protein expression in cells from patients with CAD relative to controls ( $7.691 \pm 0.353$  vs  $4.766 \pm 0.211$  ODU/ $\text{mm}^2$ ;  $P=0.0001$ ; Figure 3.8C) and in both CAD patients with ( $8.380 \pm 0.131$  vs  $4.766 \pm 0.211$  ODU/ $\text{mm}^2$ ;  $P=0.0002$ ; Figure 3.8C) and without T2D ( $7.232 \pm 0.382$  vs  $4.766 \pm 0.211$  ODU/ $\text{mm}^2$ ;  $P=0.0008$ ; Figure 3.8C) relative to controls. While expression of SOD2 was observed to be greater in cells from CAD patients with T2D as compared to those without ( $8.380 \pm 0.131$  vs  $7.232 \pm 0.382$  ODU/ $\text{mm}^2$ ;  $P=0.107$ ; Figure 3.8C), results were not statistically significant.

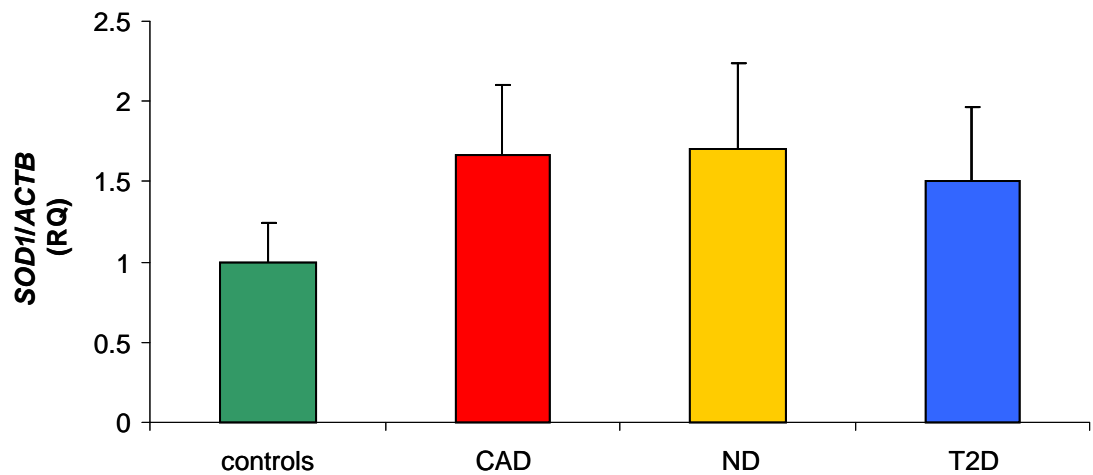


**Figure 3.7. HSVEC *SOD1* mRNA Expression Relative to  $\beta$ -actin (*ACTB*) as Assessed by TaqMan<sup>®</sup> qRT-PCR.** Expression of *SOD1* was investigated in HSVECs isolated from controls (n=6) and patients with CAD (n=23), stratified according to the absence (ND, n=17) or presence (T2D, n=6) of type 2 diabetes. A trend towards increased expression was observed in cells from CAD patients relative to those from controls but results did not reach statistical significance. Reactions were carried out in singleplex. RQ, relative quantitation.

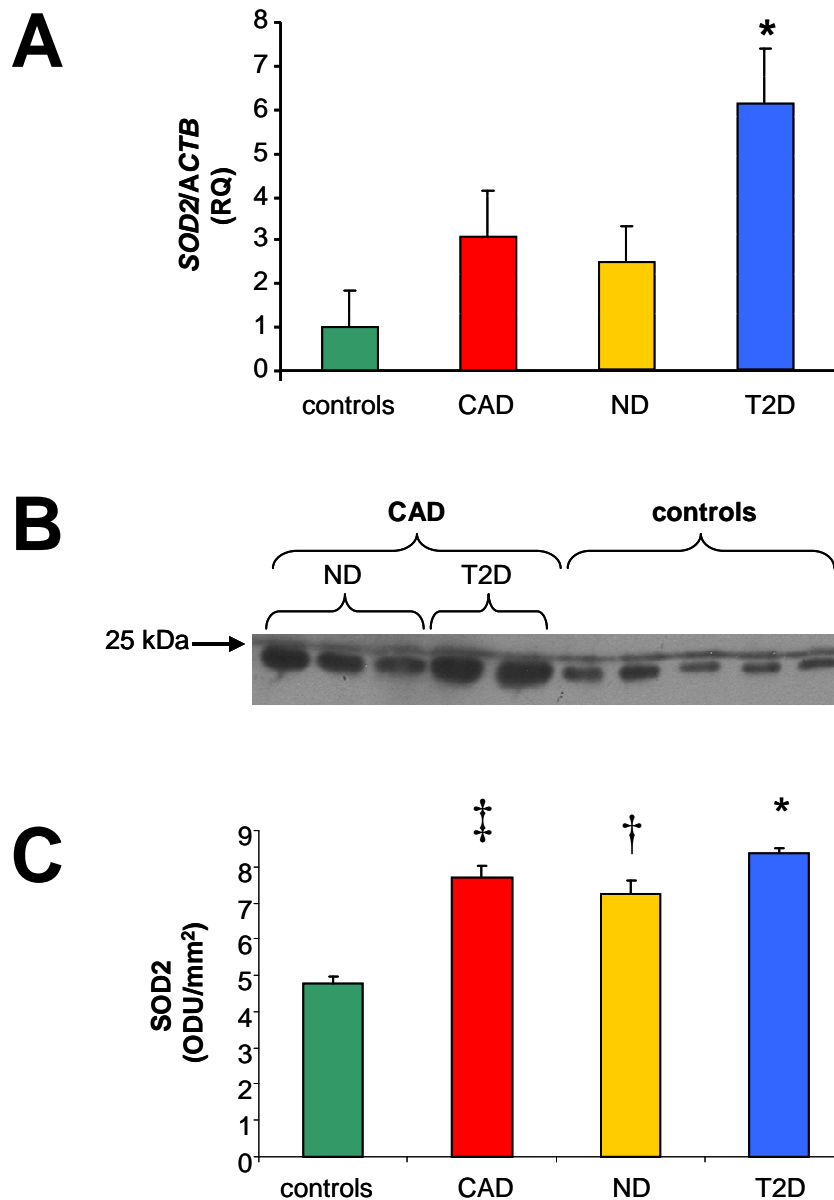


**Figure 3.8. HSVEC SOD2 mRNA and Protein Expression.** (A) Using TaqMan<sup>®</sup> qRT-PCR, expression of *SOD2* relative to  $\beta$ -actin (*ACTB*) was investigated in HSVECs isolated from controls (n=5) and patients with CAD (n=24). Reactions were carried out in singleplex. A trend towards increased expression in cells from CAD patients relative to those from controls was observed. *SOD2* expression was greater in those patients with CAD and type 2 diabetes (T2D, n=6) than in those with CAD alone (ND, n=18) and expression was significantly elevated in T2D patients as compared to controls. \*,  $P < 0.05$  vs controls. (B) *SOD2* protein expression in HSVECs isolated from controls (n=5) and CAD patients (n=5) with (T2D, n=2) and without (ND, n=3) type 2 diabetes was assessed by western blotting. A representative immunoblot is shown. (C) Densitometry revealed significantly increased *SOD2* expression in cells from the CAD patient population as a whole, CAD patients with ND, and CAD patients with T2D relative to controls with the greatest protein expression observed in HSVECs from T2D patients. ‡, †, \*,  $P < 0.001$  vs control.

### 3.3.6 Relative Quantitation of HSVEC Mitochondria by qRT-PCR

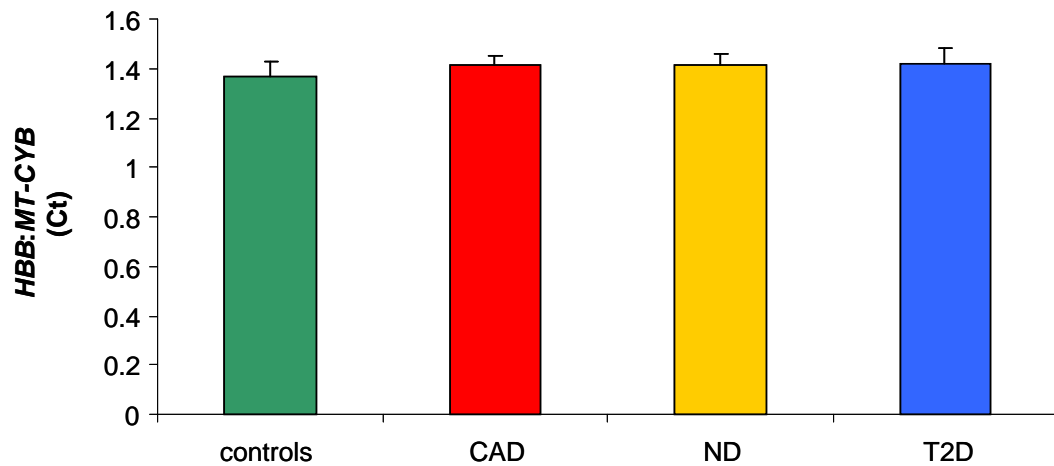
Relative to control subjects, no differences in Ct ratios were observed in the CAD patient population as a whole ( $1.367 \pm 0.062$  vs  $1.416 \pm 0.037$ ;  $P=0.500$ ; Figure 3.9), CAD patients with T2D ( $1.367 \pm 0.062$  vs  $1.421 \pm 0.064$ ;  $P=0.577$ ; Figure 3.9) and patients with CAD alone ( $1.367 \pm 0.062$  vs  $1.412 \pm 0.052$ ;  $P=0.602$ ; Figure 3.9). In addition, Ct ratios were not significantly different between HSVECs from patients with and without T2D ( $1.421 \pm 0.064$  vs  $1.412 \pm 0.052$ ;  $P=0.914$ ; Figure 3.9).

### 3.3.7 Characterisation of Enzymatic Sources of Superoxide Generation

#### 3.3.7.1 Mitochondria

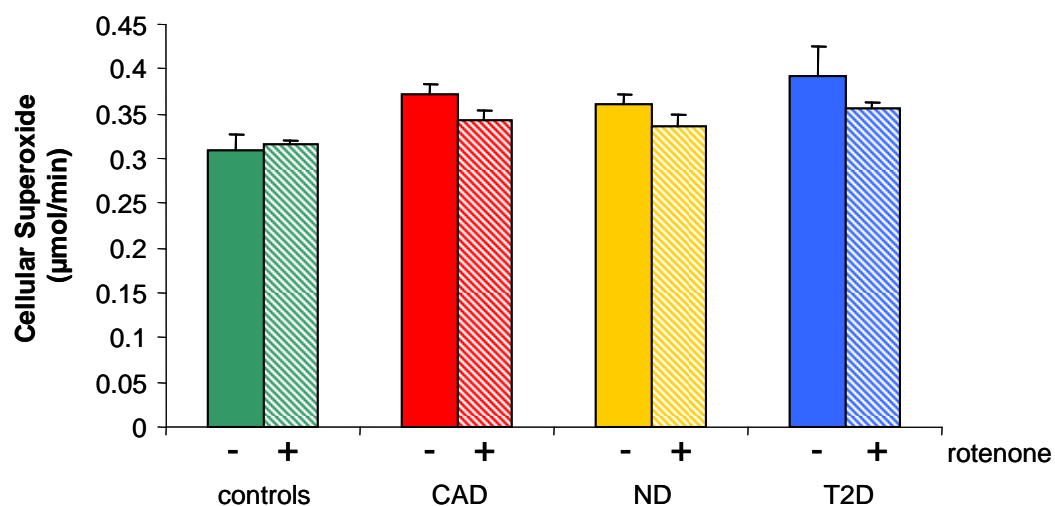
Based on SOD2 expression data (Figure 3.8), it was of interest to investigate mitochondrial  $O_2^-$  production in HSVECs. On pretreating HSVECs with rotenone, the respiratory chain inhibitor, a trend towards a greater reduction in  $O_2^-$  levels in patients with CAD as compared to control subjects, as assessed by EPR spectroscopy, was observed (Figure 3.10). However, the inhibitor caused no significant reduction in basal  $O_2^-$  levels in cells from either control subjects ( $0.308 \pm 0.019$  vs  $0.317 \pm 0.004$   $\mu\text{mol/min}$ ;  $P=0.755$ ; Figure 3.10) or patients with CAD ( $0.371 \pm 0.012$  vs  $0.343 \pm 0.010$   $\mu\text{mol/min}$ ;  $P=0.151$ ; Figure 3.10). On stratifying CAD patients according to T2D status, no significant decreases in basal  $O_2^-$  levels were observed in cells from either patients with CAD and T2D ( $0.391 \pm 0.034$  vs  $0.356 \pm 0.006$   $\mu\text{mol/min}$ ;  $P=0.359$ ; Figure 3.10) or those with CAD alone ( $0.360 \pm 0.011$  vs  $0.336 \pm 0.013$   $\mu\text{mol/min}$ ;  $P=0.297$ ; Figure 3.10).

In the absence of serum, preincubating HSVECs with the mitochondria-targeted antioxidant, MitoQ<sub>10</sub> caused a significant increase, rather than decrease, in basal  $O_2^-$  levels ( $0.400 \pm 0.012$  vs  $0.519 \pm 0.044$   $\mu\text{mol/min}$ ;  $P=0.0233$ ; Figure 3.11A), as determined by EPR spectroscopy. Pretreatment with decylTPP bromide (DTPP), the non-active control for MitoQ<sub>10</sub> (324), had no significant effect on HSVEC basal  $O_2^-$  production ( $0.400 \pm 0.012$  vs  $0.442 \pm 0.008$   $\mu\text{mol/min}$ ;  $P=0.056$ ; Figure 3.11A). In the presence of serum [20%



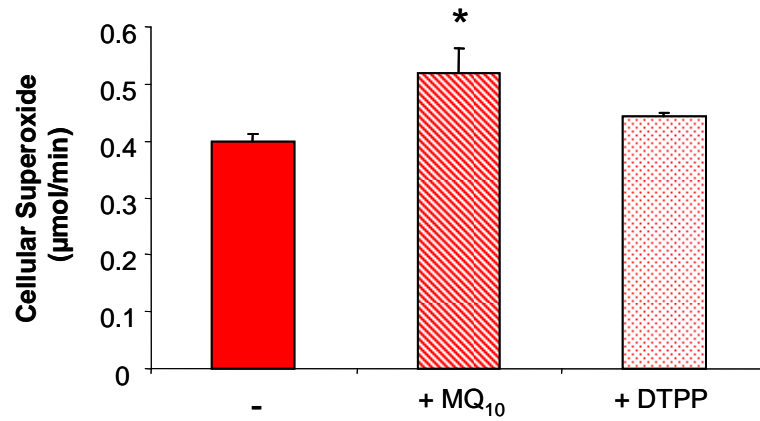
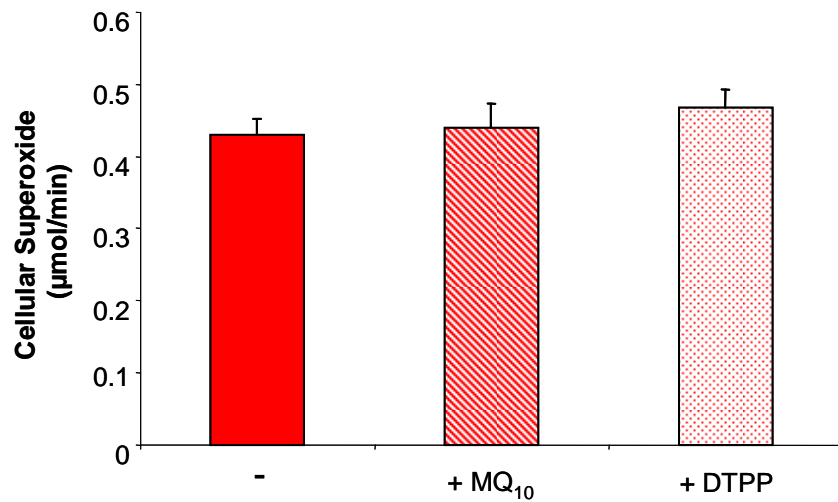
**Figure 3.9. Comparison of HSVEC Mitochondrial Numbers by Polymerase Chain Reaction.**

DNA was extracted from HSVECs isolated from controls (n=3) and patients with CAD (n=7), stratified according to the presence (T2D, n=3) or absence (ND, n=4) of type 2 diabetes. Using TaqMan<sup>®</sup> probes for single copy nuclear  $\beta$ -haemoglobin (*HBB*) and mitochondrially encoded cytochrome b (*MT-CYB*), the abundance of mitochondrial DNA relative to nuclear DNA was determined by calculating Ct (cycle value threshold value) ratios for each patient. No differences in Ct ratio were observed, suggesting mitochondrial numbers are similar between patients, irrespective of disease status.



**Figure 3.10. Effects of Mitochondrial Respiratory Chain Inhibition on HSVEC Superoxide Production as Assessed by Electron Paramagnetic Resonance Spectroscopy.** HSVECs isolated from controls (n=4) and patients with CAD (n=8) were incubated with (+) and without (-) rotenone, an inhibitor of the mitochondrial respiratory chain. CAD patients were stratified according to the presence (T2D, n=4) or absence (ND, n=4) of type 2 diabetes. On preincubation with rotenone, a greater decrease in  $O_2^-$  production in cells from CAD patients as compared to controls was observed, with the slightly larger reduction in CAD patients with T2D. However, results failed to reach statistical significance.



**A****B**

**Figure 3.11. Effects of a Mitochondria-Targeted Antioxidant on HSVEC Superoxide Production as Assessed by Electron Paramagnetic Resonance Spectroscopy.** HSVECs isolated from patients with CAD (n=3) were incubated with (+) and without (-) the mitochondria-targeted antioxidant, MitoQ<sub>10</sub> (MQ<sub>10</sub>), and the non-active control compound, decylTPP bromide (DTPP). (A) In the absence of serum, preincubation with MitoQ<sub>10</sub> resulted in a significant increase in cellular O<sub>2</sub><sup>-</sup> levels, not observed on pretreatment with DTPP. \*, *P* < 0.05. (B) In the presence of serum, neither MitoQ<sub>10</sub> nor DTPP had a significant effect on HSVEC O<sub>2</sub><sup>-</sup> levels.

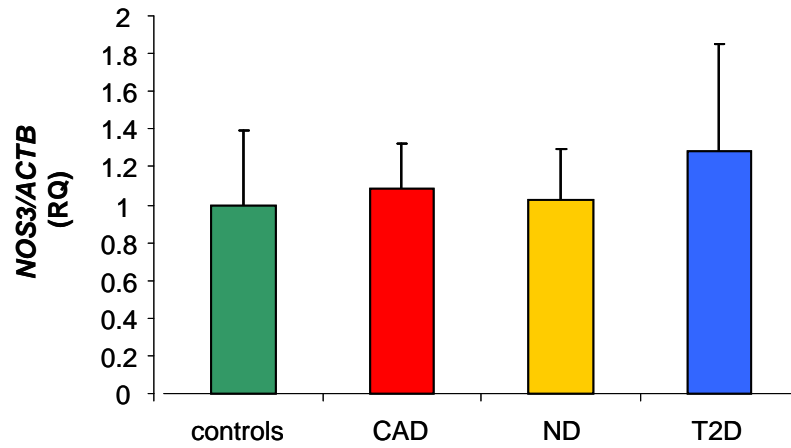
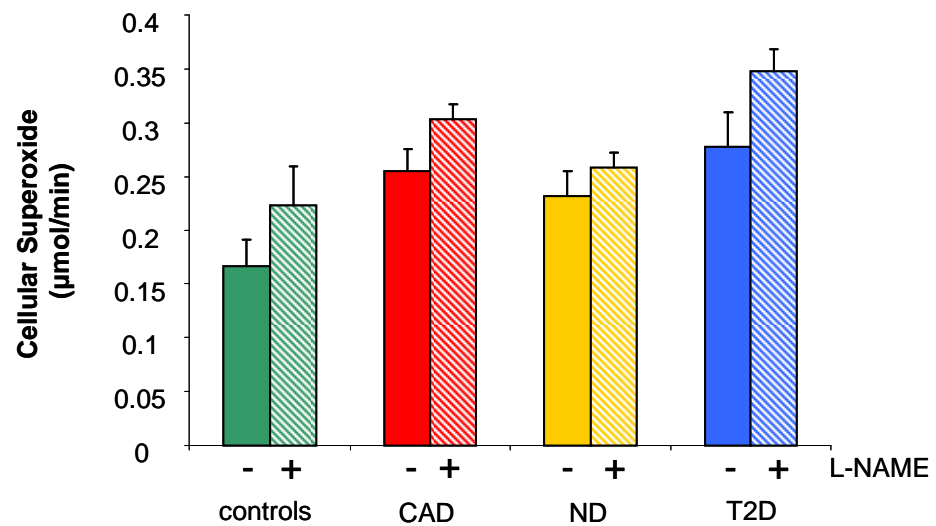
(v/v)], preincubation with neither MitoQ<sub>10</sub> ( $0.430 \pm 0.023$  vs  $0.441 \pm 0.032$   $\mu\text{mol/min}$ ;  $P=0.800$ ; Figure 3.11B ) nor DTPP ( $0.430 \pm 0.023$  vs  $0.468 \pm 0.025$   $\mu\text{mol/min}$ ;  $P=0.496$ ; Figure 3.11B) had a significant effect on cellular O<sub>2</sub><sup>-</sup> levels.

### 3.3.7.2 Endothelial Nitric Oxide Synthase

With results revealing impaired endothelium-dependent relaxation in vessels from patients with CAD (Figure 3.2) and elevated O<sub>2</sub><sup>-</sup> production in both vessels and HSVECs from these patients (Figures 3.3, 3.5 and 3.6), the contribution of uncoupled eNOS to O<sub>2</sub><sup>-</sup> generation in HSVECs from CAD patients was investigated.

Expression studies revealed no difference in *NOS3* mRNA levels between patient groups (Figure 3.12A), consistent with modulation of enzyme activity via post-translational phosphorylation. Relative to control subjects, no differences in expression were observed in the CAD patient population as a whole ( $\Delta\text{Ct}$ ,  $-6.090 \pm 0.482$  vs  $-6.211 \pm 0.279$ ;  $P=0.841$ ; Figure 3.12A), CAD patients with T2D ( $\Delta\text{Ct}$ ,  $-6.090 \pm 0.482$  vs  $-6.447 \pm 0.533$ ;  $P=0.630$ ; Figure 3.12A) and patients with CAD alone ( $\Delta\text{Ct}$ ,  $-6.090 \pm 0.482$  vs  $-6.128 \pm 0.335$ ;  $P=0.952$ ; Figure 3.12A). In addition, *NOS3* expression was not significantly different between HSVECs from patients with and without T2D ( $\Delta\text{Ct}$ ,  $-6.447 \pm 0.533$  vs  $-6.128 \pm 0.335$ ;  $P=0.627$ ; Figure 3.12A). As shown in Figure 4.7, no difference in eNOS protein expression or eNOS Ser1177 phosphorylation was observed between HSVEC lysates from patients with CAD and T2D and those with CAD alone.

Preincubating HSVECs with the eNOS inhibitor, L-NAME resulted in a non-significant, approximately equal, 20% increase in O<sub>2</sub><sup>-</sup> production for all patient groups (Figure 3.12B), as assessed by EPR spectroscopy.

**A****B**

**Figure 3.12. eNOS mRNA Expression & Contribution to Superoxide Production in HSVECs.**

(A) Using TaqMan<sup>®</sup> qRT-PCR, expression of *NOS3* relative to  $\beta$ -actin (*ACTB*) was investigated in HSVECs isolated from controls (n=6) and patients with CAD (n=23), stratified according to the presence (T2D, n=6) or absence (ND, n=17) of type 2 diabetes. Reactions were carried out in multiplex. No difference in expression was observed between patient groups. (B) HSVECs isolated from controls (n=4) and patients with CAD (n=8) were incubated with (+) and without (-) L-NAME. CAD patients were again stratified according to the presence (T2D, n=4) or absence (ND, n=4) of type 2 diabetes. Incubation with L-NAME resulted in a non-significant, approximately 20% increase in  $\text{O}_2^-$  for all patient groups, as assessed by EPR.

### 3.3.7.3 NAD(P)H Oxidase

In order to establish the contribution of NAD(P)H oxidase to  $O_2^-$  production in the endothelium of patients with CAD, mRNA expression of *CYBA*, encoding the enzyme's p22<sup>phox</sup> subunit, was investigated in HSVECs. Results demonstrated no significant difference in *CYBA* mRNA expression between patient groups (Figure 3.13A) although a trend towards increased expression in CAD patients with T2D relative to both control subjects ( $\Delta Ct$  ,4.465  $\pm$  0.384 vs 4.889  $\pm$  0.287;  $P=0.387$ ; Figure 3.13A) and CAD patients without T2D ( $\Delta Ct$  ,4.465  $\pm$  0.384 vs 4.791  $\pm$  0.266;  $P=0.524$ ; Figure 3.13A) was observed.

Attempts to confirm these findings at protein level proved unsuccessful, with failure to observe bands of the correct size on photographic film despite the use of 5 different anti-p22<sup>phox</sup> primary antibodies (Table 3.2) and varying incubation and exposure times.

However, on pretreating HSVECs with the NAD(P)H oxidase inhibitor, DPI, a statistically significant reduction in basal  $O_2^-$  production, as measured by EPR spectroscopy, was observed in cells from CAD patients (0.371  $\pm$  0.012 vs 0.270  $\pm$  0.024  $\mu\text{mol/min}$ ;  $P=0.021$ ; Figure 3.13B) but not in those from control subjects (0.308  $\pm$  0.019 vs 0.300  $\pm$  0.020  $\mu\text{mol/min}$ ;  $P=0.803$ ; Figure 3.13B). Similarly, incubation with apocynin resulted in an approximate 12% reduction in basal  $O_2^-$  levels in HSVECs from patients with CAD (0.371  $\pm$  0.012 vs 0.326  $\pm$  0.032  $\mu\text{mol/min}$ ;  $P=0.263$ ; Figure 3.13B) while only an approximately 3% reduction was observed in cells from control subjects (0.308  $\pm$  0.019 vs 0.298  $\pm$  0.024  $\mu\text{mol/min}$ ;  $P=0.774$ ; Figure 3.13B).

On stratifying patients according to the presence of T2D, incubation with DPI caused a significant, approximate 32% decrease in basal  $O_2^-$  production in HSVECs from patients with CAD alone (0.360  $\pm$  0.011 vs 0.246  $\pm$  0.035  $\mu\text{mol/min}$ ;  $P=0.010$ ; Figure 3.13B) and an approximate 18% decrease in cells from patients with CAD and T2D (0.391  $\pm$  0.034 vs 0.319  $\pm$  0.034  $\mu\text{mol/min}$ ;  $P=0.113$ ; Figure 3.13B). Pretreatment with apocynin resulted in an approximate 16% reduction in basal  $O_2^-$  levels in CAD patients without T2D (0.360  $\pm$  0.011 vs 0.302  $\pm$  0.001  $\mu\text{mol/min}$ ;  $P=0.257$ ; Figure 3.13B) but only an approximately 4% decrease in those patients with CAD and T2D (0.391  $\pm$  0.034 vs 0.375  $\pm$  0.012  $\mu\text{mol/min}$ ;  $P=0.753$ ; Figure 3.13B).

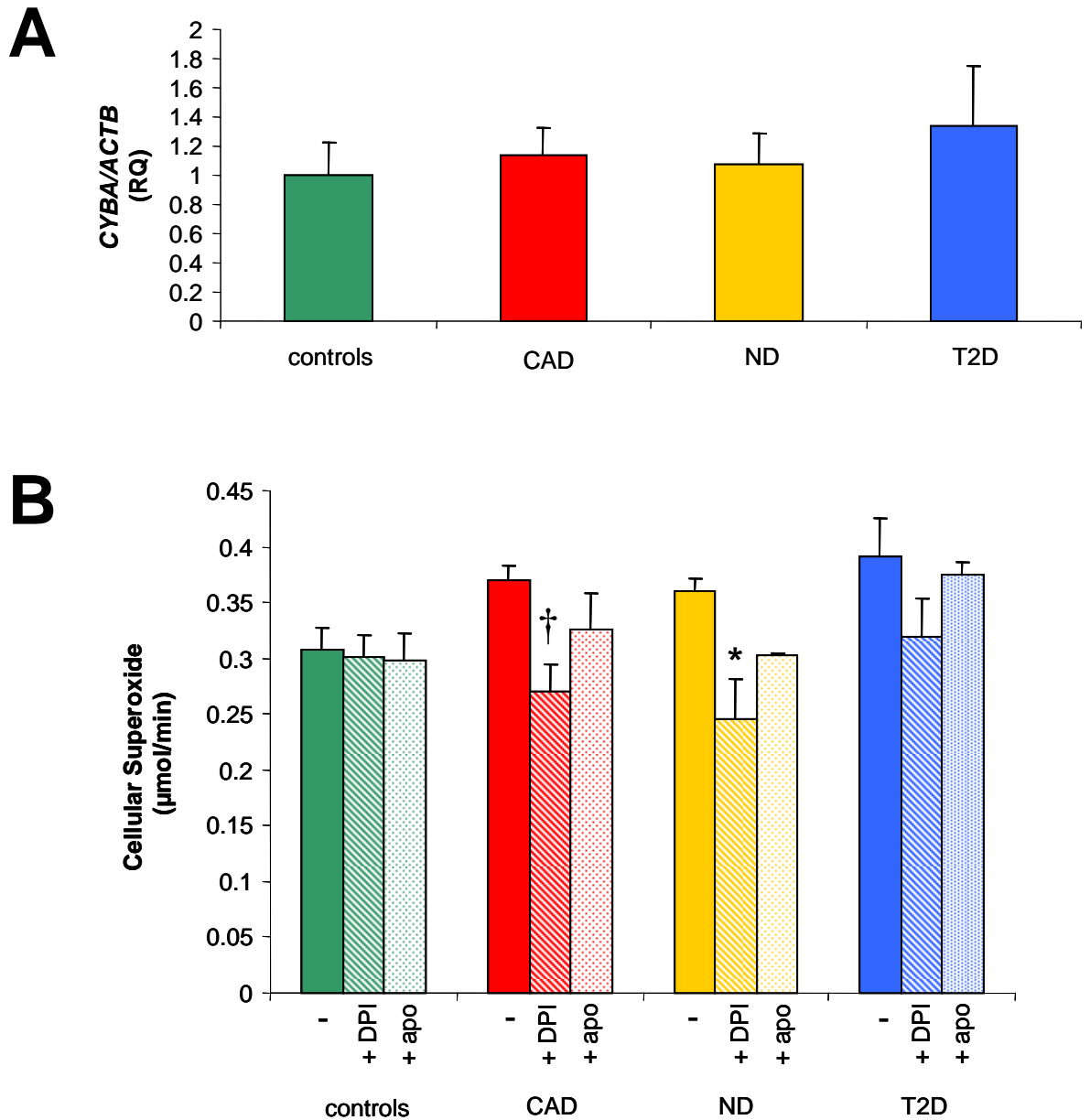


**Figure 3.13. p22<sup>phox</sup> mRNA Expression and NAD(P)H Oxidase Contribution to Superoxide Production in HSVECs.** (A) Using TaqMan<sup>®</sup> qRT-PCR, expression of *CYBA* relative to  $\beta$ -actin (*ACTB*) was investigated in HSVECs isolated from controls (n=7) and patients with CAD (n=23), stratified according to the presence (T2D, n=6) or absence (ND, n=17) of type 2 diabetes. Reactions were carried out in singleplex. No difference in expression was observed between patient groups. (B) HSVECs isolated from controls (n=4) and patients with CAD (n=8) were incubated with (+) and without (-) diphenylene iodonium (DPI) and apocynin (apo) and  $O_2^-$  production investigated using EPR. CAD patients were again stratified according to the presence (T2D, n=4) or absence (ND, n=4) of type 2 diabetes. Preincubation with both inhibitors caused a greater decrease in  $O_2^-$  production in cells from CAD patients as compared to controls, with the larger reduction in ND patients. Pretreatment with DPI caused a greater reduction in  $O_2^-$  levels than pretreatment with apocynin for all patients groups. <sup>†</sup>,  $P < 0.05$  vs untreated (-) cells from CAD patients. <sup>\*</sup>,  $P < 0.05$  vs untreated (-) cells from ND patients.

### **3.4 Discussion**

This study involved comparison of endothelial function and  $O_2^-$  production in human saphenous veins. Previous studies have demonstrated human arterial and venous basal  $O_2^-$  generation are closely related (318;334), such that results were not affected by the choice of vessel. For practical reasons, molecular studies focused on primary endothelial cells isolated from human saphenous veins. However, it is recognised that VSMCs, fibroblasts and other components of the adventitia play important roles in vascular function and pathogenesis.

As stated, endothelial dysfunction occurs in conjunction with CAD (208). Previous investigations within the group have demonstrated endothelial dysfunction in saphenous veins from patients with CAD (159) and results obtained during the course of this project have confirmed these findings (Figure 3.2A). Risk factors for CVD are almost universally associated with a degree of endothelial dysfunction in humans (87) and indeed, abnormal vascular endothelial function is a prominent feature of T2D (100;162). As shown in Figure 3.2B, a significantly greater depression of relaxation to calcium ionophore was observed in saphenous veins from patients with CAD and T2D as compared to those from patients with CAD alone, confirming poorer endothelial function in individuals with this additional CVD risk factor.

Increased vascular oxidative stress has been proposed as one potential mechanism underlying impaired endothelial function in patients with CAD and T2D (179). Investigations carried out within this laboratory have revealed endothelial dysfunction in saphenous veins from CAD patients to be associated with elevated  $O_2^-$  levels throughout the vessel wall (159), but did not consider the effect of T2D on this  $O_2^-$  production. However, a study by Guzik *et al.* has previously demonstrated significantly elevated basal  $O_2^-$  release in saphenous veins from patients with CAD and T2D relative to those with CAD alone (179). The present study served to confirm that  $O_2^-$  generation is increased in vessels from CAD patients as compared to control subjects (Figure 3.3A). However, on comparison of  $O_2^-$  levels in vessels from CAD patients with and without T2D, no statistically significant increase in  $O_2^-$  production in patients with T2D was observed (Figure 3.3B). Conversely, a trend towards reduced vascular  $O_2^-$  production was evident (Figure 3.3B). This phenomenon is likely the result of more aggressive primary and secondary prevention strategies in this vulnerable group of patients (335). Indeed, as

shown in Table 2.1, a higher percentage of study participants with CAD and T2D (78%) were found to have been prescribed ACE inhibitors/ARBs than those with CAD alone (57%). Furthermore, on comparison with T2D patients recruited by Guzik and colleagues (179), participants in the present study were subject to more intensive treatment.

To investigate the molecular basis for the increased  $O_2^-$  production and impaired endothelium-dependent relaxation in vessels from patients with CAD, endothelial cells were isolated from vascular tissue (Figure 3.4A). As isolated cells were maintained in culture for several weeks prior to investigation of  $O_2^-$  production, it seemed likely that the effects of pharmacological treatments would be lost, allowing more accurate insight into endothelial  $O_2^-$  production, particularly in vessels from patients with CAD and T2D. However, an obvious limitation of studying cultured primary endothelial cells is that there is currently no clear evidence to suggest these cells, free from physiological stresses, retain the *in vivo* phenotype.

Using lucigenin chemiluminescence,  $O_2^-$  levels were measured and found to be significantly elevated in HSVECs from patients with CAD relative to control subjects (Figures 3.5), appearing to support results obtained using intact vessel sections and implicating excess  $O_2^-$  production in attenuation of endothelium-dependent relaxation in CAD patients. However, n values were low (n=3) for these experiments and results interpreted with caution.

On increasing patient numbers and assessing  $O_2^-$  production using EPR spectroscopy, a more sensitive technique, a trend towards increased  $O_2^-$  generation was observed in cells isolated from patients with CAD (Figure 3.6) but numbers failed to reach statistical significance, raising the possibility that in culture the *in vivo* phenotype of these cells is not preserved.

The cell permeable spin probe, CMH (332) was used in conjunction with EPR spectroscopy to investigate  $O_2^-$  production. CMH detects both extra- and intracellular  $O_2^-$  (331;332;336) but does not directly react with  $H_2O_2$  (331;337;338). As described, the superoxide dismutases catalyse the conversion of  $O_2^-$  to  $H_2O_2$  and molecular oxygen (188;233;234) and increased SOD2 mRNA and protein expression was observed in HSVECs from patients with CAD (Figure 3.8). These findings provide an alternative explanation for the lack of a significant increase in  $O_2^-$  generation in cells from patients

with CAD and suggest it may be useful to investigate and compare cellular  $\text{H}_2\text{O}_2$  levels in the future.

Despite initial findings of EPR spectroscopy, CAD patients were stratified according to T2D status and  $\text{O}_2^-$  production again measured using EPR. Here, a trend towards increased  $\text{O}_2^-$  production in patients with T2D was observed (Figure 3.6), linking elevated  $\text{O}_2^-$  production in cells of the endothelium to endothelial dysfunction and indicating reduced  $\text{O}_2^-$  levels found in intact vessels could indeed be the result of enhanced pharmacological intervention within this patient group.

With results demonstrating a trend towards increased  $\text{O}_2^-$  production in HSVECs isolated from patients with CAD as compared to control subjects and in those CAD patients with T2D as compared to those without, expression of the superoxide dismutases, SOD1, SOD3 and, as previously mentioned, SOD2, was investigated in cells from all patient groups.

Expression of *SOD3* mRNA was found to be undetectable in cells from both control subjects and patients with CAD. This may be due to the fact that unlike *SOD1* and *SOD2*, expressed throughout the vessel wall, *SOD3* is largely expressed in VSMCs (339). Indeed, studies have shown *SOD3* expression to be lacking in human cultured endothelial cell lines (340;341).

SOD1 is thought to be the predominant SOD isoform in the endothelium (167). Consequently, given the significantly elevated  $\text{O}_2^-$  levels observed in vessels from CAD patients, a significant difference in *SOD1* expression may have been expected between patient groups. However, while a trend towards increased *SOD1* mRNA expression was observed in cells from patients with CAD relative to control subjects (Figure 3.7), consistent with an adaptive response to elevated  $\text{O}_2^-$  production, results did not reach statistical significance, nor was there a significant difference in expression between CAD patients with and without T2D (Figure 3.7). These findings were not surprising given results obtained on assessment of cellular  $\text{O}_2^-$  production by EPR spectroscopy (Figure 3.6). In addition, there is evidence to suggest SOD1 expression is increased in the initial stages of atherosclerosis but decreases as the condition progresses (342) and, as outlined, HSVECs were isolated from vessels of patients with advanced CAD. Furthermore, *SOD1* expression is known to be upregulated in response to shear stress (343), again raising the



question of whether cultured cells retain the *in vivo* phenotype and indicating it may be prudent to examine *SOD1* mRNA expression in vascular tissue homogenates.

Another possible explanation for cellular *SOD1* expression data may centre on the increased expression of *SOD2* mRNA and protein in HSVECs isolated from vessels of patients with CAD (Figure 3.8), an increase clearly demonstrated as not being due to differences in number of mitochondria, as determined by abundance of mtDNA (*MT-CYB*) relative to nuclear DNA (*HBB*) (Figure 3.9). Induction of *SOD2* mRNA expression is known to occur in response to oxidative stress (344), suggesting the increase represents an adaptive response to elevated mitochondrial  $O_2^-$  production in HSVECs from CAD patients, in particular those patients with T2D. Mitochondria may therefore be a principal source of excess  $O_2^-$  production in the endothelium of patients with CAD and T2D.

In order to investigate the contribution of mitochondria to endothelial  $O_2^-$  production in patients with CAD, cells were treated with rotenone, the respiratory chain inhibitor. As shown in Figure 3.10, a trend towards a greater reduction in cellular  $O_2^-$  levels was observed in CAD patients relative to control subjects and in patients with CAD and T2D relative to those with CAD alone. However, reductions in  $O_2^-$  generation were not significant as may have been expected given *SOD2* mRNA and protein expression data (Figure 3.8). Interestingly, O'Malley and colleagues (325) demonstrated rotenone markedly decreased ROS production in bovine aortic endothelial cell (BAEC) mitochondria as detected by fluorescence but had no effect on  $O_2^-$  production as assessed by EPR spectroscopy, while Guzik and colleagues (179) showed rotenone had only a minimal effect on  $O_2^-$  production in saphenous veins from CAD patients. In addition, as previously mentioned, rotenone is not a specific mitochondrial antioxidant (320) and, as such, cells were subsequently treated with MitoQ<sub>10</sub>.

Preincubating cells from CAD patients with MitoQ<sub>10</sub> caused a significant increase, rather than the anticipated decrease, in  $O_2^-$  levels (Figure 3.11A). This increase was not evident on preincubation of cells with the non-active control for MitoQ<sub>10</sub>, DTPP (Figure 3.11A), which comprises the lipophilic TTP cation but lacks the ubiquinone moiety of the antioxidant (324). Despite suggestion that MitoQ<sub>10</sub> acts to reduce mtROS production (326;345-347), like all quinones, it can redox cycle to produce  $O_2^-$ , thus acting as a prooxidant (325;348;349). Indeed, MitoQ<sub>10</sub> has been shown to enhance both mitochondrial and cellular ROS production in intact endothelial cells (348;350). Serum-free conditions

are known to greatly exacerbate MitoQ<sub>10</sub> redox cycling [(324) and personal communication with Dr Michael Murphy, MRC Mitochondrial Biology Unit, Cambridge, U.K.) and, as shown in Figure 3.11, this was confirmed to be the case in HSVECs isolated from patients with CAD. In the presence of serum, pretreatment with MitoQ<sub>10</sub> had no significant effect on HSVEC O<sub>2</sub><sup>-</sup> levels (Figure 3.11B). This result may be explained, at least in part, by data indicating MitoQ<sub>10</sub> reacts poorly with O<sub>2</sub><sup>-</sup> *per se* (351), exerting its antioxidant effect by reacting with products of lipid peroxidation (326;351;352).

With experiments involving rotenone and MitoQ<sub>10</sub> failing to provide conclusive results, it would have been of interest to examine mitochondrial O<sub>2</sub><sup>-</sup> production further in isolated mitochondria by means of EPR spectroscopy (325) or in intact cells using methods such as aconitase inactivation (353) and/or oxidation of the mitochondrially targeted hydroethidine derivative, MitoSOX<sup>™</sup> (Invitrogen) (354;355). Unfortunately, limited vascular material and time constraints meant such investigations were not possible.

As outlined, in addition to mitochondria, uncoupled eNOS is a principal source of O<sub>2</sub><sup>-</sup> production in the endothelium (173). With vessels from CAD patients, particularly those with T2D, displaying attenuated endothelium-dependent relaxation, HSVEC eNOS mRNA expression, phosphorylation and contribution to elevated O<sub>2</sub><sup>-</sup> production were investigated in CAD patients.

It has been suggested that endothelial dysfunction could be due to decreased eNOS expression (170). However, several studies have shown that CVD risk factors are associated with an increase, rather than a decrease, in eNOS expression (356). Increased expression of eNOS in vascular tissue is thought to be a consequence of an excess production of H<sub>2</sub>O<sub>2</sub> which can increase eNOS mRNA expression through transcriptional and posttranscriptional mechanisms (357). No significant difference in HSVEC *NOS3* expression was observed between patient groups (Figure 3.12A), perhaps surprising given elevated levels of SOD2 expression (Figure 3.8), associated with increased H<sub>2</sub>O<sub>2</sub> production (358), in cells from CAD patients. A number of drugs with favourable effects on CAD phenotype, including ACE inhibitors, ARBs and statins, also upregulate eNOS mRNA expression (356). With a high percentage of this study cohort prescribed such medications (Table 2.1), HSVEC *NOS3* expression data may serve to support the hypothesis that effects of pharmacological treatments are not maintained during the cell culture process. Additional findings showed eNOS protein expression and levels of eNOS

Ser1177 phosphorylation to be similar in HSVEC lysates from patients with CAD and T2D and those with CAD alone (Figure 4.7), suggesting no difference in eNOS activity between these patient groups.

Despite the apparent lack of change in HSVEC eNOS expression and activity between patient groups, poorer endothelial function in vessels from CAD patients indicates eNOS may be uncoupled, producing  $O_2^-$  rather than NO. Indeed, previous work within our group demonstrated significantly reduced  $O_2^-$  production in saphenous veins of CAD patients on pretreatment with the eNOS inhibitor, L-NAME (302). Dysfunctional eNOS has also been identified as a source of  $O_2^-$  production in vessels from patients with CAD and T2D (179). However, on preincubating HSVECs with L-NAME, cells from both control subjects and CAD patients demonstrated elevated  $O_2^-$  production (Figure 3.12B). Numbers failed to reach statistical significance, making it difficult to draw a clear conclusion from these findings, but it is possible that in cultured HSVECs, eNOS is not a major source of  $O_2^-$ . HSVEC eNOS may instead reduce vascular  $O_2^-$  release through production of NO, such that inhibiting NO production causes an increase in  $O_2^-$  levels. This has previously been shown to be the case in vessels from CAD patients denuded of endothelium (179). Alternatively, the possibility must be considered that free from physiological stresses, cultured HSVECs do not retain the *in vivo* phenotype. In the future, investigation of cellular NO and ONOO<sup>-</sup> production may provide additional insight into HSVEC eNOS activity.

NAD(P)H oxidase has been shown to be a major source of  $O_2^-$  in intact vessels from patients with CAD (208), in particular those CAD patients with T2D (179). The p22<sup>phox</sup> membrane-bound NAD(P)H oxidase subunit has been identified as crucial for enzymatic function (199) and p22<sup>phox</sup> expression is significantly increased in coronary arteries from patients with CAD relative to those from control subjects (208), and in vessels from CAD patients with T2D as compared to those from patients with CAD alone (179). To date, similar comparisons have not been carried out in primary human vascular endothelial cells. This study found no significant difference in HSVEC p22<sup>phox</sup> mRNA expression between patient groups (Figure 3.13A), indicating the increased expression previously observed by Guzik and colleagues (208) may be specific to arteries or non-endothelial cells of the vasculature.

Attempts to confirm p22<sup>phox</sup> expression data at the protein level proved unsuccessful despite using a number of anti-p22<sup>phox</sup> primary antibodies under a variety of conditions. As described, cellular extracts were used for immunoblotting. Given p22<sup>phox</sup> is a membrane-bound protein, it may have been useful to perform western blotting of cellular membrane preparations. Of note, previous studies have successfully investigated p22<sup>phox</sup> protein expression in vascular homogenates (179;208) and mononuclear cells (210). However, such investigations have not previously been performed in primary human vascular endothelial cells. As a result, with no change in p22<sup>phox</sup> mRNA expression observed, it was necessary to assume a change in protein expression between patient groups would have been unlikely.

In contrast to p22<sup>phox</sup> expression studies, inhibition of endothelial NAD(P)H oxidase indicated enzyme activity *is* altered in individuals with CAD (Figure 3.13B). DPI and apocynin, inhibitors of NAD(P)H oxidase, have been shown to significantly reduce O<sub>2</sub><sup>-</sup> production in intact portions of saphenous veins from CAD patients (159;302;318). Pretreating HSVECs with these inhibitors caused a greater reduction in O<sub>2</sub><sup>-</sup> production in CAD patients than in control subjects (Figure 3.13B). As expected, the greater of these reductions was on preincubation with the less specific of the two inhibitors, DPI, which caused a significant decrease in CAD patients. In addition to NAD(P)H oxidase, DPI inhibits nitric oxide synthases (359), xanthine oxidase (360), mitochondrial complex I (361) and cytochrome P-450 reductase (362). An attempt to address this lack of specificity was made by performing additional experiments involving apocynin which blocks assembly of the NAD(P)H oxidase complex (159). Although not statistically significant, the differential reduction in O<sub>2</sub><sup>-</sup> levels achieved by the two inhibitors implicates the aforementioned flavoproteins in endothelial O<sub>2</sub><sup>-</sup> generation in CAD. However, it has been suggested that apocynin could itself lack selectivity and may require to be metabolised by a peroxidase enzyme in order to become active (363).

Interestingly, both DPI and apocynin were observed to cause a greater decrease in cellular O<sub>2</sub><sup>-</sup> production in patients with CAD alone (Figure 3.13B), suggesting NAD(P)H oxidase may contribute to O<sub>2</sub><sup>-</sup> production to a lesser extent in T2D patients. This finding would support the earlier hypothesis that mitochondria are a major source of O<sub>2</sub><sup>-</sup> generation in the endothelium of patients with CAD and T2D.

While the contribution of xanthine oxidase to  $O_2^-$  generation in HSVECs was not considered during the course of this project, it is recognised that the enzyme has been identified as a key source of ROS production in both coronary arteries (208) and saphenous veins (159;302) from patients with CAD. In light of these published data and results obtained on treating cells with DPI and apocynin, investigation of xanthine oxidase activity and expression may represent a focus of future studies.

In summary, the findings presented in this chapter demonstrate elevated  $O_2^-$  levels and endothelial dysfunction in saphenous veins from patients with CAD, with poorer endothelial function in those CAD patients with the additional CVD risk factor, T2D. Results show increased levels of SOD2 expression in HSVECs from CAD patients, suggesting mitochondria may be a principal source of  $O_2^-$  production in the endothelium of these patients, in particular those with T2D. Findings also suggest that while HSVEC eNOS is not a major source of  $O_2^-$  generation in CAD, NAD(P)H oxidase contributes to excess  $O_2^-$  production in the endothelium of patients with this condition. Taken together, results support the idea that inhibition of vascular NAD(P)H oxidase represents a means of reducing vascular oxidative stress and progression of cardiovascular disease (364;365) and suggest that mitochondrially-targeted antioxidants, such as MitoQ<sub>10</sub>, may have therapeutic potential in patients with CAD and T2D.

## **4. Endothelial AMP-activated Protein Kinase Activity in Coronary Artery Disease**

## **4.1 Introduction**

Vascular endothelial cells are recognised as being highly glycolytic (228;366). Quintero and colleagues confirmed this to be the case in HUVECs, leading them to propose that mitochondria in these cells are not preferentially used for bioenergetic purposes but function primarily in the generation of ROS which act as signalling molecules, facilitating activation of enzymes such as AMPK (228). AMPK is now recognised as a potential target for therapeutic intervention in hyperglycaemia-induced endothelial dysfunction (section 1.5.1). Following the results outlined in Chapter 3, showing that there is increased expression of SOD2 in HSVECs isolated from patients with CAD and T2D, consistent with increased mtROS production, one objective of this project was to investigate the activity and activation of AMPK in the endothelium of patients with T2D.

As outlined in section 1.5, AMPK is a widely conserved serine/threonine protein kinase involved in the regulation of cellular and whole body energy status and has a heterotrimeric structure, comprising a catalytic  $\alpha$ -subunit ( $\alpha 1$  or  $\alpha 2$ ) and regulatory  $\beta$ - ( $\beta 1$ ,  $\beta 2$ ) and  $\gamma$ -subunits ( $\gamma 1$ ,  $\gamma 2$ ,  $\gamma 3$ ) each of which has two or more isoforms that are differentially expressed in various tissues (248). Both  $\alpha 1$  and  $\alpha 2$  catalytic subunits, encoded by *PRKAA1* and *PRKAA2* respectively, are expressed in liver, cardiomyocytes and skeletal muscle (367). However, the  $\alpha 1$  subunit has been identified as the predominant form in endothelial cells (286;297).

Activation of AMPK requires phosphorylation at Thr172 by an AMPKK. Two major AMPKKs have been identified to date, LKB1 and CaMKK (251;253;264). It has been proposed that LKB1 activity is constitutive, such that stimuli that increase the AMP/ATP ratio, including hypoxia, hypoglycaemia and ischemia, inhibit dephosphorylation at Thr172 permitting phosphorylation and activation by LKB1 (248). In contrast, activation of AMPK by  $\text{Ca}^{2+}$  is AMP-independent and mediated by the  $\alpha$  and/or  $\beta$  isoforms of CaMKK (264;265). Very recently, a third upstream kinase, transforming growth factor-1 $\beta$ -activated kinase, or TAK1, has been identified in yeast (368) and appears to be important in cardiac cells (369) but its role in other cell types is still largely undefined. Recent studies have also revealed activation of AMPK via an AMP-independent, ROS-mediated mechanism with NO (370),  $\text{H}_2\text{O}_2$  (296) and  $\text{ONOO}^-$  (289) all observed to activate the kinase in cultured cells.

There are numerous downstream targets of AMPK, including ACC and eNOS. Human ACC1 and ACC2 are phosphorylated and inhibited at Ser80 and Ser220 respectively by AMPK (287) while the kinase phosphorylates and activates eNOS at Ser1177 as previously described (176;282) (section 1.5.2).

The aims of the experimental work outlined in this chapter were as follows:

- (1) to determine whether HSVECs, like HUVECs, favour glycolysis over oxidative phosphorylation;
- (2) to compare AMPK activity in HSVECs isolated from patients with CAD alone and with CAD and T2D;
- (3) to investigate upstream mediators of AMPK activation in HSVECs, including mtROS

## **4.2 Materials & Methods**

### **4.2.1 Study Participants**

Patients with CAD were as described in section 2.2.

### **4.2.2 Human Vascular Tissue & Primary Cell Culture**

Vascular tissue was obtained and prepared as described in section 2.3 and HSVECs isolated, characterised and cultured as outlined in section 2.4. For experimental procedures carried out in Professor Moncada's laboratory (Wolfson Institute For Biomedical Research, University College London), HSVECs were cultured in endothelial cell growth medium, EGM 2 (PromoCell, Heidelberg, Germany), supplemented with 2% (v/v) FCS.



For all experiments, cells were used between passages 3 and 5 and procedures carried out when cells were approximately 80% confluent.

### **4.2.3 Determination of ATP Production in HSVECs**

Determination of the contribution of oxidative phosphorylation and glycolysis to the generation of ATP in HSVECs was carried out in Professor Moncada's laboratory, using the method of Quintero and colleagues (228). HSVECs were grown for 24 hours in 96-well plates [PerkinElmer (Waltham, MA) 3603 clear bottom, black walls, seeding density 10,000 cells per well] in phenol-red free ECM2 supplemented with 2% (v/v) FCS. On the day of the experiment, fresh medium was added and cells pretreated with 20 mM 2-deoxy-D-glucose (2DG) and 0.5  $\mu$ M rotenone (both Sigma-Aldrich Company Ltd). 2DG is a glycolytic pathway inhibitor and rotenone, as stated, is an inhibitor of the mitochondrial respiratory chain (228). ATP was measured by the luciferin/luciferase method with the PerkinElmer ATPlite<sup>™</sup> Luminescence Assay System, following the manufacturer's protocol. Chemiluminescence was determined in a TopCount (Packard Biosciences) and data analysed in Excel (Microsoft).

### **4.2.4 Western Blot Analysis**

Cell lysates were prepared as outlined in section 2.6.3 unless experiments involved treatment of cells with AICAR, the artificial activator of AMPK. For these experiments, serum-free medium was removed following overnight incubation and replaced with 5 ml KRH buffer +/- 2 mM AICAR (Sigma). Cells were then incubated for 1 hour at 37°C in a CO<sub>2</sub>-free incubator and lysates prepared as previously described. Total protein concentration of each sample was determined by Pierce BCA Protein Assay according to the manufacturer's protocol and using the Wallac Victor<sup>2</sup> plate reader. Western blots were then carried out as outlined in sections 2.8.1 unless otherwise indicated.

#### 4.2.4.1 Primary Antibodies

Primary antibodies utilised during this study are listed in Table 4.1.

#### 4.2.4.2 Secondary Antibodies

Secondary antibodies utilised during this study are listed in Table 4.2.

#### 4.2.4.3 AMPK Thr172 Phosphorylation at Different Oxygen Concentrations

Western blots to assess AMPK Thr172 phosphorylation at different O<sub>2</sub> concentrations were carried out in Professor Moncada's laboratory, using the method of Quintero and colleagues (228). On the day of the experiment, fresh medium was added and hypoxia achieved by incubating cells at 37°C in an O<sub>2</sub>-controlled hypoxic chamber (Coy Laboratory Products, Ann Arbor, MI) for 2 hours. Cells were washed with PBS, scraped off in ice-cold PhosphoSafe™ Extraction Buffer (Novagen, Nottingham, U.K.) and centrifuged for 10 minutes at 13,000 x g (4°C). From clear supernatants, protein concentration was determined using the Bio-Rad DC Protein Assay kit (Bio-Rad, Herts, U.K.) using bovine serum albumin (BSA) as control. Sample aliquots were boiled for 2 minutes, and 20 µg of total protein with equal volumes of reducing loading dye electrophoresed in precast SDS/PAGE 4-15% gradient gels (Bio-Rad). Full Range Rainbow Molecular Weight Markers were included on blots. Proteins were transferred onto Hybond-P nitrocellulose membranes overnight at 25 volts in transfer buffer and assessed for equal loading / transference by Ponceau S Solution (Sigma-Aldrich) staining. Membranes were then blocked (with shaking) in TBS-T + 5% (w/v) fat-free milk powder for approximately 45 minutes before a five hour incubation at 4°C (with shaking) in a rabbit anti-phospho-AMPK-α<sub>1</sub>-Thr-172 primary antibody solution, followed by a 45 minute incubation with HRP-conjugated goat anti-rabbit IgG. ECL (GE Healthcare) was used for detection. Films were exposed for between 30 seconds and 5 minutes and developed in a Kodak X-OMAT 1000.

<b>Epitope</b>	<b>Clonality</b>	<b>Host Species</b>	<b>Dilution</b>	<b>Diluent (w/v in TBS-T)</b>	<b>Source</b>
$\alpha$ -ACC1 N-term (cDEP)	polyclonal	sheep	1:1000	5% fat-free milk powder	A generous gift from Prof. D.G. Hardie, University of Dundee, Dundee, U.K.  CDEPSPLAKTLEL NQ (C + residues 2-15 of rat ACC) coupled to KLH
$\alpha$ -ACC Ser79	polyclonal	rabbit	1:1000	5% BSA	Cell Signalling Technology, Beverly, MA, U.S.A. (#3661)
$\alpha$ -AMPK $\alpha$ 1	polyclonal	sheep	1:1000	5% fat-free milk powder	A generous gift from Prof. D.G. Hardie (371)
$\alpha$ -AMPK $\alpha$ 2	polyclonal	sheep	1:1000	5% fat-free milk powder	A generous gift from Prof. D.G. Hardie (371)
$\alpha$ -AMPK $\alpha$ 1 Thr172	polyclonal	rabbit	1:1000	5% BSA	Cell Signalling Technology, Beverly, MA, U.S.A. (#2531)
$\alpha$ -CaMKK $\alpha$	monoclonal (clone: F-2)	mouse	1:200	5% fat-free milk powder	Santa Cruz Biotechnology, CA, U.S.A. (sc-17827)
$\alpha$ -eNOS	polyclonal	rabbit	1:5000	1% BSA	Sigma-Aldrich, St Louis, MO, U.S.A. N2643
$\alpha$ -eNOS Ser1177	polyclonal	rabbit	1:1000	5% BSA	Cell Signalling Technology, Beverly, MA, U.S.A. (#9571)

**Table 4.1. Primary Antibodies** – continued overleaf

$\alpha$ -LKB1	polyclonal	sheep	1:500	5% fat-free milk powder	<p>A generous gift from Prof. D.G. Hardie</p> <p>LKB1 antibody was raised against the whole protein in sheep and purified using protein G.</p>
----------------	------------	-------	-------	-------------------------	--

**Table 4.1. Primary Antibodies.** BSA, bovine serum albumin; KLH, keyhole limpet haemocyanin

Linked Molecule	Epitope	Host Species	Dilution	Diluent (w/v in TBST)	Source
HRP	$\alpha$ -mouse IgG	sheep	1:1000	5% fat-free milk powder or BSA	GE Healthcare U.K. Ltd, Bucks, U.K. (#NA 931)
HRP	$\alpha$ -rabbit IgG	goat	1:5000	5% fat-free milk powder	Vector Laboratories Inc., Burlingame, CA, U.S.A. (#PI-1000)
HRP	$\alpha$ -rabbit IgG	donkey	1:1000	5% fat-free milk powder or BSA	GE Healthcare U.K. Ltd, Bucks, U.K. (#NA 934)
HRP	protein G–peroxidase from <i>streptococcus</i> sp.	n/a	1:1000	5% fat-free milk powder or BSA	Sigma-Aldrich, St Louis, MO, U.S.A. (#P8170)

**Table 4.2. Secondary Antibodies.** BSA, bovine serum albumin; IgG, immunoglobulin G; n/a, not applicable

#### 4.2.4.4 Densitometric Quantification of Protein Bands

Densitometric quantification of protein bands, relative to an internal invariant control was carried out as outlined in section 2.8.2.

#### 4.2.5 *PRKAA1* & *PRKAA2* mRNA Expression

RNA was extracted from HSVECs as per section 2.5 and *PRKAA1* and *PRKAA2* mRNA expression levels assessed as outlined in section 2.7 using Applied Biosystems Custom TaqMan<sup>®</sup> Gene Expression Assays for *PRKAA1* (Hs01562315\_m1) and *PRKAA2* (Hs00178903\_m1) and TaqMan<sup>®</sup> Endogenous Control, *GAPDH* (4326317E). Reactions were carried out in singleplex.

#### 4.2.6 AMPK Activity Assay

AMPK was immunoprecipitated from lysates and assayed using the SAMS substrate peptide (HMRSAMSGHLVKRR), employing a variation on the method of Davies *et al.* (372) as outlined by Hardie and colleagues (373). SAMS peptide was synthesised by Pepceuticals Ltd (Nottingham, U.K.).

##### 4.2.6.1 Preparation of HSVEC Lysates

Cell lysates were prepared as outlined in section 2.6.3 unless experiments involved treatment of cells with test substances, AICAR (2 mM), MitoQ<sub>10</sub> (1 µM) and DTPP (1 µM). Concentrations of test substances were obtained from relevant literature (176;328). Serum-free medium was removed following overnight incubation and replaced with 5 ml KRH buffer +/- test substances as indicated. Cells were then incubated for 1 hour at 37°C in a CO<sub>2</sub>-free incubator and lysates prepared as previously described. Total protein

concentration of each sample was determined by Pierce BCA Protein Assay kit according to the manufacturer's protocol and using the Wallac Victor<sup>2</sup> plate reader.

#### 4.2.6.2 Immunoprecipitation of AMPK

5  $\mu$ l (packed volume) of Protein G-Sepharose<sup>TM</sup> 4 Fast Flow beads (GE Healthcare) were washed by centrifugation (14,000 x g, 20 seconds, 4°C) with 3 x 1 ml of immunoprecipitate (IP) buffer [50 mM Tris-HCl, pH 7.4 at 4°C, 150 mM NaCl, 50 mM NaF, 5 mM Na<sub>4</sub>P<sub>2</sub>O<sub>7</sub>, 1 mM EDTA, 1mM EGTA: 1 x stock was prepared and before use 1mM dithiothreitol (DTT), 0.1 mM benzamidine, 0.1 mM PMSF, 5  $\mu$ g/ml soybean trypsin inhibitor, 1mM NaVO<sub>3</sub>, 1% (v/v) glycerol, 1% (v/v) Triton X-100 (final concentrations) were added]. Beads were then resuspended in 200  $\mu$ l IP buffer. 2  $\mu$ g per sample of affinity-purified sheep anti-AMPK $\alpha$ 1 and  $\alpha$ 2 catalytic subunit isoform-specific antibodies were added to the Protein G-Sepharose<sup>TM</sup> slurry which was subsequently mixed by rotating for 1 hour at 4°C.

The slurry was then centrifuged (14,000 x g, 3 minutes, 4°C), supernatant removed and the remaining pellet washed, as before, with 1 ml ice cold IP buffer. The final pellet was resuspended in a volume of IP buffer sufficient to allow for one 20  $\mu$ l slurry aliquot per sample. To each 20  $\mu$ l aliquot, 200  $\mu$ g of cell lysate was added and final volumes made approximately equal by adding 200  $\mu$ l IP buffer per sample. Samples were then mixed by rotating for 2.5 hours at 4°C.

Following mixing, samples were centrifuged (14,000 x g, 3 minutes, 4°C) and supernatants removed before pellets were washed with 2 x 1ml ice-cold IP buffer containing 1 M NaCl (to remove non-specifically bound protein), 2 x 1 ml ice-cold IP buffer and, finally, 1 x 1 ml HEPES-Brij buffer [50 mM HEPES, pH 7.4, 1 mM DTT, 0.02% (v/v) Brij-35 (Sigma)]. All washes were by means of centrifugation at 14,000 x g and 4°C for 20 seconds. After the final wash, as much supernatant as possible was removed and immunoprecipitates frozen at -20 °C until activity assays were performed.

#### 4.2.6.3 Assaying AMPK Activity

Reaction mixtures (20  $\mu$ l) containing 5  $\mu$ l HEPES-Brij buffer, 5  $\mu$ l 1 mM AMP in HEPES-Brij buffer, 5  $\mu$ l 1 mM SAMS peptide in HEPES-Brij buffer and 5  $\mu$ l immunoprecipitate resuspended in HEPES-Brij buffer were prepared on ice and the reaction initiated by the addition of 5  $\mu$ l [ $\gamma$ - $^{32}$ P]ATP (Amersham) solution [1 mM [ $\gamma$ - $^{32}$ P]ATP with a specific activity in the range of 250,000 to 500,000 counts per minute per nmol (cpm nmol $^{-1}$ ), and 25 mM MgCl $_2$ ]. For each sample, reactions were carried out in duplicate. Negative control reactions were prepared for all samples by substituting SAMS with HEPES-Brij buffer. After incubation at 30°C for 10 minutes, 15  $\mu$ l of reaction mixture was removed and spotted onto 1 cm $^2$  pieces of P-81 phosphocellulose paper (Whatman plc, Kent, U.K.). Paper was then dropped into 1% (v/v) phosphoric acid to stop the reaction. The P-81 paper squares were washed in fresh phosphoric acid 3 times and then rinsed with water. Incorporation of  $^{32}$ P into the substrate peptide was determined by liquid scintillation counting using a LS 6500 Scintillation Counter [Beckman Coulter (U.K.) Ltd - Biomedical Research, Bucks, U.K] after immersing filters in Ecoscint scintillation fluid [National Diagnostics (U.K.) Ltd, Yorkshire, U.K.]

#### 4.2.7 Statistical Analysis

Statistical analyses were performed as outlined in section 2.9.

### **4.3 Results**

#### **4.3.1 HSVEC ATP Production**

In HSVECs isolated from 3 patients with CAD, on comparison with untreated cells, there was a greater decrease in intracellular ATP generation on pretreatment with 2DG (118.96  $\pm$  5.26 vs 36.26  $\pm$  2.11  $\mu$ mol/10 $^6$  cells;  $P$ <0.0001; Figure 4.1) than on pretreatment with



rotenone ( $118.96 \pm 5.26$  vs  $100.90 \pm 5.26$   $\mu\text{mol}/10^6$  cells;  $P=0.175$ ; Figure 4.1) and an additive effect when inhibitors were used in combination ( $118.96 \pm 5.26$  vs  $7.62 \pm 6.85$   $\mu\text{mol}/10^6$  cells;  $P<0.0001$ ; Figure 4.1).

### **4.3.2 Effect of Oxygen Concentration on HSVEC AMPK Thr172 Phosphorylation**

Western blotting to assess AMPK activation in HSVECs isolated from patients with CAD revealed marked phosphorylation of the enzyme across a range of oxygen concentrations, including 21% O<sub>2</sub> or 'normoxia' (Figure 4.2).

### **4.3.3 HSVEC AMPK Activity**

Based on results shown in Figure 4.2, total AMPK activity was assessed in HSVEC lysates from cells cultured at 21% O<sub>2</sub> using a synthetic peptide kinase assay. As shown in Figure 4.3, AMPK activity was increased in cells from patients with CAD as compared to those from control subjects ( $0.045 \pm 0.007$  vs  $0.022 \pm 0.006$  nmol/min/mg;  $P=0.046$ ). On comparison with control subjects, a greater increase in AMPK activity was observed in HSVECs from patients with CAD and T2D ( $0.062 \pm 0.011$  vs  $0.022 \pm 0.006$  nmol/min/mg;  $P=0.007$ ; Figure 4.3) than in cells from patients with CAD alone ( $0.031 \pm 0.005$  vs  $0.022 \pm 0.006$  nmol/min/mg;  $P=0.261$ ; Figure 4.3). AMPK activity was also significantly higher in HSVECs from patients with CAD and T2D than in those from patients with CAD alone ( $0.062 \pm 0.011$  vs  $0.031 \pm 0.005$  nmol/min/mg;  $P=0.014$ ; Figure 4.3). Treating cells with AICAR resulted in an equal, approximately two- to three-fold, increase in kinase activity for all patient groups (Figure 4.3).

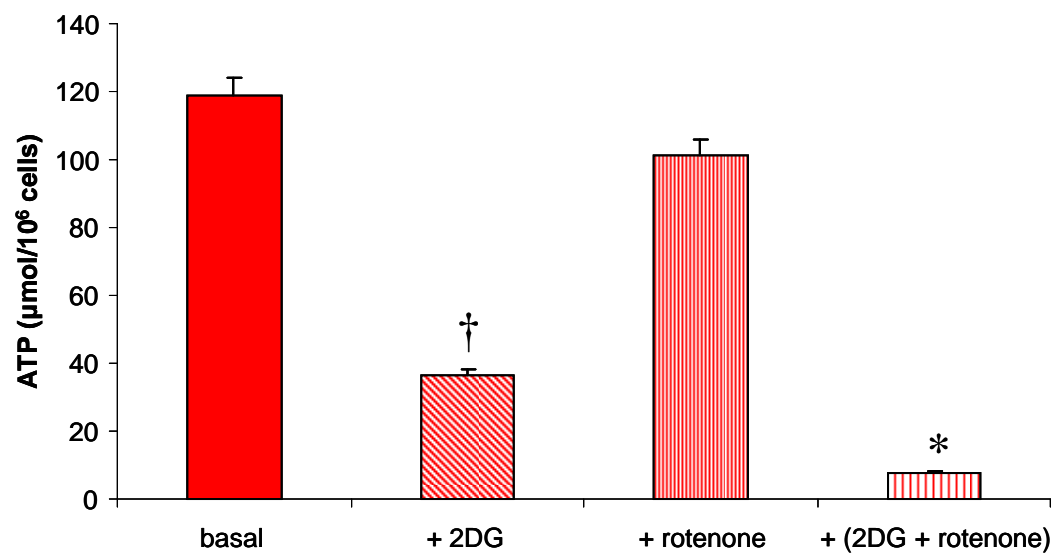


**Figure 4.1. ATP Production in HSVECs.** Using the luciferin/luciferase method, ATP production was assessed in HSVECs isolated from CAD patients (n=3). HSVECs were pretreated with (+) the glycolytic pathway inhibitor, 2-deoxy-D-glucose (2DG), and rotenone, an inhibitor of the mitochondrial respiratory chain. \*, †  $P < 0.0001$  relative to basal values for untreated cells.

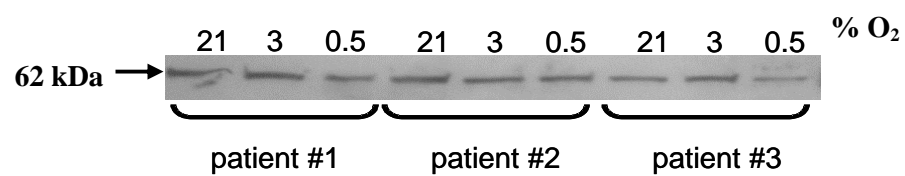


**Figure 4.2. Effect of Oxygen Concentration on AMPK $\alpha$ 1 Thr172 Phosphorylation in HSVECs from CAD Patients.** HSVECs isolated from 3 patients with CAD were incubated for 2 hours at different oxygen (O<sub>2</sub>) concentrations (21%, 3% and <0.5%) in a controlled hypoxic chamber and AMPK Thr172 phosphorylation assessed by western blotting of cell lysates.

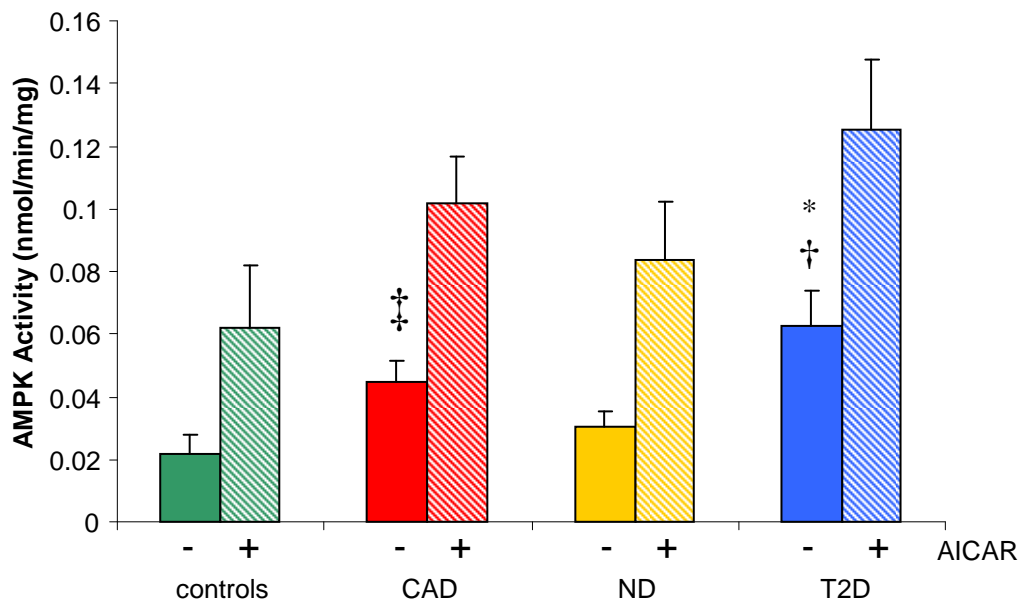


**Figure 4.3. Comparison of Total AMPK Activity in Immunoprecipitates from HSVEC Lysates Cultured at 21% Oxygen.** HSVEC lysates were prepared from cells isolated from control subjects (n=8) and patients with CAD (n=10). These CAD patients were stratified according to absence (ND, n=5) or presence (T2D, n=5) of type 2 diabetes. Cells were incubated with (+) and without (-) AICAR. ‡,  $P < 0.05$  and †,  $P < 0.01$  vs control subjects. \*,  $P < 0.05$  vs CAD patients without diabetes. Incubation with AICAR resulted in a non-significant, approximately two- to three-fold increase in AMPK activity for all patient groups.

AMPK activation at 21% O<sub>2</sub> was further investigated and compared in HSVECs from CAD patients with and without T2D by means of western blot analysis using sheep anti-AMPK $\alpha$ 1 and rabbit anti-AMPK $\alpha$ 1 Thr172 primary antibodies with donkey anti-rabbit IgG and protein G-peroxidase secondary antibodies respectively (Figure 4.4A). Patient samples were compared to an internal invariant control sample. Densitometry revealed no statistically significant difference in AMPK $\alpha$ 1 expression between patient groups (Figure 4.4B) and showed preincubating cells with AICAR had no effect on protein expression (Figure 4.4B). Densitometrical analysis demonstrated a trend towards higher levels of phosphorylation of AMPK $\alpha$ 1 in cells from CAD patients with T2D but results did not reach statistical significance (Figure 4.4C). Treatment with AICAR caused an approximately equal, three-fold increase in AMPK phosphorylation in HSVECs from both patient groups (Figures 4.4A and 4.4C).

#### **4.3.4 HSVEC *PRKAA1* & *PRKAA2* mRNA Expression**

Despite increased AMPK activity in HSVECs from patients with CAD, no change in mRNA expression of *PRKAA1*, encoding the AMPK $\alpha$ 1 catalytic subunit, was observed between patient groups (Figure 4.5), consistent with modulation of AMPK activity via post-translational phosphorylation.

Expression of *PRKAA2* mRNA, encoding the  $\alpha$ 2 subunit, was undetectable in HSVECs.

#### **4.3.5 HSVEC AMPK Substrate Phosphorylation**

Given the increased AMPK activity observed in HSVECs from patients with CAD, it was of interest to investigate phosphorylation of AMPK substrates, ACC and eNOS, in cells from these patients.

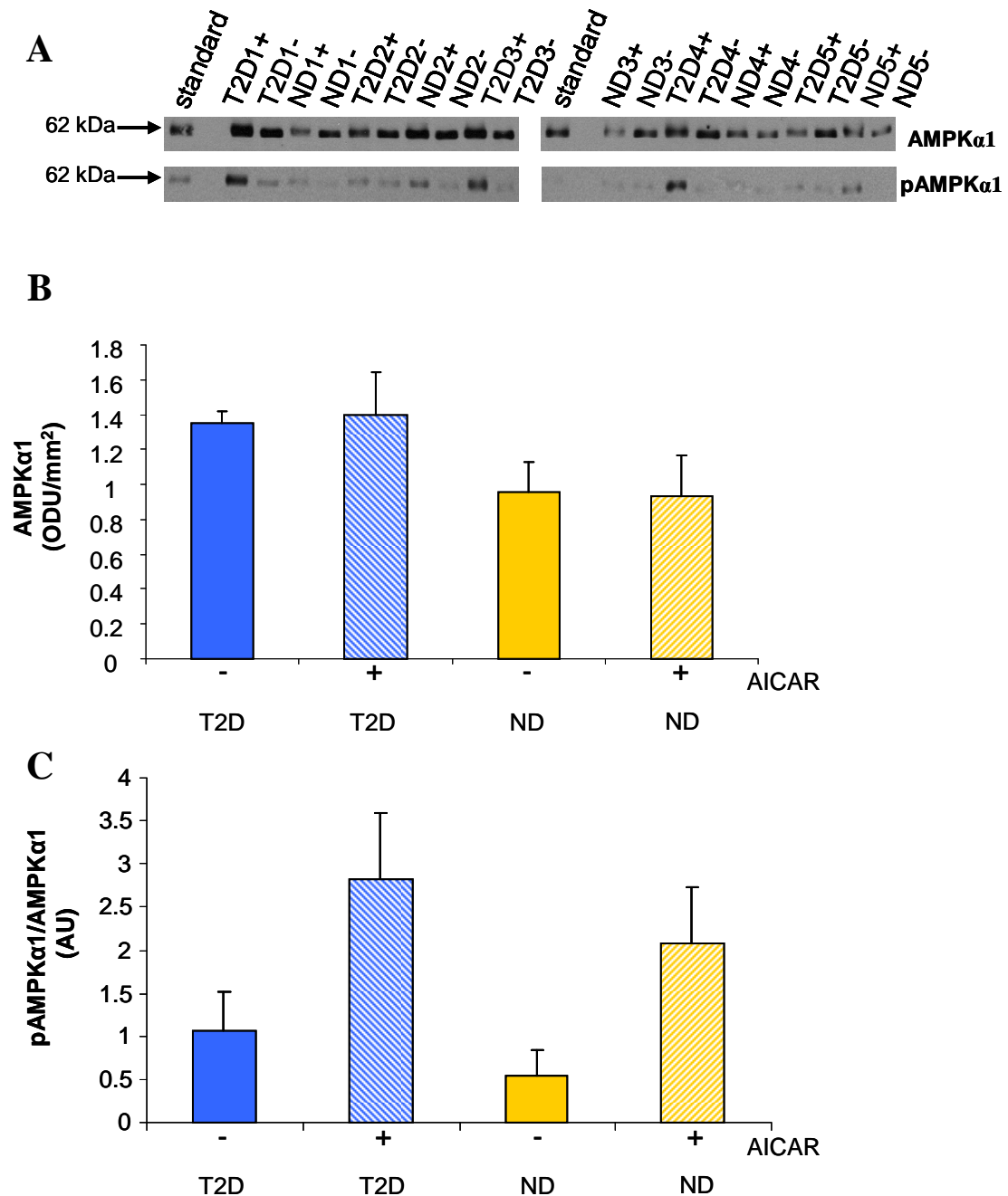


**Figure 4.4 Comparison of AMPK $\alpha$ 1 Thr172 Phosphorylation in HSVEC Lysates Cultured at 21% Oxygen.** (A) HSVECs were isolated from CAD patients with (T2D, n=5) and without (ND, n=5) type 2 diabetes and AMPK $\alpha$ 1 Thr172 phosphorylation (pAMPK $\alpha$ 1) in the presence (+) and absence (-) of AICAR assessed by western blotting of cell lysates. Representative immunoblots are shown. (B) Densitometrical analysis demonstrated no significant difference in AMPK $\alpha$ 1 expression between patient groups. Pretreatment with AICAR (+) had no effect on AMPK $\alpha$ 1 expression in cells from either group of patients. (C) Densitometry revealed a trend towards increased levels of pAMPK $\alpha$ 1 in HSVECs from T2D patients in the absence (-) of AICAR. Pretreatment with AICAR (+) caused an approximate three-fold increase in AMPK phosphorylation in HSVECs from both patient groups.

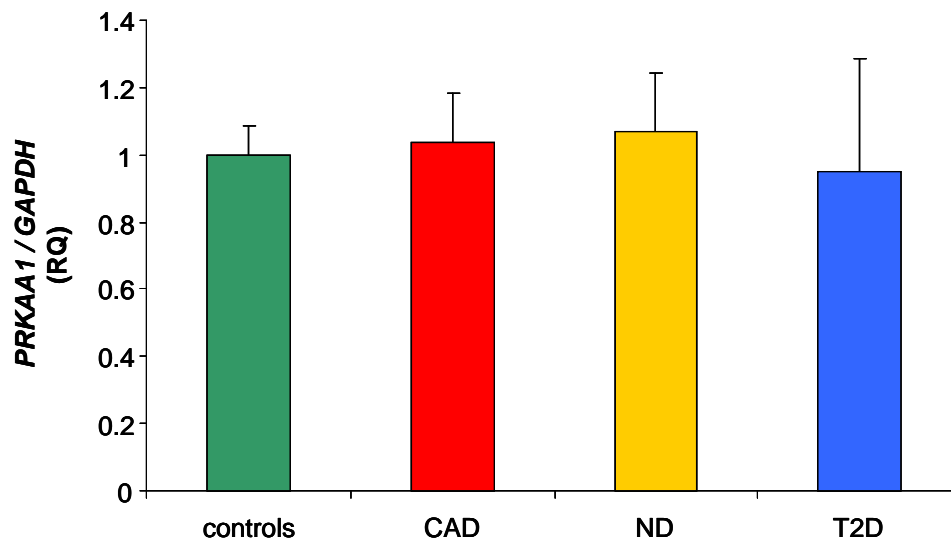


**Figure 4.5. HSVEC *PRKAA1* mRNA Expression Relative to *GAPDH* as Assessed by TaqMan® qRT-PCR.** Expression of *PRKAA1* was investigated in HSVECs isolated from controls (n=5) and patients with CAD (n=20), stratified according to the absence (ND, n=15) or presence of type 2 diabetes (T2D, n=5). No difference in *PRKAA1* expression was observed between patient groups. RQ, relative quantitation

Western blotting to assess ACC phosphorylation was carried out using rabbit anti-ACC-Ser79, an antibody which recognises both phosphorylated ACC species (ACC1 and ACC2) (Figure 4.6A). Again, an internal invariant control sample was used as a standard. Treating cells with AICAR caused a marked increase in ACC phosphorylation in HSVECs from CAD patients both with and without T2D (Figure 4.6A). Due to technical issues, ACC phosphorylation was determined relative to AMPK $\alpha$ 1 (Figure 4.4A). Densitometrical analysis demonstrated a trend towards increased ACC phosphorylation in cells from CAD patients with T2D and revealed a significant increase in ACC phosphorylation in HSVECs from both patients with CAD alone ( $0.122 \pm 0.085$  vs  $5.06 \pm 0.966$ ;  $P=0.0009$ ) and patients with CAD and T2D ( $0.441 \pm 0.239$  vs  $3.86 \pm 0.579$ ;  $P=0.0006$ ) on treatment with AICAR (Figure 4.6B).

Phosphorylation of eNOS was also assessed by means of western blot using rabbit anti-eNOS and rabbit anti-eNOS-Ser1177 antibodies using an internal invariant control sample as a standard (Figure 4.7A). Densitometry revealed a trend towards increased phosphorylation in HSVECs isolated from CAD patients with T2D as compared to those without and an increase in eNOS phosphorylation in cells from both patients groups on treatment with AICAR (Figure 4.7B).

#### **4.3.6 HSVEC AMPK Upstream Kinase Phosphorylation**

In order to determine the reason for increased AMPK activity in HSVECs from patients with CAD and T2D, protein expression of upstream AMPKKs, LKB1 and CaMKK $\alpha$  was investigated and compared in HSVECs from patients with CAD and T2D and CAD alone using an internal invariant control sample as a standard.

LKB1 western blotting showed similar band intensities in samples from HSVECs from CAD patients with and without T2D (Figure 4.8A) and densitometry revealed equal levels of LKB1 expression in cells from both patient groups (Figure 4.8B). Sheep anti-LKB1 primary antibody and protein G–peroxidase from *streptococcus* sp. secondary antibody were used.



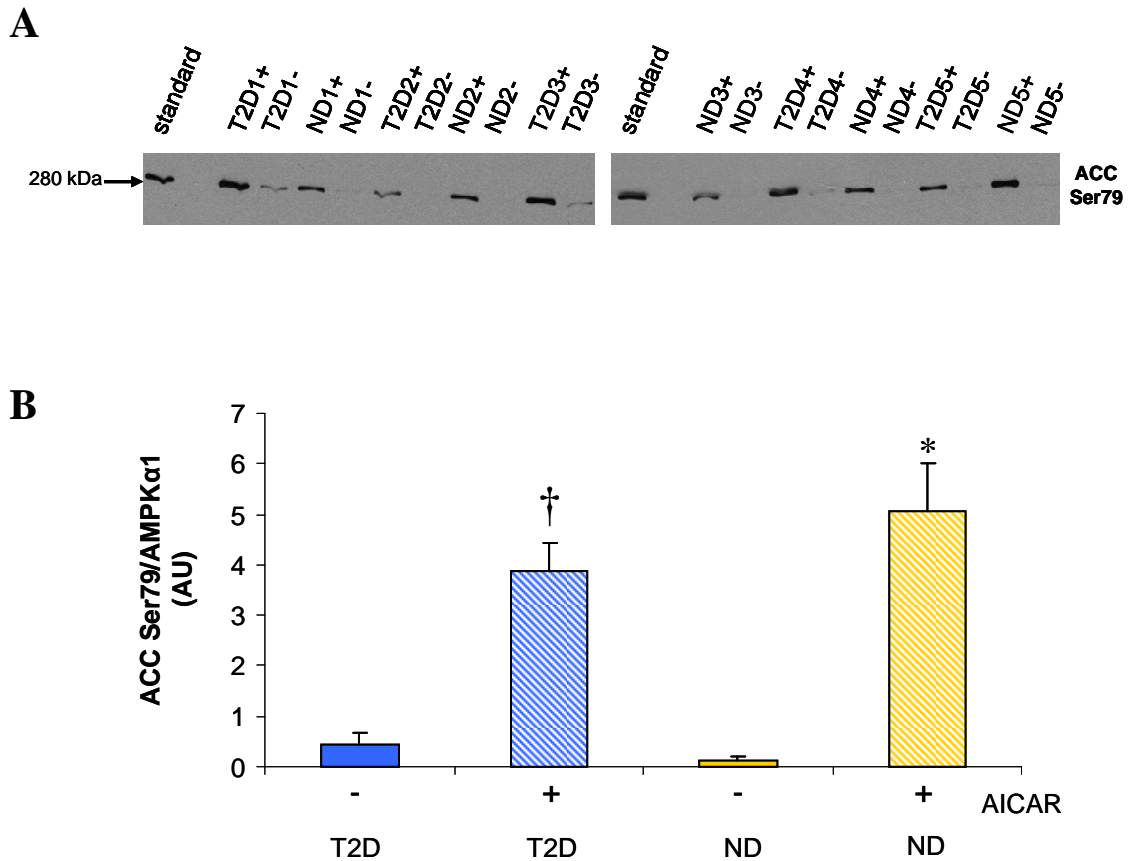
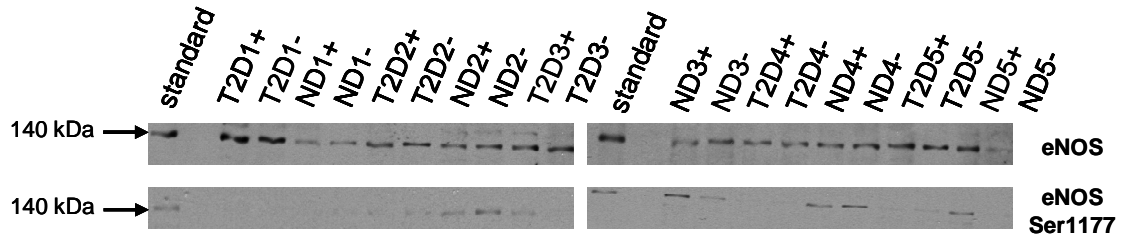
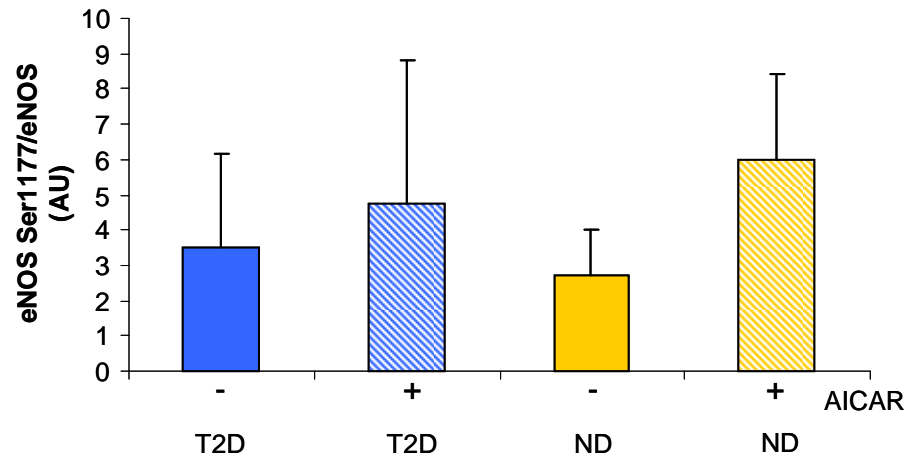


**Figure 4.6. Comparison of ACC Ser80 Phosphorylation in HSVEC Lysates Cultured at 21% Oxygen.** (A) HSVECs were isolated from CAD patients with (T2D, n=5) and without (ND, n=5) type 2 diabetes and ACC Ser79 phosphorylation in the presence (+) and absence (-) of AICAR assessed by western blotting of cell lysates. A representative immunoblot is shown. (B) Densitometry revealed a trend towards increased levels of ACC phosphorylation at Ser79 in HSVECs from T2D patients in the absence (-) of AICAR. Pretreatment with AICAR (+) caused a significant increase in ACC Ser79 phosphorylation in HSVECs from both patient groups. †,  $P < 0.001$  vs T2D (- AICAR). \*,  $P < 0.001$  vs ND (- AICAR).

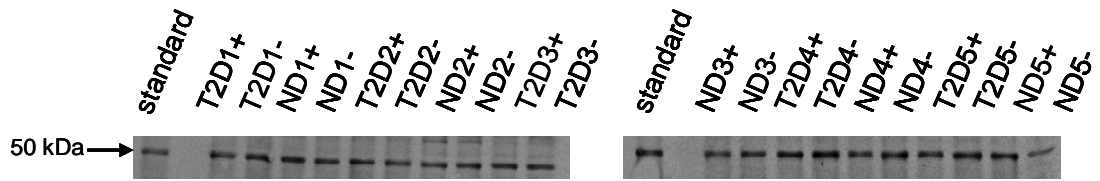
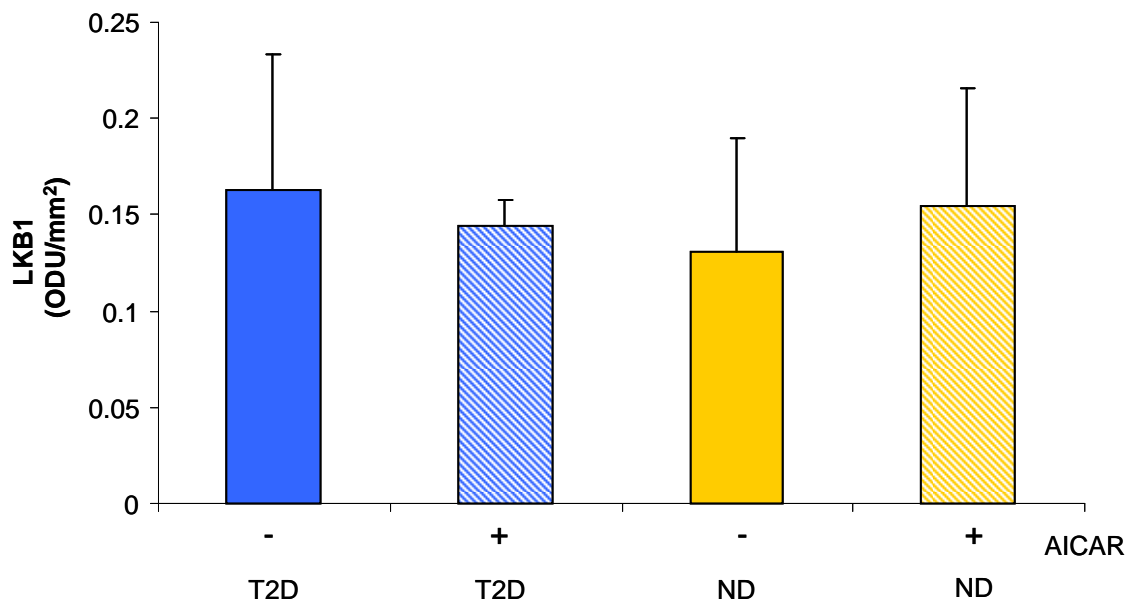
**A**



**B**



**Figure 4.7 Comparison of eNOS Ser1177 Phosphorylation in HSVEC Lysates Cultured at 21% Oxygen.** (A) HSVECs were isolated from CAD patients with (T2D, n=5) and without (ND, n=5) type 2 diabetes and eNOS Ser1177 phosphorylation in the presence (+) and absence (-) of AICAR assessed by western blotting of cell lysates. Bands of the relevant size (140 kDa) were observed for the majority of patients but were of varying density. A representative immunoblot is shown. (B) Densitometry revealed a trend towards increased levels of eNOS phosphorylation at Ser1177 in HSVECs from T2D patients in the absence of AICAR. Pretreatment with AICAR caused no significant increase in eNOS Ser1177 phosphorylation in HSVECs from either patient group.

**A****B**

**Figure 4.8. Comparison of LKB1 Protein Expression in HSVEC Lysates Cultured at 21% Oxygen.** (A) HSVECs were isolated from CAD patients with (T2D, n=5) and without (ND, n=5) type 2 diabetes and LKB1 protein expression in the presence (+) and absence (-) of AICAR assessed by western blotting of cell lysates. Bands of the relevant size (50 kDa) were observed for all patients and appeared of approximately equal density. A representative immunoblot is shown. (B) Densitometrical analysis revealed approximately equal levels of LKB1 expression across patient and treatment groups.

Western blotting to assess CaMKK $\alpha$  expression was carried out using mouse anti-CaMKK $\alpha$  primary antibody and sheep anti-mouse IgG secondary antibody (Figure 4.9A). Densitometrical analysis demonstrated no significant difference in CaMKK $\alpha$  expression in cells from either group on pretreatment with AICAR or between patient groups in the absence of AICAR (Figure 4.9B). However, on pretreatment with AICAR, expression was observed to be significantly different between patient groups (T2D vs ND;  $1.184 \pm 0.262$  vs  $4.363 \pm 1.258$ ;  $P=0.04$ ) (Figure 4.9B).

#### **4.3.7 Mitochondrial ROS-Mediated AMPK Activation in HSVECs**

The contribution of mtROS to AMPK activation was investigated by treating HSVECs from CAD patients with the mitochondria-targeted antioxidant, MitoQ<sub>10</sub>, in the presence and absence of AICAR. To control for non-specific effects of MitoQ<sub>10</sub>, cells were treated with the non-active control compound, DTPP which, as previously stated, comprises the lipophilic TTP cation but lacks the ubiquinone moiety of MitoQ<sub>10</sub> (324). Exposing HSVECs to MitoQ<sub>10</sub> resulted in a reduction in AMPK activity which was attenuated on addition of AICAR (Figure 4.10). The MitoQ<sub>10</sub>-mediated decrease in AMPK activity was greater in HSVECs from CAD patients with T2D ( $0.056 \pm 0.004$  vs  $0.009 \pm 0.01$  nmol/min/mg;  $P=0.016$ ) than in those from patients with CAD alone ( $0.035 \pm 0.005$  vs  $0.014 \pm 0.0002$  nmol/min/mg;  $P=0.052$ ) for whom the effects of MitoQ<sub>10</sub>, in both the presence and absence of AICAR, were non-significant (Figure 4.10).

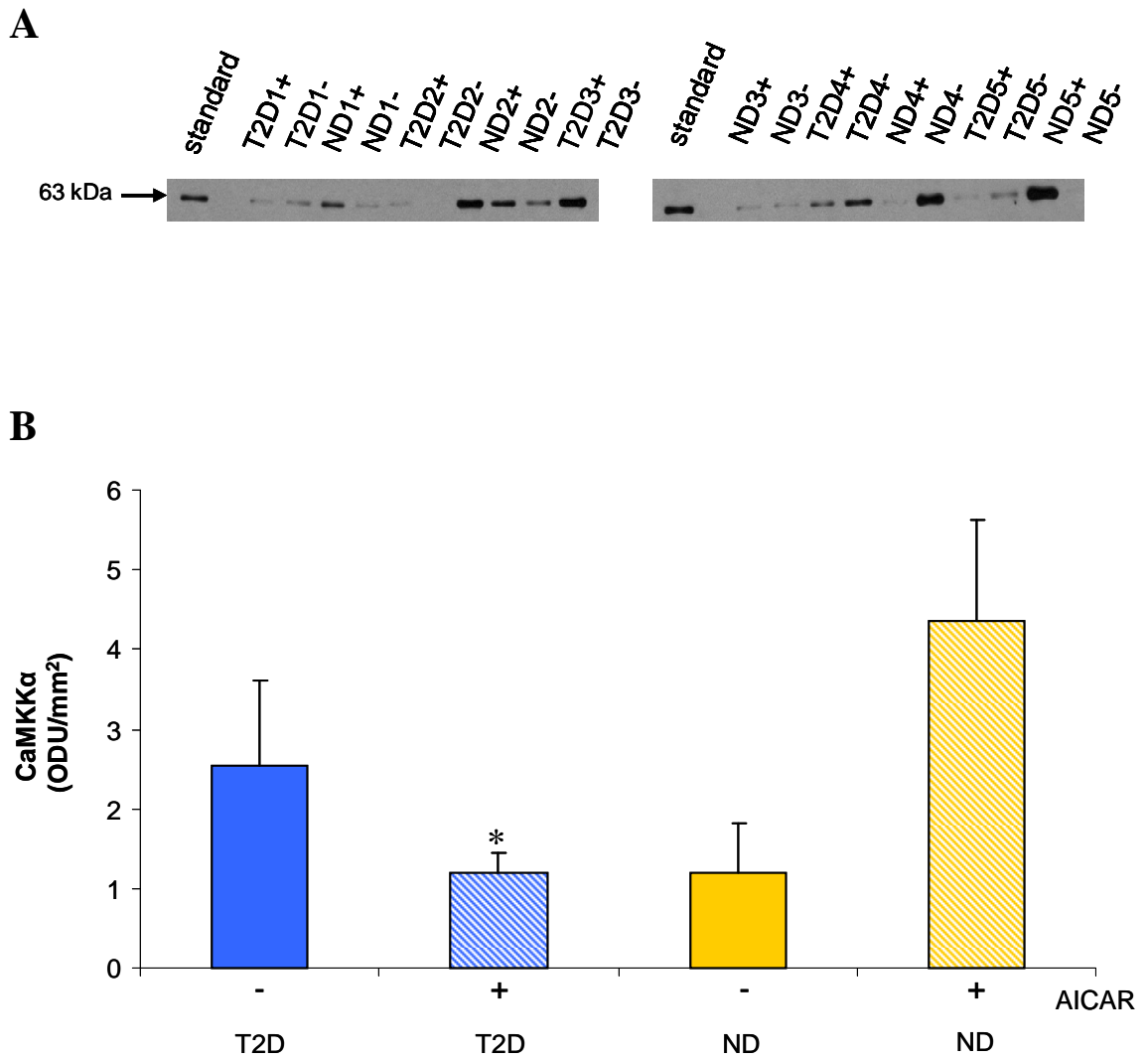


**Figure 4.9. Comparison of CaMKK $\alpha$  Protein Expression in HSVEC Lysates Cultured at 21% Oxygen.** (A) HSVECs were isolated from CAD patients with (T2D, n=5) and without (ND, n=5) type 2 diabetes and CaMKK $\alpha$  protein expression in the presence (+) and absence (-) of AICAR assessed by western blotting of cell lysates. Bands of the relevant size (63 kDa) were observed for all patients but were of varying density. (B) Densitometry revealed no significant difference in CaMKK $\alpha$  expression in cells from either group on pretreatment with AICAR or between patient groups in the absence of AICAR. CaMKK $\alpha$  expression was observed to be significantly different between patient groups on pretreatment with AICAR. \*,  $P < 0.05$  vs ND (+ AICAR).

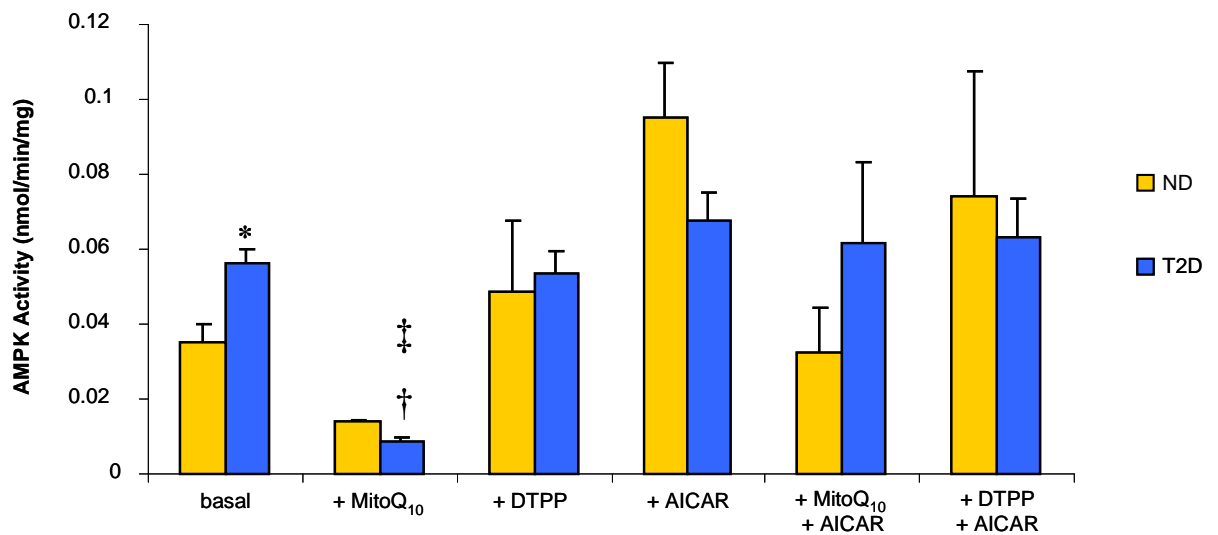


**Figure 4.10. Effect of Mitochondrial-ROS on AMPK Activation in HSVEC Lysates Cultured at 21% Oxygen.** Cells from CAD patients without type 2 diabetes (ND, n=5) and with type 2 diabetes (T2D, n=5) were incubated in the presence (+) and absence of AICAR, MitoQ<sub>10</sub> and decylTPP bromide (DTPP). Total AMPK was immunoprecipitated from lysates which were then assayed for AMPK activity. \*,  $P < 0.05$  vs basal value for cells from ND patients, †,  $P < 0.05$  vs basal value for T2D patients, ‡,  $P < 0.01$  vs value in presence of DTPP for T2D patients.

#### **4.4 Discussion**

Vascular endothelial cells are highly glycolytic (228;366) and this has been confirmed as being the case for HSVECs with results suggesting that in terms of ATP production, HSVECs can compensate more effectively when the electron transport chain is blocked than when glycolysis is blocked (Figure 4.1). A potential reason for the favouring of glycolysis by endothelial cells has been proposed by Quintero and colleagues, whereby mitochondria are not preferentially used bioenergetically in HUVECs, allowing them to function primarily in the generation of ROS for signalling purposes (228).

It is well documented that AMPK is activated in response to hypoxic stress with phosphorylation of the enzyme observed at low O<sub>2</sub> concentrations in HUVECs but undetectable at 21% O<sub>2</sub> or 'normoxia' (228). However, as shown in Figure 4.2, constitutive AMPK phosphorylation was observed in HSVECs isolated from patients with CAD, indicating cardiovascular disease phenotype is linked to enzyme activation. Indeed, at 21% O<sub>2</sub>, HSVEC AMPK activity was significantly greater in cells from patients with CAD relative to control subjects (Figure 4.3). Furthermore, on stratifying patients according to the presence of T2D, AMPK activity was significantly increased in cells from patients with CAD and T2D as compared to both control subjects and patients with CAD alone (Figure 4.3). As previously outlined, the anti-diabetic drug, metformin exerts a portion of its effect through AMPK and approximately 43% of T2D patients studied were being treated with the drug. However, for the purpose of this study, the effect of metformin treatment on AMPK activation was not considered relevant as cells were cultured for several weeks prior to preparation of lysates such that effects of pharmacological treatments were likely to have been lost. Observed differences were consequently considered to be the result of differences in the genetic backgrounds of patients.

Incubating HSVECs with AICAR resulted in a non-significant, approximately equal increase in AMPK activity for all patient groups, suggesting disease status does not affect sensitivity of cells to this artificial activator of AMPK.

On comparison of AMPK $\alpha$ 1 Thr172 phosphorylation in HSVEC lysates cultured at 21% oxygen, AICAR again caused an approximately equal increase in phosphorylation in cells from patients with and without T2D (Figure 4.4). A trend towards higher levels of phosphorylation in HSVECs from patients with CAD and T2D was observed but, unlike

for the activity assay, results failed to reach significance. This can perhaps be explained by the fact that results obtained via western blotting are far less quantifiable than those obtained by means of the more sensitive kinase assay.

Despite the increase in AMPK activity in patients with CAD relative to controls and in those CAD patients with T2D relative to both those without T2D and control subjects, no difference in AMPK $\alpha$ 1 mRNA (Figure 4.5) or protein (Figures 4.4A and 4.4B) expression was observed between patient groups, confirming modulation of AMPK activity via post-translational phosphorylation. In addition, *PRKAA2* mRNA expression was undetectable in HSVECs isolated from patients from each group, corroborating findings that the  $\alpha$ 1 subunit is the predominant form in endothelial cells.

Increased AMPK activity in HSVECs from patients with CAD and T2D relative to those with CAD alone was not mirrored by any significant increase in phosphorylation of downstream targets, ACC and eNOS, at Ser80 and Ser1177 respectively (Figures 4.6 and 4.7). However, a trend towards increased phosphorylation of both substrates in cells from T2D patients was observed (Figures 4.6 and 4.7). Again, this may be due to the fact that analysis of western blots is less quantitative than the kinase assays carried out to determine AMPK activity. Also, while there was a narrow range of expression of AMPK, there was substantial variation in expression of eNOS particularly. Furthermore, it should be noted that AMPK assays are performed in saturating AMP, and therefore reflect the increase in activity of the kinase due to phosphorylation at Thr172. However, the ACC and eNOS phosphorylation observed reflect AMPK activation that is a combination of increased phosphorylation and increased allosteric activation by AMP. As such, it is perhaps not surprising that increased AMPK activity in HSVECs from patients with CAD and T2D did not translate to a significant increase in phosphorylation of substrates.

Expression of upstream AMPKKs, LKB1 and CaMKK $\alpha$ , was investigated in an attempt to determine the mechanisms underlying the observed increase in AMPK activity in HSVECs from patients with CAD and T2D. While AICAR has no effect on expression of these kinases, lysates from HSVECs pretreated with AICAR were used in an attempt to keep samples consistent throughout experimental procedures.



As shown in Figure 4.8, LKB1 expression remained constant irrespective of patient disease status and, as expected, preincubation of cells with AICAR. Therefore, increased HSVEC AMPK activity in T2D patients does not occur as a result of elevated LKB1 expression.

For CaMKK $\alpha$ , immunoblots indicated substantial variation in protein expression between individual patient samples (Figure 4.9A). However, in lysates from cells not subject to preincubation with AICAR, CaMKK $\alpha$  expression was not found to be statistically significantly different in CAD patients with T2D as compared to those with CAD alone (Figure 4.9B), suggesting observed differences may simply represent natural variation in the human population. Interestingly, pretreatment with AICAR had no statistically significant effect on CaMKK $\alpha$  expression within patient groups but caused a significant difference in expression between groups (Figure 4.9B). As stated, AICAR does not directly affect expression of CaMKK. Consequently, the changes upon AMPK stimulation may reflect changes in subcellular localisation of CaMKK $\alpha$  such that there are apparent changes in expression within the lysates examined.

Limited cellular material meant expression of CaMKK $\beta$  was not investigated. The  $\beta$  isoform is thought to predominate in terms of AMPK activation (264;265) and so additional studies focusing on expression of this isoform are crucial in order to obtain accurate and comprehensive insight into CaMKK expression in HSVECs. Furthermore, with immunoblotting for CaMKK $\alpha$  yielding variable results, for future studies it may be useful to employ an alternative method for investigation of CaMKK-mediated AMPK activation, such as assaying AMPK activity after treatment of cells with the CaMKK inhibitor, STO-609 (287).

Given the apparent lack of change in activity of upstream AMPK kinases, the glycolytic nature of these cells and the increased expression of SOD2 (Figure 3.8), it seems likely that endothelial AMPK activation in CAD patients occurs, at least in part, in an mtROS-mediated manner and that this activation is enhanced in those CAD patients with T2D who display severe endothelial dysfunction (Figure 3.2B) and increased SOD2 expression (Figure 3.8), consistent with increased mtROS production. As previously described, within the mitochondrial matrix, SOD2 catalyses the conversion of  $O_2^-$  to  $H_2O_2$  and molecular oxygen (234). Interestingly,  $H_2O_2$  has been shown to activate AMPK under hypoxic conditions in cultured cells (295;296).

In order to test this hypothesis concerning the mtROS-mediated activation of AMPK, HSVECs isolated from vessels of CAD patients were treated with the mitochondria-targeted antioxidant, MitoQ<sub>10</sub>. As outlined in Chapter 3, MitoQ<sub>10</sub> has been shown to react poorly with O<sub>2</sub><sup>-</sup> (351) but is reported to scavenge oxidants, including H<sub>2</sub>O<sub>2</sub>, ONOO<sup>-</sup> and their derivatives, under hyperglycaemic conditions in cultured endothelial cells (374). Treatment with MitoQ<sub>10</sub> caused a significant decrease in AMPK activation in cells from CAD patients with type 2 diabetes which was attenuated on addition of AICAR, known to stimulate kinase activity in cultured endothelial cells (262;297;375) (Figure 4.10). The non-active control for MitoQ<sub>10</sub>, DTPP, had no effect on AMPK activity in a parallel experiment (Figure 4.10), indicating results can be attributed to the antioxidant action of MitoQ<sub>10</sub> specifically. The same effect was not seen in cells from CAD patients without T2D (Figure 4.10).

Taken together, these findings indicate a novel, mtROS-mediated activation of AMPK in the endothelium of patients with CAD and T2D and suggest a role for AMPK in defence against oxidative stress and endothelial dysfunction. Indeed, as described, activated AMPK phosphorylates eNOS at Ser1177 in cultured endothelial cells (176;282) and has been shown to increase endothelium-dependent vasodilation in an animal model (252). Furthermore, the anti-diabetic drug, metformin which exerts a portion of its effect through AMPK, has been reported to decrease intracellular production of mtROS in aortic endothelial cells (376), while activation of AMPK has been shown to reduce hyperglycaemia-induced mtROS production by induction of *SOD2* in HUVECs (377). In addition, Colombo and Moncada have recently shown that in HUVECs, AMPK $\alpha$ 1 is responsible for the expression of a number of genes involved in antioxidant defence, including *SOD2* (378). Thus, AMPK activation would appear to have a beneficial effect on endothelial function by suppressing oxidative stress and increasing NO bioavailability in endothelial cells.

In summary, these findings suggest AMPK is part of a feedback or adaptive mechanism in the endothelium of patients with CAD and T2D, with a role in defence against oxidative stress. It seems likely that the elevated mtROS production of T2D results in activation of AMPK which, in turn, activates eNOS, thus increasing NO bioavailability and attenuating endothelial dysfunction. Under conditions of oxidative stress, NO may react with O<sub>2</sub><sup>-</sup> to form ONOO<sup>-</sup> which has been shown to activate AMPK in the endothelium (297;379).

Endothelial AMPK may also induce SOD2 activity, resulting in production of  $\text{H}_2\text{O}_2$  which may itself activate AMPK (295;296) (Figure 4.11).

Results support a novel, mtROS-mediated mechanism for AMPK activation in the endothelium and suggest mitochondria contribute to increased  $\text{O}_2^-$  production and endothelial dysfunction in patients with coronary artery disease and type 2 diabetes. Mitochondria-targeted antioxidants, used in combination with pharmacological activators of AMPK, may therefore have potential as an early intervention strategy in the treatment of endothelial dysfunction in these patients.

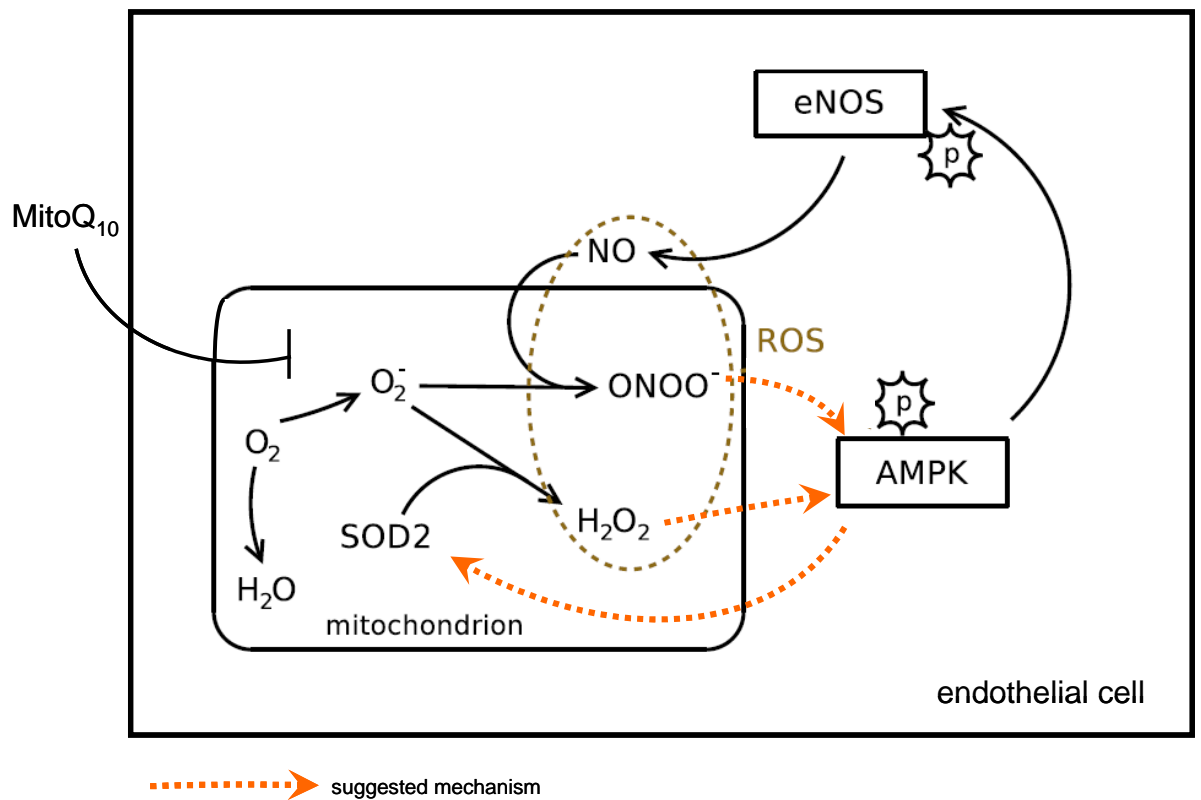


**Figure 4.11. Proposed Mechanism of Mitochondrial Reactive Oxygen Species-Mediated AMPK Activation in Endothelial Cells.** Results suggest a potentially mitochondrial reactive oxygen species (mtROS)-mediated increase in AMPK activity in patients with coronary artery disease and type 2 diabetes. AMPK may therefore be part of a feedback or adaptive mechanism with a role in defence against oxidative stress in the endothelium, regulating expression of antioxidant genes, including *SOD2*, and contributing to the control of vascular tone, via activation of endothelial nitric oxide synthase (eNOS).

## **5. Gene Expression Profiling of Endothelial Cells in Coronary Artery Disease**

## **5.1 Introduction**

Microarray technology is a powerful tool, allowing exploration of genome complexity at a fundamental level (380). Transcriptional profiling using high-density microarrays has provided unique insight into disease mechanisms, drug responses, regulatory pathways and gene function, through comparison of mRNA transcript levels in cells / tissues in a given pathological state with an appropriate control (381).

One such pathological state is CAD, where the application of microarray technology has resulted in identification of unique subsets of genes associated with specific disease processes (382). Indeed, transcript profiling has revealed associations of interesting genes, such as *ICAM-2*, with CAD (383) and identified a loss of coronary artery differentiated smooth muscle cell gene expression as a primary signature of disease progression in atherosclerosis (384).

To date, few published studies have compared gene expression profiles of CAD patients with and without T2D (381;384;385). A study by Voisine and colleagues identified quantitative and qualitative differences in gene expression profile in atrial myocardium samples from patients with T2D undergoing cardiopulmonary bypass and cardioplegic arrest, with the majority of differentially expressed genes encoding transcription activators and mediators of the inflammatory response (381). Similarly, King *et al.* (384) assessed gene expression profiles of coronary artery segments and observed differential expression of a number of genes involved in insulin signalling in vessels from diabetic patients. However, it seems likely that many of the chronic endothelial effects of T2D will be reflected in transcriptional regulation at cellular level, either as a direct response to hyperglycaemia and abnormalities of insulin signalling, or as a secondary response to the effects of these stresses. This intimates the need to examine transcript profiles of isolated endothelial cells in order to identify pathways and candidate genes that may contribute to the more severe endothelial dysfunction observed in vessels from CAD patients with T2D (Figure 3.2B). As such, this study involved comparison of gene expression profiles in primary HSVECs isolated from CAD patients with and without T2D.

The aims of the experimental work outlined in this chapter were as follows:

- 1) to identify differentially expressed genes in primary HSVECs isolated from CAD patients with and without T2D;
- 2) to analyse microarray data using Ingenuity Pathway Analysis software in order to identify canonical metabolic pathways affected by differentially expressed genes;
- 3) to confirm differential expression of selected genes using qRT PCR

## **5.2 Materials & Methods**

### **5.2.1 Study Participants**

CAD patients with and without T2D were as described in section 2.2. Twelve patients with CAD alone and six patients with CAD and T2D were selected for the study. Selected patients were age, sex and smoking status matched. All patients were male, aged between 60 and 72 years of age and non-smokers.

### **5.2.2 Human Vascular Tissue & Primary Cell Culture**

Vascular tissue was obtained and prepared as described in section 2.3 and HSVECs isolated, characterised and cultured as outlined in section 2.4.

### **5.2.3 RNA Extraction, Quantification & Validation**

Total RNA was extracted from HSVECs, DNase treated and quantified using the NanoDrop<sup>®</sup> ND-100 Spectrophotometer as per section 2.5. Total RNA sample integrity was then verified by electrophoresis of 500 ng on an Agilent Bioanalyzer 2100.

## 5.2.4 Biotinylated cRNA Synthesis

The Illumina<sup>®</sup> TotalPrep RNA Amplification Kit was used to generate biotinylated, amplified cRNA for hybridisation with Illumina Sentrix<sup>®</sup> arrays, according to the manufacturer's protocol.

### 5.2.4.1 First & Second Strand cDNA Synthesis

Reverse transcription to synthesise first strand cDNA was carried out by bringing 500 ng of total RNA to a volume of 11 µl with nuclease-free H<sub>2</sub>O before adding 9 µl Reverse Transcription Master Mix (prepared at room temperature and containing 1 µl T7 Oligo(dT) Primer, 2 µl 10 X First Strand Buffer, 4 µl dNTP Mix, 1 µl RNase Inhibitor and 1 µl ArrayScript for a single 20 µl reaction), mixing thoroughly by pipetting and incubating samples at 42°C for 2 hours.

Second strand cDNA was then synthesised immediately by adding 80 µl Second Strand Master Mix (prepared on ice and containing 63 µl nuclease-free H<sub>2</sub>O, 10 µl 10 X Second Strand Buffer, 4 µl dNTP Mix, 2 µl DNA Polymerase and 1 µl RNase H for a single 100 µl reaction) to each sample, mixing thoroughly by pipetting and flicking the tube 3-4 times before centrifuging briefly to collect the reaction in the bottom of the tube. Samples were then incubated for 2 hours at 16°C in a thermal cycler. Following the 2 hour incubation, cDNA purification was carried out straight away.

### 5.2.4.2 Double Stranded cDNA Purification

cDNA was purified to remove RNA, primers, enzymes and salts that would inhibit *in vitro* transcription. 250 µl cDNA Binding Buffer was added to each sample and the mixture mixed thoroughly by pipetting and flicking the tube before being applied to the centre of a cDNA Filter Cartridge seated in a wash tube. Cartridges were centrifuged for a minute at 10,000 x g, flow-through discarded and cartridges replaced in wash tubes. 500 µl Wash Buffer was applied to each cDNA Filter Cartridge and cartridges centrifuged at 10,000



x g for a minute. Flow-through was discarded and cartridges centrifuged for an additional minute to remove traces of Wash Buffer. Next, cDNA Filter Cartridges were transferred to cDNA Elution Tubes, 10 µl nuclease-free H<sub>2</sub>O (preheated to 50-55°C) applied to the centre of filters and samples incubated at room temperature for 2 minutes before centrifugation for 1.5 minutes at 10,000 x g. A further 9 µl preheated nuclease-free H<sub>2</sub>O was then applied to filters and samples centrifuged for 2 minutes at 10,000 x g to elute the double-stranded cDNA in an approximate volume of 17.5 µl. *In vitro* transcription (IVT) to synthesise complementary RNA (cRNA) was then carried out immediately.

#### 5.2.4.3 *In Vitro* Transcription to Synthesise cRNA

Multiple copies of biotinylated cRNA were generated from the double-stranded cDNA template by adding 7.5 µl IVT Master Mix (prepared at room temperature and containing 2.5 µl T7 10 X Reaction Buffer, 2.5 µl T7 Enzyme Mix and 2.5 µl Biotin-NTP Mix for a single 25 µl reaction) to each sample, mixing thoroughly by pipetting and flicking the tube and subsequently centrifuging briefly to collect the reaction mixture at the bottom of the tube. Samples were then incubated at 37°C for between 4 and 14 hours before 75 µl nuclease-free H<sub>2</sub>O was added to each sample to stop the reaction and bring the final volume to 100 µl. Purification of cRNA was then performed immediately.

#### 5.2.4.4 cRNA Purification & Validation

cRNA purification to remove unincorporated NTPs, salts, enzymes and inorganic phosphate involved adding 350 µl cRNA Binding Buffer followed immediately by 250 µl 100% ethanol to each sample. Samples were then mixed by pipetting before being applied to the centre of a cRNA Filter Cartridge placed in a cRNA Collection Tube. Samples were subsequently centrifuged for 1 minute at 10,000 x g, flow-through discarded and cartridges replaced in collection tubes. Next, 650 µl Wash Buffer was applied to each cartridge which was then centrifuged for 1 minute at 10,000 x g. Flow-through was again discarded and cartridges centrifuged for an additional minute to remove trace amounts of Wash Buffer. Cartridges were then transferred to fresh cRNA Collection Tubes and 100 µl nuclease-free

H<sub>2</sub>O (preheated to 50-60°C) added to the centre of the filter. Samples were left at room temperature for 2 minutes before being centrifuged for 1.5 minutes at 10,000 x g to elute purified cRNA.

Purified cRNA was quantified using the NanoDrop<sup>®</sup> ND-100 Spectrophotometer and quality assessed via electrophoresis of 500 ng on an Agilent Bioanalyzer 2100.

### **5.2.5 Microarray Hybridisation & Data Collection**

cRNA was prepared for hybridisation with Illumina<sup>®</sup> HumanWG-6 v3.0 Expression Beadchips, using the Illumina<sup>®</sup> Whole-Genome Expression Direct Hybridization Assay. Illumina<sup>®</sup> HumanWG-6 v3.0 Expression Beadchips contain 48,804 probes, targeting a total of 25,440 annotated genes. 1.5 µg of cRNA was brought to a total volume of 10 µl with RNase-free water and mixed before incubation at room temperature for 10 minutes to resuspend cRNA. Hybridisation reagents (GEX-HYB and GEX-HCB) were incubated at 58°C for 10 minutes to dissolve any salts that may have precipitated in storage. 20 µl GEX-HYB was subsequently added to each cRNA sample. 200 µl GEX-HCB was then applied to each hybridisation chamber (Hyb Chamber) and BeadChips inserted into chambers. cRNA samples were preheated at 65°C for 5 minutes then briefly vortexed and centrifuged to collect liquid. Samples were allowed to cool to room temperature before 30 µl was applied to each array. Samples were randomised on chips and technical duplicates of all T2D samples included. Hyb Chambers were incubated for 16-20 hours (overnight) in a 58°C oven rotating at 60 rpm.

Beadchips were washed and stained following standard protocols. Following overnight incubation, BeadChips were removed from Hyb Chambers and submerged in 250 ml Wash E1BC solution (prepared by adding 3 ml E1BC buffer to 1 L RNase-free H<sub>2</sub>O) before being incubated for 10 minutes in 1 X High-Temp Wash Buffer (prepared by adding 50 ml 10 X stock to 450 ml RNase-free H<sub>2</sub>O) preheated to 55°C. After 10 minutes, BeadChips were transferred to a fresh 250 ml Wash E1BC solution at room temperature and placed on an orbital shaker at maximum speed for 5 minutes. Chips were then transferred to a 250 ml 100% ethanol solution and placed on the orbital shaker (maximum speed) for 10 minutes. A 2 minute wash in a fresh Wash E1BC solution was performed before each chip was

blocked in 4 ml Block E1 buffer for 10 minutes at medium rocking speed and room temperature. Detection was performed by placing chips in 2 ml Block E1 buffer with streptavidin-Cy3 (2  $\mu$ l 1 mg/ml stock per chip), covering to protect from light and rocking at medium speed for 10 minutes. A third room temperature wash in 250 ml Wash E1BC was then carried out with shaking for 5 minutes. Finally, to dry chips, they were centrifuged for 4 minutes at 275 rcf and room temperature.

Following completion of the hybridisation procedure, BeadChips were scanned and images extracted using specific protocols on an Illumina<sup>®</sup> BeadArray Reader.

## **5.2.6 Microarray Data Analysis**

### **5.2.6.1 Quality Control**

Illumina<sup>®</sup> Gene Expression Beadchips have internal control features to monitor both sample-independent and sample-dependent data quality. Control data results were visualised with BeadStudio software.

### **5.2.6.2 Gene Expression Data Analysis**

#### ***5.2.6.2.1 Illumina<sup>®</sup> BeadStudio Analysis***

Initial analysis of microarray data was performed using Illumina<sup>®</sup> BeadStudio software. Quantile normalisation of the data was carried out without background subtraction. Each probe is represented by multiple beads (30 on average) on an Illumina<sup>®</sup> Gene Expression Beadchip. Normalised values for each bead representing a given probe were averaged to obtain the estimate of expression for that probe. Unpaired 2 sample t-tests were then conducted on these averaged values using the Illumina<sup>®</sup> custom error model (386). Differentially expressed probes were identified using a difference (diff) score cut-off of  $\pm 13.0103$ , equating to a  $P$  value  $\leq 0.05$ . Differentially expressed probes were then uploaded

to Ingenuity Pathway Analysis (IPA) software (387) and analysed to identify canonical metabolic pathways of interest containing most significantly differentially expressed genes.

#### *5.2.6.2.2 Ingenuity Pathway Analysis*

Canonical pathways analysis identified the pathways from the IPA library of canonical pathways that were most significantly associated with the data set. Genes from the data set that met the  $P$  value cut-off of 5% and were associated with a canonical pathway in the Ingenuity Pathways Knowledge Base (IPKB) were considered for the analysis. The significance of the association between the data set and the canonical pathway was measured in two ways. Firstly, a ratio of the number of genes with differentially expressed probes from the data set that mapped to the canonical pathway divided by the total number of genes with probes in the data set that mapped to the pathway was displayed. Secondly, in addition to this ratio, Fisher's exact test was used to calculate a  $P$  value determining the probability that the association between the significant genes in the data set and the canonical pathway could be explained by chance alone.

#### *5.2.6.2.3 Rosetta Resolver<sup>®</sup> Analysis*

Additional analysis of microarray data was carried out by uploading raw data from BeadStudio software to the Rosetta Resolver<sup>®</sup> Gene Expression Data Management and Analysis System. Data were normalised using Rosetta error models (388) to give one averaged, normalised value for each probe before principal component analysis (PCA) was performed. PCA is a data reduction method which identifies linear combinations of probes that explain the most variability in the data and can be used to visualise data for quality assessment purposes (389). The PCA revealed an outlier in one sample from the T2D group of patients and, after further investigation, this outlier was removed from subsequent analysis. Following PCA, an error weighted analysis of variance (ANOVA) with a false discovery rate (FDR) (390) threshold of 0.05 was used on the remaining data to identify differentially expressed probes. Again, differentially expressed probes were uploaded to IPA and analysed to identify the canonical metabolic pathways most associated with significantly differentially expressed genes.

#### 5.2.6.2.4 Integration of Analyses Results

The number of differentially expressed genes common to BeadStudio and Rosetta Resolver<sup>®</sup> analyses was identified using a Venn diagram.

### 5.2.7 TaqMan<sup>®</sup> Real-Time RT-PCR

TaqMan<sup>®</sup> qRT-PCR was utilised to confirm differential expression observed in microarray experiments. The same total RNAs isolated for microarray experiments were used as templates for the synthesis of cDNA as per section 2.7.1 and mRNA expression levels assessed as outlined in section 2.7.2. Applied Biosystems Custom TaqMan<sup>®</sup> Gene Expression Assays for *ACAD11* (Hs00259854\_m1), *AGTR2* (Hs00169126\_m1), *ATP5G3* (Hs00266085\_m1), *IDH3G* (Hs00188065\_m1), *PIK3R2* (Hs00178181\_m1), *PRKAG1* (Hs00176952\_m1) and *SDHC* (Hs00818427\_m1) were used with TaqMan<sup>®</sup> Endogenous Control,  $\beta$ -actin (*ACTB*, 4326315E). Reactions were carried out in singleplex or multiplex as indicated.

## **5.3 Results**

### **5.3.1 Total RNA & cRNA Validation**

Electrophoresis of HSVEC total RNA samples on the Agilent Bioanalyzer 2100 confirmed RNA quality prior to cDNA synthesis, as indicated by defined bands for 28S and 18S ribosomal RNA (rRNA) species and little evidence of small RNA species below the 18S band (Figure 5.1). RNA Integrity Numbers (RINs) were consistently above 9.0.

Following in vitro transcription to synthesise biotinylated cRNA, cRNA quality was also assessed by electrophoresis on the Agilent Bioanalyzer 2100. Results demonstrated

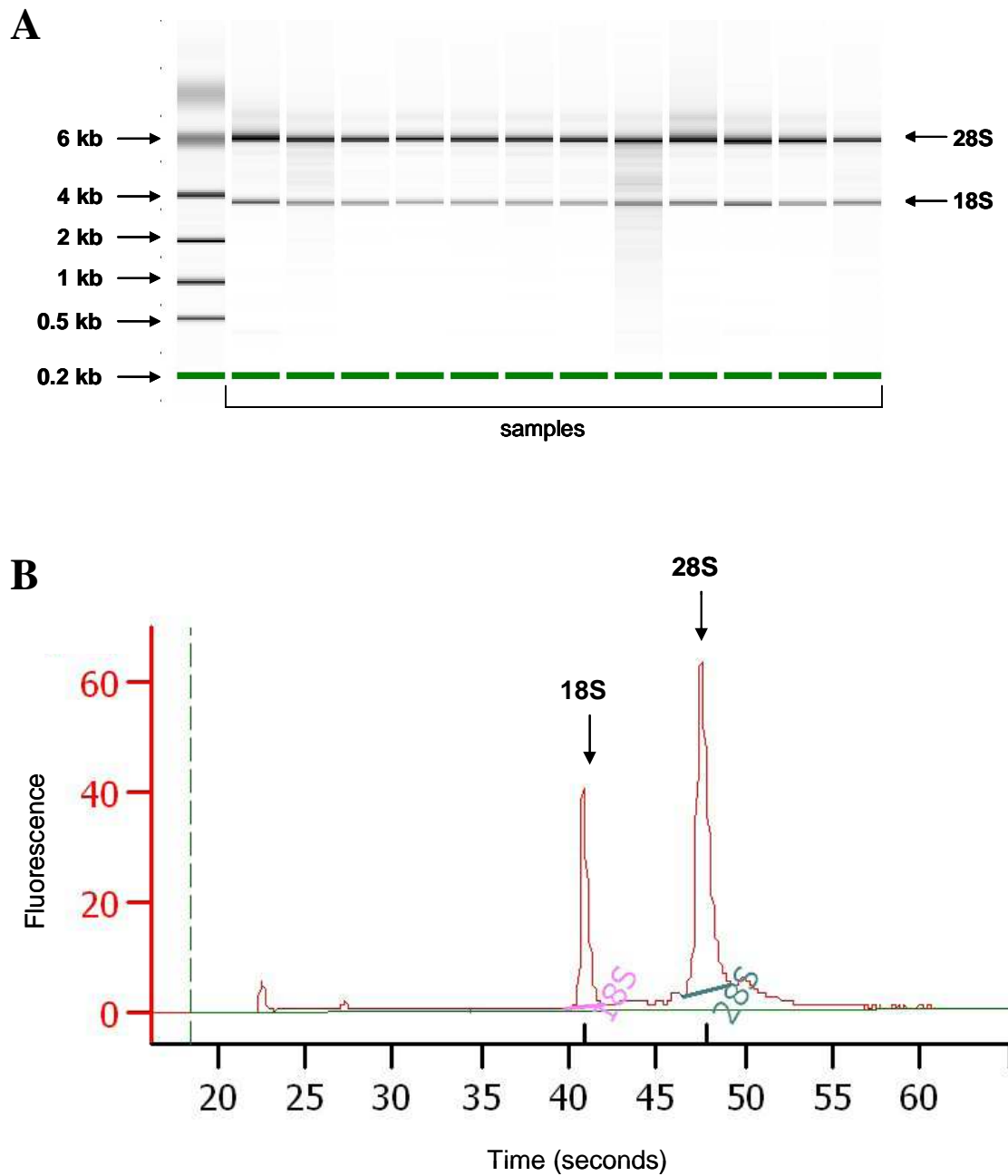


**Figure 5.1. Agilent Bioanalyzer 2100 Assessment of Total RNA Quality.** (A) Electrophoresis of representative total RNA samples revealed bands for 28S and 18S ribosomal RNA (rRNA). Green bands represent a 200 base pair size marker used to align samples and controls. kb, kilobases (B) A representative individual electropherogram showing sharp peaks for 28S and 18S rRNA. No RNA species smaller than 18S rRNA were observed, indicative of intact RNA.

approximately normal distribution of cRNA species for all samples and approximately equal concentrations (Figure 5.2).

### **5.3.2 Microarray HSVEC mRNA Expression Profiling**

#### **5.3.2.1 Microarray Data Quality Control**

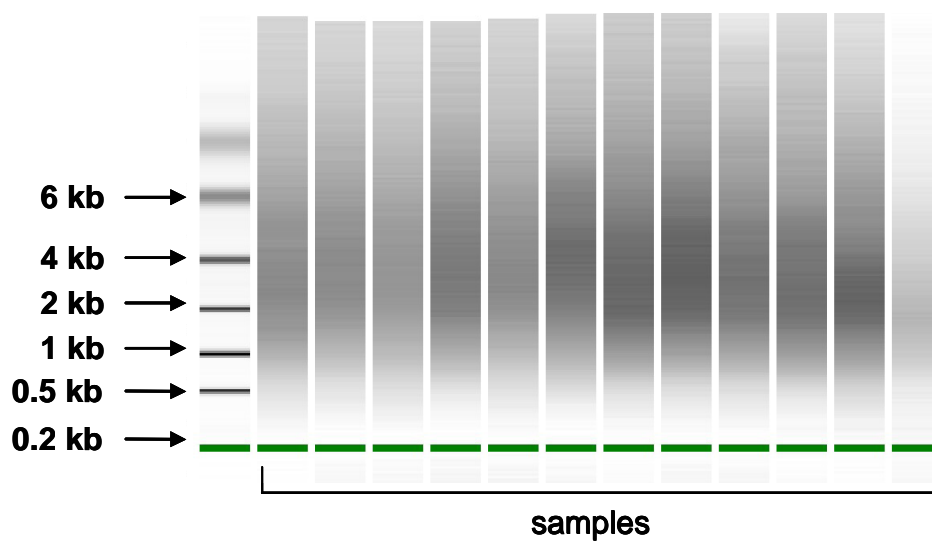
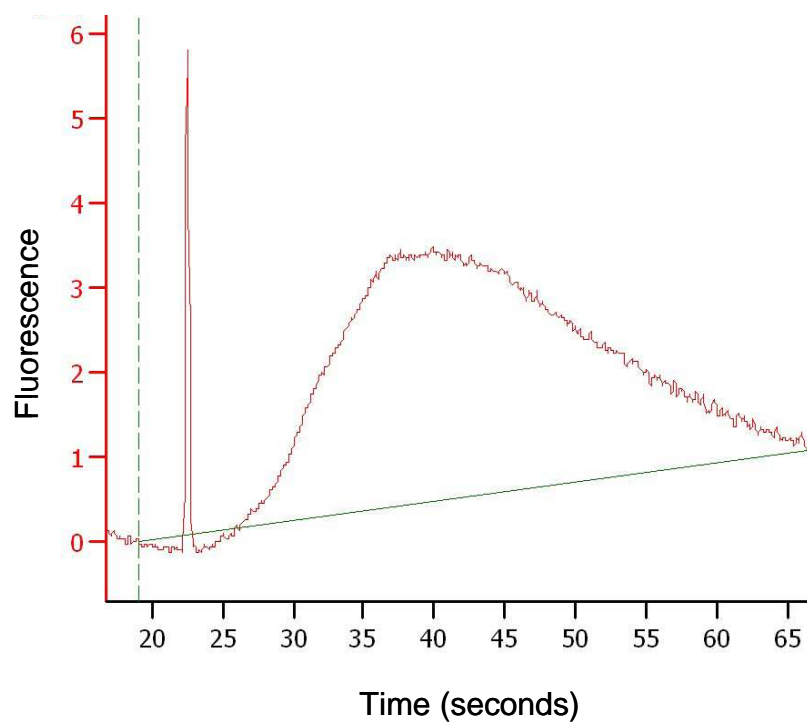
Direct Hyb Control Plots obtained for samples were consistent with BeadStudio example control plots, verifying the validity of microarray gene expression data (Figure 5.3).

#### **5.3.2.2 Beadstudio Analysis**

Using Illumina<sup>®</sup> BeadStudio software, a total of 727 probes were found to be differentially expressed between HSVECs from patients with CAD and T2D and patients with CAD alone. Expression of 293 probes was upregulated in cells from patients with T2D while 434 probes were downregulated in cells from these patients. A complete list of differentially expressed probes is included as Table A1 in the Appendix.

##### ***5.3.2.2.1 Ingenuity Pathway Analysis***

Analysis of BeadStudio microarray data using IPA software identified the citrate cycle as a canonical metabolic pathway significantly affected by the presence of T2D (Figure 5.4), with significance based on the number of genes with differentially expressed probes mapping to the pathway (Table 5.1 and Figure 5.5). Given the role of mitochondria in T2D pathogenesis (section 1.3.4.3.1), *ATP5G3*, *IDH3G* and *SDHC* were selected as candidate genes for further study. However, *SDHAL1* was identified as a pseudogene and consequently no attempt was made to confirm its differential expression.

**A****B**


**Figure 5.2. Agilent Bioanalyzer 2100 Assessment of cRNA Quality.** (A) Electrophoresis of representative samples showing the distribution of complementary RNA (cRNA) species on separation according to size. Green bands represent a 200 base pair (bp) size marker used to align samples and controls. kb, kilobases (B) Representative electropherogram showing approximately normal distribution of cRNAs. The sharp peak at the extreme left of the trace corresponds to the 200 bp size marker.



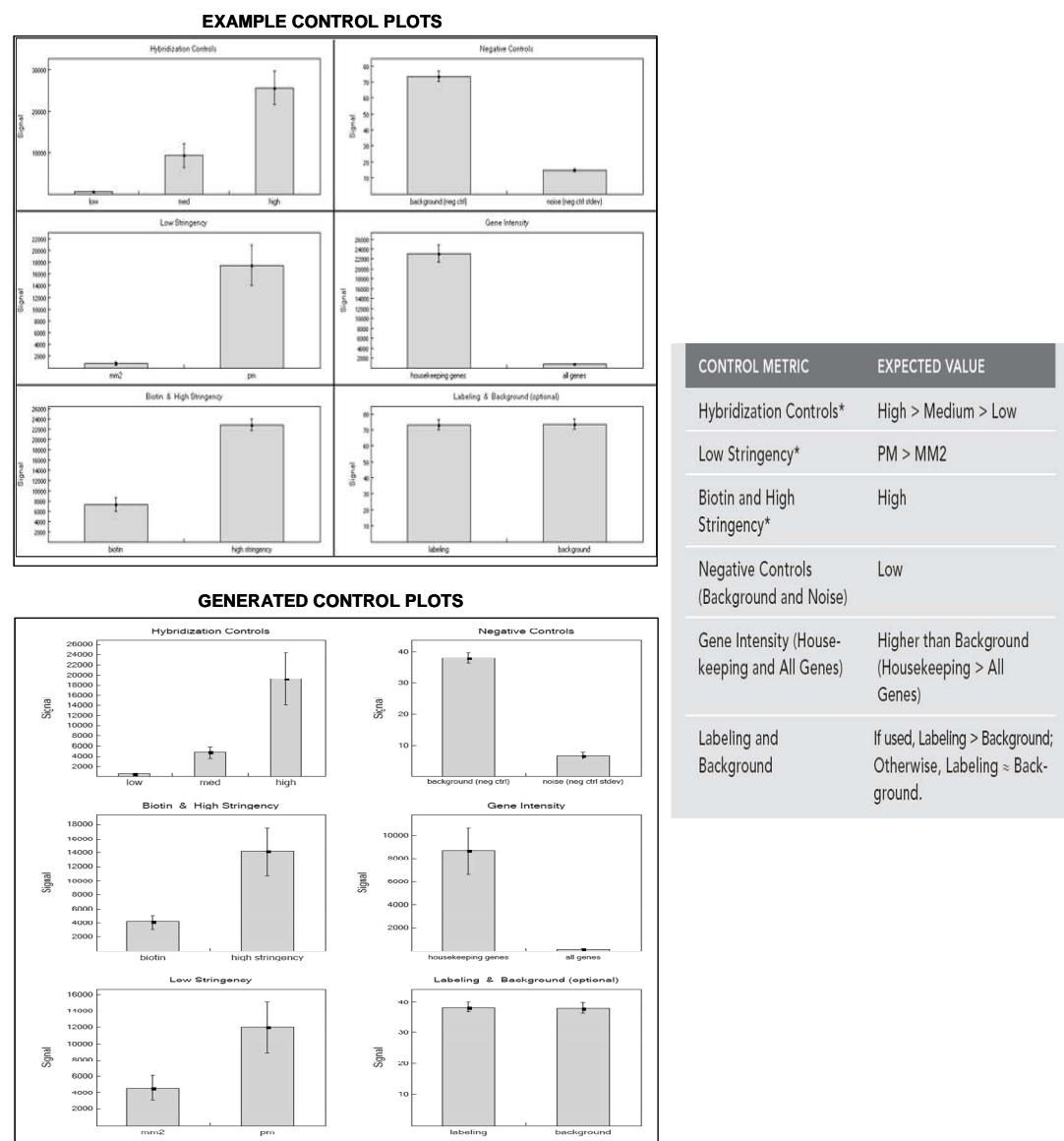
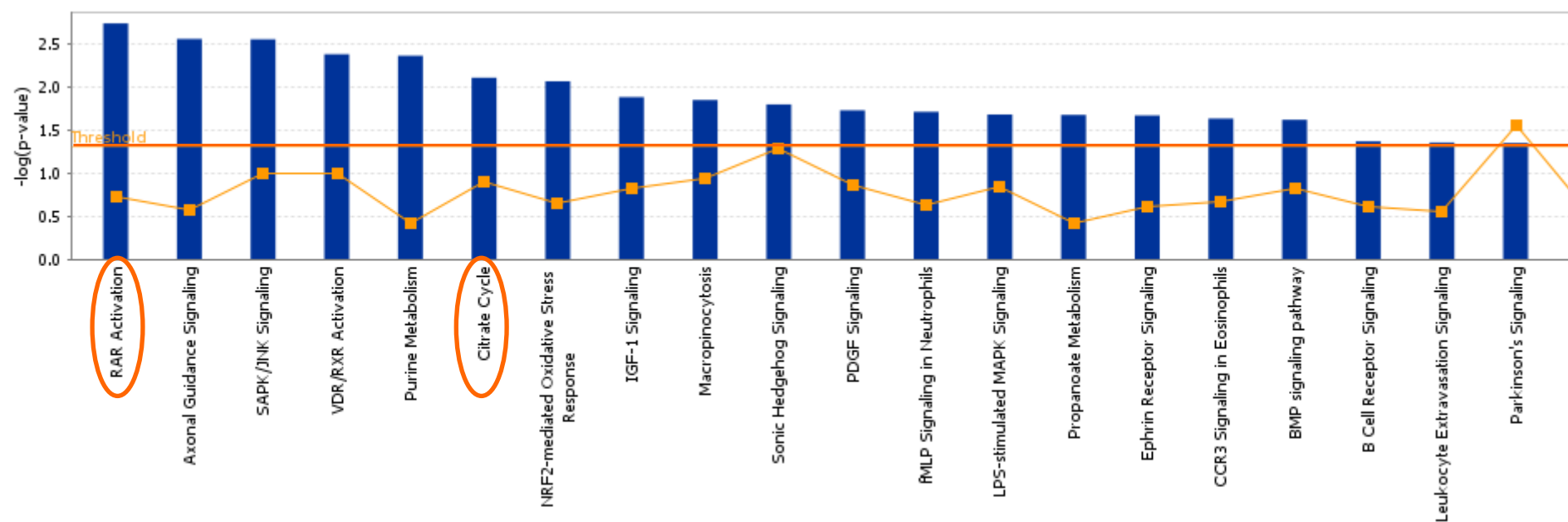


**Figure 5.3. Microarray Data Quality Control.** Quality control results for microarray data were visualised using BeadStudio software. Direct Hyb Control Plots generated for samples (bottom panel) were consistent with Beadstudio Direct Hyb Control Plot examples (top panel), verifying the validity of gene expression microarray data. Details of BeadStudio control plots are provided in the table (right hand panel). \*, sample-independent control metrics



 ratio of the number of differentially expressed genes from the data set mapping to the canonical pathway divided by the total number of genes mapping to the pathway

**Figure 5.4. IPA Canonical Pathway Analysis of BeadStudio Microarray Data.** Canonical metabolic pathways significantly affected by the presence of type 2 diabetes were observed to cross the threshold value ( $P \leq 0.05$ ). Significance is based on the number of differentially expressed genes in the pathway. Differentially expressed genes involved in the citrate cycle and retinoic acid receptor (RAR) activation were identified as candidate genes for further investigation.

Gene Symbol	Gene Name	Diff Score	Fold Change
<i>ATP5G3</i>	ATP synthase, H <sup>+</sup> transporting, mitochondrial F0 complex, subunit C3 (subunit 9)	-18.009	-1.397
<i>IDH3G</i>	isocitrate dehydrogenase 3 (NAD <sup>+</sup> ) gamma	13.807	1.306
<i>SDHAL1</i>	succinate dehydrogenase complex, subunit A, flavoprotein pseudogene 1	-15.807	-1.393
<i>SDHC</i>	succinate dehydrogenase complex, subunit C, integral membrane protein, 15kDa	-26.557	-1.346

**Table 5.1. Differentially Expressed Citrate Cycle Genes.** IPA canonical pathway analysis of BeadStudio microarray data identified 4 genes within the citrate cycle pathway as being differentially expressed in cells from patients with CAD and type 2 diabetes (T2D). *ATP5G3*, *SDHAL1* and *SDHC* were observed to be downregulated in cells from patients with T2D, while *IDH3G* was upregulated in these patients.

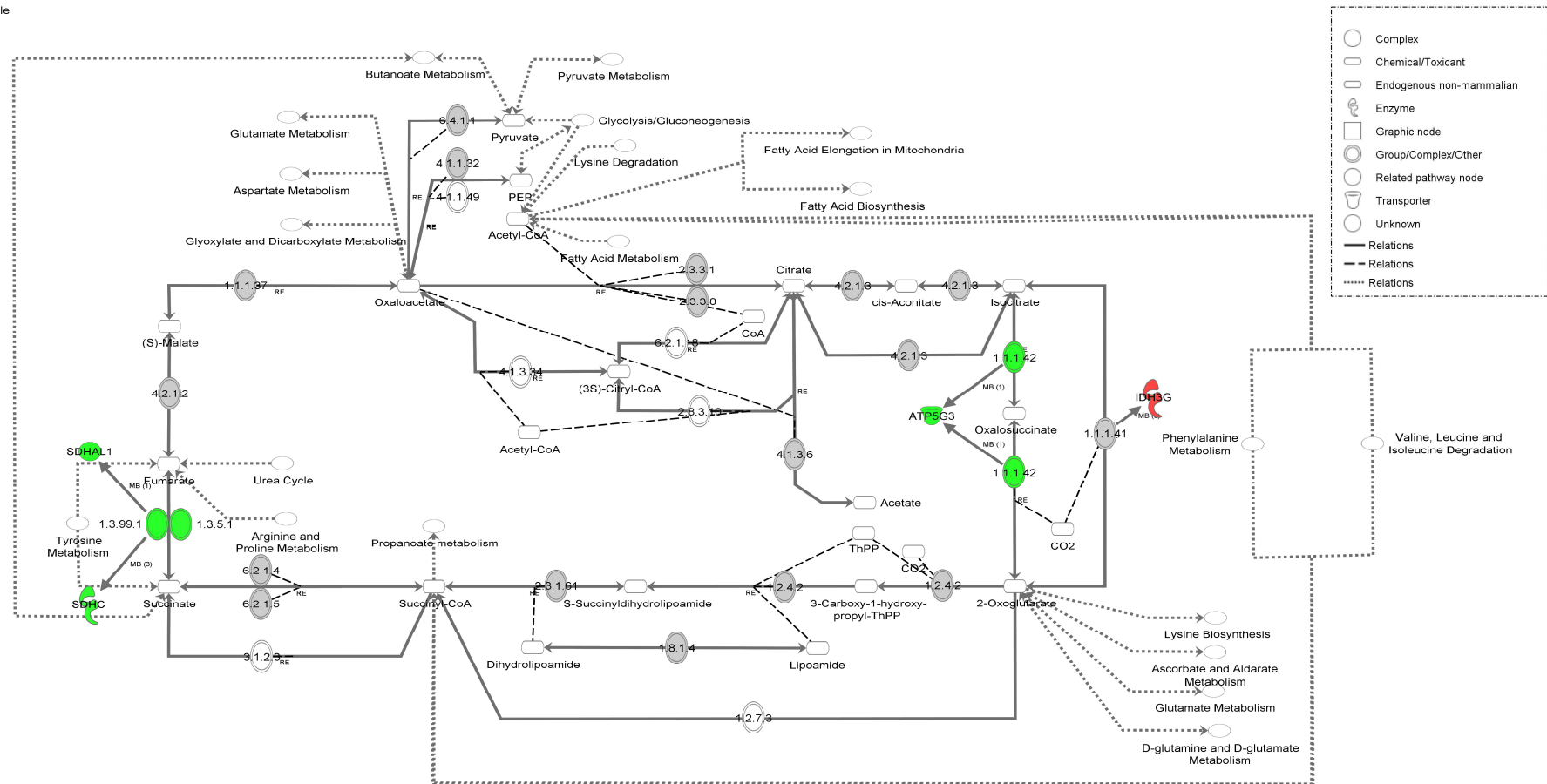


**Figure 5.5. Citrate Cycle Canonical Pathway.** The citrate cycle metabolic pathway showing candidate genes differentially expressed in HSVECs from patients with type 2 diabetes (Ingenuity Pathway Analysis).

Expression of *PRKAG1*, encoding the regulatory  $\gamma$ 1-subunit of AMPK, was observed to be significantly downregulated in CAD patients with T2D (Table A1) and involved in a number of significantly affected metabolic pathways, including retinoic acid receptor (RAR) activation, the most significantly affected canonical pathway (Table 5.2 and Figure 5.6). With AMPK implicated in T2D (section 1.5.1 and Chapter 4), *PRKAG1* was also selected as a candidate gene and its expression further investigated.

#### 5.3.2.2.2 Confirmation of Differential Expression of Candidate Genes by TaqMan<sup>®</sup> Real-Time RT-PCR

On attempting to confirm differential expression of microarray candidate genes by TaqMan<sup>®</sup> qRT-PCR, no statistically significant difference in HSVEC *ATP5G3* ( $\Delta$ Ct,  $5.706 \pm 0.412$  vs  $5.477 \pm 0.680$ ;  $P=0.763$ ; Figure 5.7A) and *IDH3G* ( $\Delta$ Ct,  $3.429 \pm 0.168$  vs  $3.659 \pm 0.223$ ;  $P=0.418$ ; Figure 5.7B) mRNA expression was found in cells isolated from CAD patients with and without T2D. Similarly, no significant difference in HSVEC *SDHC* mRNA expression was observed between patients with CAD and T2D and patients with CAD alone ( $\Delta$ Ct,  $3.556 \pm 0.176$  vs  $3.708 \pm 0.392$ ;  $P=0.692$ ; Figure 5.7C). However, the direction of change in *SDHC* expression reflected that observed on analysis of microarray data with a trend towards decreased expression in patients with CAD and T2D (Figure 5.7C).

As shown in Figure 5.7D, no significant difference in HSVEC *PRKAG1* mRNA expression was observed between patients with CAD and T2D and patients with CAD alone ( $\Delta$ Ct,  $1.315 \pm 0.317$  vs  $1.487 \pm 0.417$ ;  $P=0.746$ ) but, a trend towards decreased expression in CAD patients with T2D was noted, reflecting the direction of change observed on analysis of microarray data (Figure 5.7D).

Gene Symbol	Gene Name	Diff Score	Fold Change
<i>CCNH</i>	cyclin H	-20.875	-1.289
<i>GTF2H1</i>	general transcription factor IIH, polypeptide 1, 62kDa	13.661	1.223
<i>IL3RA</i>	interleukin 3 receptor, alpha (low affinity)	-14.374	-1.263
<i>MAP2K4</i>	mitogen-activated protein kinase kinase 4	-15.044	-1.228
<i>MAP3K1</i>	mitogen-activated protein kinase kinase kinase 1	15.91	1.259
<i>PIK3CA</i>	phosphoinositide-3-kinase, catalytic, alpha polypeptide	14.406	1.223
<i>PRKAG1</i>	protein kinase, AMP-activated, gamma 1 non-catalytic subunit	-14.846	-1.255
<i>PRKCI</i>	protein kinase C, iota	14.289	1.222
<i>RDH5</i>	retinol dehydrogenase 5 (11-cis/9-cis)	15.75	1.249
<i>RDH11</i>	retinol dehydrogenase 11 (all-trans/9-cis/11-cis)	16.835	1.253

**Table 5.2. Differentially Expressed Genes Involved in Retinoic Acid Receptor (RAR) Activation.** IPA canonical pathway analysis of BeadStudio microarray data identified 10 genes involved in the RAR activation metabolic pathway, including *PRKAG1*, as being differentially expressed in cells from patients with CAD and type 2 diabetes.



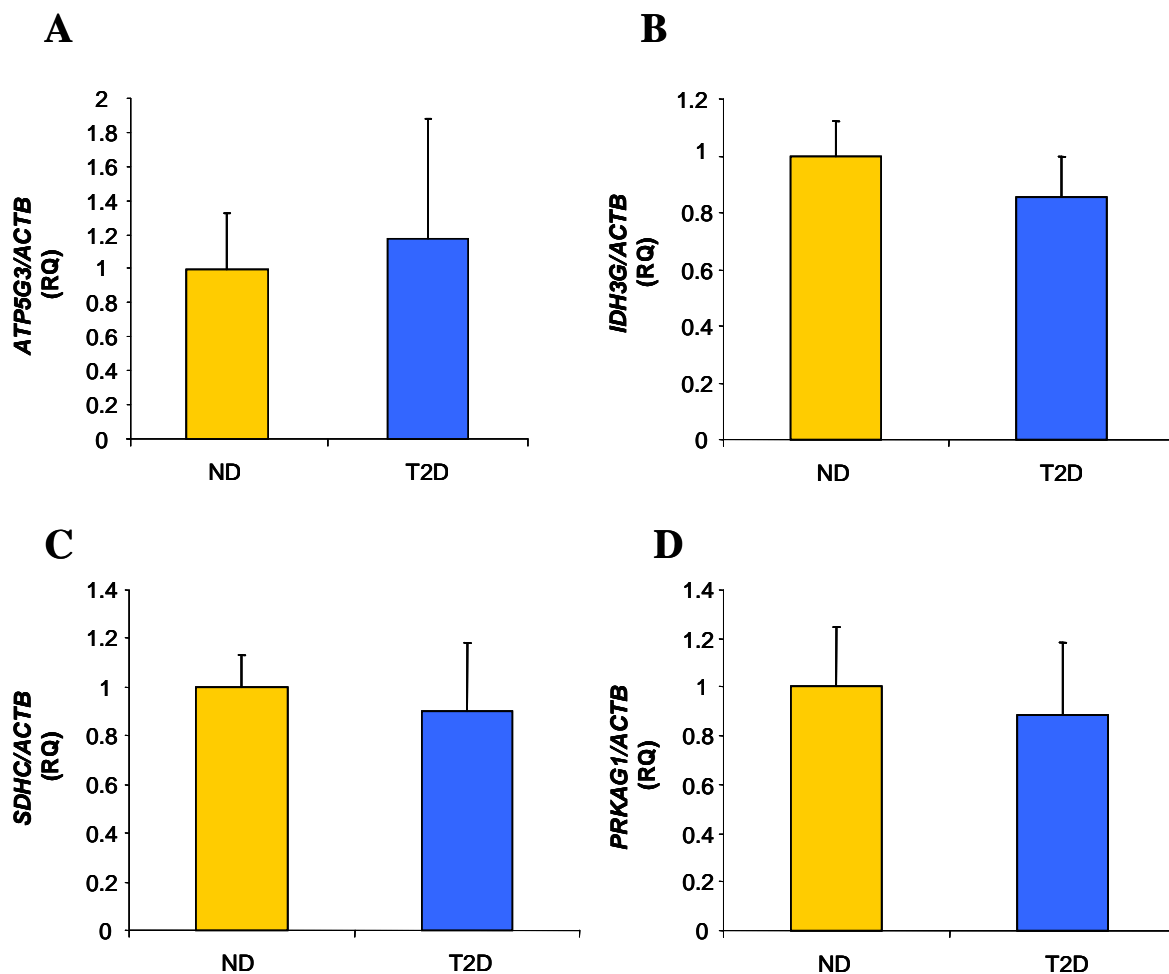


**Figure 5.7. BeadStudio Candidate Gene mRNA Expression Relative to  $\beta$ -actin (*ACTB*) as Assessed by TaqMan<sup>®</sup> qRT-PCR.** (A) *ATP5G3*, (B) *IDH3G*, (C) *SDHC* and (D) *PRKAG1* mRNA expression was investigated and compared in HSVECs isolated from CAD patients with (T2D, n=5) and without (ND, n=10) type 2 diabetes. No statistically significant differences in mRNA expression were observed. For *ATP5G3*, *IDH3G* and *PRKAG1*, reactions were carried out in singleplex. For *SDHC*, reactions were carried out in multiplex. RQ, relative quantitation



### 5.3.2.3 Rosetta Resolver<sup>®</sup> Analysis

Using Rosetta Resolver<sup>®</sup> software, a total of 92 probes were found to be differentially expressed in HSVECs from patients with CAD and T2D as compared to those from patients with CAD alone (Figure 5.8). In certain cases, more than one probe corresponded to a particular gene. This, coupled with the fact that IPA does not yet recognise all Illumina<sup>®</sup> probes, meant data generated from IPA revealed 77 genes to be differentially expressed in cells from patients with T2D. Of these 77 genes, expression of 15 genes was upregulated and expression of the remaining 62, downregulated. A complete list of these differentially expressed genes is included as Table A2 in the Appendix.

Expression of *ACAD11*, encoding acyl-Coenzyme A dehydrogenase family, member 11, was observed to be significantly downregulated in CAD patients with T2D (Table A2). Given the role of acyl-Coenzyme dehydrogenases in  $\beta$ -oxidation of fatty acids in the mitochondria and the fact that mitochondria and AMPK have been implicated in T2D, *ACAD11* was selected as a candidate gene for further investigation.

#### 5.3.2.3.1 Ingenuity Pathway Analysis

Analysis of Rosetta Resolver<sup>®</sup> microarray data using IPA software identified G-protein coupled receptor signalling as the canonical metabolic pathway most significantly affected by the presence of T2D in patients with CAD (Figure 5.9). As previously described, significance was based on the number of genes with differentially expressed probes mapping to the pathway (Table 5.3 and Figure 5.10). *AGTR2*, and *PI3KR2* were selected as candidate genes for further study.

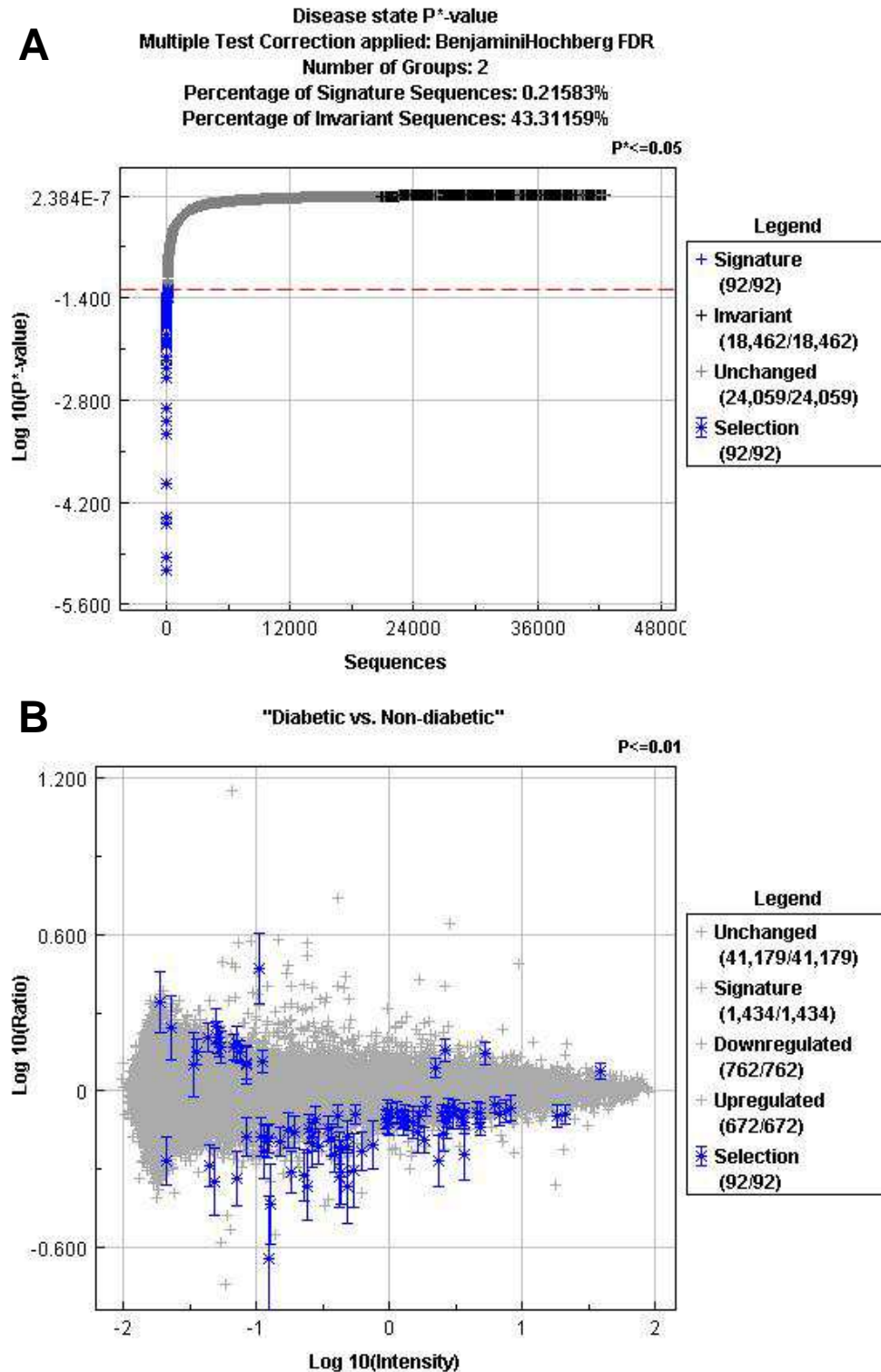
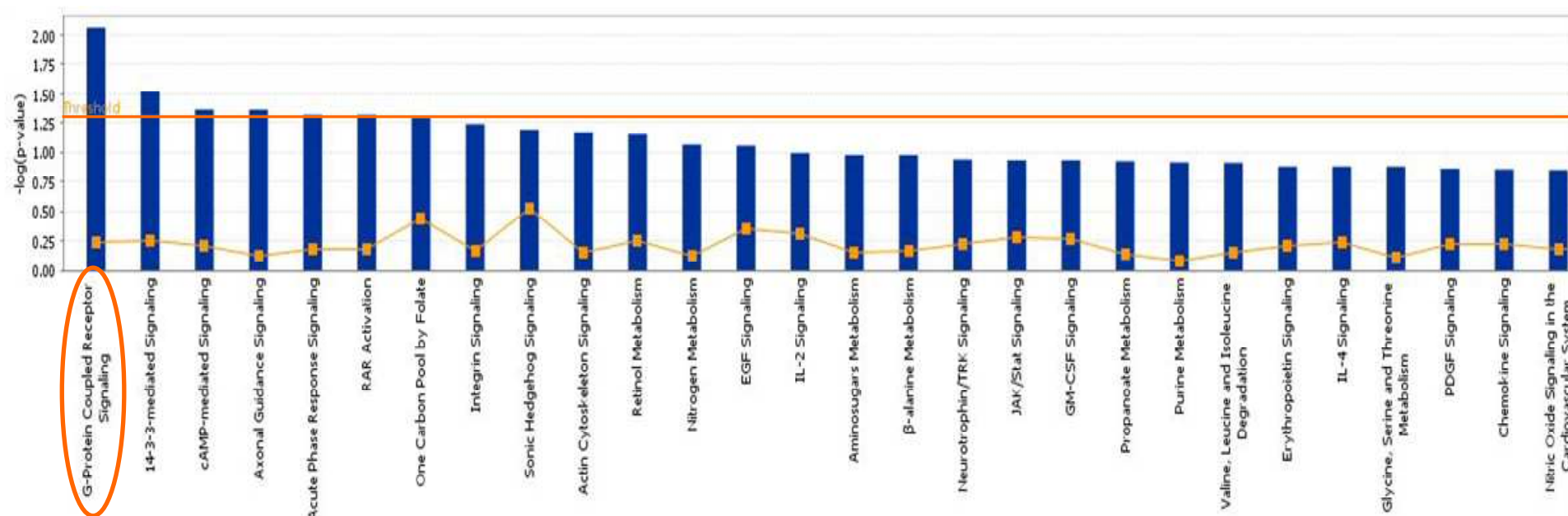


**Figure 5.8. Differentially Expressed Probes Identified by Rosetta Resolver® Analysis.** (A) The Illumina® probes' false discovery rates (FDRs) ordered on a log10 scale. The 92 in blue are below the 5% FDR cut-off, indicated by the red dashed line. Remaining probes ('Unchanged' and 'Invariant') are non-significantly differentially expressed. (B) Data displayed as log-ratios on the y-axis against mean intensity ratios on the x-axis. The 92 significantly differentially expressed probes are shown in blue, whilst remaining probes are in grey.



— ratio of the number of differentially expressed genes from the data set mapping to the canonical pathway divided by the total number of genes mapping to the pathway

**Figure 5.9. IPA Canonical Pathway Analysis of Rosetta® Resolver Microarray Data.** Canonical metabolic pathways significantly affected by the presence of type 2 diabetes were observed to cross the threshold value ( $P \leq 0.05$ ). Significance is based on the number of differentially expressed genes in the pathway. Differentially expressed genes involved in G-protein coupled receptor signalling were identified as candidate genes for further investigation.

Gene Symbol	Gene Name	Fold Change	P-value
<i>AGTR2</i>	angiotensin II receptor, type 2	1.453	0.0239
<i>PDE8A</i>	phosphodiesterase 8A	-1.263	0.0319
<i>PIK3R2</i>	phosphoinositide-3-kinase, regulatory subunit 2 (beta)	-1.221	0.0358

**Table 5.3. Differentially Expressed G-protein Coupled Receptor Signalling Genes.** IPA canonical pathway analysis of BeadStudio microarray data identified 3 genes within the G-protein coupled receptor signalling pathway as being differentially expressed in cells from patients with CAD and type 2 diabetes (T2D). *AGTR2* was observed to be upregulated in cells from patients with T2D, while *PDE8A* and *PIK3R2* were downregulated in these patients.

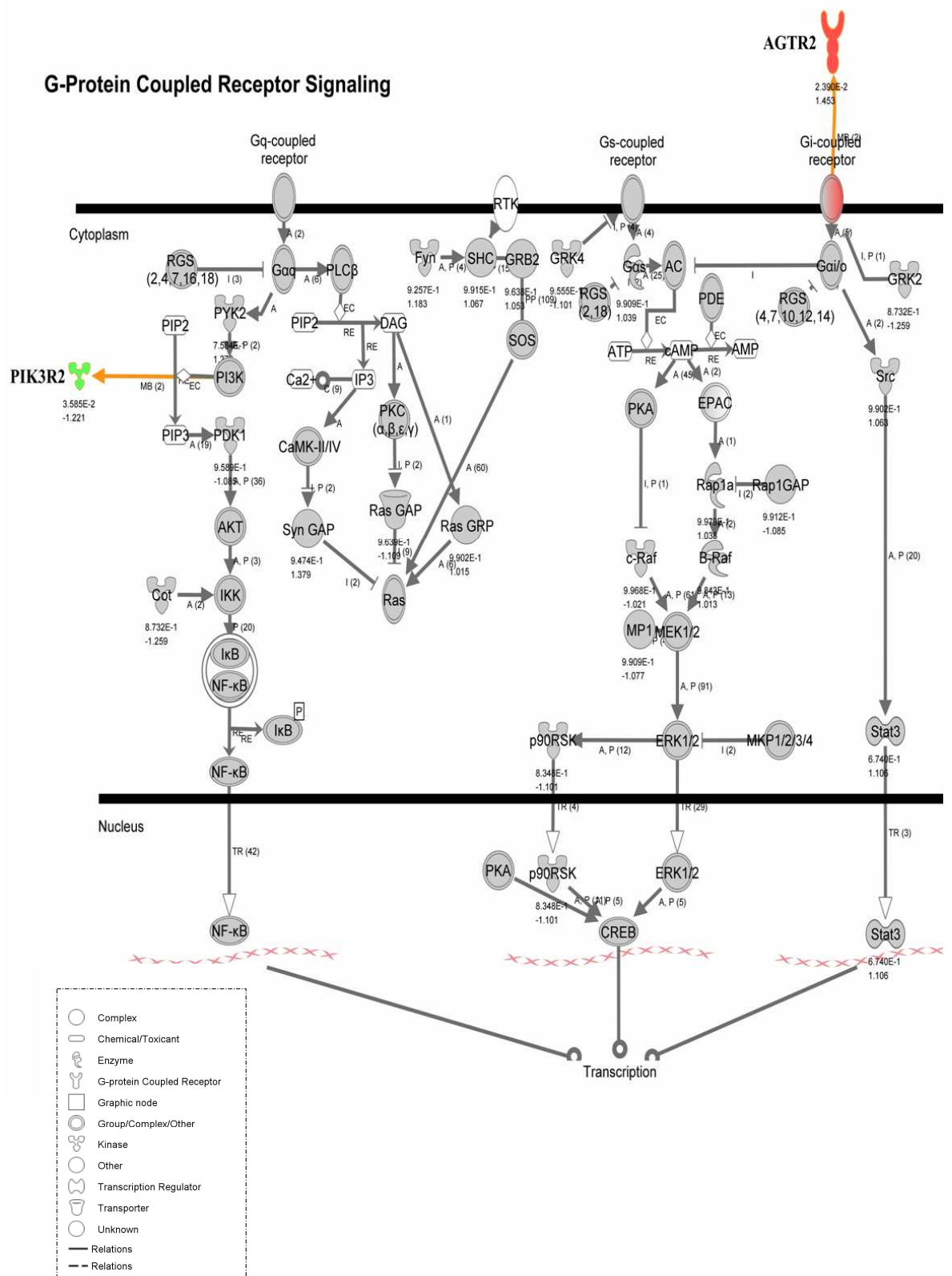


**Figure 5.10. G-protein Coupled Receptor Signalling Canonical Pathway.** G-protein coupled receptor signalling metabolic pathway showing candidate genes differentially expressed in HSVECs from patients with type 2 diabetes (Ingenuity Pathway Analysis).

#### 5.3.2.3.2 Confirmation of Differential Expression of Candidate Genes by TaqMan<sup>®</sup> Real-Time RT-PCR

As shown in Figure 5.11A, no significant difference in HSVEC *ACAD11* mRNA expression was observed between patients with CAD and T2D and patients with CAD alone ( $\Delta\text{Ct}$ ,  $7.815 \pm 0.236$  vs  $7.185 \pm 0.301$ ;  $P=0.205$ ) as assessed by TaqMan<sup>®</sup> qRT-PCR. Similarly, HSVEC *PI3KR2* mRNA expression was found not be statistically significantly different in HSVECs isolated from CAD patients with and without T2D ( $\Delta\text{Ct}$ ,  $6.161 \pm 0.186$  vs  $5.527 \pm 0.151$ ;  $P=0.067$ ; Figure 5.11B). Expression of *AGTR2* mRNA was undetectable in HSVECs from either patient group.

#### 5.3.2.4 Identification of Differentially Expressed Genes Common to BeadStudio & Rosetta Resolver<sup>®</sup> Microarray Data

A total of 45 differentially expressed genes were found to be common to both BeadStudio and Rosetta Resolver<sup>®</sup> data sets as represented in a Venn diagram (Figure 5.12) and listed in Table 5.4. Commonly differentially expressed genes included candidate genes, *ACAD11* and *AGTR2*. Other candidate genes were not found to be differentially expressed in both data sets.

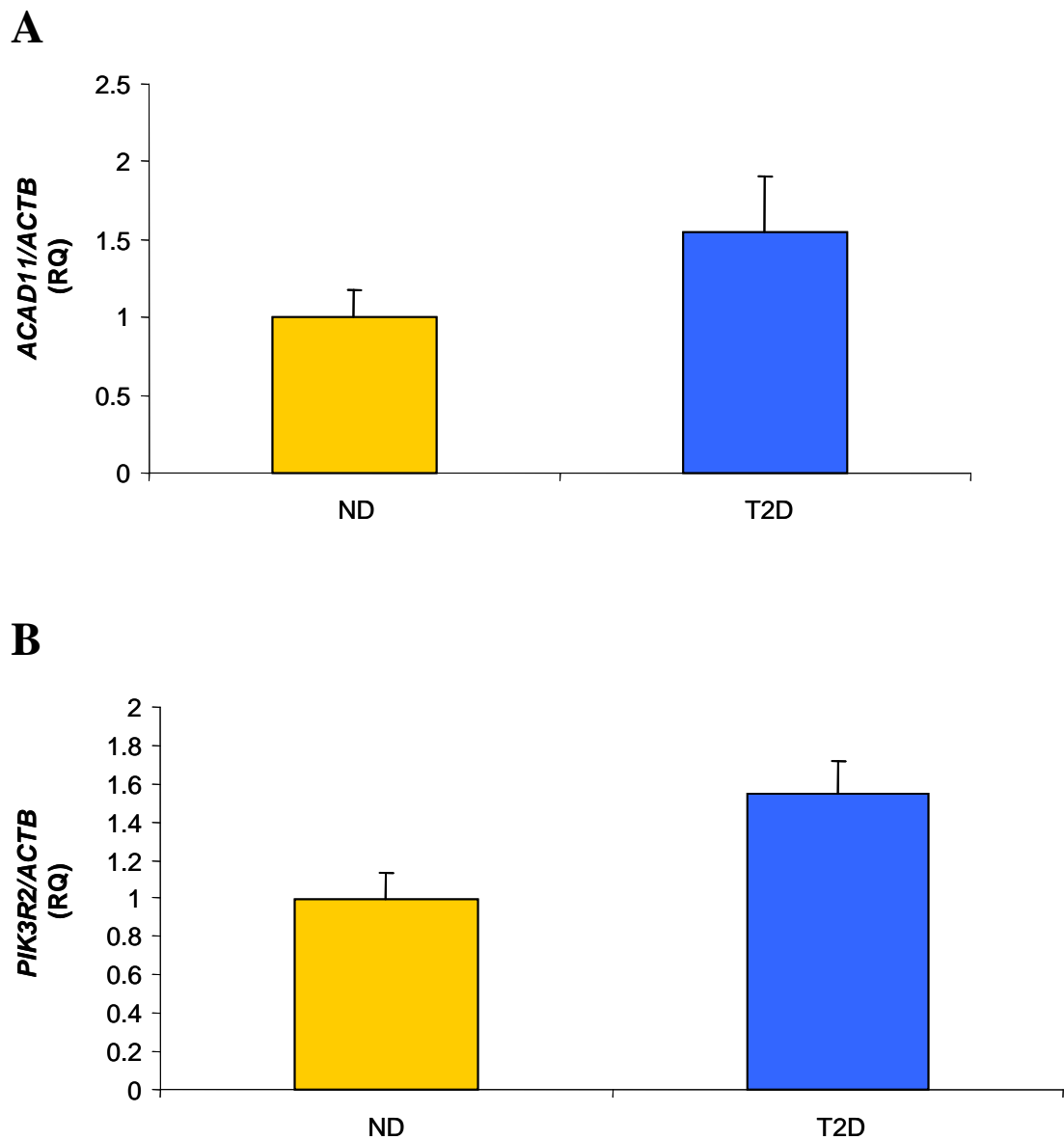


**Figure 5.11. Rosetta Resolver<sup>®</sup> Candidate Gene mRNA Expression Relative to  $\beta$ -actin (*ACTB*) as Assessed by TaqMan<sup>®</sup> qRT-PCR.** Expression of (A) *ACAD11* and (B) *PIK3R2* mRNA expression was investigated in HSVECs isolated from CAD patients with (T2D, n=5) and without (ND, n=10) type 2 diabetes. No statistically significant differences in mRNA expression were observed. Reactions were carried out in singleplex. RQ, relative quantitation



**Figure 5.12. Differentially Expressed Genes Common to BeadStudio & Rosetta Resolver® Analyses of Microarray Data.** Venn diagram illustrating that 45 differentially expressed genes were found to be common to both BeadStudio and Rosetta Resolver® data sets. For both analyses, numbers indicate differentially expressed genes rather than probes.



Gene Symbol	Gene Name
<i>ABCC5</i>	ATP-binding cassette, sub-family C (CFTR/MRP), member 5
<i>ACAD11</i>	acyl-Coenzyme A dehydrogenase family, member 11
<i>AFG3L1</i>	AFG3 ATPase family gene 3-like 1 ( <i>S. cerevisiae</i> )
<i>AGTR2</i>	angiotensin II receptor, type 2
<i>AMT</i>	aminomethyltransferase
<i>AMY2A</i>	amylase, alpha 2A (pancreatic)
<i>CCDC113</i>	coiled-coil domain containing 113
<i>CFDP1</i>	craniofacial development protein 1
<i>CROP</i>	cisplatin resistance-associated overexpressed protein
<i>DGKQ</i>	diacylglycerol kinase, theta 110kDa
<i>E4F1</i>	E4F transcription factor 1
<i>EFHD1</i>	EF-hand domain family, member D1
<i>ERGIC2</i>	ERGIC and golgi 2
<i>FAP</i>	fibroblast activation protein, alpha
<i>GNRH1</i>	gonadotropin-releasing hormone 1 (luteinizing-releasing hormone)
<i>HIP1R</i>	huntingtin interacting protein 1 related
<i>KIAA1328</i>	KIAA1328
<i>LOC283932</i>	hypothetical LOC283932
<i>LOC727762</i>	similar to NADH:ubiquinone oxidoreductase B15 subunit
<i>LOC729137</i>	hypothetical protein LOC441528
	leucine-rich repeats and calponin homology (CH) domain containing 4
<i>LRCH4</i>	
<i>LZTFL1</i>	leucine zipper transcription factor-like 1
<i>MFSD1</i>	major facilitator superfamily domain containing 1
<i>MGC42630</i>	family with sequence similarity 27, member E3
<i>NSUN5B</i>	NOL1/NOP2/Sun domain family, member 5B
<i>NUTF2</i>	nuclear transport factor 2
<i>PDE8A</i>	phosphodiesterase 8A
<i>RAB22A</i>	RAB22A, member RAS oncogene family
<i>RALBP1</i>	ralA binding protein 1
<i>RDH5</i>	retinol dehydrogenase 5 (11-cis/9-cis)
<i>RIC8B</i>	resistance to inhibitors of cholinesterase 8 homolog B ( <i>C. elegans</i> )
<i>SAA4</i>	serum amyloid A4, constitutive
<i>SETD6</i>	SET domain containing 6
<i>SLC23A3</i>	solute carrier family 23 (nucleobase transporters), member 3
<i>SLC38A6</i>	solute carrier family 38, member 6
<i>STK36</i>	serine/threonine kinase 36, fused homolog ( <i>Drosophila</i> )
<i>TDRD9</i>	tudor domain containing 9
<i>TM9SF3</i>	transmembrane 9 superfamily member 3
<i>USHBP1</i>	Usher syndrome 1C binding protein 1
<i>WDR60</i>	WD repeat domain 60
<i>ZBTB12</i>	zinc finger and BTB domain containing 12
<i>ZNF266</i>	zinc finger protein 266
<i>ZNF439</i>	zinc finger protein 439
<i>ZNF569</i>	zinc finger protein 569
<i>ZNF83</i>	zinc finger protein 83

**Table 5.4. Differentially Expressed Genes Common to BeadStudio & Rosetta Resolver® Analyses of Microarray Data.** A total of 45 differentially expressed genes were found to be common to both BeadStudio and Rosetta Resolver® data sets

## **5.4 Discussion**

Experimental work described in this chapter explored differential gene expression in primary HSVECs isolated from CAD patients with and without the additional CVD risk factor, T2D. These studies were performed in an attempt to identify candidate genes and pathways contributing to the more severe endothelial dysfunction observed in vessels from patients with CAD and T2D (Figure 3.2B). This work represents a novel investigation as previous attempts to identify differences in gene expression profiles between CAD patients with and without T2D have focused on intact cardiac tissue (381;384).

Expression profiles of over 25,000 annotated genes were assessed using Illumina<sup>®</sup> HumanWG-6 v3.0 Expression BeadChips. Primary analysis of microarray data was carried out using BeadStudio software which generated a list of 727 differentially expressed probes (Table A1).

On uploading BeadStudio data to IPA, the citrate cycle was identified as a canonical metabolic pathway significantly affected by T2D (Figure 5.4). As outlined in section 1.3.4.3.1, electron donor overproduction by the citrate cycle is known to contribute to increased mtROS production in T2D, thus facilitating progression of endothelial dysfunction (230). Furthermore, reduced glucose oxidation and storage in T2D have been observed to occur in parallel with reduced activity of the citrate cycle (391) and microarray analysis has revealed expression of a number of citrate cycle genes to be reduced in muscle biopsies from patients with T2D, including *ATP5G3* and *SDHC* (392), genes observed to be downregulated here (Table 5.1). Consequently, *ATP5G3*, *SDHC* and a third differentially expressed gene affecting the citrate cycle metabolic pathway, *IDH3G* (Table 5.1), were selected as candidate genes for further study. As shown in Table 5.1, *SDHAL1* was also recognised as a differentially expressed gene involved in the citrate cycle. However, it was identified as a pseudogene and thus no attempt was made to confirm its differential expression.

Fold changes in citrate cycle gene expression were relatively modest (Table 5.1) and therefore it is perhaps not surprising that differential expression of *ATP5G3*, *IDH3G* and *SDHC* was not confirmed using TaqMan<sup>®</sup> qRT-PCR and the  $2^{-\Delta\Delta C_t}$  comparative method, a method limited in its ability to accurately detect less than a two-fold change in gene expression (301). Given the complex nature of T2D, it seems likely that modest changes in

expression of several genes in a given pathway will be important and, as stated, previous studies have suggested that coordinated reduction in expression of genes of oxidative metabolism are implicated in T2D (392). Of note, analysis of microarray data revealed downregulation of *ATP5G3* expression and upregulation of *IDH3G* expression in cells from CAD patients with T2D (Table 5.1). The fact that TaqMan<sup>®</sup> qRT-PCR demonstrated a trend towards a change in expression in the opposite direction for both genes (Figure 5.7A and B), may be explained by the fact that due to limited human cellular material, qRT-PCR experiments did not incorporate the entire microarray patient group.

Interestingly, although not confirmed by qRT-PCR, downregulation of *ATPG3* and *SDHC* in HSVECs from patients with T2D could lead to reduced flux through the citrate cycle and a decrease in ATP synthesis which, in turn, would lead to an increase in AMPK activity (248). Reduced expression of citrate cycle genes in the endothelium of CAD patients with T2D may therefore contribute to the increased AMPK activity observed in HSVECs isolated from these patients (Figure 4.3).

*PRKAG1* encodes the regulatory  $\gamma$ 1-subunit of AMPK and was observed to be involved in a number of metabolic pathways significantly affected by T2D, including IGF-1 signalling (Figure 5.4) and the most significantly affected pathway, RAR activation (Figure 5.4, Table 5.2 and Figure 5.6). As outlined, AMPK is recognised as a therapeutic target in T2D (137;143) and with results suggesting AMPK activity is increased in HSVECs isolated from patients with both CAD and T2D (Figure 4.3), *PRKAG1* was selected as a fourth candidate gene from BeadStudio microarray data. Again, BeadStudio analysis revealed a modest reduction in *PRKAG1* expression which was not confirmed by TaqMan<sup>®</sup> qRT-PCR. This finding was perhaps to be expected as AMPK subunits do not exist as single entities, found only within heterotrimers of  $\alpha$ -,  $\beta$ - and  $\gamma$ -subunits (248) and expression of all three should therefore remain the same. No difference in expression of *PRKAA1*, encoding the  $\alpha$ 1-catalytic subunit, was observed in HSVECs from CAD patients with T2D (Figure 4.5). Therefore, if *PRKAG1* expression was indeed downregulated in cells from these patients, it would follow that expression of *PRKAG2* and/or *PRKAG3*, encoding the  $\gamma$ 2- and  $\gamma$ 3-subunits respectively, would be upregulated. However, neither *PRKAG2* nor *PRKAG3* were identified as being differentially expressed on analysis of microarray data and, as such, downregulation of *PRKAG1* appears to be a spurious finding, potentially representing a false positive outcome.

NRF2-mediated oxidative stress response and IGF-1 signalling, canonical metabolic pathways significantly affected by the presence of T2D (Figure 5.4), were of potential interest in terms of T2D pathogenesis. However, it should be noted that BeadStudio analysis had limited statistical merit as no FDR cut-off was applied or background subtraction of data performed. This may explain why differential expression of candidate genes was not confirmed by qRT-PCR and is why, with human cellular material limited, differentially expressed genes involved in additional canonical pathways were not investigated further. Instead, a more statistically robust analysis of microarray data using Rosetta Resolver<sup>®</sup> software was performed.

Uploading microarray data to the Rosetta Resolver<sup>®</sup> Gene Expression Data Management and Analysis System permitted identification of an outlier using PCA. This outlier, a T2D patient, was subsequently excluded from further analysis. Rosetta Resolver<sup>®</sup> analysis, incorporating more stringent statistical limits, generated a list of fewer significantly differentially expressed genes (Table A2) than BeadStudio analysis. In addition, IPA revealed a decrease in the number of canonical metabolic pathways significantly affected (Figure 5.9). G-protein coupled receptor signalling was observed to be the pathway most significantly affected by the presence of T2D (Figure 5.9) with *AGTR2* and *PIK3R2* identified as differentially expressed genes involved in this metabolic process (Table 5.3).

Expression of *AGTR2*, encoding the Ang II type 2 receptor, was found to be modestly upregulated in HSVECs from patients with T2D (Table 5.3). Ang II is one of the main effector molecules of the RAS, known to play a deleterious role in the initiation and progression of atherosclerosis (393). Ang II mediates its physiological effects by binding Ang II type 1 (AT<sub>1</sub>) and type 2 (AT<sub>2</sub>) receptors on the cell membrane (394;395) (Figure 5.13). AT<sub>1</sub> receptor binding has been shown to mediate vasoconstrictor responses and cell growth and proliferation of VSMCs, cardiomyocytes and coronary endothelial cells. As such, the AT<sub>1</sub> receptor has been implicated in various cardiovascular pathologies, including atherosclerosis and stroke (393;395) and ARBs act to block the adverse effects of Ang II through direct interaction with this receptor (393;396). Conversely, the AT<sub>2</sub> receptor mediates vasodilatory responses and biological processes that counteract the trophic responses mediated through AT<sub>1</sub> receptor (395;397).

Previously described findings of this study suggest CAD patients with T2D have poorer endothelial function (Figure 3.2) and are subject to increased oxidative stress in the

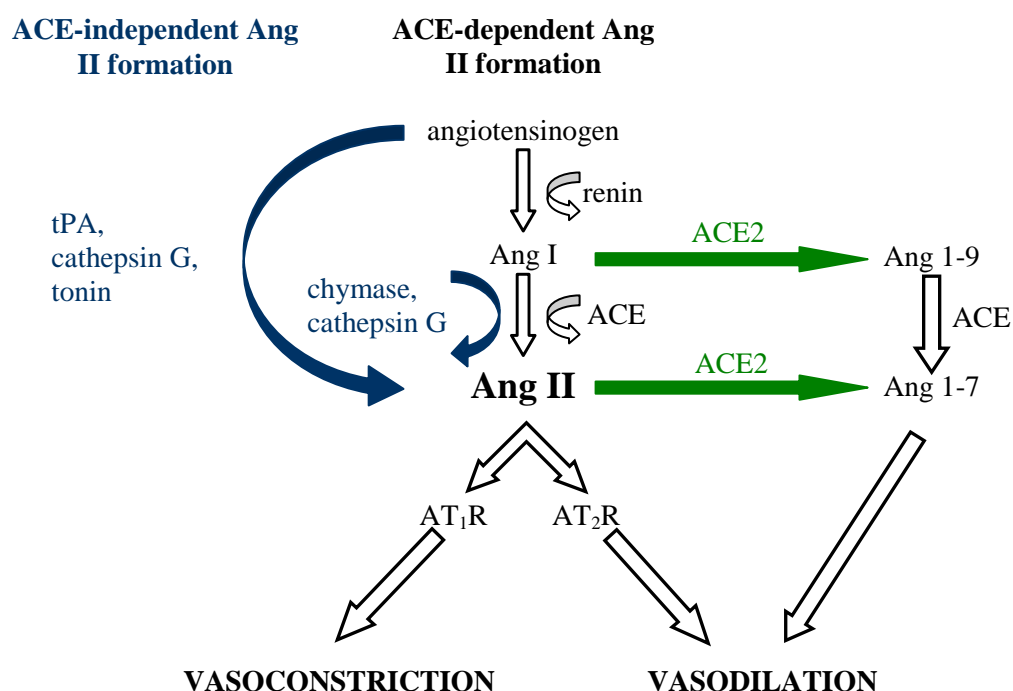


**Figure 5.13. Renin-Angiotensin System Enzymatic Cascades.** The main effector molecule of the renin-angiotensin system (RAS), angiotensin II (Ang II), can be generated in an angiotensin converting enzyme (ACE)-dependent or independent manner. ACE-dependent Ang II formation occurs via a two step reaction: renin catalyses the conversion of angiotensinogen to angiotensin I (Ang I) which is subsequently hydrolysed by ACE to form Ang II. Alternatively, the direct conversion of angiotensinogen to Ang I can occur independently of ACE via enzymes such as tissue plasminogen activator (tPA), cathepsin G and tonin. In addition, chymase and cathepsin G are able to catalyse the ACE-independent hydrolysis of Ang I to Ang II. Ang II mediates its physiological effects by binding angiotensin II type I (AT<sub>1</sub>) and angiotensin II type 2 (AT<sub>2</sub>) receptors on the cell membrane. The receptors display a heterogenous tissue distribution with the AT<sub>1</sub> receptor present in adult cardiovascular tissues and the AT<sub>2</sub> receptor observed to be highly expressed during foetal development. AT<sub>1</sub> receptor binding has been shown to mediate vasoconstrictor responses. Conversely, the AT<sub>2</sub> receptor mediates vasodilatory responses. A recently discovered ACE-related carboxypeptidase (ACE2) catalyses the cleavage of Ang I to angiotensin 1-9 (Ang 1-9) and mediates the transformation of Ang II into angiotensin 1-7 (Ang 1-7), a known vasodilator (398;399). Ang 1-9 may also be directly converted to Ang 1-7 by ACE. Adapted from (395;396).

endothelium (Figure 3.8) as compared to patients with CAD alone. As such, it seemed possible that upregulation of *AGTR2* expression in cells from T2D patients represented an adaptive response to adverse effects of the AT<sub>1</sub> receptor. However, while analysis of microarray data revealed differential expression of *AGTR2*, expression levels detected were very low. Consequently, on attempting to confirm differential expression of the gene using TaqMan<sup>®</sup> qRT-PCR, *AGTR2* mRNA levels were undetectable. This finding is concordant with previous studies which have found that the AT<sub>2</sub> receptor is highly expressed during foetal development, with mRNA levels less abundant in adult cardiovascular tissue (394;395).

Identified as a second candidate gene from the Rosetta Resolver<sup>®</sup> data set (Table 5.3 and Figure 5.10), *PIK3R2* encodes the regulatory (IRS-binding) subunit of PI3K, p85 $\beta$  (400). As outlined in section 1.1, PI3K plays a pivotal role in insulin signalling and development of T2D and the p85 $\beta$  subunit has been shown to be involved in insulin sensitivity in mice (401). Differential expression of *PIK3R2* in the endothelium of patients with T2D could therefore contribute to reduced sensitivity to insulin, leading to a decrease in NO synthesis and the attenuated endothelial function observed in these patients (Figure 3.2). In this instance, microarray data analysis again revealed a modest fold change in gene expression which was not confirmed by TaqMan<sup>®</sup> qRT-PCR (Figure 5.11B). Indeed, once more qRT-PCR demonstrated a trend towards a change in expression in the direction opposite to that observed on analysis of microarray data (Table 5.3 and Figure 5.11B), possibly the result of PCR experiments involving only a subset of microarray patients. Given the potential significance of differential *PIK3R2* expression in the endothelium of patients with T2D, this kinase may merit further investigation in the future.

Although not observed to be involved in metabolic pathways significantly affected by T2D, *ACAD11* was found to be differentially expressed on Rosetta Resolver<sup>®</sup> analysis of microarray data (Table A2). The gene encodes one of the most recently identified subtypes of the acyl-Coenzyme A dehydrogenase (ACAD) family and is, as yet, of unknown function (402). However, with a number of ACAD subtypes involved in mitochondrial  $\beta$ -oxidation of fatty acids (402;403), a process implicated in development of T2D and insulin resistance (230), *ACAD11* was selected for further investigation.

*ACAD11* expression was observed to be downregulated in cells from patients with T2D on Rosetta Resolver<sup>®</sup> analysis of microarray data (Table A2). Although presently

uncharacterised, if *ACAD11* represents an ACAD family member required for  $\beta$ -oxidation of fatty acids, downregulation of its expression may imply impaired  $\beta$ -oxidation and thus reliance on glucose oxidation in the endothelium of patients with T2D. This situation could potentially be associated with the increased AMPK activity observed in HSVECs isolated from patients with CAD and T2D (Figure 4.3), as increasing activity of the kinase, with a view to stimulating fatty acid oxidation, could be an attempt to overcome the problem of increased glucose oxidation. However, TaqMan<sup>®</sup> qRT-PCR failed to confirm differential expression of *ACAD11*, instead revealing a trend towards increased expression in CAD patients with T2D (Figure 5.11A).

On examination of both microarray data sets, a total of 45 differentially expressed genes were identified as being common to both BeadStudio and Rosetta Resolver<sup>®</sup> analyses (Table 5.4 and Figure 5.12). Perhaps unsurprisingly, given the limited statistical merit of the analysis, none of the candidate genes identified from the BeadStudio data set were included in the list of common genes, supporting the notion that this analysis may have given rise to a number of false positives. *AGTR2* and *ACAD11*, candidate genes selected from Rosetta Resolver<sup>®</sup> analysis, were found to be common to both lists of differentially expressed genes. However, *PIK3R2* was not identified as a common gene. This gene was selected from the more statistically robust Rosetta Resolver<sup>®</sup> data set and so despite its absence from the BeadStudio list, it is still an interesting candidate. *PDE8A*, encoding phosphodiesterase 8A, was another gene identified as common to both data sets. Rosetta Resolver<sup>®</sup> analysis revealed *PDE8A* to be modestly downregulated in patients with T2D and involved in G-protein coupled receptor signalling (Figure 5.9 and Table 5.3). Further investigation of *PDE8A* expression was not carried out due to limited human cellular material and time constraints but, with the isoenzyme, PDE8B suggested to have a role in insulin response to glucose in rat pancreatic  $\beta$ -cells (404), *PDE8A* may represent a focus of future studies.

The transcriptional profiling described in this chapter represents the first human microarray study to be carried out within this laboratory and was not without limitations and difficulties. The application of stringent statistical limits resulted in relatively few genes being identified as differentially expressed between patient groups. There may be a number of potential explanations for this, including, as previously suggested, that human endothelial cells fail to retain the *in vivo* phenotype in culture. One possible strategy to overcome this issue could involve microarray analysis of pooled RNAs from passage 0

cells. Furthermore, complex diseases, such as T2D, are likely to be the result of low-magnitude alterations in expression of multiple genes and therefore the small subject numbers in this study limits the power to detect differences between groups. In addition, as previously discussed, using TaqMan<sup>®</sup> qRT-PCR and the  $2^{-\Delta\Delta C_t}$  method to validate differential expression means anything less than a two-fold change in gene expression is considered insignificant (301). Given these limitations, complementary methodologies, including proteomics and microRNA (miRNA) profiling, may aid in the elucidation of molecular mechanisms adversely affected in the endothelium of patients with CAD and T2D. With increasing evidence to implicate endothelial dysfunction in T2D disease progression (162), integration of these technologies, allowing examination of gene transcription and translation in the endothelium of CAD patients with T2D, seems key to understanding diabetic vascular complications.



## **6. General Discussion**

Endothelial dysfunction occurs in conjunction with CAD and is observed in both the coronary and peripheral vasculature (405). Accumulating evidence suggests a causative role for vascular oxidative stress in endothelial dysfunction and the pathogenesis of CAD (159). The prevalence of CAD in patients with T2D is more than ten times greater than in the general population and poorer clinical outcomes are observed in CAD patients with T2D than in those without (335;406;407). Previous investigations carried out within this laboratory have demonstrated endothelial dysfunction and elevated  $O_2^-$  production in saphenous veins from patients with advanced CAD (159). In addition to confirming these findings, this study has considered the effects of T2D on endothelial function and vascular  $O_2^-$  production, revealing more severe endothelial dysfunction in vessels from those CAD patients with T2D. Through application of a wide range of molecular techniques, cellular mechanisms underlying this oxidative stress and endothelial dysfunction have been investigated in primary endothelial cells isolated from CAD patients.

Having confirmed elevated  $O_2^-$  production in vessels from patients with CAD and with Al Benna *et al.* reporting that this increase occurs throughout the vessel wall (159), preliminary cellular work involved investigation of HSVEC  $O_2^-$  production. EPR spectroscopy failed to confirm significantly increased  $O_2^-$  release in cells from CAD patients relative to those from controls, raising the possibility that cultured primary cells, free from physiological stresses, do not retain the *in vivo* phenotype. While it is acknowledged that this may represent a potential limitation of the study, in focusing on cultured primary endothelial cells, a pragmatic approach to the exploration of endothelium-specific mechanisms of oxidative stress has been adopted.

Subsequent investigations revealed increased HSVEC SOD2 protein and mRNA expression in CAD patients, in particular those with T2D. This increase in SOD2 expression is likely to represent an adaptive response to elevated mitochondrial  $O_2^-$  production as accumulating evidence suggests mitochondrially-derived ROS contribute to oxidative stress and endothelial dysfunction in a range of cardiovascular pathologies, including CAD and T2D (222;224;225). Attempts to establish the contribution of mitochondria to cellular  $O_2^-$  production involved treatment of HSVECs with rotenone and MitoQ<sub>10</sub>. The results of these studies were inconclusive but the role of mitochondria in HSVEC  $O_2^-$  generation clearly merits further investigation. As such, alternative methods, including MitoSOX<sup>™</sup> (Invitrogen) staining, will be employed to this end in the future.

With HSVECs isolated from CAD patients failing to retain the significantly elevated  $O_2^-$  phenotype but displaying increased SOD2 expression,  $H_2O_2$  may represent a more useful marker of oxidative stress in the endothelium of these patients. Known to induce endothelial dysfunction (408),  $H_2O_2$  is a more stable molecule than  $O_2^-$  which may render its detection in HSVECs less challenging. Thus, in addition to assessment of mitochondrial  $O_2^-$  production, future studies are likely to involve comparisons of cellular  $H_2O_2$ , using Amplex<sup>®</sup> Red (Invitrogen) technology or EPR spectroscopy, employing the method recently described by Dikalov and colleagues (409).

Expression of *SOD2* mRNA was significantly increased in HSVECs from CAD patients with T2D relative to those from patients with CAD alone, as assessed by TaqMan<sup>®</sup> qRT-PCR. However, this differential expression was not confirmed on comparison of global gene expression profiles in cells from these patients. This was perhaps not surprising, given qRT-PCR and microarray experiments did not involve investigation of gene expression in cells isolated from the same clinical subjects, a consequence of limited vascular material. This finding therefore serves to highlight the difficulty of studying gene expression in outbred human populations.

Despite obvious limitations of the microarray experiment described in Chapter 5, it remains the first study of its kind to examine global gene expression in primary endothelial cells from CAD patients with and without T2D. Furthermore, in revealing differential expression of a number of genes potentially linked to mitochondrial function, the study serves to support a key role for mitochondrial dysfunction in the pathogenesis of CAD and T2D. However, the difficulties associated with small subject numbers and confirmation of differential expression of candidate genes, in addition to the possibility that cultured cells do not retain the *in vivo* phenotype, indicates alternative or complementary technologies may prove more successful in elucidating molecular mechanisms adversely affected in patients with CAD and T2D. Proteomics, which involves the identification of polymorphic protein expression and isoforms between samples, is increasingly being applied in complex disease research and has been utilised within this laboratory in the context of CAD; urinary protein biomarkers were assayed in control subjects and patients with CAD and a signature polypeptide pattern specific to CAD patients distinguished (410).

In addition to proteomics, miRNA technology has attracted considerable research interest in recent years. MicroRNAs are non-coding RNA molecules involved in post-

transcriptional control of gene expression (411). The ability of miRNAs to affect expression of complex diseases such as CAD and T2D is considered likely since they are known to target multiple mRNAs (412). Indeed, genome-wide expression profiling of miRNAs in patients with heart disease (ischaemic cardiomyopathy, dilated cardiomyopathy and aortic stenosis) revealed disease-specific miRNA expression patterns particular to each condition on comparison with healthy control subjects (413). In terms of diabetes, specific miRNAs involved in insulin production, secretion and action have been identified in recent years (414;415). In particular, studies involving murine models have reported miR-9 and miR-375 to be involved in regulation of insulin secretion (416;417), while miR-124a2 has recently been implicated in pancreatic  $\beta$ -cell development and function (418). However, despite growing evidence that miRNAs are important in T2D, few studies of global miRNA expression in human insulin target tissues have been published to date. The present study was limited due to the majority of samples being collected before well established techniques to capture miRNAs became available but future studies may focus on these small RNA components.

While the microarray experiment of Chapter 5 represents a novel piece of work, the key findings of this project centre around AMPK. Recently identified as a potential therapeutic target in vascular disease (419), AMPK is currently the subject of extensive research. A paper from Professor Salvador Moncada's group, published in 2006, revealed that the kinase is activated in a mtROS-mediated manner in endothelial cells (228). Consequently, the finding that SOD2 expression is significantly increased in HSVECs from patients with CAD, consistent with increased mtROS production, led to investigation of AMPK activity in these cells. Activity of the kinase was observed to be significantly increased in the endothelium of CAD patients with T2D despite no change in activity of upstream kinases, LKB1 and CaMKK, suggesting an alternative, potentially mtROS-mediated method of activation in these individuals. Indeed, it seemed likely that these patients, with an extra risk factor for CVD, poorer endothelial function and significantly increased endothelial SOD2 expression, would be subject to increased mitochondrially-produced ROS in the endothelium, resulting in the increased AMPK activity observed. As described in Chapter 4, treatment of cells with the mitochondria-targeted antioxidant, MitoQ<sub>10</sub> revealed AMPK is indeed activated in a mtROS-mediated manner in the endothelium of patients with CAD and T2D, representing the major, novel finding of this project.

In terms of what mtROS-mediated activation of AMPK means in relation to enzymatic function, it appears AMPK is part of a feedback or adaptive mechanism with a role in defence against oxidative stress in the endothelium of patients with CAD and T2D. The kinase may contribute to control of vascular tone through phosphorylation of eNOS and stimulation of NO production (176;282), or by inducing expression of genes involved in antioxidant defence, including *SOD2* itself (377;378). As such, assessment of HSVEC *SOD2* expression following treatment of cells with AICAR and MitoQ<sub>10</sub> will be carried out in the near future.

In addition to inducing expression of *SOD2*, there is now evidence to suggest AMPK inhibits production of O<sub>2</sub><sup>-</sup> by NAD(P)H oxidase. A recent study by Alba and colleagues demonstrated that AMPK inhibits activation of NAD(P)H oxidase in neutrophils by phosphorylating the p47<sup>phox</sup> subunit, thus preventing its translocation to the plasma membrane (420). The findings described in Chapter 3 of this thesis indicate a lesser contribution of vascular NAD(P)H oxidase to O<sub>2</sub><sup>-</sup> production in endothelial cells of patients with CAD and T2D than in cells from patients with CAD alone. This result may therefore be explained by the fact that increased endothelial AMPK activity in CAD patients with T2D results in suppression of NAD(P)H oxidase activation in the endothelium of these patients.

With vascular complications the leading cause of death in patients with CAD and T2D (8;30), the body of work presented here further supports the idea that a well tolerated therapeutic activator of AMPK should successfully improve glycaemic control while maintaining or restoring endothelial function. Agents presently known to activate AMPK, such as metformin, appear to act indirectly and exhibit a number of unpleasant side effects (419). Attempts have been made to generate alternative AMPK-activating agents, including the thienopyridone A769662, which induces AMPK activity via a mechanism involving the β- and γ-subunits (421). However, this compound may have potentially limiting side effects and is reported to inhibit the function of the 26S proteasome by an AMPK-independent mechanism, leading to cell cycle arrest in mouse embryonic fibroblasts *in vitro* (422). Despite this observation, treatment of ob/ob mice with A769662 lowered plasma glucose, reduced body weight gain, and significantly decreased both plasma and liver triglyceride levels (423). It remains to be determined whether the compound can improve vascular function.

Results presented here suggest activators of AMPK will prove most useful when administered in conjunction with mitochondria-targeted antioxidants, such as MitoQ<sub>10</sub>. The ubiquinone has recently been shown to improve endothelial function and attenuate cardiac hypertrophy in a rodent model of CVD, the SHRSP (424). In addition, it has reached two human phase 2 clinical trials and is reported to be protective against liver damage in a small study of patients with chronic hepatitis C (425) and well tolerated when taken over the period of a year by patients with Parkinson's disease (426). At the time of writing, an application has been made by this group to the Medicines and Healthcare products Regulatory Agency (MHRA) for a clinical trial of MitoQ<sub>10</sub> in patients with CAD undergoing CABG surgery. Should this application prove successful, the contribution of mitochondrially-derived ROS to oxidative stress and endothelial dysfunction, and the translational relevance of modulation of AMPK activity by mtROS could be determined through examination of vessels and cells isolated from trial participants. Alternatively, future *in vivo* studies may utilise the SHRSP, with investigations of mtROS production and kinase activity following oral administration of MitoQ<sub>10</sub>.

In conclusion, the findings presented in this thesis confirm CAD is associated with endothelial dysfunction and elevated vascular O<sub>2</sub><sup>-</sup> production and provide insight into the cellular mechanisms underlying these processes in the endothelium. This study demonstrates a novel, mtROS-mediated mechanism for AMPK activation in the endothelium of patients with coronary artery disease and type 2 diabetes and suggests mitochondria contribute to increased O<sub>2</sub><sup>-</sup> production and endothelial dysfunction in these patients. In terms of clinical perspective, results indicate that mitochondria-targeted antioxidants, used in combination with pharmacological activators of AMPK, may have therapeutic potential as an early intervention strategy in the treatment of endothelial dysfunction in these patients.

## **Appendix**

<b>Illumina® Probe ID</b>	<b>Gene Symbol</b>	<b>T2D Diff Score</b>	<b>Illumina® Probe ID</b>	<b>Gene Symbol</b>	<b>T2D Diff Score</b>
ILMN_1862910		-51.512	ILMN_1776428	STK17A	-20.689
ILMN_1722397	LOC729137	-41.691	ILMN_1813769	ARRDC3	-20.636
ILMN_1788955	PDLIM1	-40.376	ILMN_1750722	RPS7	-20.494
ILMN_1752269	ACSS1	-33.752	ILMN_1694075	GADD45A	-20.261
ILMN_1719949	LOC644019	-31.901	ILMN_1699022	ENDOD1	-20.221
ILMN_1740466	FAM46A	-28.802	ILMN_1777849	IL7R	-20.189
ILMN_1663765	LOC647346	-28.787	ILMN_1696810	ADMR	-20.078
ILMN_1669404	KISS1	-28.355	ILMN_1765633	FAM10A7	-20.03
ILMN_1732575	SEC14L1	-27.921	ILMN_1675684	APOBEC3C	-19.899
ILMN_1730201	DTNA	-27.194	ILMN_1874778	LOC729310	-19.813
ILMN_1703140	NEDD4	-27.098	ILMN_1705364	BAT3	-19.752
ILMN_1696537	DDIT4L	-26.676	ILMN_1731639	CASP3	-19.464
ILMN_1746241	SDHC	-26.557	ILMN_1675797	EPDR1	-19.464
ILMN_1652763	LOC389203	-26.039	ILMN_1656327	GLT1D1	-19.396
ILMN_1659365	LOC653071	-25.739	ILMN_1803375	ODZ1	-19.368
ILMN_1794505	SHFM1	-24.905	ILMN_1794038	FAM49A	-19.24
ILMN_1759344	LOC652226	-24.892	ILMN_1662097	SLC25A43	-19.035
ILMN_1720430	C20orf149	-24.198	ILMN_1683494	TMEM154	-18.807
ILMN_1806266	RAP1GDS1	-23.93	ILMN_1694100	PRIM2	-18.801
ILMN_1665865	IGFBP4	-23.751	ILMN_1821335		-18.582
ILMN_1652638	LRRC58	-23.634	ILMN_1655222	LOC389833	-18.483
ILMN_1749078	TIMP2	-23.12	ILMN_1725705	CLPP	-18.439
ILMN_1745578	ETS2	-22.945	ILMN_1705630	LOC641700	-18.309
ILMN_1745593	STMN1	-22.764	ILMN_1707356	CFL2	-18.264
ILMN_1880421		-22.471	ILMN_1830906		-18.235
ILMN_1757387	UCHL1	-22.451	ILMN_1836185		-18.189
	TNFRSF10				
ILMN_1666022	D	-22.167	ILMN_1675312	LOC389833	-18.144
ILMN_1716407	SORBS2	-22.01	ILMN_1770466	ATP5G3	-18.009
ILMN_1655236	GFPT2	-21.798	ILMN_1695872	LOC641992	-17.995
ILMN_1673676	SNX5	-21.759	ILMN_1654563	EFNB1	-17.95
ILMN_1687538	ETS1	-21.695	ILMN_1742065	GCNT4	-17.95
ILMN_1667970	LOC728825	-21.661	ILMN_1717855	PFDN1	-17.881
ILMN_1751851	CECR1	-21.569	ILMN_1767556	C10orf10	-17.85
ILMN_1702168	HSD17B12	-21.535	ILMN_1665736	LOC648024	-17.809
ILMN_1655046	NUTF2	-21.535	ILMN_1764261	TMEM128	-17.782
ILMN_1675156	CDC42	-21.522	ILMN_1665682	IL15RA	-17.762
ILMN_1701613	RARRES3	-21.431	ILMN_1736356	STK32B	-17.664
ILMN_1698478	SNAPC2	-21.333	ILMN_1764225	GAGE6	-17.569
ILMN_1800837	CFDP1	-21.281	ILMN_1780060	FCN3	-17.45
ILMN_1718182	THRA	-21.167	ILMN_1674620	SGCE	-17.404
ILMN_1716518	NACA	-21.145	ILMN_1662016	SCRN2	-17.269
ILMN_1694569	LOC650224	-20.899	ILMN_1800131	LOC652826	-17.267
ILMN_1721535	COG5	-20.883	ILMN_1726415	CCNA1	-17.258
ILMN_1742250	CCNH	-20.875	ILMN_1693108	RUVBL1	-17.253
ILMN_1808041	RPL10A	-20.855	ILMN_1774545	LOC339240	-17.21
ILMN_1656651	MR1	-20.853	ILMN_1756862	APOL3	-17.115

**Table A1** – continued overleaf



<b>Illumina® Probe ID</b>	<b>Gene Symbol</b>	<b>T2D Diff Score</b>	<b>Illumina® Probe ID</b>	<b>Gene Symbol</b>	<b>T2D Diff Score</b>
ILMN_1792814	FLJ43870	-17.075	ILMN_1683375	MCL1	-15.397
ILMN_1726523	OR10G3	-17.072	ILMN_1841025		-15.39
ILMN_1660248	WTAP	-17.061	ILMN_1779213	TFG	-15.371
ILMN_1911874		-17.033	ILMN_1836965		-15.352
ILMN_1801661	KRT7	-16.965	ILMN_1772743	PIGK	-15.351
ILMN_1810941	COMT	-16.964	ILMN_1677483	EXOSC1	-15.309
ILMN_1750225	MYCT1	-16.914	ILMN_1815032	SOX7	-15.298
ILMN_1765701	LOC399942	-16.887	ILMN_1788283	COTL1	-15.296
ILMN_1677610	OVCA2	-16.768	ILMN_1676289	NCAM1	-15.273
ILMN_1869431		-16.701	ILMN_1831325		-15.236
ILMN_1676173	PARVB	-16.676	ILMN_1783681	MRPL34	-15.235
ILMN_1711899	ANXA2	-16.659	ILMN_1671267	NF2	-15.219
ILMN_1908488		-16.655	ILMN_1774086	CBX3	-15.209
ILMN_1690063	LOC651143	-16.52	ILMN_1827211		-15.168
ILMN_1729142	PRR6	-16.439	ILMN_1912500		-15.145
ILMN_1713574	LOC643493	-16.369	ILMN_1669376	DRAM	-15.13
ILMN_1705982	LOC645284	-16.347	ILMN_1748591	ODC1	-15.11
ILMN_1889126		-16.313	ILMN_1754249	LOC442535	-15.106
ILMN_1726354	EXOSC7	-16.276	ILMN_1673363	CD97	-15.088
ILMN_1658639	SLC46A3	-16.275	ILMN_1690125	PDLIM7	-15.067
ILMN_1781270	LOC646071	-16.236	ILMN_1739534	MAP2K4	-15.044
ILMN_1737163	SH3BGRL3	-16.163	ILMN_1763989	SEC63	-15.036
ILMN_1697665	LOC653972	-16.162	ILMN_1877681		-15.035
ILMN_1762071	C17orf80	-16.112	ILMN_1661825	TNFRSF6B	-15.027
ILMN_1727402	HCLS1	-16.11	ILMN_1687887	PSMC4	-15.018
ILMN_1801020	ADK	-16.064	ILMN_1815656	SERINC3	-15.012
ILMN_1682935	LYPLAL1	-15.954	ILMN_1853049		-14.97
ILMN_1680579	ATP2B4	-15.918	ILMN_1882522		-14.941
ILMN_1757347	C22orf9	-15.897	ILMN_1667597	LOC644865	-14.935
ILMN_1906438		-15.836	ILMN_1763688	C17orf49	-14.877
ILMN_1707815	SDHALP1	-15.807	ILMN_1758939	RIPK2	-14.855
ILMN_1740591	LOC649292	-15.771	ILMN_1774687	PRKAG1	-14.846
ILMN_1846641		-15.752	ILMN_1854518		-14.841
ILMN_1794875	MAG1	-15.672	ILMN_1801043	GSN	-14.836
ILMN_1711928	FLJ20920	-15.665	ILMN_1775634	AGTR2	-14.792
	SLC22A18				
ILMN_1691048	AS	-15.663	ILMN_1785284	ALDH6A1	-14.756
ILMN_1661417	MAGED2	-15.652	ILMN_1716859	TDO2	-14.737
ILMN_1690566	RASSF4	-15.652	ILMN_1732916	CCDC17	-14.723
ILMN_1672922	CYTL1	-15.634	ILMN_1827239		-14.715
ILMN_1654322	ATP1B3	-15.567	ILMN_1697945	FRMD4B	-14.703
ILMN_1787750	CD200	-15.555	ILMN_1800487	CDC26	-14.693
ILMN_1685240	PTRH1	-15.513	ILMN_1660718	GABBR2	-14.691
ILMN_1652549	DTNA	-15.496	ILMN_1808713	HSD17B2	-14.68
ILMN_1790249	F8A1	-15.423	ILMN_1658053	DYNLRB1	-14.668
ILMN_1739103	MPZL1	-15.404	ILMN_1790271	EEF1B2	-14.658
ILMN_1705116	C6orf85	-15.403	ILMN_1678312	LOC388397	-14.656

**Table A1**-continued oveleaf

<b>Illumina® Probe ID</b>	<b>Gene Symbol</b>	<b>T2D Diff Score</b>	<b>Illumina® Probe ID</b>	<b>Gene Symbol</b>	<b>T2D Diff Score</b>
ILMN_1817598		-14.654	ILMN_1740777	ZBTB12	-13.921
ILMN_1820226		-14.647	ILMN_1708605	LOC652481	-13.884
ILMN_1682112	PCDHA10	-14.627	ILMN_1829475		-13.88
ILMN_1669923	SSR2	-14.591	ILMN_1886034		-13.878
ILMN_1870248		-14.501	ILMN_1879243		-13.871
ILMN_1689467	CCDC86	-14.497	ILMN_1894376		-13.828
ILMN_1912718		-14.49	ILMN_1774949	PIGP	-13.82
ILMN_1688178	CGI-96	-14.448	ILMN_1795944	PRR13	-13.818
ILMN_1785692	LOC728098	-14.445	ILMN_1651329	LOC651538	-13.797
ILMN_1851746		-14.428	ILMN_1862963		-13.796
ILMN_1767006	PSMB8	-14.425	ILMN_1856010		-13.745
ILMN_1676333	LOC645465	-14.388	ILMN_1807492	LOC643668	-13.736
ILMN_1747344	IL3RA	-14.374	ILMN_1728914	PRUNE	-13.732
ILMN_1714752	ZNF658	-14.366	ILMN_1730553	DDR2	-13.73
ILMN_1679949	SLC25A23	-14.352	ILMN_1852928		-13.701
ILMN_1741259	LOC649209	-14.32	ILMN_1686610	APBA3	-13.675
ILMN_1652205	LOC645785	-14.309	ILMN_1916026		-13.643
ILMN_1743432	DGUOK	-14.3	ILMN_1839168		-13.628
ILMN_1884228		-14.27	ILMN_1886655		-13.603
ILMN_1764573	XIST	-14.267	ILMN_1917294		-13.585
ILMN_1766643	HOP	-14.255	ILMN_1794046	MTX2	-13.568
ILMN_1710482	APLP2	-14.251	ILMN_1749907	LOC441241	-13.539
ILMN_1679133	SERPINB1	-14.249	ILMN_1674315	POLA	-13.522
ILMN_1692077	MXRA7	-14.223	ILMN_1666174	CECR1	-13.512
ILMN_1665040	RBMS3	-14.189	ILMN_1780988	LOC401720	-13.504
ILMN_1915629		-14.177	ILMN_1751124	RGMB	-13.504
ILMN_1680280	LOC644923	-14.175	ILMN_1728071	KRAS	-13.484
ILMN_1870679		-14.167	ILMN_1807981	SIGIRR	-13.482
ILMN_1769027	CDC42SE1	-14.164	ILMN_1880671		-13.467
ILMN_1879882		-14.155	ILMN_1657348	LOC650909	-13.436
ILMN_1822952		-14.146	ILMN_1732750	CHCHD8	-13.43
ILMN_1800000	FAM131B	-14.14	ILMN_1888844		-13.424
ILMN_1752562	CXCL5	-14.087	ILMN_1663754	ZNF442	-13.42
ILMN_1899777		-14.086	ILMN_1656621	CHMP2A	-13.418
ILMN_1706571	SLC35D2	-14.079	ILMN_1679700	LOC389672	-13.404
ILMN_1815081	AQP1	-14.075	ILMN_1712347	LOC644422	-13.404
ILMN_1689669	MDK	-14.074	ILMN_1914595		-13.396
ILMN_1740487	CMTM7	-14.062	ILMN_1811303	NR5A2	-13.363
ILMN_1800224	NOLC1	-14.044	ILMN_1814998	FKSG30	-13.323
ILMN_1661351	C17orf81	-14.038	ILMN_1912586		-13.298
ILMN_1692733	NRARP	-14.026	ILMN_1694140	AFAP1L1	-13.29
ILMN_1658743	CCNDBP1	-14.004	ILMN_1803277	MVP	-13.29
ILMN_1692916	LOC646135	-13.969	ILMN_1693233	KIAA0513	-13.227
ILMN_1654462	LOC440084	-13.966	ILMN_1709440	CPM	-13.207
ILMN_1884842		-13.962	ILMN_1817948		-13.193
ILMN_1753924	KRT19	-13.956	ILMN_1888230		-13.191

**Table A1**-continued overleaf

<b>Illumina® Probe ID</b>	<b>Gene Symbol</b>	<b>T2D Diff Score</b>	<b>Illumina® Probe ID</b>	<b>Gene Symbol</b>	<b>T2D Diff Score</b>
ILMN_1704471	NR1D2	-13.188	ILMN_1802096	ABTB1	13.398
ILMN_1850685		-13.161	ILMN_1694399	ICA1	13.429
ILMN_1770071	IFITM4P	-13.157	ILMN_1811535	JUB	13.451
ILMN_1905101		-13.143	ILMN_1720431	ZNF420	13.457
ILMN_1851207		-13.139	ILMN_1789074	HSPA1A	13.46
ILMN_1718852	PLCL1	-13.113	ILMN_1688479	LRRC42	13.468
ILMN_1733841	TCF7L1	-13.112	ILMN_1735765	RAB14	13.481
ILMN_1709643	TMEM69	-13.11	ILMN_1699206	KIAA1727	13.488
ILMN_1714144	GPR108	-13.101	ILMN_1673817	REP15	13.489
ILMN_1786331	TRIM16	-13.076	ILMN_1719149	LOC653663	13.494
ILMN_1712525	UBE2E3	-13.049	ILMN_1859908		13.497
ILMN_1915123		-13.04	ILMN_1782247	GCN5L2	13.5
ILMN_1797666	SLC27A6	-13.039	ILMN_1752510	FAM13A1	13.504
ILMN_1903877		-13.032	ILMN_1655702	ABHD5	13.526
ILMN_1680341	PPIE	-13.027	ILMN_1809139	AHCTF1	13.535
ILMN_1768867	AP3B1	-13.021	ILMN_1722423	SHPRH	13.539
ILMN_1811222	LOC643213	-13	ILMN_1881865		13.542
ILMN_1839051		13.005	ILMN_1707464	MST1	13.589
ILMN_1736901	ZDHHC23	13.017	ILMN_1709227	CCDC84	13.617
ILMN_1728180	CROP	13.028	ILMN_1664139	FAM29A	13.624
ILMN_1708485	BIN3	13.033	ILMN_1743402	SIX4	13.643
ILMN_1655167	ZNF502	13.043	ILMN_1799381	SNORD14A	13.643
ILMN_1687303	ACAD10	13.046	ILMN_1707481	BTBD15	13.654
ILMN_1806809	ZNF189	13.057	ILMN_1726693	GTF2H1	13.661
ILMN_1696806	CTNND1	13.06	ILMN_1810385	ATR	13.667
ILMN_1786024	POLR3H	13.07	ILMN_1832120		13.685
ILMN_1717112	LOC642787	13.083	ILMN_1701991	SYNJ1	13.692
ILMN_1804111	CETN3	13.089	ILMN_1793290	WDR60	13.703
ILMN_1699767	PDE8A	13.099	ILMN_1776094	PPCS	13.725
ILMN_1799688	CDC23	13.118	ILMN_1725644	UBE2D2	13.731
ILMN_1662130	LOC730316	13.12	ILMN_1915783		13.735
ILMN_1737878	FLJ34047	13.164	ILMN_1708110	TMEM144	13.738
ILMN_1730118	ZNF644	13.204	ILMN_1753393	OSGEP	13.752
ILMN_1720844	SSX2IP	13.232	ILMN_1716733	MYOM2	13.755
ILMN_1743288	LOC652570	13.236	ILMN_1737635	RAD1	13.771
ILMN_1696757	TTC14	13.244	ILMN_1685820	RAB40B	13.772
ILMN_1884750		13.258	ILMN_1863592		13.777
ILMN_1743078	LOC643031	13.3	ILMN_1655922	SAPS2	13.779
ILMN_1724017	LOC732450	13.307	ILMN_1713752	SERINC3	13.781
ILMN_1813603	SF3B1	13.307	ILMN_1703891	TBC1D9	13.801
ILMN_1736077	LIAS	13.314	ILMN_1682762	IDH3G	13.807
ILMN_1870668		13.327	ILMN_1659082	ZCRB1	13.807
ILMN_1708064	MAP4	13.36	ILMN_1767665	LOC493869	13.812
ILMN_1749081	AUTS2	13.361	ILMN_1767642	C11orf46	13.816
ILMN_1666082	HEATR3	13.373	ILMN_1812208	SUV420H2	13.822
ILMN_1669982	CCDC85A	13.397	ILMN_1698365	LOC387921	13.824

**Table A1**-continued overleaf

<b>Illumina® Probe ID</b>	<b>Gene Symbol</b>	<b>T2D Diff Score</b>	<b>Illumina® Probe ID</b>	<b>Gene Symbol</b>	<b>T2D Diff Score</b>
ILMN_1785661	FAM108B1	13.828	ILMN_1759074	DUSP19	14.451
ILMN_1717263	PRELID2	13.849	ILMN_1761833	SLC40A1	14.458
ILMN_1798448	IDS	13.869	ILMN_1749838	MZF1	14.497
ILMN_1700896	SAP30	13.872	ILMN_1656132	PNLDC1	14.5
ILMN_1821052		13.889	ILMN_1701434	RAP1B	14.529
ILMN_1672302	STK32C	13.891	ILMN_1806601	GRSF1	14.598
ILMN_1692429	PQBP1	13.911	ILMN_1701247	LOC132241	14.616
ILMN_1684183	RAD9A	13.916	ILMN_1707240	PTBP2	14.621
ILMN_1671992	LOC650128	13.917	ILMN_1807704	LOC338799	14.632
ILMN_1856932		13.931	ILMN_1736042	ME1	14.657
ILMN_1711828	ANKRD10	13.94	ILMN_1914800		14.669
ILMN_1895385		13.942	ILMN_1794522	EIF5A	14.683
ILMN_1690783	TREML1	13.954	ILMN_1840934		14.685
ILMN_1704431	LOC554203	13.981	ILMN_1717834	MGC11102	14.695
ILMN_1800164	PPFIA1	14.02	ILMN_1692041	POT1	14.715
ILMN_1751474	ARHGAP29	14.046	ILMN_1765310	TCEAL2	14.72
ILMN_1704398	FZD9	14.061	ILMN_1765019	SACM1L	14.728
ILMN_1772658	KIAA0947	14.063	ILMN_1707434	LOC653778	14.735
ILMN_1688464	MAP6D1	14.083	ILMN_1757052	SLC16A1	14.738
ILMN_1786976	RAB22A	14.086	ILMN_1667510	C12orf65	14.742
ILMN_1688056	UGP2	14.104	ILMN_1853116		14.771
ILMN_1775328	MTG1	14.141	ILMN_1683533	CCDC66	14.773
ILMN_1671839	TAF1C	14.16	ILMN_1784436	KIAA1688	14.79
ILMN_1733084	LOC147645	14.172	ILMN_1770818	LOC642342	14.792
ILMN_1668027	LOC727762	14.175	ILMN_1728517	FNTB	14.806
ILMN_1784037	ZBTB40	14.179	ILMN_1683129	CCNL1	14.813
ILMN_1697024	LOC730432	14.198	ILMN_1664833	MRPL50	14.815
ILMN_1800676	TMEM49	14.208	ILMN_1812559	SLC7A6	14.815
ILMN_1691290	CELSR3	14.211	ILMN_1758679	TMEM168	14.816
ILMN_1727738	RAB33B	14.223	ILMN_1866464		14.822
ILMN_1810514	SLC25A44	14.254	ILMN_1795407	CRYZL1	14.85
ILMN_1698007	LOC651872	14.27	ILMN_1712027	RSBN1L	14.862
ILMN_1787826	SLC36A1	14.272	ILMN_1666178	TP53I13	14.863
ILMN_1725188	PRKCI	14.289	ILMN_1913678		14.865
ILMN_1684278	SNORD38A	14.315	ILMN_1752798	LOC642780	14.886
ILMN_1747442	P4HA1	14.316	ILMN_1753413	TRIOBP	14.908
ILMN_1716658	ZNF543	14.37	ILMN_1758941	REEP5	14.938
ILMN_1757660	CAPS	14.391	ILMN_1661107	SNORD34	14.973
ILMN_1677165	SF3B1	14.405	ILMN_1835722		14.978
ILMN_1705468	PIK3CA	14.406	ILMN_1775423	C10orf88	14.986
ILMN_1671221	GAPVD1	14.429	ILMN_1685703	ACOX2	14.99
ILMN_1656656	COX19	14.43	ILMN_1665290	LOC643995	15.024
ILMN_1789095	BMPR2	14.435	ILMN_1703985	C19orf25	15.055
ILMN_1899404		14.436	ILMN_1830984		15.063
ILMN_1761058	ACAD11	14.437	ILMN_1774945	NRG3	15.1
ILMN_1904135		14.442	ILMN_1750256	ALS2	15.122

**Table A1**-continued overleaf

<b>Illumina® Probe ID</b>	<b>Gene Symbol</b>	<b>T2D Diff Score</b>	<b>Illumina® Probe ID</b>	<b>Gene Symbol</b>	<b>T2D Diff Score</b>
ILMN_1807031	C14orf28	15.165	ILMN_1788237	LOC652755	16.216
ILMN_1767601	C21orf94	15.215	ILMN_1813240	EIF1AX	16.225
ILMN_1706608	LOC338799	15.232	ILMN_1815035	DENND2C	16.254
ILMN_1811117	LOC400986	15.256	ILMN_1803018	KIFC2	16.27
ILMN_1696935	RBM39	15.318	ILMN_1723418	CEL	16.306
ILMN_1753607	PNO1	15.319	ILMN_1785933	C19orf18	16.323
ILMN_1664449	ALG5	15.364	ILMN_1652736	RPS6KA3	16.385
ILMN_1703273	UACA	15.374	ILMN_1683112	FANCC	16.437
ILMN_1672947	CAST	15.391	ILMN_1786789	FAM102B	16.445
ILMN_1829768		15.446	ILMN_1682757	PFKFB2	16.447
ILMN_1743933	TSHZ3	15.456	ILMN_1816925	LOC730459	16.487
ILMN_1693538	STK36	15.466	ILMN_1675541	EEF1B2	16.554
ILMN_1766195	ZNF558	15.476	ILMN_1689086	CTSC	16.634
ILMN_1660125	SFMBT2	15.51	ILMN_1678904	ENO3	16.67
ILMN_1694367	SNORD35B	15.534	ILMN_1768754	PILRB	16.694
ILMN_1711208	CELSR2	15.542	ILMN_1715351	SCYE1	16.729
ILMN_1707337	MSTO1	15.553	ILMN_1768004	PDCD4	16.745
ILMN_1736623	NCKIPSD	15.568	ILMN_1736184	GSTM3	16.75
ILMN_1770152	ADAMTS18	15.591	ILMN_1773992	CCRL1	16.772
ILMN_1715096	C6orf168	15.64	ILMN_1736017	LOC643834	16.802
ILMN_1706825	PKN2	15.654	ILMN_1768719	RDH11	16.835
ILMN_1657619	DNAJB14	15.667	ILMN_1688455	KIAA0564	16.842
ILMN_1762262	PKIA	15.698	ILMN_1766950	PCDHB13	16.863
ILMN_1787813	SLC5A3	15.698	ILMN_1654518	LRCH4	16.866
ILMN_1788778	Sep-11	15.701	ILMN_1664802	WSB1	16.941
ILMN_1770892	YY1	15.707	ILMN_1715526	ZDHHC21	16.979
ILMN_1773395	RDH5	15.75	ILMN_1656378	NMT2	17.001
ILMN_1677963	TMCC1	15.757	ILMN_1852793		17.015
ILMN_1785266	OFD1	15.796	ILMN_1782487	LOC400759	17.018
ILMN_1786168	LOC400464	15.807	ILMN_1791840	RALBP1	17.036
ILMN_1677484	SNAPC4	15.818	ILMN_1800401	ZNF69	17.061
ILMN_1741506	LOC149134	15.843	ILMN_1745389	KIAA1328	17.096
ILMN_1698521	SH2B1	15.86	ILMN_1683487	ZNF154	17.243
ILMN_1723020	MAP3K1	15.91	ILMN_1665331	AMT	17.329
ILMN_1734011	RP13- 15M17.2	15.912	ILMN_1658809	SEZ6	17.35
ILMN_1801869	WDR75	15.963	ILMN_1682038	SNORA25	17.392
ILMN_1696043	FLVCR2	16.013	ILMN_1666690	ACRC	17.4
ILMN_1683023	PDGFC	16.013	ILMN_1718932	MTRR	17.415
ILMN_1862001		16.079	ILMN_1788931	DOCK8	17.518
ILMN_1714283	TLE2	16.081	ILMN_1664096	ZNF491	17.548
ILMN_1746208	CCAR1	16.086	ILMN_1813344	C20orf7	17.573
ILMN_1774265	UNQ830	16.096	ILMN_1736237	DLAT	17.621
ILMN_1774589	IQCC	16.102	ILMN_1741468	FAP	17.634
ILMN_1739587	UTY	16.155	ILMN_1737561	LOC88523	17.697
ILMN_1776347	TCP1	16.158	ILMN_1663532	RIC8B	17.699
ILMN_1695079	ZNF101	16.204	ILMN_1748374	LOC400304	17.703

**Table A1**-continued overleaf

<b>Illumina® Probe ID</b>	<b>Gene Symbol</b>	<b>T2D Diff Score</b>	<b>Illumina® Probe ID</b>	<b>Gene Symbol</b>	<b>T2D Diff Score</b>
ILMN_1657701	TMEM137	17.711	ILMN_1666615	PREPL	19.068
ILMN_1676946	AP3M2	17.723	ILMN_1721657	RSU1	19.093
ILMN_1755222	C9orf82	17.747	ILMN_1743280	LRRC37B	19.162
ILMN_1739583	ROCK1	17.761	ILMN_1695606	EFNB3	19.177
ILMN_1712719	MAP7	17.79	ILMN_1698261	PDE6B	19.198
ILMN_1664177	ATXN7L2	17.791	ILMN_1752117	TMEM55A	19.289
ILMN_1729515	PIN4	17.856	ILMN_1813179	LOC401074	19.316
ILMN_1685052	DNAH1	17.936	ILMN_1709747	ENDOGL1	19.475
ILMN_1767279	LOC648245	18.061	ILMN_1724789	CD59	19.54
ILMN_1741219	RRAGB	18.061	ILMN_1866216		19.562
ILMN_1784706	GABRE	18.096	ILMN_1670752	KIAA0907	19.614
ILMN_1890175		18.108	ILMN_1815705	LZTFL1	19.626
ILMN_1660864	RHBDL1	18.139	ILMN_1767558	LRP5	19.668
ILMN_1748427	ZNF239	18.146	ILMN_1892638		19.688
ILMN_1764764	MUM1	18.163	ILMN_1908989		19.748
ILMN_1682589	M6PR	18.173	ILMN_1801045	SPIN3	19.778
ILMN_1860821		18.272	ILMN_1749253	TUBD1	19.817
ILMN_1653794	C6orf160	18.306	ILMN_1723124	GALK2	19.907
ILMN_1678998	LRRC14	18.328	ILMN_1784783	NME5	19.924
ILMN_1760281	PRPF4B	18.391	ILMN_1677532	TARDBP	20.007
ILMN_1795835	LOC338758	18.397	ILMN_1726989	C1orf86	20.083
ILMN_1757910	HIP1R	18.404	ILMN_1810533	SLC6A15	20.147
ILMN_1747650	BMP6	18.429	ILMN_1749915	C1orf63	20.209
ILMN_1891455		18.465	ILMN_1727553	LOC63920	20.236
ILMN_1738749	MAST3	18.483	ILMN_1706506	ZNF454	20.439
ILMN_1720916	SETD7	18.49	ILMN_1868805		20.491
ILMN_1681367	ZNF642	18.529	ILMN_1759084	INTS8	20.527
ILMN_1768117	RBM25	18.55	ILMN_1778464	TMEM1	20.75
ILMN_1691395	ZBTB11	18.565	ILMN_1722450	NSUN5B	20.769
ILMN_1813430	TRIM69	18.584	ILMN_1672565	RG9MTD1	20.778
ILMN_1679558	LOC283874	18.622	ILMN_1782222	KIAA1033	20.793
ILMN_1707051	NFATC1	18.63	ILMN_1721034	ZNF227	20.839
ILMN_1898124		18.764	ILMN_1798826	MRPS25	20.848
ILMN_1674297	HCFC2	18.77	ILMN_1726368	ZNF135	20.957
ILMN_1712798	ZNF608	18.778	ILMN_1759407	USHBP1	20.984
ILMN_1669931	TM9SF3	18.79	ILMN_1796119	C6orf113	21.051
ILMN_1721741	ATPBD1B	18.8	ILMN_1672122	PH-4	21.137
ILMN_1757408	ZNF256	18.816	ILMN_1696469	LOC648509	21.184
ILMN_1843756		18.865	ILMN_1734867	NR2C1	21.285
ILMN_1893633	LOC439949	18.897	ILMN_1758105	ZNF791	21.299
ILMN_1788118	SLC23A3	18.943	ILMN_1743427	SCYL3	21.302
ILMN_1801762	PFDN4	18.952	ILMN_1716921	ZNF83	21.387
ILMN_1790103	ZNF569	18.96	ILMN_1673478	C5orf5	21.414
ILMN_1713744	C14orf132	18.977	ILMN_1746782	LRRC16	21.506
ILMN_1792109	AFG3L1	19.025	ILMN_1779448	EFHD1	21.634
ILMN_1670322	FCHO2	19.052	ILMN_1789364	ZNF789	21.681

**Table A1**-continued overleaf

Illumina® Probe ID	Gene Symbol	T2D Diff Score	Illumina® Probe ID	Gene Symbol	T2D Diff Score
ILMN_1657011	LOC286208	21.689	ILMN_1781361	LOC400986	24.518
ILMN_1681760	LOC728518	21.713	ILMN_1910120	LOC730092	24.876
ILMN_1703555	SNORD31	21.737	ILMN_1751362	FASTKD1	24.938
ILMN_1756992	MUC1	21.765	ILMN_1898691		25.009
ILMN_1668055	SAA4	21.911	ILMN_1652147	MRPL43	25.102
ILMN_1798085	EID2B	21.916	ILMN_1809894	TMEM117	25.126
ILMN_1714848	ZNF354A	21.965	ILMN_1747824	ZNF85	25.136
ILMN_1665810	CCDC113	22.105	ILMN_1663646	DMXL1	25.519
ILMN_1827736		22.113	ILMN_1735275	WDSUB1	25.636
ILMN_1754757	SCNN1D	22.21	ILMN_1727466	KCNMB4	25.708
ILMN_1730888	ZNF680	22.392	ILMN_1710954	LOC283932	25.954
ILMN_1690839	PPAPDC3	22.455	ILMN_1759062	NIPBL	26.188
ILMN_1788689	PHIP	22.456	ILMN_1782098	SMO	26.524
ILMN_1720287	E4F1	22.493	ILMN_1753823	IL17D	26.709
ILMN_1793578	ZFP37	22.555	ILMN_1745501	DNALI1	27.223
ILMN_1791006	AHI1	22.619	ILMN_1712766	ERGIC2	27.338
ILMN_1761044	GNB1L	22.632	ILMN_1849693		27.408
ILMN_1670379	ANTXR1	22.692	ILMN_1802519	VPS36	27.821
ILMN_1745790	MRPL42P5	22.696	ILMN_1807136	LOC729559	27.938
ILMN_1814221	NPTX1	22.721	ILMN_1867188		28.015
ILMN_1745991	GNRH1	22.742	ILMN_1676302	FAM113A	28.406
ILMN_1684726	C2orf27	22.773	ILMN_1802053	ZNF91	28.983
ILMN_1811050	CCDC88A	22.996	ILMN_1811029	TLK1	29.073
ILMN_1719064	KCTD10	23.165	ILMN_1727923	ZNF140	29.289
ILMN_1746924	ZNF610	23.185	ILMN_1716264	ANKRD1	29.505
ILMN_1696004	LRRK1	23.209	ILMN_1651964	ABCC5	29.711
ILMN_1892548		23.238	ILMN_1789751	MFSD1	29.818
ILMN_1651364	PCBD2	23.25	ILMN_1737818	C12orf43	29.866
ILMN_1719290	CRYZL1	23.268	ILMN_1913641		30.162
ILMN_1665135	RBBP6	23.445	ILMN_1893511		31.152
ILMN_1812666	DNAJC15	23.698	ILMN_1662147	MANEAL	32.856
ILMN_1745852	WDR33	23.704	ILMN_1724009	SETD6	34.229
ILMN_1691772	ZSCAN29	23.731	ILMN_1662038	LARGE	34.239
ILMN_1753782	ZNF266	24.006	ILMN_1811110	TDRD9	35.458
ILMN_1873278	LOC731895	24.021	ILMN_1698185	WDR90	36.252
				NGFRAP1L	
ILMN_1793017	DGKQ	24.026	ILMN_1806473	1	36.806
ILMN_1801303	AMY2A	24.081	ILMN_1818617		37.692
ILMN_1738124	ZNF772	24.146	ILMN_1716555	MGC42630	40.455
ILMN_1751393	ZNF684	24.302	ILMN_1696622	SLC38A6	44.889
ILMN_1811301	INPP5E	24.314	ILMN_1792972	ZNF439	47.176
ILMN_1849186		24.316	ILMN_1725314	GBP3	49.23
ILMN_1911717		24.513			

**Table A1. Differentially Expressed Probes Identified on BeadStudio Analysis of Microarray Data.** A total of 727 probes were found to be differentially expressed in endothelial cells from patients with coronary artery disease and type 2 diabetes (T2D).

Gene Symbol	Gene Name	GenBank Accession Number	P value	Fold Change
ABCC5	ATP-binding cassette, sub-family C (CFTR/MRP), member 5	NM_005688.2	0.00958	-1.25529
ACAD11	acyl-Coenzyme A dehydrogenase family, member 11	NM_032169.4	0.00412	-1.44834
AFG3L1	AFG3 ATPase family gene 3-like 1 (S. cerevisiae)	NR_003226.1	3.00E-05	-1.64806
AGTR2	angiotensin II receptor, type 2	NM_000686.4	0.0239	1.45261
AMT (includes EG:275)	aminomethyltransferase	NM_000481.2	0.03663	-2.06699
AMY2A	amylase, alpha 2A (pancreatic)	NM_000699.2	0.04685	-1.52472
BLZF1	basic leucine zipper nuclear factor 1 (JEM-1)	NM_003666.2	0.01698	-1.23465
C10ORF120	chromosome 10 open reading frame 120	NM_001010912.1	0.01645	1.23922
C10ORF97	chromosome 10 open reading frame 97	NM_024948.2	0.02841	-1.17917
C14ORF39	chromosome 14 open reading frame 39	NM_174978.1	0.03079	1.51268
C17ORF54	chromosome 17 open reading frame 54	NM_182564.1	0.00842	1.5758
C19ORF18	chromosome 19 open reading frame 18	NM_152474.3	0.03607	-1.54723
C1ORF63	chromosome 1 open reading frame 63	NM_020317.3	0.00588	-1.88027
C6ORF123	chromosome 6 open reading frame 123	NM_014356.2	0.02219	1.71414
CCDC113	coiled-coil domain containing 113	NM_014157.2	0.00116	-1.45675
CFDP1	craniofacial development protein 1	NM_006324.2	0.03607	1.37673
CFL1	cofilin 1 (non-muscle)	NM_005507.2	0.01086	1.17496
CROP	cisplatin resistance-associated overexpressed protein	NM_006107.2	0.01538	-2.04803
DGKQ	diacylglycerol kinase, theta 110kDa	NM_001347.2	0.03809	-1.33223
E4F1	E4F transcription factor 1	NM_004424.3	0.01635	-1.33492
EFHD1	EF-hand domain family, member D1	NM_025202.2	0.01086	-4.45841
ERGIC2	ERGIC and golgi 2	NM_016570.2	0.03412	-1.28905
FAP	fibroblast activation protein, alpha	NM_004460.2	0.01538	-2.34487
FLJ21062	hypothetical protein FLJ21062	NM_001039706.1	0.03663	-1.30533
GDF2	growth differentiation factor 2	NM_016204.1	0.01726	1.2736
GNL2	guanine nucleotide binding protein-like 2 (nucleolar)	NM_013285.1	0.026	-1.1826

**Table A2**-continued overleaf



Gene Symbol	Gene Name	GenBank Accession Number	P value	Fold Change
GNRH1	gonadotropin-releasing hormone 1 (luteinizing-releasing hormone)	NM_000825.3	0.0198	-1.58069
HIP1R	huntingtin interacting protein 1 related	XM_001132864.1	0.03809	-1.52871
KIAA0556	KIAA0556	NM_015202.1	0.04851	-1.23184
KIAA0574	KIAA0574 protein	XM_001127362.1	0.96044	1.07003
KIAA1328	KIAA1328	NM_020776.1	0.03557	-1.40981
KIAA2013	KIAA2013	NM_138346.1	0.02921	1.21295
KLK4	kallikrein-related peptidase 4	NM_004917.3	0.02841	2.15663
LOC283932	hypothetical LOC283932	NM_175901.3	0.03079	-1.42516
LOC440748	hypothetical gene supported by AK124556	XM_498841.3	0.04054	1.39778
LOC727762	similar to NADH:ubiquinone oxidoreductase B15 subunit	XM_001125898.1	0.0238	-1.7181
LOC729137	hypothetical protein LOC441528 leucine-rich repeats and calponin homology (CH) domain containing 4	XM_001129423.1	1.10E-04	2.9142
LRCH4	containing 4	NM_002319.2	0.0238	-1.60402
LSM14A	LSM14A, SCD6 homolog A (S. cerevisiae)	NM_015578.1	0.04685	-1.14405
LZTFL1	leucine zipper transcription factor-like 1	NM_020347.2	0.01963	-1.30391
MFSD1	major facilitator superfamily domain containing 1	NM_022736.1	6.99E-06	-1.39625
MGC12760	ciliary rootlet coiled-coil, rootletin-like 1	XM_001130627.1	0.01784	-1.72953
MGC42630	family with sequence similarity 27, member E3	NM_175923.3	0.01634	-1.51369
NSUN5B	NOL1/NOP2/Sun domain family, member 5B	NM_001039575.1	0.01086	-1.57828
NUTF2	nuclear transport factor 2	NM_005796.1	0.01086	1.41546
PDE8A	phosphodiesterase 8A	NM_173457.1	0.03186	-1.2629
PIK3R2	phosphoinositide-3-kinase, regulatory subunit 2 (beta)	NM_005027.2	0.03585	-1.22074
RAB22A	RAB22A, member RAS oncogene family	NM_020673.2	0.01199	-1.28058
RALBP1	ralA binding protein 1	NM_006788.3	0.03117	-1.23267
RDH5	retinol dehydrogenase 5 (11-cis/9-cis)	NM_002905.2	0.03117	-1.43216
RIC8B	resistance to inhibitors of cholinesterase 8 homolog B (C. elegans)	NM_018157.2	0.00412	-1.31425
SAA4	serum amyloid A4, constitutive	NM_006512.1	0.03762	-1.96613

**Table A2**-continued overleaf

Gene Symbol	Gene Name	GenBank Accession Number	P value	Fold Change
SETD6	SET domain containing 6	NM_024860.1	7.70E-04	-1.5567
SGSM2	small G protein signaling modulator 2	NM_014853.2	0.03186	-1.21567
SLC23A3	solute carrier family 23 (nucleobase transporters), member 3	NM_144712.2	0.03607	-2.3497
SLC25A28	solute carrier family 25, member 28	NM_031212.3	0.0238	-1.23134
SLC38A6	solute carrier family 38, member 6	NM_153811.1	0.0092	-1.5712
SRMS	src-related kinase lacking C-terminal regulatory tyrosine and N-terminal myristylation sites	NM_080823.2	0.02963	-1.86829
STK35	serine/threonine kinase 35	NM_080836.2	0.03186	-1.15512
STK36	serine/threonine kinase 36, fused homolog (Drosophila)	NM_015690.2	0.04624	-1.33175
TCFL5	transcription factor-like 5 (basic helix-loop-helix)	NM_006602.2	0.04014	-1.26548
TDRD9	tudor domain containing 9	NM_153046.1	7.70E-04	-2.18596
TM9SF3	transmembrane 9 superfamily member 3	NM_020123.2	0.01199	-1.2211
TSPAN6	tetraspanin 6	NM_003270.2	0.02841	-1.18427
ULK1	unc-51-like kinase 1 (C. elegans)	XM_001133335.1	0.0092	-1.24957
USHBP1	Usher syndrome 1C binding protein 1	NM_031941.3	0.01538	-2.16837
WDR60	WD repeat domain 60	NM_018051.3	0.01226	-1.33403
ZBTB12	zinc finger and BTB domain containing 12	NM_181842.1	0.01784	1.57687
ZDHHC8	zinc finger, DHHC-type containing 8	NM_013373.2	0.01086	-1.266
ZMYM2	zinc finger, MYM-type 2	NM_197968.1	0.00311	-1.26863
ZNF212	zinc finger protein 212	NM_012256.2	0.01645	-1.20548
ZNF266	zinc finger protein 266	NM_006631.2	4.00E-05	-1.33324
ZNF439	zinc finger protein 439	NM_152262.2	0.01925	-1.68406
ZNF486	zinc finger protein 486	XM_371152.3	0.0471	-1.24292
ZNF569	zinc finger protein 569	NM_152484.2	0.01086	-1.29198
ZNF83	zinc finger protein 83	NM_018300.2	0.02596	-1.47467
ZUFSP	zinc finger with UFM1-specific peptidase domain	NM_145062.1	0.01949	-1.34485

**Table A2. Differentially Expressed Genes Identified From Ingenuity Pathway Analysis (IPA) of Rosetta Resolver® Microarray Data.** IPA identified 77 differentially expressed genes ( $P \leq 0.005$ ) within the Rosetta Resolver® data set.

## Reference List

- (1) World Health Organisation: Cardiovascular Diseases.  
<http://www.who.int/mediacentre/factsheets/fs317/en/index.html>. 2009.
- (2) Coronary Heart Disease Statistics 2008.  
<http://www.heartstats.org/datapage.asp?id=7998>. 2009.
- (3) Dominiczak AF, Graham D, McBride MW, Brain NJ, Lee WK, Charchar FJ et al. Corcoran Lecture. Cardiovascular genomics and oxidative stress. *Hypertension* 2005; 45(4):636-642.
- (4) Delles C, McBride MW, Padmanabhan S, Dominiczak AF. The genetics of cardiovascular disease. *Trends Endocrinol Metab* 2008; 19(9):309-316.
- (5) Samani NJ, Erdmann J, Hall AS, Hengstenberg C, Mangino M, Mayer B et al. Genomewide association analysis of coronary artery disease. *N Engl J Med* 2007; 357(5):443-453.
- (6) Yusuf S, Hawken S, Ounpuu S, Dans T, Avezum A, Lanas F et al. Effect of potentially modifiable risk factors associated with myocardial infarction in 52 countries (the INTERHEART study): case-control study. *Lancet* 2004; 364(9438):937-952.
- (7) Beckman JA, Creager MA, Libby P. Diabetes and atherosclerosis: epidemiology, pathophysiology, and management. *JAMA* 2002; 287(19):2570-2581.
- (8) Morrish NJ, Wang SL, Stevens LK, Fuller JH, Keen H. Mortality and causes of death in the WHO Multinational Study of Vascular Disease in Diabetes. *Diabetologia* 2001; 44 Suppl 2:S14-S21.
- (9) Saltiel AR. New perspectives into the molecular pathogenesis and treatment of type 2 diabetes. *Cell* 2001; 104(4):517-529.
- (10) World Health Organisation: Diabetes.  
<http://www.who.int/mediacentre/factsheets/fs312/en/index.html>. 2009.
- (11) Conrad MC. Large and small artery occlusion in diabetics and nondiabetics with severe vascular disease. *Circulation* 1967; 36(1):83-91.
- (12) Silva JA, Escobar A, Collins TJ, Ramee SR, White CJ. Unstable angina. A comparison of angioscopic findings between diabetic and nondiabetic patients. *Circulation* 1995; 92(7):1731-1736.
- (13) Vigorita VJ, Moore GW, Hutchins GM. Absence of correlation between coronary arterial atherosclerosis and severity or duration of diabetes mellitus of adult onset. *Am J Cardiol* 1980; 46(4):535-542.
- (14) Waller BF, Palumbo PJ, Lie JT, Roberts WC. Status of the coronary arteries at necropsy in diabetes mellitus with onset after age 30 years. Analysis of 229 diabetic patients with and without clinical evidence of coronary heart disease and comparison to 183 control subjects. *Am J Med* 1980; 69(4):498-506.

- (15) Diabetes. Beware the silent assassin. Diabetes U.K.  
[http://www.diabetes.org.uk/Documents/Reports/Silent\\_assassin\\_press\\_report.pdf](http://www.diabetes.org.uk/Documents/Reports/Silent_assassin_press_report.pdf). 2008.
- (16) Ridderstrale M, Groop L. Genetic dissection of type 2 diabetes. *Mol Cell Endocrinol* 2009; 297(1-2):10-17.
- (17) Diabetes U.K.: What is diabetes? [http://www.diabetes.org.uk/Guide-to-diabetes/Introduction-to-diabetes/What\\_is\\_diabetes/](http://www.diabetes.org.uk/Guide-to-diabetes/Introduction-to-diabetes/What_is_diabetes/). 2009.
- (18) Gonzalez EL, Johansson S, Wallander MA, Rodriguez LA. Trends in the prevalence and incidence of diabetes in the UK: 1996-2005. *J Epidemiol Community Health* 2009; 63(4):332-336.
- (19) Glucose tolerance and cardiovascular mortality: comparison of fasting and 2-hour diagnostic criteria. *Arch Intern Med* 2001; 161(3):397-405.
- (20) Fox CS, Coady S, Sorlie PD, D'Agostino RB, Sr., Pencina MJ, Vasan RS et al. Increasing cardiovascular disease burden due to diabetes mellitus: the Framingham Heart Study. *Circulation* 2007; 115(12):1544-1550.
- (21) Smith SC, Jr. Multiple risk factors for cardiovascular disease and diabetes mellitus. *Am J Med* 2007; 120(3 Suppl 1):S3-S11.
- (22) Cohen Y, Raz I, Merin G, Mozes B. Comparison of factors associated with 30-day mortality after coronary artery bypass grafting in patients with versus without diabetes mellitus. Israeli Coronary Artery Bypass (ISCAB) Study Consortium. *Am J Cardiol* 1998; 81(1):7-11.
- (23) Eberly LE, Cohen JD, Prineas R, Yang L. Impact of incident diabetes and incident nonfatal cardiovascular disease on 18-year mortality: the multiple risk factor intervention trial experience. *Diabetes Care* 2003; 26(3):848-854.
- (24) Fietsam R, Jr., Bassett J, Glover JL. Complications of coronary artery surgery in diabetic patients. *Am Surg* 1991; 57(9):551-557.
- (25) Haffner SM, Lehto S, Ronnemaa T, Pyorala K, Laakso M. Mortality from coronary heart disease in subjects with type 2 diabetes and in nondiabetic subjects with and without prior myocardial infarction. *N Engl J Med* 1998; 339(4):229-234.
- (26) Malmberg K, Ryden L, Efendic S, Herlitz J, Nicol P, Waldenstrom A et al. Randomized trial of insulin-glucose infusion followed by subcutaneous insulin treatment in diabetic patients with acute myocardial infarction (DIGAMI study): effects on mortality at 1 year. *J Am Coll Cardiol* 1995; 26(1):57-65.
- (27) Pajunen P, Koukkunen H, Ketonen M, Jerkkola T, Immonen-Raiha P, Karja-Koskenkari P et al. Myocardial infarction in diabetic and non-diabetic persons with and without prior myocardial infarction: the FINAMI Study. *Diabetologia* 2005; 48(12):2519-2524.
- (28) Luciani N, Nasso G, Gaudino M, Abbate A, Gliaca F, Alessandrini F et al. Coronary artery bypass grafting in type II diabetic patients: a comparison between insulin-dependent and non-insulin-dependent patients at short- and mid-term follow-up. *Ann Thorac Surg* 2003; 76(4):1149-1154.

- (29) Matata BM, Galinanes M. Cardiopulmonary bypass exacerbates oxidative stress but does not increase proinflammatory cytokine release in patients with diabetes compared with patients without diabetes: regulatory effects of exogenous nitric oxide. *J Thorac Cardiovasc Surg* 2000; 120(1):1-11.
- (30) Mulnier HE, Seaman HE, Raleigh VS, Soedamah-Muthu SS, Colhoun HM, Lawrenson RA. Mortality in people with type 2 diabetes in the UK. *Diabet Med* 2006; 23(5):516-521.
- (31) Bansal P, Wang Q. Insulin as a physiological modulator of glucagon secretion. *Am J Physiol Endocrinol Metab* 2008; 295(4):E751-E761.
- (32) Unger RH, Orci L. Physiology and pathophysiology of glucagon. *Physiol Rev* 1976; 56(4):778-826.
- (33) Ferrannini E, Galvan AQ, Gastaldelli A, Camastra S, Sironi AM, Toschi E et al. Insulin: new roles for an ancient hormone. *Eur J Clin Invest* 1999; 29(10):842-852.
- (34) Saltiel AR, Kahn CR. Insulin signalling and the regulation of glucose and lipid metabolism. *Nature* 2001; 414(6865):799-806.
- (35) Zeng G, Quon MJ. Insulin-stimulated production of nitric oxide is inhibited by wortmannin. Direct measurement in vascular endothelial cells. *J Clin Invest* 1996; 98(4):894-898.
- (36) Formoso G, Chen H, Kim JA, Montagnani M, Consoli A, Quon MJ. Dehydroepiandrosterone mimics acute actions of insulin to stimulate production of both nitric oxide and endothelin 1 via distinct phosphatidylinositol 3-kinase- and mitogen-activated protein kinase-dependent pathways in vascular endothelium. *Mol Endocrinol* 2006; 20(5):1153-1163.
- (37) Potenza MA, Marasciulo FL, Chieppa DM, Brigiani GS, Formoso G, Quon MJ et al. Insulin resistance in spontaneously hypertensive rats is associated with endothelial dysfunction characterized by imbalance between NO and ET-1 production. *Am J Physiol Heart Circ Physiol* 2005; 289(2):H813-H822.
- (38) Potenza MA, Marasciulo FL, Tarquinio M, Quon MJ, Montagnani M. Treatment of spontaneously hypertensive rats with rosiglitazone and/or enalapril restores balance between vasodilator and vasoconstrictor actions of insulin with simultaneous improvement in hypertension and insulin resistance. *Diabetes* 2006; 55(12):3594-3603.
- (39) Muniyappa R, Montagnani M, Koh KK, Quon MJ. Cardiovascular actions of insulin. *Endocr Rev* 2007; 28(5):463-491.
- (40) Stumvoll M, Goldstein BJ, van Haeften TW. Type 2 diabetes: principles of pathogenesis and therapy. *Lancet* 2005; 365(9467):1333-1346.
- (41) Lizcano JM, Alessi DR. The insulin signalling pathway. *Curr Biol* 2002; 12(7):R236-R238.
- (42) Rosen OM. Banting lecture 1989. Structure and function of insulin receptors. *Diabetes* 1989; 38(12):1508-1511.

- (43) Sun XJ, Rothenberg P, Kahn CR, Backer JM, Araki E, Wilden PA et al. Structure of the insulin receptor substrate IRS-1 defines a unique signal transduction protein. *Nature* 1991; 352(6330):73-77.
- (44) Withers DJ, White M. Perspective: The insulin signaling system--a common link in the pathogenesis of type 2 diabetes. *Endocrinology* 2000; 141(6):1917-1921.
- (45) Cohen P. The twentieth century struggle to decipher insulin signalling. *Nat Rev Mol Cell Biol* 2006; 7(11):867-873.
- (46) Kane S, Sano H, Liu SC, Asara JM, Lane WS, Garner CC et al. A method to identify serine kinase substrates. Akt phosphorylates a novel adipocyte protein with a Rab GTPase-activating protein (GAP) domain. *J Biol Chem* 2002; 277(25):22115-22118.
- (47) Roach WG, Chavez JA, Miinea CP, Lienhard GE. Substrate specificity and effect on GLUT4 translocation of the Rab GTPase-activating protein Tbc1d1. *Biochem J* 2007; 403(2):353-358.
- (48) Baumann CA, Ribon V, Kanzaki M, Thurmond DC, Mora S, Shigematsu S et al. CAP defines a second signalling pathway required for insulin-stimulated glucose transport. *Nature* 2000; 407(6801):202-207.
- (49) Chiang SH, Baumann CA, Kanzaki M, Thurmond DC, Watson RT, Neudauer CL et al. Insulin-stimulated GLUT4 translocation requires the CAP-dependent activation of TC10. *Nature* 2001; 410(6831):944-948.
- (50) Ribon V, Saltiel AR. Insulin stimulates tyrosine phosphorylation of the proto-oncogene product of c-Cbl in 3T3-L1 adipocytes. *Biochem J* 1997; 324 ( Pt 3):839-845.
- (51) Cross DA, Alessi DR, Cohen P, Andjelkovich M, Hemmings BA. Inhibition of glycogen synthase kinase-3 by insulin mediated by protein kinase B. *Nature* 1995; 378(6559):785-789.
- (52) Agati JM, Yeagley D, Quinn PG. Assessment of the roles of mitogen-activated protein kinase, phosphatidylinositol 3-kinase, protein kinase B, and protein kinase C in insulin inhibition of cAMP-induced phosphoenolpyruvate carboxykinase gene transcription. *J Biol Chem* 1998; 273(30):18751-18759.
- (53) Dickens M, Svitek CA, Culbert AA, O'Brien RM, Tavare JM. Central role for phosphatidylinositide 3-kinase in the repression of glucose-6-phosphatase gene transcription by insulin. *J Biol Chem* 1998; 273(32):20144-20149.
- (54) Buchkovich NJ, Yu Y, Zampieri CA, Alwine JC. The TORrid affairs of viruses: effects of mammalian DNA viruses on the PI3K-Akt-mTOR signalling pathway. *Nat Rev Microbiol* 2008; 6(4):266-275.
- (55) Buchkovich NJ, Yu Y, Zampieri CA, Alwine JC. The TORrid affairs of viruses: effects of mammalian DNA viruses on the PI3K-Akt-mTOR signalling pathway. *Nat Rev Microbiol* 2008; 6(4):266-275.

- (56) Miron M, Verdu J, Lachance PE, Birnbaum MJ, Lasko PF, Sonenberg N. The translational inhibitor 4E-BP is an effector of PI(3)K/Akt signalling and cell growth in *Drosophila*. *Nat Cell Biol* 2001; 3(6):596-601.
- (57) Thomas G, Hall MN. TOR signalling and control of cell growth. *Curr Opin Cell Biol* 1997; 9(6):782-787.
- (58) Boulton TG, Nye SH, Robbins DJ, Ip NY, Radziejewska E, Morgenbesser SD et al. ERKs: a family of protein-serine/threonine kinases that are activated and tyrosine phosphorylated in response to insulin and NGF. *Cell* 1991; 65(4):663-675.
- (59) Montagnani M, Golovchenko I, Kim I, Koh GY, Goalstone ML, Mundhekar AN et al. Inhibition of phosphatidylinositol 3-kinase enhances mitogenic actions of insulin in endothelial cells. *J Biol Chem* 2002; 277(3):1794-1799.
- (60) Montagnani M, Ravichandran LV, Chen H, Esposito DL, Quon MJ. Insulin receptor substrate-1 and phosphoinositide-dependent kinase-1 are required for insulin-stimulated production of nitric oxide in endothelial cells. *Mol Endocrinol* 2002; 16(8):1931-1942.
- (61) Zeng G, Nystrom FH, Ravichandran LV, Cong LN, Kirby M, Mostowski H et al. Roles for insulin receptor, PI3-kinase, and Akt in insulin-signaling pathways related to production of nitric oxide in human vascular endothelial cells. *Circulation* 2000; 101(13):1539-1545.
- (62) Rader DJ. Effect of insulin resistance, dyslipidemia, and intra-abdominal adiposity on the development of cardiovascular disease and diabetes mellitus. *Am J Med* 2007; 120(3 Suppl 1):S12-S18.
- (63) Luan B, Zhao J, Wu H, Duan B, Shu G, Wang X et al. Deficiency of a beta-arrestin-2 signal complex contributes to insulin resistance. *Nature* 2009; 457(7233):1146-1149.
- (64) Pessin JE, Saltiel AR. Signaling pathways in insulin action: molecular targets of insulin resistance. *J Clin Invest* 2000; 106(2):165-169.
- (65) McFarlane SI, Banerji M, Sowers JR. Insulin resistance and cardiovascular disease. *J Clin Endocrinol Metab* 2001; 86(2):713-718.
- (66) Petersen KF, Shulman GI. Etiology of insulin resistance. *Am J Med* 2006; 119(5 Suppl 1):S10-S16.
- (67) Lebovitz HE, Banerji MA. Point: visceral adiposity is causally related to insulin resistance. *Diabetes Care* 2005; 28(9):2322-2325.
- (68) Banerji MA, Lebowitz J, Chaiken RL, Gordon D, Kral JG, Lebovitz HE. Relationship of visceral adipose tissue and glucose disposal is independent of sex in black NIDDM subjects. *Am J Physiol* 1997; 273(2 Pt 1):E425-E432.
- (69) Tchernof A, Lamarche B, Prud'homme D, Nadeau A, Moorjani S, Labrie F et al. The dense LDL phenotype. Association with plasma lipoprotein levels, visceral obesity, and hyperinsulinemia in men. *Diabetes Care* 1996; 19(6):629-637.

- (70) Bergman RN, Ader M. Free fatty acids and pathogenesis of type 2 diabetes mellitus. *Trends Endocrinol Metab* 2000; 11(9):351-356.
- (71) Machann J, Haring H, Schick F, Stumvoll M. Intramyocellular lipids and insulin resistance. *Diabetes Obes Metab* 2004; 6(4):239-248.
- (72) Hotamisligil GS. Role of endoplasmic reticulum stress and c-Jun NH2-terminal kinase pathways in inflammation and origin of obesity and diabetes. *Diabetes* 2005; 54 Suppl 2:S73-S78.
- (73) Carey AL, Bruce CR, Sacchetti M, Anderson MJ, Olsen DB, Saltin B et al. Interleukin-6 and tumor necrosis factor-alpha are not increased in patients with Type 2 diabetes: evidence that plasma interleukin-6 is related to fat mass and not insulin responsiveness. *Diabetologia* 2004; 47(6):1029-1037.
- (74) Carey AL, Febbraio MA. Interleukin-6 and insulin sensitivity: friend or foe? *Diabetologia* 2004; 47(7):1135-1142.
- (75) Hotamisligil GS, Spiegelman BM. Tumor necrosis factor alpha: a key component of the obesity-diabetes link. *Diabetes* 1994; 43(11):1271-1278.
- (76) Hotamisligil GS, Budavari A, Murray D, Spiegelman BM. Reduced tyrosine kinase activity of the insulin receptor in obesity-diabetes. Central role of tumor necrosis factor-alpha. *J Clin Invest* 1994; 94(4):1543-1549.
- (77) Christiansen T, Richelsen B, Bruun JM. Monocyte chemoattractant protein-1 is produced in isolated adipocytes, associated with adiposity and reduced after weight loss in morbid obese subjects. *Int J Obes (Lond)* 2005; 29(1):146-150.
- (78) Bastard JP, Jardel C, Bruckert E, Blondy P, Capeau J, Laville M et al. Elevated levels of interleukin 6 are reduced in serum and subcutaneous adipose tissue of obese women after weight loss. *J Clin Endocrinol Metab* 2000; 85(9):3338-3342.
- (79) Dyck DJ, Heigenhauser GJ, Bruce CR. The role of adipokines as regulators of skeletal muscle fatty acid metabolism and insulin sensitivity. *Acta Physiol (Oxf)* 2006; 186(1):5-16.
- (80) Yamauchi T, Kamon J, Minokoshi Y, Ito Y, Waki H, Uchida S et al. Adiponectin stimulates glucose utilization and fatty-acid oxidation by activating AMP-activated protein kinase. *Nat Med* 2002; 8(11):1288-1295.
- (81) Goldstein BJ, Scalia R. Adiponectin: A novel adipokine linking adipocytes and vascular function. *J Clin Endocrinol Metab* 2004; 89(6):2563-2568.
- (82) Rajala MW, Scherer PE. Minireview: The adipocyte--at the crossroads of energy homeostasis, inflammation, and atherosclerosis. *Endocrinology* 2003; 144(9):3765-3773.
- (83) Executive Summary of The Third Report of The National Cholesterol Education Program (NCEP) Expert Panel on Detection, Evaluation, And Treatment of High Blood Cholesterol In Adults (Adult Treatment Panel III). *JAMA* 2001; 285(19):2486-2497.



- (84) Executive Summary of The Third Report of The National Cholesterol Education Program (NCEP) Expert Panel on Detection, Evaluation, And Treatment of High Blood Cholesterol In Adults (Adult Treatment Panel III). JAMA 2001; 285(19):2486-2497.
- (85) Grundy SM, Brewer HB, Jr., Cleeman JI, Smith SC, Jr., Lenfant C. Definition of metabolic syndrome: report of the National Heart, Lung, and Blood Institute/American Heart Association conference on scientific issues related to definition. Arterioscler Thromb Vasc Biol 2004; 24(2):e13-e18.
- (86) Haffner SM, Stern MP, Hazuda HP, Mitchell BD, Patterson JK. Cardiovascular risk factors in confirmed prediabetic individuals. Does the clock for coronary heart disease start ticking before the onset of clinical diabetes? JAMA 1990; 263(21):2893-2898.
- (87) Endemann DH, Schiffrin EL. Endothelial dysfunction. J Am Soc Nephrol 2004; 15(8):1983-1992.
- (88) Madamanchi NR, Runge MS. Mitochondrial dysfunction in atherosclerosis. Circ Res 2007; 100(4):460-473.
- (89) Goh SY, Cooper ME. Clinical review: The role of advanced glycation end products in progression and complications of diabetes. J Clin Endocrinol Metab 2008; 93(4):1143-1152.
- (90) Wellen KE, Hotamisligil GS. Obesity-induced inflammatory changes in adipose tissue. J Clin Invest 2003; 112(12):1785-1788.
- (91) Brown NJ, Kim KS, Chen YQ, Blevins LS, Nadeau JH, Meranze SG et al. Synergistic effect of adrenal steroids and angiotensin II on plasminogen activator inhibitor-1 production. J Clin Endocrinol Metab 2000; 85(1):336-344.
- (92) Chen YQ, Su M, Walia RR, Hao Q, Covington JW, Vaughan DE. Sp1 sites mediate activation of the plasminogen activator inhibitor-1 promoter by glucose in vascular smooth muscle cells. J Biol Chem 1998; 273(14):8225-8231.
- (93) Meigs JB, D'Agostino RB, Sr., Wilson PW, Cupples LA, Nathan DM, Singer DE. Risk variable clustering in the insulin resistance syndrome. The Framingham Offspring Study. Diabetes 1997; 46(10):1594-1600.
- (94) Schneider DJ, Sobel BE. Augmentation of synthesis of plasminogen activator inhibitor type 1 by insulin and insulin-like growth factor type I: implications for vascular disease in hyperinsulinemic states. Proc Natl Acad Sci U S A 1991; 88(22):9959-9963.
- (95) Meigs JB, D'Agostino RB, Sr., Wilson PW, Cupples LA, Nathan DM, Singer DE. Risk variable clustering in the insulin resistance syndrome. The Framingham Offspring Study. Diabetes 1997; 46(10):1594-1600.
- (96) Ridker PM, Cushman M, Stampfer MJ, Tracy RP, Hennekens CH. Inflammation, aspirin, and the risk of cardiovascular disease in apparently healthy men. N Engl J Med 1997; 336(14):973-979.

- (97) Nathan DM, Cleary PA, Backlund JY, Genuth SM, Lachin JM, Orchard TJ et al. Intensive diabetes treatment and cardiovascular disease in patients with type 1 diabetes. *N Engl J Med* 2005; 353(25):2643-2653.
- (98) Stratton IM, Adler AI, Neil HA, Matthews DR, Manley SE, Cull CA et al. Association of glycaemia with macrovascular and microvascular complications of type 2 diabetes (UKPDS 35): prospective observational study. *BMJ* 2000; 321(7258):405-412.
- (99) Schleicher ED, Wagner E, Nerlich AG. Increased accumulation of the glycoxidation product N(epsilon)-(carboxymethyl)lysine in human tissues in diabetes and aging. *J Clin Invest* 1997; 99(3):457-468.
- (100) Giugliano D, Marfella R, Coppola L, Verrazzo G, Acampora R, Giunta R et al. Vascular effects of acute hyperglycemia in humans are reversed by L-arginine. Evidence for reduced availability of nitric oxide during hyperglycemia. *Circulation* 1997; 95(7):1783-1790.
- (101) Kaprio J, Tuomilehto J, Koskenvuo M, Romanov K, Reunanen A, Eriksson J et al. Concordance for type 1 (insulin-dependent) and type 2 (non-insulin-dependent) diabetes mellitus in a population-based cohort of twins in Finland. *Diabetologia* 1992; 35(11):1060-1067.
- (102) Newman B, Selby JV, King MC, Slemenda C, Fabsitz R, Friedman GD. Concordance for type 2 (non-insulin-dependent) diabetes mellitus in male twins. *Diabetologia* 1987; 30(10):763-768.
- (103) Lyssenko V, Almgren P, Anevski D, Perfekt R, Lahti K, Nissen M et al. Predictors of and longitudinal changes in insulin sensitivity and secretion preceding onset of type 2 diabetes. *Diabetes* 2005; 54(1):166-174.
- (104) Brosseau JD, Eelkema RC, Crawford AC, Abe TA. Diabetes among the three affiliated tribes: correlation with degree of Indian inheritance. *Am J Public Health* 1979; 69(12):1277-1278.
- (105) Serjeantson SW, Owerbach D, Zimmet P, Nerup J, Thoma K. Genetics of diabetes in Nauru: effects of foreign admixture, HLA antigens and the insulin-gene-linked polymorphism. *Diabetologia* 1983; 25(1):13-17.
- (106) Lebovitz HE. Type 2 diabetes: an overview. *Clin Chem* 1999; 45(8 Pt 2):1339-1345.
- (107) Fajans SS, Bell GI, Polonsky KS. Molecular mechanisms and clinical pathophysiology of maturity-onset diabetes of the young. *N Engl J Med* 2001; 345(13):971-980.
- (108) Florez JC. Clinical review: the genetics of type 2 diabetes: a realistic appraisal in 2008. *J Clin Endocrinol Metab* 2008; 93(12):4633-4642.
- (109) Dina C, Meyre D, Gallina S, Durand E, Korner A, Jacobson P et al. Variation in FTO contributes to childhood obesity and severe adult obesity. *Nat Genet* 2007; 39(6):724-726.

- (110) Frayling TM, Timpson NJ, Weedon MN, Zeggini E, Freathy RM, Lindgren CM et al. A common variant in the FTO gene is associated with body mass index and predisposes to childhood and adult obesity. *Science* 2007; 316(5826):889-894.
- (111) Grarup N, Andersen G, Krarup NT, Albrechtsen A, Schmitz O, Jorgensen T et al. Association testing of novel type 2 diabetes risk alleles in the JAZF1, CDC123/CAMK1D, TSPAN8, THADA, ADAMTS9, and NOTCH2 loci with insulin release, insulin sensitivity, and obesity in a population-based sample of 4,516 glucose-tolerant middle-aged Danes. *Diabetes* 2008; 57(9):2534-2540.
- (112) Loos RJ, Lindgren CM, Li S, Wheeler E, Zhao JH, Prokopenko I et al. Common variants near MC4R are associated with fat mass, weight and risk of obesity. *Nat Genet* 2008; 40(6):768-775.
- (113) Saxena R, Voight BF, Lyssenko V, Burt NP, de Bakker PI, Chen H et al. Genome-wide association analysis identifies loci for type 2 diabetes and triglyceride levels. *Science* 2007; 316(5829):1331-1336.
- (114) Scott LJ, Mohlke KL, Bonnycastle LL, Willer CJ, Li Y, Duren WL et al. A genome-wide association study of type 2 diabetes in Finns detects multiple susceptibility variants. *Science* 2007; 316(5829):1341-1345.
- (115) Unoki H, Takahashi A, Kawaguchi T, Hara K, Horikoshi M, Andersen G et al. SNPs in KCNQ1 are associated with susceptibility to type 2 diabetes in East Asian and European populations. *Nat Genet* 2008; 40(9):1098-1102.
- (116) Yasuda K, Miyake K, Horikawa Y, Hara K, Osawa H, Furuta H et al. Variants in KCNQ1 are associated with susceptibility to type 2 diabetes mellitus. *Nat Genet* 2008; 40(9):1092-1097.
- (117) Zeggini E, Weedon MN, Lindgren CM, Frayling TM, Elliott KS, Lango H et al. Replication of genome-wide association signals in UK samples reveals risk loci for type 2 diabetes. *Science* 2007; 316(5829):1336-1341.
- (118) Zeggini E, Scott LJ, Saxena R, Voight BF, Marchini JL, Hu T et al. Meta-analysis of genome-wide association data and large-scale replication identifies additional susceptibility loci for type 2 diabetes. *Nat Genet* 2008; 40(5):638-645.
- (119) NEEL JV. Diabetes mellitus: a "thrifty" genotype rendered detrimental by "progress"? *Am J Hum Genet* 1962; 14:353-362.
- (120) Hales CN, Barker DJ. Type 2 (non-insulin-dependent) diabetes mellitus: the thrifty phenotype hypothesis. *Diabetologia* 1992; 35(7):595-601.
- (121) Tuomilehto J, Lindstrom J, Eriksson JG, Valle TT, Hamalainen H, Ilanne-Parikka P et al. Prevention of type 2 diabetes mellitus by changes in lifestyle among subjects with impaired glucose tolerance. *N Engl J Med* 2001; 344(18):1343-1350.
- (122) Knowler WC, Barrett-Connor E, Fowler SE, Hamman RF, Lachin JM, Walker EA et al. Reduction in the incidence of type 2 diabetes with lifestyle intervention or metformin. *N Engl J Med* 2002; 346(6):393-403.

- (123) Pan XR, Li GW, Hu YH, Wang JX, Yang WY, An ZX et al. Effects of diet and exercise in preventing NIDDM in people with impaired glucose tolerance. The Da Qing IGT and Diabetes Study. *Diabetes Care* 1997; 20(4):537-544.
- (124) Altshuler D, Hirschhorn JN, Klannemark M, Lindgren CM, Vohl MC, Nemesh J et al. The common PPARgamma Pro12Ala polymorphism is associated with decreased risk of type 2 diabetes. *Nat Genet* 2000; 26(1):76-80.
- (125) Horikawa Y, Oda N, Cox NJ, Li X, Orho-Melander M, Hara M et al. Genetic variation in the gene encoding calpain-10 is associated with type 2 diabetes mellitus. *Nat Genet* 2000; 26(2):163-175.
- (126) Gloyn AL, Weedon MN, Owen KR, Turner MJ, Knight BA, Hitman G et al. Large-scale association studies of variants in genes encoding the pancreatic beta-cell KATP channel subunits Kir6.2 (KCNJ11) and SUR1 (ABCC8) confirm that the KCNJ11 E23K variant is associated with type 2 diabetes. *Diabetes* 2003; 52(2):568-572.
- (127) Grant SF, Thorleifsson G, Reynisdottir I, Benediktsson R, Manolescu A, Sainz J et al. Variant of transcription factor 7-like 2 (TCF7L2) gene confers risk of type 2 diabetes. *Nat Genet* 2006; 38(3):320-323.
- (128) Sladek R, Rocheleau G, Rung J, Dina C, Shen L, Serre D et al. A genome-wide association study identifies novel risk loci for type 2 diabetes. *Nature* 2007; 445(7130):881-885.
- (129) Pascoe L, Tura A, Patel SK, Ibrahim IM, Ferrannini E, Zeggini E et al. Common variants of the novel type 2 diabetes genes CDKAL1 and HHEX/IDE are associated with decreased pancreatic beta-cell function. *Diabetes* 2007; 56(12):3101-3104.
- (130) Steinthorsdottir V, Thorleifsson G, Reynisdottir I, Benediktsson R, Jonsdottir T, Walters GB et al. A variant in CDKAL1 influences insulin response and risk of type 2 diabetes. *Nat Genet* 2007; 39(6):770-775.
- (131) Grarup N, Rose CS, Andersson EA, Andersen G, Nielsen AL, Albrechtsen A et al. Studies of association of variants near the HHEX, CDKN2A/B, and IGF2BP2 genes with type 2 diabetes and impaired insulin release in 10,705 Danish subjects: validation and extension of genome-wide association studies. *Diabetes* 2007; 56(12):3105-3111.
- (132) Staiger H, Stancakova A, Zilinskaite J, Vanttinen M, Hansen T, Marini MA et al. A candidate type 2 diabetes polymorphism near the HHEX locus affects acute glucose-stimulated insulin release in European populations: results from the EUGENE2 study. *Diabetes* 2008; 57(2):514-517.
- (133) Gudmundsson J, Sulem P, Steinthorsdottir V, Bergthorsson JT, Thorleifsson G, Manolescu A et al. Two variants on chromosome 17 confer prostate cancer risk, and the one in TCF2 protects against type 2 diabetes. *Nat Genet* 2007; 39(8):977-983.
- (134) Molavi B, Rassouli N, Bagwe S, Rasouli N. A review of thiazolidinediones and metformin in the treatment of type 2 diabetes with focus on cardiovascular complications. *Vasc Health Risk Manag* 2007; 3(6):967-973.

- (135) DeFronzo RA, Barzilai N, Simonson DC. Mechanism of metformin action in obese and lean noninsulin-dependent diabetic subjects. *J Clin Endocrinol Metab* 1991; 73(6):1294-1301.
- (136) Stumvoll M, Nurjhan N, Perriello G, Dailey G, Gerich JE. Metabolic effects of metformin in non-insulin-dependent diabetes mellitus. *N Engl J Med* 1995; 333(9):550-554.
- (137) Shaw RJ, Lamia KA, Vasquez D, Koo SH, Bardeesy N, DePinho RA et al. The kinase LKB1 mediates glucose homeostasis in liver and therapeutic effects of metformin. *Science* 2005; 310(5754):1642-1646.
- (138) Bailey CJ, Turner RC. Metformin. *N Engl J Med* 1996; 334(9):574-579.
- (139) Cusi K, Consoli A, DeFronzo RA. Metabolic effects of metformin on glucose and lactate metabolism in noninsulin-dependent diabetes mellitus. *J Clin Endocrinol Metab* 1996; 81(11):4059-4067.
- (140) Mamputu JC, Wiernsperger NF, Renier G. Antiatherogenic properties of metformin: the experimental evidence. *Diabetes Metab* 2003; 29(4 Pt 2):6S71-6S76.
- (141) Nolan JJ, Ludvik B, Beerdsen P, Joyce M, Olefsky J. Improvement in glucose tolerance and insulin resistance in obese subjects treated with troglitazone. *N Engl J Med* 1994; 331(18):1188-1193.
- (142) Nolan JJ, Ludvik B, Beerdsen P, Joyce M, Olefsky J. Improvement in glucose tolerance and insulin resistance in obese subjects treated with troglitazone. *N Engl J Med* 1994; 331(18):1188-1193.
- (143) LeBrasseur NK, Kelly M, Tsao TS, Farmer SR, Saha AK, Ruderman NB et al. Thiazolidinediones can rapidly activate AMP-activated protein kinase in mammalian tissues. *Am J Physiol Endocrinol Metab* 2006; 291(1):E175-E181.
- (144) Yki-Jarvinen H. Thiazolidinediones. *N Engl J Med* 2004; 351(11):1106-1118.
- (145) Cockcroft JR. Exploring vascular benefits of endothelium-derived nitric oxide. *Am J Hypertens* 2005; 18(12 Pt 2):177S-183S.
- (146) Feletou M, Vanhoutte PM. Endothelial dysfunction: a multifaceted disorder (The Wiggers Award Lecture). *Am J Physiol Heart Circ Physiol* 2006; 291(3):H985-1002.
- (147) Moncada S, Higgs EA. Nitric oxide and the vascular endothelium. *Handb Exp Pharmacol* 2006;(176 Pt 1):213-254.
- (148) Yetik-Anacak G, Catravas JD. Nitric oxide and the endothelium: history and impact on cardiovascular disease. *Vascul Pharmacol* 2006; 45(5):268-276.
- (149) Beny JL, Brunet P, Huggel H. Interaction of bradykinin and des-Arg9-bradykinin with isolated pig coronary arteries: mechanical and electrophysiological events. *Regul Pept* 1987; 17(4):181-190.

- (150) Chen G, Suzuki H, Weston AH. Acetylcholine releases endothelium-derived hyperpolarizing factor and EDRF from rat blood vessels. *Br J Pharmacol* 1988; 95(4):1165-1174.
- (151) Palmer RM, Ferrige AG, Moncada S. Nitric oxide release accounts for the biological activity of endothelium-derived relaxing factor. *Nature* 1987; 327(6122):524-526.
- (152) Ignarro LJ, Buga GM, Wood KS, Byrns RE, Chaudhuri G. Endothelium-derived relaxing factor produced and released from artery and vein is nitric oxide. *Proc Natl Acad Sci U S A* 1987; 84(24):9265-9269.
- (153) Moncada S, Gryglewski R, Bunting S, Vane JR. An enzyme isolated from arteries transforms prostaglandin endoperoxides to an unstable substance that inhibits platelet aggregation. *Nature* 1976; 263(5579):663-665.
- (154) Yanagisawa M, Kurihara H, Kimura S, Tomobe Y, Kobayashi M, Mitsui Y et al. A novel potent vasoconstrictor peptide produced by vascular endothelial cells. *Nature* 1988; 332(6163):411-415.
- (155) Simionescu M. Implications of early structural-functional changes in the endothelium for vascular disease. *Arterioscler Thromb Vasc Biol* 2007; 27(2):266-274.
- (156) Schachinger V, Britten MB, Zeiher AM. Prognostic impact of coronary vasodilator dysfunction on adverse long-term outcome of coronary heart disease. *Circulation* 2000; 101(16):1899-1906.
- (157) Schachinger V, Britten MB, Zeiher AM. Prognostic impact of coronary vasodilator dysfunction on adverse long-term outcome of coronary heart disease. *Circulation* 2000; 101(16):1899-1906.
- (158) Widlansky ME, Gokce N, Keaney JF, Jr., Vita JA. The clinical implications of endothelial dysfunction. *J Am Coll Cardiol* 2003; 42(7):1149-1160.
- (159) Al Benna S, Hamilton CA, McClure JD, Rogers PN, Berg GA, Ford I et al. Low-density lipoprotein cholesterol determines oxidative stress and endothelial dysfunction in saphenous veins from patients with coronary artery disease. *Arterioscler Thromb Vasc Biol* 2006; 26(1):218-223.
- (160) Kawashima S, Yokoyama M. Dysfunction of endothelial nitric oxide synthase and atherosclerosis. *Arterioscler Thromb Vasc Biol* 2004; 24(6):998-1005.
- (161) Kawashima S, Yokoyama M. Dysfunction of endothelial nitric oxide synthase and atherosclerosis. *Arterioscler Thromb Vasc Biol* 2004; 24(6):998-1005.
- (162) Hadi HA, Suwaidi JA. Endothelial dysfunction in diabetes mellitus. *Vasc Health Risk Manag* 2007; 3(6):853-876.
- (163) Irani K. Oxidant signaling in vascular cell growth, death, and survival : a review of the roles of reactive oxygen species in smooth muscle and endothelial cell mitogenic and apoptotic signaling. *Circ Res* 2000; 87(3):179-183.

- (164) Li PF, Dietz R, von Harsdorf R. Differential effect of hydrogen peroxide and superoxide anion on apoptosis and proliferation of vascular smooth muscle cells. *Circulation* 1997; 96(10):3602-3609.
- (165) Li PF, Dietz R, von Harsdorf R. Reactive oxygen species induce apoptosis of vascular smooth muscle cell. *FEBS Lett* 1997; 404(2-3):249-252.
- (166) Wolin MS, Gupte SA, Oeckler RA. Superoxide in the vascular system. *J Vasc Res* 2002; 39(3):191-207.
- (167) Cai H, Harrison DG. Endothelial dysfunction in cardiovascular diseases: the role of oxidant stress. *Circ Res* 2000; 87(10):840-844.
- (168) Fridovich I. Superoxide anion radical ( $O_2^-$ ), superoxide dismutases, and related matters. *J Biol Chem* 1997; 272(30):18515-18517.
- (169) Darley-Usmar V, Wiseman H, Halliwell B. Nitric oxide and oxygen radicals: a question of balance. *FEBS Lett* 1995; 369(2-3):131-135.
- (170) Forstermann U, Munzel T. Endothelial nitric oxide synthase in vascular disease: from marvel to menace. *Circulation* 2006; 113(13):1708-1714.
- (171) Palmer RM, Rees DD, Ashton DS, Moncada S. L-arginine is the physiological precursor for the formation of nitric oxide in endothelium-dependent relaxation. *Biochem Biophys Res Commun* 1988; 153(3):1251-1256.
- (172) Schmidt HH, Nau H, Wittfoht W, Gerlach J, Prescher KE, Klein MM et al. Arginine is a physiological precursor of endothelium-derived nitric oxide. *Eur J Pharmacol* 1988; 154(2):213-216.
- (173) Vasquez-Vivar J, Kalyanaraman B, Martasek P, Hogg N, Masters BS, Karoui H et al. Superoxide generation by endothelial nitric oxide synthase: the influence of cofactors. *Proc Natl Acad Sci U S A* 1998; 95(16):9220-9225.
- (174) Moncada S, Higgs EA. The discovery of nitric oxide and its role in vascular biology. *Br J Pharmacol* 2006; 147 Suppl 1:S193-S201.
- (175) Michell BJ, Griffiths JE, Mitchelhill KI, Rodriguez-Crespo I, Tiganis T, Bozinovski S et al. The Akt kinase signals directly to endothelial nitric oxide synthase. *Curr Biol* 1999; 9(15):845-848.
- (176) Morrow VA, Fougelle F, Connell JM, Petrie JR, Gould GW, Salt IP. Direct activation of AMP-activated protein kinase stimulates nitric-oxide synthesis in human aortic endothelial cells. *J Biol Chem* 2003; 278(34):31629-31639.
- (177) Mitchell JA, Ali F, Bailey L, Moreno L, Harrington LS. Role of nitric oxide and prostacyclin as vasoactive hormones released by the endothelium. *Exp Physiol* 2008; 93(1):141-147.
- (178) Tare M, Parkington HC, Coleman HA, Neild TO, Dusting GJ. Hyperpolarization and relaxation of arterial smooth muscle caused by nitric oxide derived from the endothelium. *Nature* 1990; 346(6279):69-71.

- (179) Guzik TJ, Mussa S, Gastaldi D, Sadowski J, Ratnatunga C, Pillai R et al. Mechanisms of increased vascular superoxide production in human diabetes mellitus: role of NAD(P)H oxidase and endothelial nitric oxide synthase. *Circulation* 2002; 105(14):1656-1662.
- (180) Rajagopalan S, Kurz S, Munzel T, Tarpey M, Freeman BA, Griending KK et al. Angiotensin II-mediated hypertension in the rat increases vascular superoxide production via membrane NADH/NADPH oxidase activation. Contribution to alterations of vasomotor tone. *J Clin Invest* 1996; 97(8):1916-1923.
- (181) Warnholtz A, Nickenig G, Schulz E, Macharzina R, Brasen JH, Skatchkov M et al. Increased NADH-oxidase-mediated superoxide production in the early stages of atherosclerosis: evidence for involvement of the renin-angiotensin system. *Circulation* 1999; 99(15):2027-2033.
- (182) Zeiher AM, Schachinger V, Minners J. Long-term cigarette smoking impairs endothelium-dependent coronary arterial vasodilator function. *Circulation* 1995; 92(5):1094-1100.
- (183) Wilcox JN, Subramanian RR, Sundell CL, Tracey WR, Pollock JS, Harrison DG et al. Expression of multiple isoforms of nitric oxide synthase in normal and atherosclerotic vessels. *Arterioscler Thromb Vasc Biol* 1997; 17(11):2479-2488.
- (184) Shimokawa H, Flavahan NA, Vanhoutte PM. Loss of endothelial pertussis toxin-sensitive G protein function in atherosclerotic porcine coronary arteries. *Circulation* 1991; 83(2):652-660.
- (185) Harrison D, Griending KK, Landmesser U, Hornig B, Drexler H. Role of oxidative stress in atherosclerosis. *Am J Cardiol* 2003; 91(3A):7A-11A.
- (186) Ignarro LJ. Nitric oxide as a unique signaling molecule in the vascular system: a historical overview. *J Physiol Pharmacol* 2002; 53(4 Pt 1):503-514.
- (187) Hamilton CA, Miller WH, Al Benna S, Brosnan MJ, Drummond RD, McBride MW et al. Strategies to reduce oxidative stress in cardiovascular disease. *Clin Sci (Lond)* 2004; 106(3):219-234.
- (188) Li JM, Shah AM. Endothelial cell superoxide generation: regulation and relevance for cardiovascular pathophysiology. *Am J Physiol Regul Integr Comp Physiol* 2004; 287(5):R1014-R1030.
- (189) Griending KK, Ushio-Fukai M, Lassegue B, Alexander RW. Angiotensin II signaling in vascular smooth muscle. New concepts. *Hypertension* 1997; 29(1 Pt 2):366-373.
- (190) Ray R, Shah AM. NADPH oxidase and endothelial cell function. *Clin Sci (Lond)* 2005; 109(3):217-226.
- (191) Soccio M, Toniato E, Evangelista V, Carluccio M, De Caterina R. Oxidative stress and cardiovascular risk: the role of vascular NAD(P)H oxidase and its genetic variants. *Eur J Clin Invest* 2005; 35(5):305-314.



- (192) Suzuki H, Swei A, Zweifach BW, Schmid-Schonbein GW. In vivo evidence for microvascular oxidative stress in spontaneously hypertensive rats. Hydroethidine microfluorography. *Hypertension* 1995; 25(5):1083-1089.
- (193) Boveris A, Oshino N, Chance B. The cellular production of hydrogen peroxide. *Biochem J* 1972; 128(3):617-630.
- (194) Chance B, Sies H, Boveris A. Hydroperoxide metabolism in mammalian organs. *Physiol Rev* 1979; 59(3):527-605.
- (195) Jezek P, Hlavata L. Mitochondria in homeostasis of reactive oxygen species in cell, tissues, and organism. *Int J Biochem Cell Biol* 2005; 37(12):2478-2503.
- (196) Turrens JF. Mitochondrial formation of reactive oxygen species. *J Physiol* 2003; 552(Pt 2):335-344.
- (197) Milstien S, Katusic Z. Oxidation of tetrahydrobiopterin by peroxynitrite: implications for vascular endothelial function. *Biochem Biophys Res Commun* 1999; 263(3):681-684.
- (198) Griendling KK, Minieri CA, Ollerenshaw JD, Alexander RW. Angiotensin II stimulates NADH and NADPH oxidase activity in cultured vascular smooth muscle cells. *Circ Res* 1994; 74(6):1141-1148.
- (199) Ushio-Fukai M, Zafari AM, Fukui T, Ishizaka N, Griendling KK. p22phox is a critical component of the superoxide-generating NADH/NADPH oxidase system and regulates angiotensin II-induced hypertrophy in vascular smooth muscle cells. *J Biol Chem* 1996; 271(38):23317-23321.
- (200) Bayraktutan U, Draper N, Lang D, Shah AM. Expression of functional neutrophil-type NADPH oxidase in cultured rat coronary microvascular endothelial cells. *Cardiovasc Res* 1998; 38(1):256-262.
- (201) De Keulenaer GW, Chappell DC, Ishizaka N, Nerem RM, Alexander RW, Griendling KK. Oscillatory and steady laminar shear stress differentially affect human endothelial redox state: role of a superoxide-producing NADH oxidase. *Circ Res* 1998; 82(10):1094-1101.
- (202) Mohazzab KM, Kaminski PM, Wolin MS. NADH oxidoreductase is a major source of superoxide anion in bovine coronary artery endothelium. *Am J Physiol* 1994; 266(6 Pt 2):H2568-H2572.
- (203) Zalba G, San Jose G, Moreno MU, Fortuno MA, Fortuno A, Beaumont FJ et al. Oxidative stress in arterial hypertension: role of NAD(P)H oxidase. *Hypertension* 2001; 38(6):1395-1399.
- (204) De Keulenaer GW, Alexander RW, Ushio-Fukai M, Ishizaka N, Griendling KK. Tumour necrosis factor alpha activates a p22phox-based NADH oxidase in vascular smooth muscle. *Biochem J* 1998; 329 ( Pt 3):653-657.
- (205) Marumo T, Schini-Kerth VB, Fisslthaler B, Busse R. Platelet-derived growth factor-stimulated superoxide anion production modulates activation of transcription factor NF-kappaB and expression of monocyte chemoattractant protein 1 in human aortic smooth muscle cells. *Circulation* 1997; 96(7):2361-2367.

- (206) Guzik TJ, West NE, Black E, McDonald D, Ratnatunga C, Pillai R et al. Vascular superoxide production by NAD(P)H oxidase: association with endothelial dysfunction and clinical risk factors. *Circ Res* 2000; 86(9):E85-E90.
- (207) Hamilton CA, Brosnan MJ, Al Benna S, Berg G, Dominiczak AF. NAD(P)H oxidase inhibition improves endothelial function in rat and human blood vessels. *Hypertension* 2002; 40(5):755-762.
- (208) Guzik TJ, Sadowski J, Guzik B, Jopek A, Kapelak B, Przybylowski P et al. Coronary artery superoxide production and nox isoform expression in human coronary artery disease. *Arterioscler Thromb Vasc Biol* 2006; 26(2):333-339.
- (209) Moreno MU, San Jose G, Orbe J, Paramo JA, Beloqui O, Diez J et al. Preliminary characterisation of the promoter of the human p22(phox) gene: identification of a new polymorphism associated with hypertension. *FEBS Lett* 2003; 542(1-3):27-31.
- (210) San Jose G, Moreno MU, Olivan S, Beloqui O, Fortuno A, Diez J et al. Functional effect of the p22phox -930A/G polymorphism on p22phox expression and NADPH oxidase activity in hypertension. *Hypertension* 2004; 44(2):163-169.
- (211) Inoue N, Kawashima S, Kanazawa K, Yamada S, Akita H, Yokoyama M. Polymorphism of the NADH/NADPH oxidase p22 phox gene in patients with coronary artery disease. *Circulation* 1998; 97(2):135-137.
- (212) Sorescu D, Weiss D, Lassegue B, Clempus RE, Szocs K, Sorescu GP et al. Superoxide production and expression of nox family proteins in human atherosclerosis. *Circulation* 2002; 105(12):1429-1435.
- (213) Azumi H, Inoue N, Ohashi Y, Terashima M, Mori T, Fujita H et al. Superoxide generation in directional coronary atherectomy specimens of patients with angina pectoris: important role of NAD(P)H oxidase. *Arterioscler Thromb Vasc Biol* 2002; 22(11):1838-1844.
- (214) Guzik TJ, Chen W, Gongora MC, Guzik B, Lob HE, Mangalat D et al. Calcium-dependent NOX5 nicotinamide adenine dinucleotide phosphate oxidase contributes to vascular oxidative stress in human coronary artery disease. *J Am Coll Cardiol* 2008; 52(22):1803-1809.
- (215) Kim YK, Lee MS, Son SM, Kim IJ, Lee WS, Rhim BY et al. Vascular NADH oxidase is involved in impaired endothelium-dependent vasodilation in OLETF rats, a model of type 2 diabetes. *Diabetes* 2002; 51(2):522-527.
- (216) Ding H, Aljofan M, Triggle CR. Oxidative stress and increased eNOS and NADPH oxidase expression in mouse microvessel endothelial cells. *J Cell Physiol* 2007; 212(3):682-689.
- (217) Ulker S, McMaster D, McKeown PP, Bayraktutan U. Antioxidant vitamins C and E ameliorate hyperglycaemia-induced oxidative stress in coronary endothelial cells. *Diabetes Obes Metab* 2004; 6(6):442-451.
- (218) Weidig P, McMaster D, Bayraktutan U. High glucose mediates pro-oxidant and antioxidant enzyme activities in coronary endothelial cells. *Diabetes Obes Metab* 2004; 6(6):432-441.

- (219) Kanie N, Kamata K. Effects of chronic administration of the novel endothelin antagonist J-104132 on endothelial dysfunction in streptozotocin-induced diabetic rat. *Br J Pharmacol* 2002; 135(8):1935-1942.
- (220) Wautier MP, Chappey O, Corda S, Stern DM, Schmidt AM, Wautier JL. Activation of NADPH oxidase by AGE links oxidant stress to altered gene expression via RAGE. *Am J Physiol Endocrinol Metab* 2001; 280(5):E685-E694.
- (221) Yan SD, Schmidt AM, Anderson GM, Zhang J, Brett J, Zou YS et al. Enhanced cellular oxidant stress by the interaction of advanced glycation end products with their receptors/binding proteins. *J Biol Chem* 1994; 269(13):9889-9897.
- (222) Ballinger SW. Mitochondrial dysfunction in cardiovascular disease. *Free Radic Biol Med* 2005; 38(10):1278-1295.
- (223) Murphy MP. How mitochondria produce reactive oxygen species. *Biochem J* 2009; 417(1):1-13.
- (224) Corral-Debrinski M, Shoffner JM, Lott MT, Wallace DC. Association of mitochondrial DNA damage with aging and coronary atherosclerotic heart disease. *Mutat Res* 1992; 275(3-6):169-180.
- (225) Lowell BB, Shulman GI. Mitochondrial dysfunction and type 2 diabetes. *Science* 2005; 307(5708):384-387.
- (226) Cleeter MW, Cooper JM, Darley-Usmar VM, Moncada S, Schapira AH. Reversible inhibition of cytochrome c oxidase, the terminal enzyme of the mitochondrial respiratory chain, by nitric oxide. Implications for neurodegenerative diseases. *FEBS Lett* 1994; 345(1):50-54.
- (227) Palacios-Callender M, Quintero M, Hollis VS, Springett RJ, Moncada S. Endogenous NO regulates superoxide production at low oxygen concentrations by modifying the redox state of cytochrome c oxidase. *Proc Natl Acad Sci U S A* 2004; 101(20):7630-7635.
- (228) Quintero M, Colombo SL, Godfrey A, Moncada S. Mitochondria as signaling organelles in the vascular endothelium. *Proc Natl Acad Sci U S A* 2006; 103(14):5379-5384.
- (229) Doughan AK, Harrison DG, Dikalov SI. Molecular mechanisms of angiotensin II-mediated mitochondrial dysfunction: linking mitochondrial oxidative damage and vascular endothelial dysfunction. *Circ Res* 2008; 102(4):488-496.
- (230) Nishikawa T, Edelstein D, Du XL, Yamagishi S, Matsumura T, Kaneda Y et al. Normalizing mitochondrial superoxide production blocks three pathways of hyperglycaemic damage. *Nature* 2000; 404(6779):787-790.
- (231) Zhang DX, Gutterman DD. Mitochondrial reactive oxygen species-mediated signaling in endothelial cells. *Am J Physiol Heart Circ Physiol* 2007; 292(5):H2023-H2031.
- (232) Du X, Edelstein D, Obici S, Higham N, Zou MH, Brownlee M. Insulin resistance reduces arterial prostacyclin synthase and eNOS activities by increasing endothelial fatty acid oxidation. *J Clin Invest* 2006; 116(4):1071-1080.

- (233) Leopold JA, Loscalzo J. Oxidative enzymopathies and vascular disease. *Arterioscler Thromb Vasc Biol* 2005; 25(7):1332-1340.
- (234) Zelko IN, Mariani TJ, Folz RJ. Superoxide dismutase multigene family: a comparison of the CuZn-SOD (SOD1), Mn-SOD (SOD2), and EC-SOD (SOD3) gene structures, evolution, and expression. *Free Radic Biol Med* 2002; 33(3):337-349.
- (235) Fennell JP, Brosnan MJ, Frater AJ, Hamilton CA, Alexander MY, Nicklin SA et al. Adenovirus-mediated overexpression of extracellular superoxide dismutase improves endothelial dysfunction in a rat model of hypertension. *Gene Ther* 2002; 9(2):110-117.
- (236) Zanetti M, Sato J, Katusic ZS, O'Brien T. Gene transfer of superoxide dismutase isoforms reverses endothelial dysfunction in diabetic rabbit aorta. *Am J Physiol Heart Circ Physiol* 2001; 280(6):H2516-H2523.
- (237) Li Q, Bolli R, Qiu Y, Tang XL, Murphree SS, French BA. Gene therapy with extracellular superoxide dismutase attenuates myocardial stunning in conscious rabbits. *Circulation* 1998; 98(14):1438-1448.
- (238) Chung DJ, Wright AE, Clerch LB. The 3' untranslated region of manganese superoxide dismutase RNA contains a translational enhancer element. *Biochemistry* 1998; 37(46):16298-16306.
- (239) Fridovich I. Oxygen toxicity: a radical explanation. *J Exp Biol* 1998; 201(Pt 8):1203-1209.
- (240) Muzykantov VR. Targeting of superoxide dismutase and catalase to vascular endothelium. *J Control Release* 2001; 71(1):1-21.
- (241) Durand E, Al Haj ZA, Addad F, Brasselet C, Caligiuri G, Vinchon F et al. Adenovirus-mediated gene transfer of superoxide dismutase and catalase decreases restenosis after balloon angioplasty. *J Vasc Res* 2005; 42(3):255-265.
- (242) Wu G, Fang YZ, Yang S, Lupton JR, Turner ND. Glutathione metabolism and its implications for health. *J Nutr* 2004; 134(3):489-492.
- (243) Hayes JD, Flanagan JU, Jowsey IR. Glutathione transferases. *Annu Rev Pharmacol Toxicol* 2005; 45:51-88.
- (244) Fu Y, Porres JM, Lei XG. Comparative impacts of glutathione peroxidase-1 gene knockout on oxidative stress induced by reactive oxygen and nitrogen species in mouse hepatocytes. *Biochem J* 2001; 359(Pt 3):687-695.
- (245) Zhang Y, Handy DE, Loscalzo J. Adenosine-dependent induction of glutathione peroxidase 1 in human primary endothelial cells and protection against oxidative stress. *Circ Res* 2005; 96(8):831-837.
- (246) Weiss N, Zhang YY, Heydrick S, Bierl C, Loscalzo J. Overexpression of cellular glutathione peroxidase rescues homocyst(e)ine-induced endothelial dysfunction. *Proc Natl Acad Sci U S A* 2001; 98(22):12503-12508.

- (247) Hardie DG. Role of AMP-activated protein kinase in the metabolic syndrome and in heart disease. *FEBS Lett* 2008; 582(1):81-89.
- (248) Hardie DG. AMPK: a key regulator of energy balance in the single cell and the whole organism. *Int J Obes (Lond)* 2008; 32 Suppl 4:S7-12.
- (249) Carling D. The AMP-activated protein kinase cascade--a unifying system for energy control. *Trends Biochem Sci* 2004; 29(1):18-24.
- (250) Hardie DG, Hawley SA, Scott JW. AMP-activated protein kinase--development of the energy sensor concept. *J Physiol* 2006; 574(Pt 1):7-15.
- (251) Carling D, Sanders MJ, Woods A. The regulation of AMP-activated protein kinase by upstream kinases. *Int J Obes (Lond)* 2008; 32 Suppl 4:S55-S59.
- (252) Zou MH, Wu Y. AMP-activated protein kinase activation as a strategy for protecting vascular endothelial function. *Clin Exp Pharmacol Physiol* 2008; 35(5-6):535-545.
- (253) Hawley SA, Boudeau J, Reid JL, Mustard KJ, Udd L, Makela TP et al. Complexes between the LKB1 tumor suppressor, STRAD alpha/beta and MO25 alpha/beta are upstream kinases in the AMP-activated protein kinase cascade. *J Biol* 2003; 2(4):28.
- (254) Shaw RJ, Kosmatka M, Bardeesy N, Hurley RL, Witters LA, DePinho RA et al. The tumor suppressor LKB1 kinase directly activates AMP-activated kinase and regulates apoptosis in response to energy stress. *Proc Natl Acad Sci U S A* 2004; 101(10):3329-3335.
- (255) Towler MC, Hardie DG. AMP-activated protein kinase in metabolic control and insulin signaling. *Circ Res* 2007; 100(3):328-341.
- (256) Hardie DG. Minireview: the AMP-activated protein kinase cascade: the key sensor of cellular energy status. *Endocrinology* 2003; 144(12):5179-5183.
- (257) Leff T. AMP-activated protein kinase regulates gene expression by direct phosphorylation of nuclear proteins. *Biochem Soc Trans* 2003; 31(Pt 1):224-227.
- (258) Young LH, Li J, Baron SJ, Russell RR. AMP-activated protein kinase: a key stress signaling pathway in the heart. *Trends Cardiovasc Med* 2005; 15(3):110-118.
- (259) Kola B, Hubina E, Tucci SA, Kirkham TC, Garcia EA, Mitchell SE et al. Cannabinoids and ghrelin have both central and peripheral metabolic and cardiac effects via AMP-activated protein kinase. *J Biol Chem* 2005; 280(26):25196-25201.
- (260) Minokoshi Y, Kim YB, Peroni OD, Fryer LG, Muller C, Carling D et al. Leptin stimulates fatty-acid oxidation by activating AMP-activated protein kinase. *Nature* 2002; 415(6869):339-343.
- (261) Tomas E, Tsao TS, Saha AK, Murrey HE, Zhang CC, Itani SI et al. Enhanced muscle fat oxidation and glucose transport by ACRP30 globular domain: acetyl-CoA carboxylase inhibition and AMP-activated protein kinase activation. *Proc Natl Acad Sci U S A* 2002; 99(25):16309-16313.

- (262) Corton JM, Gillespie JG, Hawley SA, Hardie DG. 5-aminoimidazole-4-carboxamide ribonucleoside. A specific method for activating AMP-activated protein kinase in intact cells? *Eur J Biochem* 1995; 229(2):558-565.
- (263) Narkar VA, Downes M, Yu RT, Embler E, Wang YX, Banayo E et al. AMPK and PPARdelta agonists are exercise mimetics. *Cell* 2008; 134(3):405-415.
- (264) Hawley SA, Pan DA, Mustard KJ, Ross L, Bain J, Edelman AM et al. Calmodulin-dependent protein kinase kinase-beta is an alternative upstream kinase for AMP-activated protein kinase. *Cell Metab* 2005; 2(1):9-19.
- (265) Woods A, Dickerson K, Heath R, Hong SP, Momcilovic M, Johnstone SR et al. Ca<sup>2+</sup>/calmodulin-dependent protein kinase kinase-beta acts upstream of AMP-activated protein kinase in mammalian cells. *Cell Metab* 2005; 2(1):21-33.
- (266) Toyoda T, Hayashi T, Miyamoto L, Yonemitsu S, Nakano M, Tanaka S et al. Possible involvement of the alpha1 isoform of 5'AMP-activated protein kinase in oxidative stress-stimulated glucose transport in skeletal muscle. *Am J Physiol Endocrinol Metab* 2004; 287(1):E166-E173.
- (267) Kramer HF, Witczak CA, Fujii N, Jessen N, Taylor EB, Arnolds DE et al. Distinct signals regulate AS160 phosphorylation in response to insulin, AICAR, and contraction in mouse skeletal muscle. *Diabetes* 2006; 55(7):2067-2076.
- (268) Treebak JT, Glund S, Deshmukh A, Klein DK, Long YC, Jensen TE et al. AMPK-mediated AS160 phosphorylation in skeletal muscle is dependent on AMPK catalytic and regulatory subunits. *Diabetes* 2006; 55(7):2051-2058.
- (269) Lochhead PA, Salt IP, Walker KS, Hardie DG, Sutherland C. 5-aminoimidazole-4-carboxamide riboside mimics the effects of insulin on the expression of the 2 key gluconeogenic genes PEPCK and glucose-6-phosphatase. *Diabetes* 2000; 49(6):896-903.
- (270) Koo SH, Flechner L, Qi L, Zhang X, Sreaton RA, Jeffries S et al. The CREB coactivator TORC2 is a key regulator of fasting glucose metabolism. *Nature* 2005; 437(7062):1109-1111.
- (271) Woods A, Azzout-Marniche D, Foretz M, Stein SC, Lemarchand P, Ferre P et al. Characterization of the role of AMP-activated protein kinase in the regulation of glucose-activated gene expression using constitutively active and dominant negative forms of the kinase. *Mol Cell Biol* 2000; 20(18):6704-6711.
- (272) Merrill GF, Kurth EJ, Hardie DG, Winder WW. AICA riboside increases AMP-activated protein kinase, fatty acid oxidation, and glucose uptake in rat muscle. *Am J Physiol* 1997; 273(6 Pt 1):E1107-E1112.
- (273) Zong H, Ren JM, Young LH, Pypaert M, Mu J, Birnbaum MJ et al. AMP kinase is required for mitochondrial biogenesis in skeletal muscle in response to chronic energy deprivation. *Proc Natl Acad Sci U S A* 2002; 99(25):15983-15987.
- (274) Um SH, Frigerio F, Watanabe M, Picard F, Joaquin M, Sticker M et al. Absence of S6K1 protects against age- and diet-induced obesity while enhancing insulin sensitivity. *Nature* 2004; 431(7005):200-205.

- (275) Salt IP, Connell JM, Gould GW. 5-aminoimidazole-4-carboxamide ribonucleoside (AICAR) inhibits insulin-stimulated glucose transport in 3T3-L1 adipocytes. *Diabetes* 2000; 49(10):1649-1656.
- (276) Song XM, Fiedler M, Galuska D, Ryder JW, Fernstrom M, Chibalin AV et al. 5-Aminoimidazole-4-carboxamide ribonucleoside treatment improves glucose homeostasis in insulin-resistant diabetic (ob/ob) mice. *Diabetologia* 2002; 45(1):56-65.
- (277) Buhl ES, Jessen N, Pold R, Ledet T, Flyvbjerg A, Pedersen SB et al. Long-term AICAR administration reduces metabolic disturbances and lowers blood pressure in rats displaying features of the insulin resistance syndrome. *Diabetes* 2002; 51(7):2199-2206.
- (278) Iglesias MA, Ye JM, Frangioudakis G, Saha AK, Tomas E, Ruderman NB et al. AICAR administration causes an apparent enhancement of muscle and liver insulin action in insulin-resistant high-fat-fed rats. *Diabetes* 2002; 51(10):2886-2894.
- (279) Brunmair B, Staniek K, Gras F, Scharf N, Althaym A, Clara R et al. Thiazolidinediones, like metformin, inhibit respiratory complex I: a common mechanism contributing to their antidiabetic actions? *Diabetes* 2004; 53(4):1052-1059.
- (280) Kubota N, Terauchi Y, Kubota T, Kumagai H, Itoh S, Satoh H et al. Pioglitazone ameliorates insulin resistance and diabetes by both adiponectin-dependent and -independent pathways. *J Biol Chem* 2006; 281(13):8748-8755.
- (281) Nawrocki AR, Rajala MW, Tomas E, Pajvani UB, Saha AK, Trumbauer ME et al. Mice lacking adiponectin show decreased hepatic insulin sensitivity and reduced responsiveness to peroxisome proliferator-activated receptor gamma agonists. *J Biol Chem* 2006; 281(5):2654-2660.
- (282) Chen ZP, Mitchelhill KI, Michell BJ, Stapleton D, Rodriguez-Crespo I, Witters LA et al. AMP-activated protein kinase phosphorylation of endothelial NO synthase. *FEBS Lett* 1999; 443(3):285-289.
- (283) Zhang Y, Lee TS, Kolb EM, Sun K, Lu X, Sladek FM et al. AMP-activated protein kinase is involved in endothelial NO synthase activation in response to shear stress. *Arterioscler Thromb Vasc Biol* 2006; 26(6):1281-1287.
- (284) Boyle JG, Logan PJ, Ewart MA, Reihill JA, Ritchie SA, Connell JM et al. Rosiglitazone stimulates nitric oxide synthesis in human aortic endothelial cells via AMP-activated protein kinase. *J Biol Chem* 2008; 283(17):11210-11217.
- (285) Chen H, Montagnani M, Funahashi T, Shimomura I, Quon MJ. Adiponectin stimulates production of nitric oxide in vascular endothelial cells. *J Biol Chem* 2003; 278(45):45021-45026.
- (286) Davis BJ, Xie Z, Viollet B, Zou MH. Activation of the AMP-activated kinase by antidiabetes drug metformin stimulates nitric oxide synthesis in vivo by promoting the association of heat shock protein 90 and endothelial nitric oxide synthase. *Diabetes* 2006; 55(2):496-505.

- (287) Reihill JA, Ewart MA, Hardie DG, Salt IP. AMP-activated protein kinase mediates VEGF-stimulated endothelial NO production. *Biochem Biophys Res Commun* 2007; 354(4):1084-1088.
- (288) Zou MH, Hou XY, Shi CM, Nagata D, Walsh K, Cohen RA. Modulation by peroxynitrite of Akt- and AMP-activated kinase-dependent Ser1179 phosphorylation of endothelial nitric oxide synthase. *J Biol Chem* 2002; 277(36):32552-32557.
- (289) Zou MH, Hou XY, Shi CM, Kirkpatrick S, Liu F, Goldman MH et al. Activation of 5'-AMP-activated kinase is mediated through c-Src and phosphoinositide 3-kinase activity during hypoxia-reoxygenation of bovine aortic endothelial cells. Role of peroxynitrite. *J Biol Chem* 2003; 278(36):34003-34010.
- (290) Nagata D, Mogi M, Walsh K. AMP-activated protein kinase (AMPK) signaling in endothelial cells is essential for angiogenesis in response to hypoxic stress. *J Biol Chem* 2003; 278(33):31000-31006.
- (291) Ouchi N, Kobayashi H, Kihara S, Kumada M, Sato K, Inoue T et al. Adiponectin stimulates angiogenesis by promoting cross-talk between AMP-activated protein kinase and Akt signaling in endothelial cells. *J Biol Chem* 2004; 279(2):1304-1309.
- (292) Prasad R, Giri S, Nath N, Singh I, Singh AK. 5-aminoimidazole-4-carboxamide-1-beta-4-ribofuranoside attenuates experimental autoimmune encephalomyelitis via modulation of endothelial-monocyte interaction. *J Neurosci Res* 2006; 84(3):614-625.
- (293) Ewart MA, Kohlhaas CF, Salt IP. Inhibition of tumor necrosis factor alpha-stimulated monocyte adhesion to human aortic endothelial cells by AMP-activated protein kinase. *Arterioscler Thromb Vasc Biol* 2008; 28(12):2255-2257.
- (294) Hattori Y, Suzuki K, Hattori S, Kasai K. Metformin inhibits cytokine-induced nuclear factor kappaB activation via AMP-activated protein kinase activation in vascular endothelial cells. *Hypertension* 2006; 47(6):1183-1188.
- (295) Choi SL, Kim SJ, Lee KT, Kim J, Mu J, Birnbaum MJ et al. The regulation of AMP-activated protein kinase by H(2)O(2). *Biochem Biophys Res Commun* 2001; 287(1):92-97.
- (296) Emerling BM, Weinberg F, Snyder C, Burgess Z, Mutlu GM, Viollet B et al. Hypoxic activation of AMPK is dependent on mitochondrial ROS but independent of an increase in AMP/ATP ratio. *Free Radic Biol Med* 2009; 46(10):1386-1391.
- (297) Zou MH, Kirkpatrick SS, Davis BJ, Nelson JS, Wiles WG, Schlattner U et al. Activation of the AMP-activated protein kinase by the anti-diabetic drug metformin in vivo. Role of mitochondrial reactive nitrogen species. *J Biol Chem* 2004; 279(42):43940-43951.
- (298) Lee WJ, Lee IK, Kim HS, Kim YM, Koh EH, Won JC et al. Alpha-lipoic acid prevents endothelial dysfunction in obese rats via activation of AMP-activated protein kinase. *Arterioscler Thromb Vasc Biol* 2005; 25(12):2488-2494.



- (299) Jaffe EA, Nachman RL, Becker CG, Minick CR. Culture of human endothelial cells derived from umbilical veins. Identification by morphologic and immunologic criteria. *J Clin Invest* 1973; 52(11):2745-2756.
- (300) Southgate K, Newby AC. Serum-induced proliferation of rabbit aortic smooth muscle cells from the contractile state is inhibited by 8-Br-cAMP but not 8-Br-cGMP. *Atherosclerosis* 1990; 82(1-2):113-123.
- (301) Livak KJ, Schmittgen TD. Analysis of relative gene expression data using real-time quantitative PCR and the 2(-Delta Delta C(T)) Method. *Methods* 2001; 25(4):402-408.
- (302) Delles C, Zimmerli LU, McGrane DJ, Koh-Tan CH, Pathi VL, McKay AJ et al. Vascular stiffness is related to superoxide generation in the vessel wall. *J Hypertens* 2008; 26(5):946-955.
- (303) Hink U, Li H, Mollnau H, Oelze M, Matheis E, Hartmann M et al. Mechanisms underlying endothelial dysfunction in diabetes mellitus. *Circ Res* 2001; 88(2):E14-E22.
- (304) Tsao PS, Niebauer J, Buitrago R, Lin PS, Wang BY, Cooke JP et al. Interaction of diabetes and hypertension on determinants of endothelial adhesiveness. *Arterioscler Thromb Vasc Biol* 1998; 18(6):947-953.
- (305) Mollnau H, Wendt M, Szocs K, Lassegue B, Schulz E, Oelze M et al. Effects of angiotensin II infusion on the expression and function of NAD(P)H oxidase and components of nitric oxide/cGMP signaling. *Circ Res* 2002; 90(4):E58-E65.
- (306) Hamilton CA, Brosnan MJ, McIntyre M, Graham D, Dominiczak AF. Superoxide excess in hypertension and aging: a common cause of endothelial dysfunction. *Hypertension* 2001; 37(2 Part 2):529-534.
- (307) Kerr S, Brosnan MJ, McIntyre M, Reid JL, Dominiczak AF, Hamilton CA. Superoxide anion production is increased in a model of genetic hypertension: role of the endothelium. *Hypertension* 1999; 33(6):1353-1358.
- (308) Afanas'ev IB. Lucigenin chemiluminescence assay for superoxide detection. *Circ Res* 2001; 89(11):E46.
- (309) Liochev SI, Fridovich I. Lucigenin (bis-N-methylacridinium) as a mediator of superoxide anion production. *Arch Biochem Biophys* 1997; 337(1):115-120.
- (310) Munzel T, Afanas'ev IB, Kleschyov AL, Harrison DG. Detection of superoxide in vascular tissue. *Arterioscler Thromb Vasc Biol* 2002; 22(11):1761-1768.
- (311) Dikalov S, Griendling KK, Harrison DG. Measurement of reactive oxygen species in cardiovascular studies. *Hypertension* 2007; 49(4):717-727.
- (312) Zhao H, Joseph J, Fales HM, Sokoloski EA, Levine RL, Vasquez-Vivar J et al. Detection and characterization of the product of hydroethidine and intracellular superoxide by HPLC and limitations of fluorescence. *Proc Natl Acad Sci U S A* 2005; 102(16):5727-5732.

- (313) Valgimigli L, Pedulli GF, Paolini M. Measurement of oxidative stress by EPR radical-probe technique. *Free Radic Biol Med* 2001; 31(6):708-716.
- (314) Dudley SC, Jr., Hoch NE, McCann LA, Honeycutt C, Diamandopoulos L, Fukai T et al. Atrial fibrillation increases production of superoxide by the left atrium and left atrial appendage: role of the NADPH and xanthine oxidases. *Circulation* 2005; 112(9):1266-1273.
- (315) Dikalov S, Skatchkov M, Fink B, Bassenge E. Quantification of superoxide radicals and peroxynitrite in vascular cells using oxidation of sterically hindered hydroxylamines and electron spin resonance. *Nitric Oxide* 1997; 1(5):423-431.
- (316) Hwang J, Saha A, Boo YC, Sorescu GP, McNally JS, Holland SM et al. Oscillatory shear stress stimulates endothelial production of O<sub>2</sub><sup>-</sup> from p47phox-dependent NAD(P)H oxidases, leading to monocyte adhesion. *J Biol Chem* 2003; 278(47):47291-47298.
- (317) McNally JS, Davis ME, Giddens DP, Saha A, Hwang J, Dikalov S et al. Role of xanthine oxidoreductase and NAD(P)H oxidase in endothelial superoxide production in response to oscillatory shear stress. *Am J Physiol Heart Circ Physiol* 2003; 285(6):H2290-H2297.
- (318) Berry C, Hamilton CA, Brosnan MJ, Magill FG, Berg GA, McMurray JJ et al. Investigation into the sources of superoxide in human blood vessels: angiotensin II increases superoxide production in human internal mammary arteries. *Circulation* 2000; 101(18):2206-2212.
- (319) Graham D, Huynh NN, Hamilton CA, Beattie E, Smith RA, Cocheme HM et al. Mitochondria-Targeted Antioxidant MitoQ10 Improves Endothelial Function and Attenuates Cardiac Hypertrophy. *Hypertension* 2009.
- (320) Li N, Ragheb K, Lawler G, Sturgis J, Rajwa B, Melendez JA et al. Mitochondrial complex I inhibitor rotenone induces apoptosis through enhancing mitochondrial reactive oxygen species production. *J Biol Chem* 2003; 278(10):8516-8525.
- (321) Murphy MP, Smith RA. Drug delivery to mitochondria: the key to mitochondrial medicine. *Adv Drug Deliv Rev* 2000; 41(2):235-250.
- (322) Murphy MP. Targeting lipophilic cations to mitochondria. *Biochim Biophys Acta* 2008; 1777(7-8):1028-1031.
- (323) James AM, Cocheme HM, Smith RA, Murphy MP. Interactions of mitochondria-targeted and untargeted ubiquinones with the mitochondrial respiratory chain and reactive oxygen species. Implications for the use of exogenous ubiquinones as therapies and experimental tools. *J Biol Chem* 2005; 280(22):21295-21312.
- (324) Ross MF, Prime TA, Abakumova I, James AM, Porteous CM, Smith RA et al. Rapid and extensive uptake and activation of hydrophobic triphenylphosphonium cations within cells. *Biochem J* 2008; 411(3):633-645.
- (325) O'Malley Y, Fink BD, Ross NC, Prisinzano TE, Sivitz WI. Reactive oxygen and targeted antioxidant administration in endothelial cell mitochondria. *J Biol Chem* 2006; 281(52):39766-39775.

- (326) Dhanasekaran A, Kotamraju S, Kalivendi SV, Matsunaga T, Shang T, Keszler A et al. Supplementation of endothelial cells with mitochondria-targeted antioxidants inhibit peroxide-induced mitochondrial iron uptake, oxidative damage, and apoptosis. *J Biol Chem* 2004; 279(36):37575-37587.
- (327) Adlam VJ, Harrison JC, Porteous CM, James AM, Smith RA, Murphy MP et al. Targeting an antioxidant to mitochondria decreases cardiac ischemia-reperfusion injury. *FASEB J* 2005; 19(9):1088-1095.
- (328) Lowes DA, Thottakam BM, Webster NR, Murphy MP, Galley HF. The mitochondria-targeted antioxidant MitoQ protects against organ damage in a lipopolysaccharide-peptidoglycan model of sepsis. *Free Radic Biol Med* 2008; 45(11):1559-1565.
- (329) Murphy MP, Smith RA. Targeting antioxidants to mitochondria by conjugation to lipophilic cations. *Annu Rev Pharmacol Toxicol* 2007; 47:629-656.
- (330) Hamilton CA, Berg G, McIntyre M, Mcphaden AR, Reid JL, Dominiczak AF. Effects of nitric oxide and superoxide on relaxation in human artery and vein. *Atherosclerosis* 1997; 133(1):77-86.
- (331) Dikalov SI, Li W, Mehranpour P, Wang SS, Zafari AM. Production of extracellular superoxide by human lymphoblast cell lines: comparison of electron spin resonance techniques and cytochrome C reduction assay. *Biochem Pharmacol* 2007; 73(7):972-980.
- (332) Kuzkaya N, Weissmann N, Harrison DG, Dikalov S. Interactions of peroxynitrite, tetrahydrobiopterin, ascorbic acid, and thiols: implications for uncoupling endothelial nitric-oxide synthase. *J Biol Chem* 2003; 278(25):22546-22554.
- (333) Miller FJ, Rosenfeldt FL, Zhang C, Linnane AW, Nagley P. Precise determination of mitochondrial DNA copy number in human skeletal and cardiac muscle by a PCR-based assay: lack of change of copy number with age. *Nucleic Acids Res* 2003; 31(11):e61.
- (334) Guzik TJ, Sadowski J, Kapelak B, Jopek A, Rudzinski P, Pillai R et al. Systemic regulation of vascular NAD(P)H oxidase activity and nox isoform expression in human arteries and veins. *Arterioscler Thromb Vasc Biol* 2004; 24(9):1614-1620.
- (335) Scrutinio D, Giannuzzi P. Comorbidity in patients undergoing coronary artery bypass graft surgery: impact on outcome and implications for cardiac rehabilitation. *Eur J Cardiovasc Prev Rehabil* 2008; 15(4):379-385.
- (336) Dikalova A, Clempus R, Lassegue B, Cheng G, McCoy J, Dikalov S et al. Nox1 overexpression potentiates angiotensin II-induced hypertension and vascular smooth muscle hypertrophy in transgenic mice. *Circulation* 2005; 112(17):2668-2676.
- (337) Khatri JJ, Johnson C, Magid R, Lessner SM, Laude KM, Dikalov SI et al. Vascular oxidant stress enhances progression and angiogenesis of experimental atheroma. *Circulation* 2004; 109(4):520-525.

- (338) Dikalov SI, Vitek MP, Mason RP. Cupric-amyloid beta peptide complex stimulates oxidation of ascorbate and generation of hydroxyl radical. *Free Radic Biol Med* 2004; 36(3):340-347.
- (339) Stralin P, Karlsson K, Johansson BO, Marklund SL. The interstitium of the human arterial wall contains very large amounts of extracellular superoxide dismutase. *Arterioscler Thromb Vasc Biol* 1995; 15(11):2032-2036.
- (340) Marklund SL. Expression of extracellular superoxide dismutase by human cell lines. *Biochem J* 1990; 266(1):213-219.
- (341) Marklund SL. Extracellular superoxide dismutase in human tissues and human cell lines. *J Clin Invest* 1984; 74(4):1398-1403.
- (342) 't Hoen PA, Van der Lans CA, Van Eck M, Bijsterbosch MK, Van Berkel TJ, Twisk J. Aorta of ApoE-deficient mice responds to atherogenic stimuli by a prelesional increase and subsequent decrease in the expression of antioxidant enzymes. *Circ Res* 2003; 93(3):262-269.
- (343) Inoue N, Ramasamy S, Fukai T, Nerem RM, Harrison DG. Shear stress modulates expression of Cu/Zn superoxide dismutase in human aortic endothelial cells. *Circ Res* 1996; 79(1):32-37.
- (344) Miao L, Clair DK. Regulation of Superoxide Dismutase Genes: Implications in Diseases. *Free Radic Biol Med* 2009.
- (345) Esplugues JV, Rocha M, Nunez C, Bosca I, Ibiza S, Herance JR et al. Complex I dysfunction and tolerance to nitroglycerin: an approach based on mitochondrial-targeted antioxidants. *Circ Res* 2006; 99(10):1067-1075.
- (346) Kelso GF, Porteous CM, Coulter CV, Hughes G, Porteous WK, Ledgerwood EC et al. Selective targeting of a redox-active ubiquinone to mitochondria within cells: antioxidant and antiapoptotic properties. *J Biol Chem* 2001; 276(7):4588-4596.
- (347) Skulachev VP. How to clean the dirtiest place in the cell: cationic antioxidants as intramitochondrial ROS scavengers. *IUBMB Life* 2005; 57(4-5):305-310.
- (348) Doughan AK, Dikalov SI. Mitochondrial redox cycling of mitoquinone leads to superoxide production and cellular apoptosis. *Antioxid Redox Signal* 2007; 9(11):1825-1836.
- (349) Plecita-Hlavata L, Jezek J, Jezek P. Pro-oxidant mitochondrial matrix-targeted ubiquinone MitoQ10 acts as anti-oxidant at retarded electron transport or proton pumping within Complex I. *Int J Biochem Cell Biol* 2009; 41(8-9):1697-1707.
- (350) Mukherjee TK, Mishra AK, Mukhopadhyay S, Hoidal JR. High concentration of antioxidants N-acetylcysteine and mitoquinone-Q induces intercellular adhesion molecule 1 and oxidative stress by increasing intracellular glutathione. *J Immunol* 2007; 178(3):1835-1844.
- (351) Koopman WJ, Verkaart S, Visch HJ, van der Westhuizen FH, Murphy MP, van den Heuvel LW et al. Inhibition of complex I of the electron transport chain causes O<sub>2</sub>·- mediated mitochondrial outgrowth. *Am J Physiol Cell Physiol* 2005; 288(6):C1440-C1450.

- (352) James AM, Smith RA, Murphy MP. Antioxidant and prooxidant properties of mitochondrial Coenzyme Q. *Arch Biochem Biophys* 2004; 423(1):47-56.
- (353) Gardner PR, Raineri I, Epstein LB, White CW. Superoxide radical and iron modulate aconitase activity in mammalian cells. *J Biol Chem* 1995; 270(22):13399-13405.
- (354) Robinson KM, Janes MS, Pehar M, Monette JS, Ross MF, Hagen TM et al. Selective fluorescent imaging of superoxide in vivo using ethidium-based probes. *Proc Natl Acad Sci U S A* 2006; 103(41):15038-15043.
- (355) Zhao H, Joseph J, Fales HM, Sokoloski EA, Levine RL, Vasquez-Vivar J et al. Detection and characterization of the product of hydroethidine and intracellular superoxide by HPLC and limitations of fluorescence. *Proc Natl Acad Sci U S A* 2005; 102(16):5727-5732.
- (356) Li H, Wallerath T, Munzel T, Forstermann U. Regulation of endothelial-type NO synthase expression in pathophysiology and in response to drugs. *Nitric Oxide* 2002; 7(3):149-164.
- (357) Drummond GR, Cai H, Davis ME, Ramasamy S, Harrison DG. Transcriptional and posttranscriptional regulation of endothelial nitric oxide synthase expression by hydrogen peroxide. *Circ Res* 2000; 86(3):347-354.
- (358) Dasgupta J, Subbaram S, Connor KM, Rodriguez AM, Tirosh O, Beckman JS et al. Manganese superoxide dismutase protects from TNF-alpha-induced apoptosis by increasing the steady-state production of H<sub>2</sub>O<sub>2</sub>. *Antioxid Redox Signal* 2006; 8(7-8):1295-1305.
- (359) Stuehr DJ, Fasehun OA, Kwon NS, Gross SS, Gonzalez JA, Levi R et al. Inhibition of macrophage and endothelial cell nitric oxide synthase by diphenyleneiodonium and its analogs. *FASEB J* 1991; 5(1):98-103.
- (360) Doussiere J, Vignais PV. Diphenylene iodonium as an inhibitor of the NADPH oxidase complex of bovine neutrophils. Factors controlling the inhibitory potency of diphenylene iodonium in a cell-free system of oxidase activation. *Eur J Biochem* 1992; 208(1):61-71.
- (361) Li Y, Trush MA. Diphenyleneiodonium, an NAD(P)H oxidase inhibitor, also potently inhibits mitochondrial reactive oxygen species production. *Biochem Biophys Res Commun* 1998; 253(2):295-299.
- (362) Prabhakar NR. Oxygen sensing by the carotid body chemoreceptors. *J Appl Physiol* 2000; 88(6):2287-2295.
- (363) Delles C, Miller WH, Dominiczak AF. Targeting reactive oxygen species in hypertension. *Antioxid Redox Signal* 2008; 10(6):1061-1077.
- (364) Cai H, Griendling KK, Harrison DG. The vascular NAD(P)H oxidases as therapeutic targets in cardiovascular diseases. *Trends Pharmacol Sci* 2003; 24(9):471-478.

- (365) Jacobson GM, Dourron HM, Liu J, Carretero OA, Reddy DJ, Andrzejewski T et al. Novel NAD(P)H oxidase inhibitor suppresses angioplasty-induced superoxide and neointimal hyperplasia of rat carotid artery. *Circ Res* 2003; 92(6):637-643.
- (366) Mann GE, Yudilevich DL, Sobrevia L. Regulation of amino acid and glucose transporters in endothelial and smooth muscle cells. *Physiol Rev* 2003; 83(1):183-252.
- (367) Cheung PC, Salt IP, Davies SP, Hardie DG, Carling D. Characterization of AMP-activated protein kinase gamma-subunit isoforms and their role in AMP binding. *Biochem J* 2000; 346 Pt 3:659-669.
- (368) Momcilovic M, Hong SP, Carlson M. Mammalian TAK1 activates Snf1 protein kinase in yeast and phosphorylates AMP-activated protein kinase in vitro. *J Biol Chem* 2006; 281(35):25336-25343.
- (369) Xie M, Zhang D, Dyck JR, Li Y, Zhang H, Morishima M et al. A pivotal role for endogenous TGF-beta-activated kinase-1 in the LKB1/AMP-activated protein kinase energy-sensor pathway. *Proc Natl Acad Sci U S A* 2006; 103(46):17378-17383.
- (370) Zhang J, Xie Z, Dong Y, Wang S, Liu C, Zou MH. Identification of nitric oxide as an endogenous activator of the AMP-activated protein kinase in vascular endothelial cells. *J Biol Chem* 2008; 283(41):27452-27461.
- (371) Woods A, Salt I, Scott J, Hardie DG, Carling D. The alpha1 and alpha2 isoforms of the AMP-activated protein kinase have similar activities in rat liver but exhibit differences in substrate specificity in vitro. *FEBS Lett* 1996; 397(2-3):347-351.
- (372) Davies SP, Carling D, Hardie DG. Tissue distribution of the AMP-activated protein kinase, and lack of activation by cyclic-AMP-dependent protein kinase, studied using a specific and sensitive peptide assay. *Eur J Biochem* 1989; 186(1-2):123-128.
- (373) Hardie D.G., Haystead T.A.J., Salt I.P., Davies S.P. Assay and purification of protein: serine / threonine kinases. In: Hardie D.G., editor. *Protein Phosphorylation: A Practical Approach*. Oxford University Press, Oxford U.K., 1999: 201-209.
- (374) Quijano C, Castro L, Peluffo G, Valez V, Radi R. Enhanced mitochondrial superoxide in hyperglycemic endothelial cells: direct measurements and formation of hydrogen peroxide and peroxynitrite. *Am J Physiol Heart Circ Physiol* 2007; 293(6):H3404-H3414.
- (375) Wu Y, Song P, Xu J, Zhang M, Zou MH. Activation of protein phosphatase 2A by palmitate inhibits AMP-activated protein kinase. *J Biol Chem* 2007; 282(13):9777-9788.
- (376) Ouslimani N, Peynet J, Bonnefont-Rousselot D, Therond P, Legrand A, Beaudoux JL. Metformin decreases intracellular production of reactive oxygen species in aortic endothelial cells. *Metabolism* 2005; 54(6):829-834.
- (377) Kukidome D, Nishikawa T, Sonoda K, Imoto K, Fujisawa K, Yano M et al. Activation of AMP-activated protein kinase reduces hyperglycemia-induced mitochondrial reactive oxygen species production and promotes mitochondrial

- biogenesis in human umbilical vein endothelial cells. *Diabetes* 2006; 55(1):120-127.
- (378) Colombo SL, Moncada S. AMPK $\alpha$ 1 regulates the antioxidant status of vascular endothelial cells. *Biochem J* 2009.
  - (379) Xie Z, Dong Y, Zhang M, Cui MZ, Cohen RA, Riek U et al. Activation of protein kinase C  $\zeta$  by peroxynitrite regulates LKB1-dependent AMP-activated protein kinase in cultured endothelial cells. *J Biol Chem* 2006; 281(10):6366-6375.
  - (380) Dufva M. Introduction to microarray technology. *Methods Mol Biol* 2009; 529:1-22.
  - (381) Voisine P, Ruel M, Khan TA, Bianchi C, Xu SH, Kohane I et al. Differences in gene expression profiles of diabetic and nondiabetic patients undergoing cardiopulmonary bypass and cardioplegic arrest. *Circulation* 2004; 110(11 Suppl 1):II280-II286.
  - (382) Archacki SR, Wang QK. Microarray analysis of cardiovascular diseases. *Methods Mol Med* 2006; 129:1-13.
  - (383) Archacki SR, Angheloiu G, Tian XL, Tan FL, DiPaola N, Shen GQ et al. Identification of new genes differentially expressed in coronary artery disease by expression profiling. *Physiol Genomics* 2003; 15(1):65-74.
  - (384) King JY, Ferrara R, Tabibiazar R, Spin JM, Chen MM, Kuchinsky A et al. Pathway analysis of coronary atherosclerosis. *Physiol Genomics* 2005; 23(1):103-118.
  - (385) Lu H, Raptis M, Black E, Stan M, Amar S, Graves DT. Influence of diabetes on the exacerbation of an inflammatory response in cardiovascular tissue. *Endocrinology* 2004; 145(11):4934-4939.
  - (386) BeadStudio Normalization Algorithms for Gene Expression Data. [http://www.illumina.com/downloads/GXBeadStudioNormalization\\_TechNote.pdf](http://www.illumina.com/downloads/GXBeadStudioNormalization_TechNote.pdf). 2009.
  - (387) Ingenuity® Systems. <http://www.ingenuity.com/>. 2009.
  - (388) Weng L, Dai H, Zhan Y, He Y, Stepaniants SB, Bassett DE. Rosetta error model for gene expression analysis. *Bioinformatics* 2006; 22(9):1111-1121.
  - (389) Wit E, McClure J. *Statistics For Microarrays: Design Analysis, and Inference*. Wiley & Sons, 2004.
  - (390) Benjamini Y, Hochberg Y. Controlling the false discovery rate: a practical and powerful approach to multiple testing. *Journal of the Royal Statistical Society Series B* 1995; 57:289-300.
  - (391) Simoneau JA, Veerkamp JH, Turcotte LP, Kelley DE. Markers of capacity to utilize fatty acids in human skeletal muscle: relation to insulin resistance and obesity and effects of weight loss. *FASEB J* 1999; 13(14):2051-2060.
  - (392) Patti ME, Butte AJ, Crunkhorn S, Cusi K, Berria R, Kashyap S et al. Coordinated reduction of genes of oxidative metabolism in humans with insulin resistance and

- diabetes: Potential role of PGC1 and NRF1. *Proc Natl Acad Sci U S A* 2003; 100(14):8466-8471.
- (393) Mazzolai L, Hayoz D. The renin-angiotensin system and atherosclerosis. *Curr Hypertens Rep* 2006; 8(1):47-53.
  - (394) Lavoie JL, Sigmund CD. Minireview: overview of the renin-angiotensin system--an endocrine and paracrine system. *Endocrinology* 2003; 144(6):2179-2183.
  - (395) Unger T. The role of the renin-angiotensin system in the development of cardiovascular disease. *Am J Cardiol* 2002; 89(2A):3A-9A.
  - (396) Schindler C, Bramlage P, Kirch W, Ferrario CM. Role of the vasodilator peptide angiotensin-(1-7) in cardiovascular drug therapy. *Vasc Health Risk Manag* 2007; 3(1):125-137.
  - (397) Ishii K, Takekoshi K, Shibuya S, Kawakami Y, Isobe K, Nakai T. Angiotensin subtype-2 receptor (AT<sub>2</sub>) negatively regulates subtype-1 receptor (AT<sub>1</sub>) in signal transduction pathways in cultured porcine adrenal medullary chromaffin cells. *J Hypertens* 2001; 19(11):1991-1999.
  - (398) Crackower MA, Sarao R, Oudit GY, Yagil C, Kozieradzki I, Scanga SE et al. Angiotensin-converting enzyme 2 is an essential regulator of heart function. *Nature* 2002; 417(6891):822-828.
  - (399) Donoghue M, Hsieh F, Baronas E, Godbout K, Gosselin M, Stagliano N et al. A novel angiotensin-converting enzyme-related carboxypeptidase (ACE2) converts angiotensin I to angiotensin 1-9. *Circ Res* 2000; 87(5):E1-E9.
  - (400) Otsu M, Hiles I, Gout I, Fry MJ, Ruiz-Larrea F, Panayotou G et al. Characterization of two 85 kd proteins that associate with receptor tyrosine kinases, middle-T/pp60c-src complexes, and PI3-kinase. *Cell* 1991; 65(1):91-104.
  - (401) Ueki K, Fruman DA, Yballe CM, Fasshauer M, Klein J, Asano T et al. Positive and negative roles of p85 alpha and p85 beta regulatory subunits of phosphoinositide 3-kinase in insulin signaling. *J Biol Chem* 2003; 278(48):48453-48466.
  - (402) Shen YQ, Lang BF, Burger G. Diversity and dispersal of a ubiquitous protein family: acyl-CoA dehydrogenases. *Nucleic Acids Res* 2009.
  - (403) Ensenaer R, He M, Willard JM, Goetzman ES, Corydon TJ, Vandahl BB et al. Human acyl-CoA dehydrogenase-9 plays a novel role in the mitochondrial beta-oxidation of unsaturated fatty acids. *J Biol Chem* 2005; 280(37):32309-32316.
  - (404) Dov A, Abramovitch E, Warwar N, Neshet R. Diminished phosphodiesterase-8B potentiates biphasic insulin response to glucose. *Endocrinology* 2008; 149(2):741-748.
  - (405) Drexler H. Endothelial dysfunction: clinical implications. *Prog Cardiovasc Dis* 1997; 39(4):287-324.
  - (406) Berry C, Tardif JC, Bourassa MG. Coronary heart disease in patients with diabetes: part II: recent advances in coronary revascularization. *J Am Coll Cardiol* 2007; 49(6):643-656.



- (407) Berry C, Tardif JC, Bourassa MG. Coronary heart disease in patients with diabetes: part I: recent advances in prevention and noninvasive management. *J Am Coll Cardiol* 2007; 49(6):631-642.
- (408) Boulden BM, Widder JD, Allen JC, Smith DA, Al Baldawi RN, Harrison DG et al. Early determinants of H<sub>2</sub>O<sub>2</sub>-induced endothelial dysfunction. *Free Radic Biol Med* 2006; 41(5):810-817.
- (409) Dikalov SI, Dikalova AE, Bikineyeva AT, Schmidt HH, Harrison DG, Griendling KK. Distinct roles of Nox1 and Nox4 in basal and angiotensin II-stimulated superoxide and hydrogen peroxide production. *Free Radic Biol Med* 2008; 45(9):1340-1351.
- (410) Zimmerli LU, Schiffer E, Zurbig P, Good DM, Kellmann M, Mous L et al. Urinary proteomic biomarkers in coronary artery disease. *Mol Cell Proteomics* 2008; 7(2):290-298.
- (411) Herrera BM, Lockstone HE, Taylor JM, Wills QF, Kaisaki PJ, Barrett A et al. MicroRNA-125a is over-expressed in insulin target tissues in a spontaneous rat model of Type 2 Diabetes. *BMC Med Genomics* 2009; 2(1):54.
- (412) Lim LP, Lau NC, Garrett-Engele P, Grimson A, Schelter JM, Castle J et al. Microarray analysis shows that some microRNAs downregulate large numbers of target mRNAs. *Nature* 2005; 433(7027):769-773.
- (413) Ikeda S, Kong SW, Lu J, Bisping E, Zhang H, Allen PD et al. Altered microRNA expression in human heart disease. *Physiol Genomics* 2007; 31(3):367-373.
- (414) Poy MN, Spranger M, Stoffel M. microRNAs and the regulation of glucose and lipid metabolism. *Diabetes Obes Metab* 2007; 9 Suppl 2:67-73.
- (415) Tang X, Tang G, Ozcan S. Role of microRNAs in diabetes. *Biochim Biophys Acta* 2008; 1779(11):697-701.
- (416) Plaisance V, Abderrahmani A, Perret-Menoud V, Jacquemin P, Lemaigre F, Regazzi R. MicroRNA-9 controls the expression of Granuphilin/Slp4 and the secretory response of insulin-producing cells. *J Biol Chem* 2006; 281(37):26932-26942.
- (417) Poy MN, Eliasson L, Krutzfeldt J, Kuwajima S, Ma X, Macdonald PE et al. A pancreatic islet-specific microRNA regulates insulin secretion. *Nature* 2004; 432(7014):226-230.
- (418) Baroukh N, Ravier MA, Loder MK, Hill EV, Bounacer A, Scharfmann R et al. MicroRNA-124a regulates Foxa2 expression and intracellular signaling in pancreatic beta-cell lines. *J Biol Chem* 2007; 282(27):19575-19588.
- (419) Fisslthaler B, Fleming I. Activation and signaling by the AMP-activated protein kinase in endothelial cells. *Circ Res* 2009; 105(2):114-127.
- (420) Alba G, El Bekay R, Alvarez-Maqueda M, Chacon P, Vega A, Monteseirin J et al. Stimulators of AMP-activated protein kinase inhibit the respiratory burst in human neutrophils. *FEBS Lett* 2004; 573(1-3):219-225.

- (421) Scott JW, van Denderen BJ, Jorgensen SB, Honeyman JE, Steinberg GR, Oakhill JS et al. Thienopyridone drugs are selective activators of AMP-activated protein kinase beta1-containing complexes. *Chem Biol* 2008; 15(11):1220-1230.
- (422) Moreno D, Knecht E, Viollet B, Sanz P. A769662, a novel activator of AMP-activated protein kinase, inhibits non-proteolytic components of the 26S proteasome by an AMPK-independent mechanism. *FEBS Lett* 2008; 582(17):2650-2654.
- (423) Cool B, Zinker B, Chiou W, Kifle L, Cao N, Perham M et al. Identification and characterization of a small molecule AMPK activator that treats key components of type 2 diabetes and the metabolic syndrome. *Cell Metab* 2006; 3(6):403-416.
- (424) Graham D, Huynh NN, Hamilton CA, Beattie E, Smith RA, Cocheme HM et al. Mitochondria-targeted antioxidant MitoQ10 improves endothelial function and attenuates cardiac hypertrophy. *Hypertension* 2009; 54(2):322-328.
- (425) Gane EJ, Orr DW, Weilert F, Keogh GF, Gibson M, Murphy MP et al. Phase II study of the mitochondrial antioxidant mitoquinone for hepatitis C. *Journal of Hepatology* 2008; 48:S318 (meeting abstract 847).
- (426) Snow BJ, Rolfe FL, Murphy MP, Smith RA, Lockhart MM, Frampton CM et al. Phase II study of the mitochondrial antioxidant mitoquinone for Parkinson's disease. *Neurology* 2008; 70:A483-A484.